UNIVERSITAT POLITÉCNICA DE VALENCIA

DEPARTAMENTO DE COMUNICACIONES

Optical Orthogonal Frequency Division Multiplexed communication systems: analysis, design and optimization

Ph.D. Thesis

by

Christian Sánchez Costa

Ph.D. Supervisors:

Beatriz Ortega Tamarit

José Capmany Francoy

Valencia, July 2014

UNIVERSITAT POLITÉCNICA DE VALENCIA

DEPARTAMENTO DE COMUNICACIONES

Optical Orthogonal Frequency Division Multiplexed communication systems: analysis, design and optimization

Christian Sánchez Costa, M.Sc.
Optical and Quantum Communications Group (OQCG)
ITEAM Research Institute
Universitat Politècnica de València (UPV)
Camí de Vera s/n, 46022 València, SPAIN
crisanco@iteam.upv.es

Ph.D. Supervisors:
Beatriz Ortega Tamarit
José Capmany Francoy

To my wife Teresa,
and parents Dolores and José María
Teresa and Barto

Acknowledgements

I would like to thank the financial support given by the European Comission FP7 under project ALPHA (Architectures for fLexible Photonic Home and Access networks, grant no. 212352) and the Spanish Ministry of Economy and Competitiveness under the project NEWTON (Nueva generación de técnicas ópticas de transmissión OFDM para futuras redes WDM PONs", grant no. TEC2011-26642).

I would like to give my sincere thanks to my Ph.D. supervisors Beatriz Ortega and José Capmany for their wise guidance during these years and giving me the opportunity to do this Ph.D. work in the Optical and Quantum Communications Group (OQCG). I would not like to let the opportunity get away without also thanking to Beatriz Ortega for her patience, help and support.

I wish also to express my gratitude to all the present and past colleagues from the OQCG, for the helpful conversations on the scientific challenges and problems which have appeared on the way and have allowed me to get other perspectives, and for contributing to get a nice and good work atmosphere.

At this point, I must also thank to Prof. Jianming Tang for hosting me for a research stay in the Optical Communications Research group at the School of Electronic Engineering, Bangor University. I could know fantastic people there, and, for their support and collaborative assistance during that time and nowadays, it is my must to give special thanks to Jinlong Wei and Emilio-Hugues.

Beyond the professional environment, I would like to thank my parents, firstly for trusting me and giving me the opportunity to develop my university studies, and, secondly, for being an example of strength to adversity. My warmest regard to my parents in law Barto and Teresa, for their understanding, support and love during all these years. And to all the members of my family and friends, for so many good moments.

To my dear wife Teresa, because she is an essential support to me and living with her is the best thing has ever occurred to me. She is a source of understanding, love, affection and accepts me with all my faults. She has made possible the finishing of this Ph.D. thesis.

To all of them, thank you.

Abstract

In this work we carry out an intensive theoretical labor to describe optical communication systems which employ orthogonal frequency division multiplexing (OFDM), and, more concretely, those systems which use direct laser intensity modulation and direct detection. Placed within the unceasing search process of higher transmission rate and functionality of optical communication systems, OFDM, a widespread technique in other communication systems, has attracted a great interest during the last years due to its ease of linear effects equalization, flexibility, scalability and high use of well-known and mature signal processing techniques. Optical metro and access networks is one of the scenarios where it has raised a great interest, where the link reach is in the order of tens of kilometers, and the cost-effectiveness is of the main concern.

Optical OFDM (OOFDM) is different to subcarrier multiplexing (SCM) technique because subcarrier's data spectral content overlap one to another, but it can be detected correctly thanks to its orthogonality property. Besides, its detection and generation can be done electrically through the calculation of the Fast Fourier transform and its inverse, respectively. Under a proper design, OOFDM offers an easy equalization of the linear communication system effects, though its high peak-to-average power ratio is one of its main disadvantages.

As starting point, we propose an analytical model to study in detail all those phenomena which affect the signal information detected at the receiver. Such phenomena are the laser nonlinearity, laser phase and intensity modulations, propagation through the optical fiber taking into account the chromatic dispersion, and the intensity detection by means of a square-law detector. This analytical model is validated through comparisons with simulation results obtained by means of commercial software. Given the singularity of OFDM signal due to its multi-carrier nature, the amplitude of the generated signal is random, and the analytical model is complemented with a study of signal clipping at the transmitter. Moreover, filtering effects affecting the signal through the communication system are also taken into account. With the analytical model reported we can describe in a rather comprehensive way the main phenomena as well as exploring and optimizing the final system performance of OOFDM systems with direct modulation and detection.

Since the optical communication systems with direct modulation and detected are severely affected by nonlinear distortion, and for multi-carrier signals such as OFDM signals it means the mixing of the information symbols carried by the different subcarriers, we propose in Chapter 5 a pre-distortion technique based on the analytical model previously proposed. This technique improves the modulation efficiency, making possible to increase the signal information term without increasing the nonlinear distortion at the receiver. Great nonlinear distortion cancellation efficiency values are achieved, and our technique is also compared to another one previously published in order to evaluate its performance.

Another technique for the improvement of systems with direct modulation and detection is the employment of optical filtering. Though it is understood in an intuitive way for traditional optical modulation formats, it is necessary to have a mathematical formulae for OOFDM signals in order to understand exactly its working principle, the improvement obtained, as well as its potentiality. For such purpose, in Chapter 6 we present an analytical model which extends that previously proposed. The simplification of the mathematical expressions just obtained allows us to systematically explore the different effects involved in the final performance obtained, the study of OOFDM systems with different optical filtering structures, as well as the possibility of optimization in a quick and efficient manner different optical filtering structures. In our particular case, we study an optical filter based on Mach Zehnder interferometer and uniform fiber-Bragg grating structures.

To put it briefly, with this Ph.D. Thesis we have pretended to contribute on getting a greater understanding and a better design of optical communication systems employing OOFDM as well as exploring alternatives for their improvement.

Resumen

En este trabajo se realiza una intensiva labor teórica de descripción de sistemas de comunicaciones ópticas que utilizan la técnica de multiplexación por división de frecuencias ortogonales (OFDM en inglés), más concretamente en sistemas con modulación directa de la intensidad de un láser y detección directa. Enmarcada en el incensante proceso de búsqueda de mayores tasas de transmisión y de funcionalidad de los sistemas de comunicaciones ópticas, OFDM, una técnica muy popular en otros sistemas de comunicaciones, ha atraído un gran interés para sistemas de comunicaciones ópticas en los últimos años debido a la facilidad de ecualización de efectos lineales, flexibilidad, escalabilidad y alto uso de técnicas conocidas y maduras de procesamiento de señal. Uno de los escenarios donde ha suscitado un gran interés ha sido el de redes ópticas metropolitanas y de acceso, donde el alcance es del orden de decenas de kilómetros, y la eficiencia en los costes es de primordial importancia.

OFDM óptico (OOFDM en inglés) se distingue de la técnica de multiplexación por subportadoras (SCM en inglés) en que el contenido de las subportadoras se solapan espectralmente, pero se puede detectar correctamente gracias a su propiedad de ortogonalidad. Además, su detección y generación se puede realizar eléctricamente mediante el cálculo de la transformada rápida de Fourier y su inversa, respectivamente. Bajo un apropiado diseño, OOFDM ofrece una fácil ecualización de los efectos lineales del sistema de comunicaciones, aunque su alto ratio de “valor de pico a potencia media" es una de sus principales desventajas.

Como punto de partida, planteamos un modelo analítico que estudia con detalle todos aquellos fenómenos que afectan a la señal de información detectada en el receptor. Tales fenómenos son la nolinealidad del láser, las modulaciones de intensidad y de fase ópticas, la propagación a través de la fibra óptica teniendo en cuenta la dispersión cromática, y la detección de intensidad óptica final mediante un detector de ley cuadrática. Este modelo analítico es validado mediante comparaciones con resultados obtenidos a través de simulaciones con software comercial. Dada la singularidad de las señales OFDM, debida a su naturaleza multi-portadora, la amplitud de la señal generada es aleatoria, y el modelo analítico es complementado con un estudio que contempla el recorte o “clipping" en el transmisor. Además, se tiene en cuenta los efectos de filtrado de la señal a lo largo de sistema de comunicaciones. Con el modelo analítico desarrollado se está en disposición de realizar una descripción bastante completa de los principales fenómenos así como explorar y optimizar el funcionamiento final de sistemas OOFDM con modulación y detección directa.

Puesto que los sistemas de comunicaciones ópticas con modulación y detección directa se ven perjudicados por la distorsión no lineal, que para señales multi-portadora como OFDM se traduce en la mezcla de los símbolos de información que transportan las diferentes subportadoras, se propone en el Capítulo 5 una técnica de pre-distorsión que se basa en el modelo analítico previamente propuesto. Esta técnica mejora la eficiencia de modulación, haciendo

posible incrementar el término de la señal de información sin que se vea incrementada la distorsión no lineal en el receptor. Valores muy altos de cancelación de la distorsión no lineal se consiguen, y la técnica aquí propuesta se compara también con otra ya publicada con el objetivo de evaluar su funcionamiento.

Otra técnica para la mejora de sistemas con modulación y detección directas es la realizada mediante filtrado óptico. Aunque se conoce de forma intuitiva su funcionamiento para formatos de modulación ópticos tradicionales, es preciso disponer de una formulación matemática para señales ópticas OFDM para entender de forma exacta su principio de operación, las mejoras obtenidas, así como su potencial. En el Capítulo 6 se desarrolla un modelo analítico para tal fin que extiende el análisis teórico previamente propuesto. La simplificación de las expresiones matemáticas obtenidas nos permite explorar de forma sistemática los diferentes efectos que afectan el funcionamiento final obtenido, estudiar el sistema OOFDM con diversas estructuras de filtrado óptico, así como la posibilidad de optimizar de forma rápida y eficiente diferentes estructuras de filtrado. En nuestro caso particular, se estudian un filtro basado en un interferómetro Mach Zehnder y una red uniforme de Bragg grabada en fibra óptica.

En definitiva, con este trabajo de tesis doctoral se ha pretendido contribuir a conseguir un mayor entendimiento y mejor diseño de sistemas de comunicaciones ópticas que emplean OOFDM y explorar alternativas para su mejora.

Resum

En aquest treball, es realitza una intensiva labor teòrica de descripció de sistemes de comunicacions òptiques, que utilitzen la tècnica de multiplexació per divisió de freqüencies ortogonals (OFDM en anglès); més concretament, en sistemes amb modulació directa de la intensitat d'un làser i detecció directa. Emmarcada en l'incessant procés de cerca de majors taxes de transmissió i de funcionalitat dels sistemes de comunicacions òptiques, OFDM, una tècnica molt popular en altres sistemes de comunicacions, ha atret un gran interès en els últims anys, a causa de la facilitat d'equalització d'efectes lineals, flexibilitat, escalabilitat i alt ús de tècniques conegudes i madures de processament de senyal. Un dels escenaris on ha suscitat un gran interès ha estat en el de xarxes òptiques metropolitanes i d'accés, on l'abast és de l'ordre de desenes de quilòmetres i l'eficiència en els costos és de primordial importància.

OFDM òptic (OOFDM en anglès) es distingeix de la tècnica de multiplexació per subportadores (SCM en anglès) en que el contingut de les subportadores es solapen espectralment; però, es pot detectar correctament gràcies a la seua propietat d'ortogonalitat. A més, la seua detecció i generació es pot realitzar elèctricament, mitjançant el càlcul de la transformada ràpida de Fourier i la seua inversa, respectivament. Sota un apropiat disseny, OOFDM ofereix una fàcil equalització dels efectes lineals del sistema de comunicacions, encara que la seua alta ràtio de valor de pic a potència mitjana, és una de les seues principals desavantatges.

Com a punt de partida, plantegem un model analític que estudia amb detall, tots aquells fenòmens que afecten al senyal d'informació detectada en el receptor. Tals fenòmens són la no-linealitat del làser, les modulacions d'intensitat i de fase òptica, la propagació a través de la fibra òptica tenint en compte la dispersió cromàtica i la detecció d'intensitat òptica final mitjançant un detector de llei quadràtica. Aquest model analític és validat mitjançant comparacions amb resultats obtinguts a través de simulacions amb programa comercial. Donada la singularitat, dels senyals OFDM, deguda a la seua naturalesa multi-portadora, l'amplitud del senyal generat és aleatòria i el model analític és complementat amb un estudi que contempla la retallada o clipping en el transmissor. A més, es té en compte els efectes de filtrat del senyal al llarg del sistema de comunicacions. Amb el model analític desenvolupat s'està en disposició de realitzar una descripció, bastant completa, dels principals fenòmens; així, com explorar i optimitzar el funcionament final de sistemes OOFDM amb modulació i detecció directa.

Ja que els sistemes de comunicacions òptiques amb modulació i detecció directa es veuen perjudicats per la distorsió no lineal, que per a senyals multi-portadores, com OFDM, es tradueix en la mescla dels símbols d'informació que transporten les diferents subportadores, es proposa, en el Capítol 5, una tècnica de pre-distorsió, que es basa en el model analític prèviament proposat. Aquesta tècnica millora l'eficiència de modulació, fent possible in-

crementar el terme del senyal d'informació, sense que es veja incrementada la distorsió no lineal en el receptor. Valors molt alts de cancel·lació de la distorsió no lineal s'aconsegueixen i la tècnica, ací proposada, es compara també amb una altra ja publicada, amb l'objectiu d'avaluar el seu funcionament.

Una altra tècnica per a la millora de sistemes amb modulació i detecció directes és la realitzada mitjançant filtrat òptic. Encara que es coneix, de forma intuïtiva, el seu funcionament per a formats de modulació òptics tradicionals, cal disposar, d'una formulació matemàtica per a senyals òptics OFDM, per entendre de forma exacta el seu principi d'operació, les millores obtingudes, així com el seu potencial. En el Capítol 6 es desenvolupa un model analític per a tal fi, que estén l'anàlisi teòrica prèviament proposat. La simplificació de les expressions matemàtiques obtingudes, ens permet explorar de forma sistemàtica els diferents efectes que afecten el funcionament final obtingut, estudiar el sistema OOFDM amb diverses estructures de filtrat òptic, així com la possibilitat d'optimitzar de forma ràpida i eficient diferents estructures de filtrat. En el nostre cas particular, s'estudien un filtre basat en un interferòmetre Mach Zehnder i una xarxa uniforme de Bragg gravada en fibra òptica.

En definitiva, amb aquest treball de tesi doctoral s'ha pretès contribuir a aconseguir un major enteniment i millor disseny de sistemes de comunicacions òptiques que empren OOFDM i explorar alternatives per a la seua millora.

List of Figures

List of Tables

Contents

Chapter 1

Introduction

1.1 Context

1.1.1 The need for further transmission capacity

In the so-called “information age", only two windows of the electromagnetism spectrum are nowadays used for supporting the huge worldwide information traffic [1]: the first one spans from long-wave radio to millimeter wave (100KHz to 300GHz), whilst the second one is located in the infrared lightwave region (30THz-300THz). Applications such as radio and TV broadcast, wireless local area networks or mobile phone communications make use of the first one, providing bit rates up to the order of Gbits/s. On the other hand, lightwave systems which make use of the second window, due to its huger available spectrum and thus the potentiality of supporting Tbits/s capacities over many thousand kilometers, are the backbone to the modern-day information infrastructure.

Telecommunications have become a central element of society's daily life and newly emerged communication services such as IPTV, video conference, remote medical support, online gaming or social networking are adopted at a rapid speed. These huge bandwidth demanding services require the transport of large information flows from one place to another, passing through different segments of the communication network until reaching the end-users, as illustrated in Fig. 1.1.

As result, there is a relentless demand for more network capacity, putting a great pressure on the communication network infrastructures at every scale, from core to metro, access networks and in-building or in-house networks. In order to put it in numbers, Fig. 1.2 shows a forecast of the global Internet Protocol traffic for the years 2012-2017 extracted from [2]: the expected Internet Protol traffic per month at 2017 is expected to be 120.6 exabytes from 69 exabytes per month in 2014, showing an increase of around 23% per year.

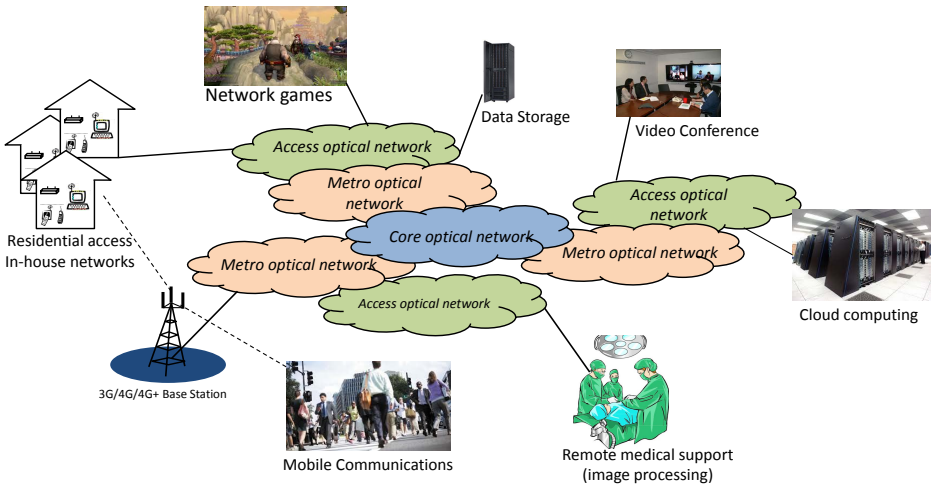

Figure 1.1: Information network

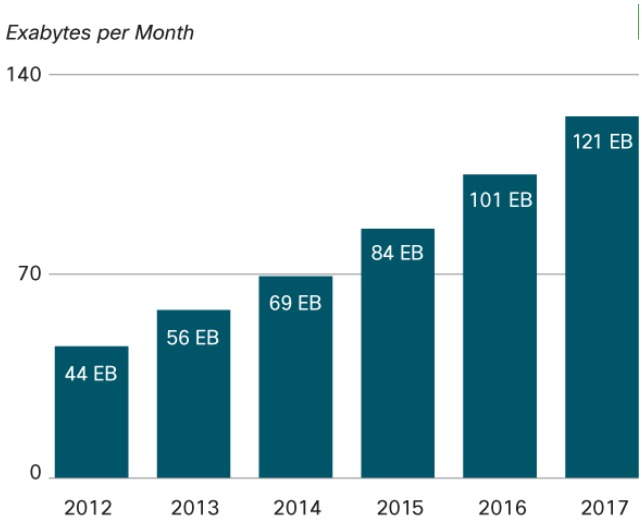

Figure 1.2: Global Internet Protocol traffic.

1.1.2 Technical advances on optical communications

Fueled by this endless demand for more transmission capacity, technical advances brought by research on optical communications have allowed the achievement of higher data rates, longer distances, lower cost and more functionality [3, 4]: advanced modulation formats, coherent systems with digital signal processing (DSP), advanced coding, low-loss optical components, low-noise optical amplifiers and advanced optical fibers. Among these, research on advanced modulation formats and the employment of digital signal processing techniques are of special importance to understand the motivation of this work.

Until recently, most of the installed optical networks used traditional intensity-modulation direct-detection (IMDD) formats based on nonreturn-to-zero (NRZ). Smaller separation between wavelength channels is required in order to get a more efficient exploitation of the available fiber spectrum, and, thus, more efficient ways of encoding the information sig-

nal into narrower frequency bins. Furthermore, apart from lowering the cost per information bit, the employment of advanced modulation formats may provide salient advantages such as robustness to fiber impairment effects (chromatic dispersion, fiber nonlinearities, polarization-mode dispersion,...), to optical component penalty effects (e.g., optical filtering due to optical add-drop multiplexers), and also adaptability, flexibility, amongst others.

Chromatic dispersion on single-mode fiber (SMF) has been the main fiber impairment to overcome in optical communications, and, for such, dispersion compensating fibers have been traditionally employed along the optical fiber link. However, in 2005, Nortel demonstrated the transmission of a 10Gbits/s return-to-zero differential phase-shift keying signal through 5120 km of standard SMF, with no optical dispersion [5]. The optical field was modulated by a precompensated signal using a inphase-quadrature optical modulator. This electronic approach for the dispersion compensation represented a solution with a smaller cost and ease for adaptation than its optical counterpart. In the following years, the research on digital signal processing techniques in optical communication systems has been very extensive[6–16]. The performance improvement in CMOS technology, manifested by the doubling of transistors in electronic integrated circuits as foreseen by the Moore's, is the underlying force which makes feasible such complex DSP techniques operating at speeds of Gsam/s.

In this context, one may wonder what orthogonal-frequency division multiplexing (OFDM) brings to the optical communications world and why it has become so popular in a so relatively short period of time. The next advantages of optical OFDM (OOFDM) [1] can help to answer these questions and understand our motivation to carry out this research work on it:

- Scalability. The information on OFDM signals is managed in the frequency domain, and so it is relatively easy to achieve greater capacities by making use of broader transmission spectrums. The migration to higher information rates can be made smoothly without incurring significant expenses as result of the substitution of hardware and software.

- Adaptability. OOFDM, thanks to its easy equalization, can easily adapt to any optical dispersion and meet the actual conditions of the fiber link (length, single or multi mode, mechanical variations,...). On the other hand, by means of some additional digital signal processing, the information transmission can be adapted to the channel conditions by changing the modulation format and/or the power of each subcarrier, or its code rate.

- Sub-carrier granularity. Although routed wavelength division multiplexed (WDM) networks offer well known advantages, their rigid and coarse granularity leads to inefficient capacity utilization. It may be benefitial to get access to parts of the traffic for subsequent routing until the end-user, and OOFDM bands and subcarriers are promising candidates to provide such fine granularity.

Amongst the great variety of scenarios where OOFDM has been proposed [1, 17, 18], in this work we focus on communication applications with short/medium reach links (up to around 100km of standard single mode fiber). Thus, this work must be placed within the research literature on optical metro networks, but, mainly on conventional and reach-extended optical access networks.

1.1.3 Optical access networks

The access network is that part of the telecommunications network that connects service providers central office (CO) to end users [19]. Conventional communication technologies employed in this part of the network based on twisted-pair telephony and coaxial cable are struggling to meet the end-users demands for larger data rates, whose provision come at the expense of shorter reach [20]. Due to its enormous volume, the upgrade of this part of the telecommunications networks yields large cost expenses, but communication carriers are finally adopting commercial solutions based on optical fiber due to its low loss and huge bandwidth. The penetration of optical fibre directly to the home, referred to as fibre to the home (FTTH) or more generally FTTx (x can be H for home, B for building, and C for curb), has consequently undergone a rapid mass deployment.

Passive optical network (PON) is an attractive solution for realizing FTTH, since the cost maintenance is lowered and simplified because the absence of active components. In Fig. 1.3 the point-to-point and point-to-multipoint architectures are shown.

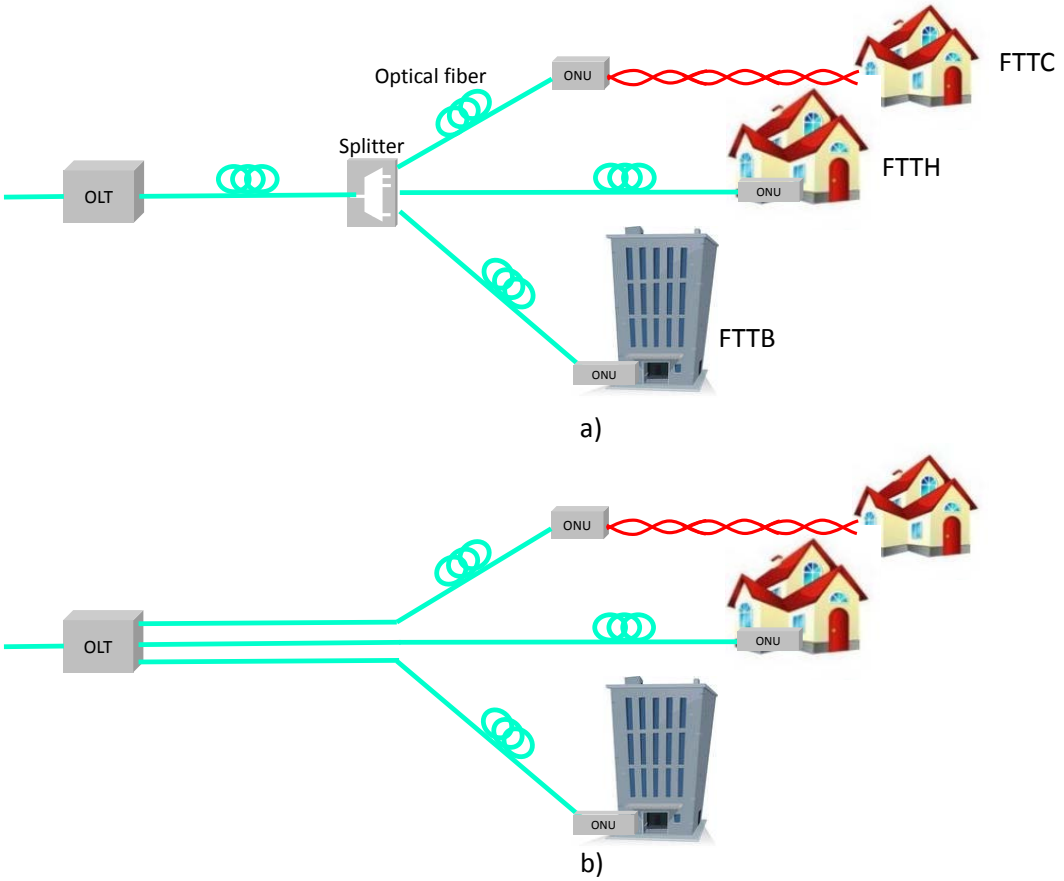

Figure 1.3: a) Point-to-multipoint PON. b) Point-to-point PON.

The point-to-multipoint configuration shown in Fig. 1.3(a) employs a power splitter to distribute the signal from the optical line terminal (OLT) to users at different optical network units (ONUs). Another type of PON called WDM-PON uses a wavelength multiplexer as

the remote distribution node. Table 1.1 summarizes the current different standardized PON technologies [21].

It is also worth to remark the interest on a new type of optical access network, the so-called long-reach passive optical network (LR-PONs) [22–24]. LR-PON aims to simplify the telecommunication network by integrating access networks with metro networks and extend the coverage span of PONs from the traditional range 20km to 100km and beyond by exploiting optical amplifier and wavelength-division multiplexing technologies.

Capital cost and operational expenses for deployment of optical access as "future-proof" solution are the main concern for operators. Some of the desired features for a highly scalable new generation PON are [25, 26]:

- High splitting ratio, long reach and speed.
- Tolerance to low-cost opto-electronic components.
- Higher spectral efficiency and more robustness to fibre dispersion compared to conventional techniques used in current PONs.
- Passive.
- Simple upgradeability.
- Centralized management.
- Dynamic resource allocation.
- Compatibility with the already deployed PON infrastructures.

As indicated in Table 1.1, 10G-PON standard defines a maximum transmission capacity of 10Gb/s. This speed is achieved by employing conventional signal modulation schemes, which are now reaching the limit where further increasing transmission capacity whilst maintaining cost-effectiveness is highly challenging. Requirements for future PON impose heavy restrictions on optical transceiver designs in terms of available bandwidth, scalability requirements, ONU simplicity and dynamic bandwidth allocation capacity. DSP-enabled advanced modulation and multiplexing approaches are a reasonable way to increase data rate to 20-40Gbits/s and beyond [27].

1.1.4 OOFDM in optical access networks. State of the art

As we will see in Chapter 2, OOFDM has been proposed for a myriad of optical communication scenarios, with diverse architectures. In the context of optical access networks, intensity-modulated and direct-detection is an attractive alternative due mainly to its low-cost and reduced complexity. In this subsection we outline some of the works which have been published in the last years on IM/DD OOFDM systems, although we must remark that coherent detection is attracting more interest as the time even for its application in optical access networks [28].

Bangor University's optical communications research group has extensively contributed to the work on OOFDM transceivers, being the first research group on demonstrating a real-time operation of an OOFDM system at Gbits/s. For these reasons, we remark some of

Table 1.1: Standardized PON technologies

Technology	Standard	Data rate
Gigabit-PON	ITU-T G.984	2.5Gbits/s downstream 1.25Gbits/s upstream
10G-PON	ITU-T G.987	10Gbits/s downstream 2.5Gbits/s upstream
Ethernet-PON	IEEE 802.3ah	1Gbits/s symmetric
10G-EPON	IEEE 802.3av	10Gbits/s downstream 1Gbits/s upstream[†] 10Gbits/s upstream

[†] Co-existence with EPON

their most important achievements in Table 1.2. The systems were tested with SMF and multi-mode fiber (MMF), and with several intensity modulators: distributed-feedback laser (DFB), reflective semiconductor optical amplifier (RSOA), electro-absorption modulated laser (EML), electro-absorption modulator (REAM), and vertical-cavity surface emitting laser (VCSEL) [29–37].

Table 1.2: Real-time transceivers OOFDM achievements of Bangor University

Modulator	Fiber	Single-band Multi-band	Bit rate	Reach
DFB	MMF	Single-band	1.5Gbits/s	500m
DFB	MMF	Single-band	3Gbits/s	500m
DFB	MMF	Single-band	6Gbits/s	300m
RSOA	SMF	Single-band	7.5Gbits/s	25km
DFB	MMF	Single-band	11.25Gbits/s	500
VCSEL	SMF	Single-band	11.25Gbits/s	25km
EML	SMF	Multi-band	19.25Gbits/s	25km
REAM	SMF	Multi-band	19.25Gbits/s	25km
EML	MMF	Multi-band	25.25Gbits/s	300m

Since the results were achieved in a real-time system implemented using field-programmable gate array technology, much attention in these works was paid to implementation issues. An excellent report of the progress achieved during the past recent years is found in [38]. Recently, other groups [39, 40] have also demonstrated a real-time operation of an OOFDM system targeted at PON applications, whilst the great majority of literature with experimental results on OOFDM has been achieved through off-line processing.

There has been also an increasing interest on using DSP technique for the mitigation of nonlinearities in directly modulated/detected (DM/DD) OOFDM systems. For example, in

[41] an iterative equalization to mitigate the distortion at the receiver without the knowledge of the transmitted data is proposed, achieving a reach extension from 10km to 100km with a DML 30-Gbps OFDM signal. In [42] a similar but improved iterative equalization technique is employed to demonstrate a 32.25-Gbits/s OOFDM system over 100km using an EAM as intensity modulator. These works are based on a previously published work [43] which reported a small-signal analysis of DM/DD OOFDM systems, whose theory was used to reconstruct the nonlinear distortion at the receiver.

NEC laboratories research group proposed in 2007 the so-called OFDMA technique to share the same feeder optical fiber among the multiple ONUs in a PON [44]. Recent advances of NEC laboratories have demonstrated an OFDMA-PON with a downstream signal line bit rate 40Gbits/s using external intensity modulation and, by introducing polarization multiplexing with direct detection in conjunction with novel 4×4 multiple-input multiple-output (MIMO) DSP equalization, allowed them to achieve a record 108 Gbits/s downstream OFDMA-PON transmission [45]. In [46] they demonstrate the feasibility of a WDM-OFDMA-PON to support a total capacity in the order of Tbits/s over 90km SMF and a 1:32 passive split; worthy to mention that OLT receiver employs coherent detection in order to avoid signal $\times$ signal beat interference as result of the upstream transmission by the different ONUs.

These works represent a very small sample of the work done in OOFDM systems for short/medium reach. For example, OFDM radio-over-fiber systems have been also focus of research [47, 48], or the employment of OOFDM for in-building networks [49]. Externally-field modulated OODFM signals have been proposed for medium reach in [50, 51]. And many other OOFDM systems for its application in PONs have been proposed [52–54].

In this context, part of the work developed in the present Ph.D. Thesis has been realized under the framework of the European FP7 ALPHA project (Architectures for fLexible Photonic Home and Access networks), grant agreement no.: 212 352, which main goal was the development of innovative architectural and transmission solutions for access and in-building integrated multi-service Internet/Intranet and 3G/B3G networks with adequate management and control. This project, with a duration of 39 months since January 1st 2008, was coordinated by ACREO AB (Sweden) and integrated by the following European institutions: the Universitat Politècnica de València, Interdisciplinair Instituut Voor Breedbandtechnologie vzw, Danish University of Technology, Homefibre Digital Network GmbH, 3S Photonics and Telekomunikacja Polska R&D. st, France Telecom R&D, Alcatel-Lucent Bell Labs France, CommScope Italy Srl, University of Bologna, Telefonica I+D, Technical University of Eindhoven, Telsey S.p.A., Bangor University, Politechnico di Torino, Luceat S.p.A.

The rest of work was developed under the framework of national project “NEW generation optical OFDM transmission Techniques for future WDM-PONs" (NEWTON/TEC2011-26642) granted by the Ministerio de Economía y Competitividad since 1st Jan, 2012 until now, which main goals are to investigate and develop further potentialities of OOFDM signal transmission.

1.2 Objectives

The global objective of this Ph.D. Thesis is to develop a model to understand and describe DM/DD OOFDM transmission systems, aimed to explore the potentiality of these systems, overcome the main limitations and optimize the conditions to obtain the highest performance in terms of transmission capacity and maximum achievable reach link. Some of the essential partial objectives for the accomplishment of this global goal are:

- To carry out a theoretical analysis to study the main transmission effects in DM/DD systems with regard the performance of the received OOFDM signals. Due to the sensibility of OFDM signals to nonlinearities, such theoretical analysis must go beyond the description provided by an analysis based on a small-signal approximation aimed to describe only linear effects and provide an accurate description also of the nonlinear distortion of the transmission system: namely, laser nonlinearities, propagation of the chirped OOFDM signal through the dispersive optical fiber and the final optical intensity detection.

- To check the validity of the proposed theoretical analysis by comparing it with simulation results provided by commercial software (in particular, Matlab® and VPI-transmission-Maker®) and explore its feasibility to describe DM/DD OOFDM in variant operating conditions.

- The development of a relatively straightforward software tool for the comprehensive evaluation of DM/DD OOFDM systems. Those who have had the opportunity to work with OFDM signals know its powerful features, but also how complicated the influence of its manifold determining system parameters is and, thus, how interesting a tool for the systematic and separately evaluation of the influence of each of these parameters is. Due to its importance on the design of OOFDM systems, the influence of two system parameters such as the clipping level and the length of cyclic extensions must be included in the derivation.

- The proposal of a DSP technique to improve the system performance of a DM/DD OOFDM system beyond to that offered by a conventional one. As commented in Section 1.1, an important advance on optical communication systems has been the application of DSP techniques to optical communication systems. Besides, all of them, to a large extent, are based on a deep knowledge of the communication system effects on the received signals. We pretend to take advantage of the theoretical derivation previously presented, and, particularly, of the simplified analytical model of the nonlinear distortion, to implement and test a DSP technique to allow the increase of the transmission information rate of OOFDM signals.

- The provision of an end-to-end analytical model of optically filtered DM/DD OOFDM systems in order to grasp the foundations of its operation and find out its potentiality and limitations, as well as the rapid evaluation of the achieved system performance with different optical filters. All-optical signal processing techniques are destined to play an important role in the system performance improvement of optical communication systems. The employment of optical filtering techniques in DM/DD systems for its system performance increase has been proposed for traditional intensity modulation formats during the last years; although it has also been studied recently for OOFDM systems, there is a lack of understanding on its foundation, potentiality and limitations.

Although this Ph.D. Thesis focuses on optical communication systems with short/medium reach links with direct modulation/detection, it has been our goal to address the presented objectives in a broad and accurate way in order to make our contribution easily usable to other optical scenarios with different transmission/detection architectures.

1.3 Thesis Structure

This Ph.D. Thesis comprises seven chapters. In this first chapter we have presented the context in which this work has been carried out, as well as the objectives pursued. Chapter 2 presents the basics of the OFDM technique in order to facilitate its understanding: we start by explaining the generation of OFDM signal waveforms, how this technique takes advantage of the division of the available bandwidth into multiple frequency bins to allocate the OFDM subcarriers, the principle of orthogonality between overlapping subcarriers and its detection at the transmitter in order to extract the data information. Then, its implementation based on efficient DSP algorithms is explained, together with important concepts such as cyclic pre- and post-fixes, clipping of the generated signal, power and bit loading techniques, as well as how linear effects affect the received signal and its easy equalization at the receiver. The different OOFDM optical communication system architectures proposed in the last years are also briefly discussed, with an emphasis on directly modulated/detected configurations.

Chapter 3 presents the analytical formulation used to mathematically understand and characterize DM/DD OOFDM systems. Concretely, the analysis starts by deriving a mathematical expression of the optical signal at the output of the directly modulated laser (DML), accounting for the linear and nonlinear effects of the direct modulation. Effects of the optical fiber are limited to those due to second order chromatic dispersion, and the operation of a p-i-n photodiode is modeled by an square-law detector. The results obtained through the evaluation of the analytical model and those obtained through simulations using commercial software are compared.

Chapter 4 extends and simplify the theory presented in Chapter 3. The aim of extending the previously presented theory is to include the effects of important design OOFDM parameters and explore the potentiality of DM/DD OOFDM systems in a comprehensive and quick manner. To this respect, we explain how to determine the effects of clipping by calculating the power spectral density of the clipping noise, and we propose its refinement by taking into account the impulsive nature of the clipping process; besides, the effects of inter-symbol interference (ISI) and inter-carrier interference (ICI) also included in the analytical model, and simplified expressions of the nonlinear distortion are derived. With the help of this simplified analytical model, we explore the potentiality of DM/DD OOFDM systems and investigate the inter-related effects on the system performance of some of the main design system parameters.

In Chapter 5 we propose a novel pre-distortion technique for the mitigation of the nonlinear distortion present in DM/DD systems. The proposed technique is based on the reconstruction of the interference terms following the analytical model reported in the previous chapter. In order to perform such interference reconstruction, our proposal also includes a simple feedback mechanism for the identification of essential magnitudes such as the transfer function of the laser intensity modulation. The potentiality of the proposed technique is studied and the performance obtained is compared with that provided by a conventional DM/DD OOFDM system.

The insertion of an optical filter in the optical link of an DM/DD OOFDM system is analytically studied in Chapter 6. The first part of this chapter can be considered to be an extension of the theory presented in Chapter 3 and the effects of the optical filtering are included in a straight manner in the analytical model. Similarly to that done in Chapter 4, in order to account for the nonlinear distortion in this new optical scenario, simplified expressions of the nonlinear distortion are derived in order to perform quick evaluations of its effects. Power budget improvements obtained with different optical filters are quantified and characteristic parameters of Mach-Zehnder and uniform fiber Bragg grating based optical filters are optimized in order to obtain an optimized working operation. To finish this chapter, the underlying operation of such technique as well as its limitations are discussed.

Finally, in Chapter 7 we summarize the main conclusion of this work and outline possible futures lines of work.

Further mathematical details on the derivations are included in Appendixes A, B, C and D.

Chapter 2

Fundamentals of (O)OFDM

2.1 Introduction

Orthogonal-frequency division multiplexing is a multicarrier multiplexing technique, which means that the data information is carried over a set of lower rate subcarriers. Its robustness to channel delay spread and its ease of channel estimation and compensation of linear channel effects in time-varying environments has made of it a popular technique.

The concept of OFDM was already suggested in the 1960s, but it has been necessary the development of very large-scale integrated (VLSI) CMOS chips for the beginning of its broad usage, and OFDM is currently employed in a great variety of guided and RF communications scenarios. Among the important standards that incorporate OFDM modulation technology are the European digital video broadcasting (DVB), wireless local area networks (Wi-Fi, IEEE 802.11a/g), wireless metropolitan area networks (WiMAX; 802.16e), asymmetric digital subscriber line (ADSL; ITU G.992.1), and the fourth-generation mobile communications system (long-term evolution)[1].

This chapter is structured as follows: firstly, the mathematical basis behind OFDM as well as a description of a typical OFDM system are explained; important concepts related to OFDM such as the cyclic extensions appended to each OFDM symbol, the peak-to-average power ratio (PAPR) of OFDM signals and the fine granularity at a subcarrier level OFDM offers us. Finally, we discuss briefly the application of OFDM in optical communications.

2.2 Orthogonal Frequency Division Multiplexing Basics

2.2.1 OFDM Signal Waveform

The driving principle of OFDM technology is rather simple: one OFDM symbol is composed of a set of subcarriers, and each of them is modulated by an information symbol with its corresponding quadrature and in-phase component. This is very similar to subcarrier multiplexing (SCM) technique, except that subcarriers in OFDM overlap as it is described below to maximize the spectral efficiency.

Mathematically, the definition of orthogonality between two symbols $A_n(t)$ and $A_m(t)$ (which are basically functions defined in a time interval $0 \leq t \leq T$) is

$$\frac{1}{T}\int_0^T A_n(t)\cdot A_m^*(t)dt = 0 \text{ if } m \neq n \tag{2.1}$$

In the particular case of OFDM, we have:

$$A_n(t) = \begin{cases} exp\big(j\Omega_n t\big), & 0 \leq t < T \\ 0, & \text{otherwise} \end{cases} \tag{2.2}$$

and substituing in Eq. (2.1):

$$\begin{aligned} &\frac{1}{T}\int_0^T exp\big(j\Omega_n t\big)\cdot exp\big(-j\Omega_m t\big)dt = \\ &\frac{1}{T}\int_0^T exp\big(j2\pi\frac{n}{T}t\big)\cdot exp\big(-2\pi\frac{m}{T}t\big)dt = \begin{cases} 0, & \text{if } m \neq n \\ 1, & \text{if } m = n \end{cases} \end{aligned} \tag{2.3}$$

Therefore, the defining condition in OFDM to ensure orthogonality is that the spacing frequency between adjacent subcarriers is equal to the period of integration T. This orthogonality between subcarriers allows a more efficient employment of the available bandwidth for transmission, since the spectrum of the subcarriers are allowed to overlap, but the information is not corrupted provided that the orthogonality between subcarriers is maintained.

The low-pass equivalent representation of the OFDM signal is then given by the sum of a certain number of these fundamental waveforms:

$$s_B(t) = \sum_{i=-\infty}^{\infty}\sum_{k=-N/2}^{N/2-1} X_{i,k}\cdot rect\Big(\frac{t-T/2-iT}{T}\Big)\cdot exp\Big(\Omega_k\cdot\big(t-iT\big)\Big) \tag{2.4}$$

where $X_{i,k}$ is the encoded data symbol at the kth subcarrier of the ith OFDM symbol, N is the number of subcarriers, T is the OFDM symbol duration and $rect(\frac{t-T/2-iT}{T})$ is the rectangular function centered at $T/2+iT$ and with duration T. By applying that the Discrete Fourier Transform (DFT) of the rectangular function $rect(\frac{t}{T})$ is a *sinc* function, some DFT properties and using the fact that the crosscorrelation between $X_{i,m}$ and $X_{i,n}$ is

$$\langle X_{i,m}\cdot X_{j,n}^*\rangle = \begin{cases} 0, \text{ for } i \neq j \text{ or } m \neq n \\ \sigma_x^2, \text{ for } i = j \text{ and } m = n \end{cases} \tag{2.5}$$

the power spectral density of the OFDM signal can be expressed as [55]:

$$P_s(\Omega) = \frac{\sigma_x^2}{T} \sum_{k=-N/2}^{N/2-1} \frac{1}{2\pi} \cdot T^2 sinc^2(\Omega - k \cdot \Delta\Omega) \tag{2.6}$$

where $sinc(x) = sin(\pi \cdot x)/(\pi \cdot x)$ and $\Delta\Omega = 2\pi \cdot 1/T$. A plot of Eq. (2.6) is shown in Fig. 2.1.

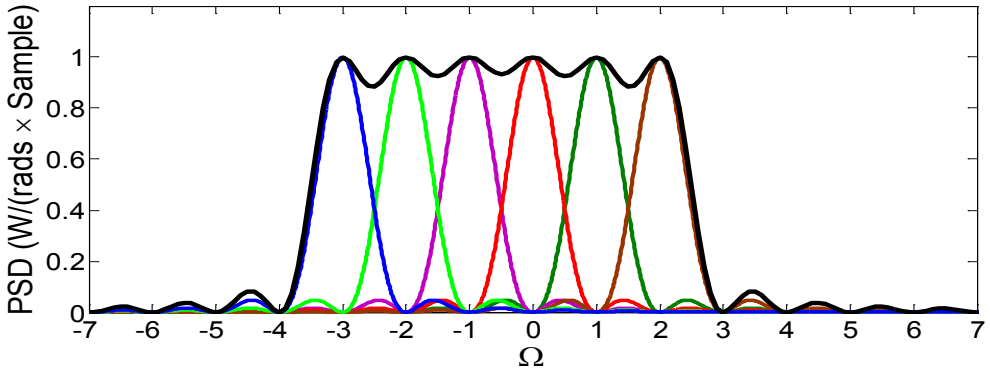

Figure 2.1: Power spectral density (PSD) of an OFDM signal with $N = 7$, $\sigma_x^2 = 1$ and $T = 1$ (black line).

We note in Fig. 2.1 that the OFDM spectrum has a nearly rectangular shape and the signal power is smoothly spread over the used bandwidth (similar to white noise), which is one of the advantages of OFDM. If we use the null-to-null bandwidth definition, the OFDM signal's bandwidth is equal to:

$$B_{OFDM} = (N+1) \cdot \Delta\Omega = 2\pi \frac{(N+1)}{T} \tag{2.7}$$

2.2.2 Description of a typical OFDM System

The direct generation and detection of N RF tones by using oscillators becomes unfeasible when N increases to values of tens or hundreds. Luckily, the Inverse Discrete Fourier Transform (IDFT) makes possible the generation of multi-tone signals, and the Inverse Fast Fourier Transform (IFFT) algorithm provides an efficient implementation of it; meanwhile, the Discrete Fourier Transform (DFT), through its Fast Fourier transform (FFT) implementation, offers an efficient way to perform the detection operation, taking advantage of the orthogonality given by Eq. (2.3). In Fig. 2.2 we show an OFDM system which employs the IFFT and the FFT operations at the transmitter and at the receiver, respectively:

Firstly, a fragment of the information binary data stream is converted into a set of information symbols. These information symbols may belong to any type of modulation, such as differential phase shift keying (DPSK), M-phase shift keying (M-PSK) or M-quadrature amplitude modulation (M-QAM). The input at the IFFT processor is a vector of values denoted as ($X_{-FS/2}$, $X_{-FS/2+1}$,..., $X_{FS/2-1}$), where FS is the IFFT size, and the discrete output is given by:

$$x[m] = \sum_{k=-FS/2}^{FS/2-1} X_k \cdot exp\Big(j \cdot 2\pi \cdot k \cdot \frac{m}{FS}\Big), m = 0, 1, 2, ..., FS - 1. \tag{2.8}$$

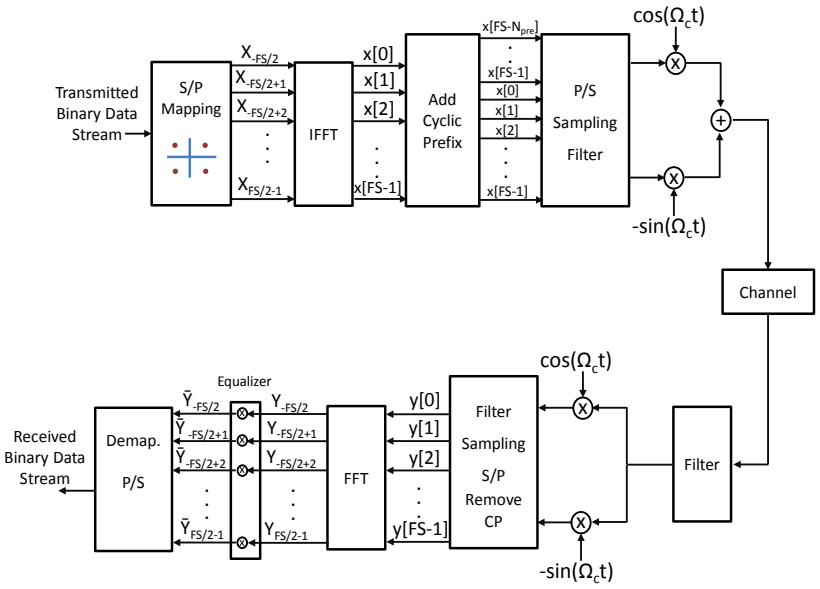

Figure 2.2: Schematic illustration of an OFDM system

Therefore, the m-th sample of an OFDM symbol is given by the sum of FS complex exponential functions. For the sake of clarity, the binary information to complex symbols mapping as well as the IFFT operation is schematically illustrated in Fig. 2.3. The two

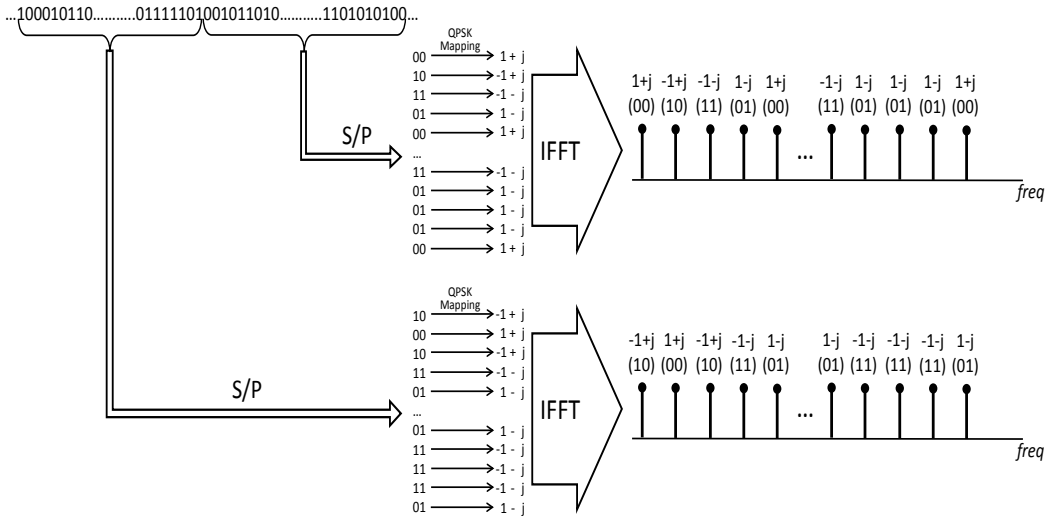

Figure 2.3: Binary information to QPSK complex symbols mapping and IFFT operation.

OFDM symbols shown in Fig. 2.3 are transmitted subsequently through the communication system after being conveniently physically adapted, which requires its conversion to an analog signal. With a digital-to-analog converter (DAC) working at a sampling rate equal to f_{sam}, the Nyquist frequency is equal to $f_{sam}/2$. OFDM provides an easy way to carry out oversampling just by not using the whole spectral content from $-f_{sam}/2$ to $f_{sam}/2$, that is, setting to zero a determined number of subcarriers at those frequencies closer to the Nyquist frequency. Generally, the sampling rate is designed so that $f_{sam} = FS/T$. The oversampling

facilitates the analog filtering requirements at the transmitter and receiver. Fig. 2.4 shows a typical symbol/subcarrier arrangement for the sake of clarity.

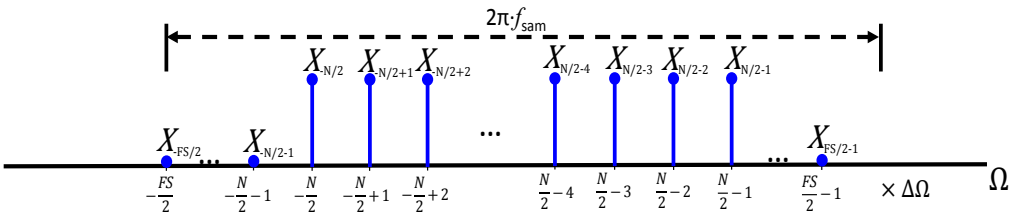

Figure 2.4: Data symbols/subcarrier arrangement.

After DAC, the signal must be frequency up-converted in order to transmit its in-phase and quadrature components. The generated analog signal at an OFDM transmitter with up-conversion at a frequency Ω_c has typically the next expression:

$$s(t) = Re\left\{ \sum_{i=-\infty}^{\infty} \sum_{k=-N/2}^{N/2-1} X_k \cdot exp\Big(\Omega_k\big(t-iT\big)\Big) * h_{trx}(t) \cdot exp\Big(\Omega_c \cdot \big(t-iT\big)\Big) \right\} \tag{2.9}$$

where $Re\{\cdot\}$ stands for the real part of a complex quantity and $h_{trx}(t)$ is the impulse response of the transmitter filter.

If one is interested on not using a frequency up-conversion stage for hardware simplicity, $x[m]$ can be forced to be a discrete real-valued signal by imposing the Hermitian symmetry on the information symbols at the input of the IFFT:

$$\begin{aligned} X_0 &= X_{-FS/2} = 0 \\ X_k &= X^*_{-k}, k = 1, 2, ...FS/2 - 1 \end{aligned} \tag{2.10}$$

Then, the analog OFDM symbol may be expressed as:

$$s(t) = \sum_{k=1}^{N} |X_k| \cdot cos\big(\Omega_k \cdot t + \varphi_{X_k}\big) * h_{trx}(t), 0 \leq t < T \tag{2.11}$$

where N is still the number of subcarriers with information, having set the rest of subcarriers to zero. This variant of OFDM is sometimes called discrete multi-tone (DMT) [56].

After passing through the channel, with impulse response $h_{channel}(t)$, the received signal is then frequency down-converted and passed through an analog-to-digital converter (ADC), to generate the discrete received OFDM symbol:

$$y[m] = \sum_{k=-FS/2}^{FS/2-1} X_k \cdot exp\Big(j \cdot 2\pi \cdot k \cdot \frac{m}{FS}\Big) * h[m], 0 \leq m \leq FS - 1 \tag{2.12}$$

where $h[m] = h_{trx}[m] * h_{channel}[m] * h_{rx}[m]$, being $h_{rx}[m]$ the sampled impulse response of the electronic filters at the receiver. The information symbols contained in the signal $r[m]$ can finally be recovered as in Eq. (2.3) by calculating its FFT:

$$Y[r] = \sum_{m=-FS/2}^{FS/2-1} y[m] \cdot exp\Big(-j \cdot 2\pi \cdot m \cdot \frac{r}{FS}\Big), r = -FS/2, -FS/2+1, 2, ..., FS/2-1 \tag{2.13}$$

In the next subsection we see how the linear effects of the whole communication system affect the received symbols $Y[1], ...Y[N]$.

2.2.2.1 Cyclic extension

In [57] it was proposed the use of a cyclic extension with a sufficient length in order to make the transmitted "sequence ... appear periodic to" the communication channel. In Fig. 2.5(a) we show the appending of a cyclic prefix of length N_{pre} samples, and Fig. 2.5(b) we show the same operation, but with both pre- and post-fix extensions.

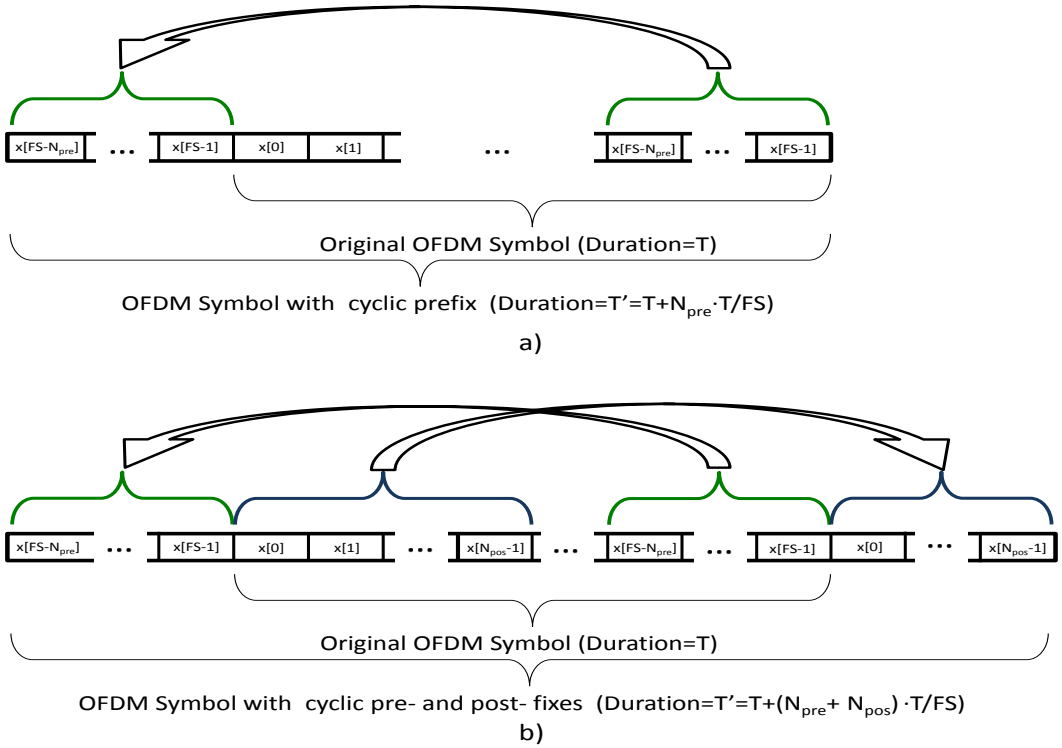

Figure 2.5: Time domain OFDM symbol showing the appending of cyclic extensions.

Cyclic prefix involves the extension of the transmitted OFDM symbol $[x[0], x[1] ..., x[FS-1]]$ by N_{pre} samples. Since each sample represents a sample period equals to T/FS, the appending of N_{pre} extra samples results in a new OFDM symbol with duration $T' = T + N_{pre} \cdot T/FS$. For two-sided channel impulses responses, the actual received OFDM symbol is affected by the previous and the next OFDM symbol, and we must append both a pre- and a post-fix. In this last case, the resulting symbol duration is equal to $T' = T + (N_{pre} + N_{pos}) \cdot T/FS$.

The goal of the cyclic extensions is to avoid inter-symbol interference (ISI) due to multi-path effect or frequency dispersion. Provided that the length of the cyclic prefix is sufficiently long, the corrupted samples due to ISI are discarded at the receiver-end side. Besides, with a proper value of cyclic extension length(s), the transmitted sequence appears to be periodic

to the channel and the linear convolution in Eq. (2.12) mimics a circular convolution:

$$y[m] = x[m] \circledast h[m], 0 \leq m \leq FS - 1 \tag{2.14}$$

where $\circledast$ denotes circular convolution. Thus, given the properties of the DFT, we can write:

$$Y[r] = X[r] \cdot H[r], r = -FS/2, -FS/2 + 1, 2, ..., FS/2 - 1 \tag{2.15}$$

This equation represents one of the main advantages of OFDM, since it indicates that linear channel effects can be equalized once we know the coefficients of the system transfer function $H[r], r = -FS/2, -FS/2 + 1, 2, ..., FS/2 - 1$. By designing a correct training strategy, we can obtain an estimation of the transfer function coefficients, $\hat{H}[r], r = -FS/2, -FS/2 + 1, 2, ..., FS/2 - 1$, and the equalized symbols are given by:

$$\begin{aligned} \hat{Y}[r] &= X[r] \cdot H[r] \cdot \frac{1}{\hat{H}[r]} = \{\hat{H}[r] = H[r]\} \\ &= X[r], r = -FS/2, -FS/2 + 1, 2, ..., FS/2 - 1 \end{aligned} \tag{2.16}$$

However, the addition of cyclic extensions means the transmission of redundant information, and thus a waste of information transmission rate, given by:

$$R(bits/s) = \frac{No.\ bits/OFDM\ symbol}{Total\ OFDM\ symbol\ duration}$$

$$= \begin{cases} \dfrac{log_2(M) \cdot N}{T/FS \cdot (FS + N_{pre})}, & \text{with pre-fix} \quad (2.17) \\ \dfrac{log_2(M) \cdot N}{T/FS \cdot (FS + N_{pre} + N_{pos})}, & \text{with pre- and post-fix} \quad (2.18) \end{cases}$$

where M stands for the constellation size of the QAM format used. The length of the cyclic extension is under a trade-off between robustness to interference due to filtering effects and the achieved transmission information rate.

2.2.2.2 Peak-to-Average Power Ratio and Clipping

PAPR is considered by literature the most important drawback of OFDM [58]. From previous section, we know that each discrete signal value at the IFFT output is the result of a random sum of N exponential functions, each one with its corresponding amplitude and phase, determined by its corresponding information complex symbol. The distribution of the amplitude may then be approximated by a Gaussian distribution, in which the tails represent the relative small propability that a high amplitude peak occurs, and values around the mean (zero) represent the most likely amplitude values. For illustration, Fig. 2.6 shows a numerically generated discrete real value signal $x[m]$ and the associated amplitude distribution.

The PAPR, in the discrete domain, is defined as:

$$PAPR = \frac{max_m\{|x[m]|^2\}}{\langle |x[m]|^2 \rangle}, m \in \mathbb{Z} \tag{2.19}$$

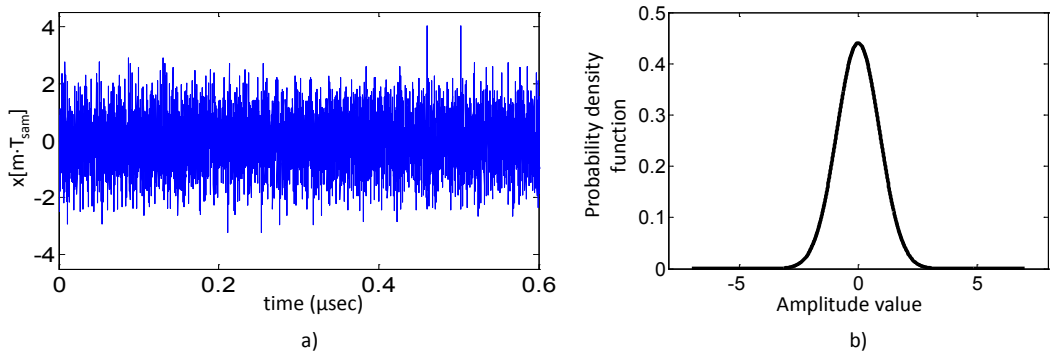

Figure 2.6: a) Real-valued discrete OFDM signal and b) amplitude probability density function

where $max_m\{|x[m]|^2\}$ is the maximum peak value squared of the signal $x[m]$ and $\langle|x[m]|^2\rangle$ is the average signal power. A high value of PAPR is undesirable, since it determines the dynamic range of electronic components such as DAC or amplifiers, and optical components such as DMLs or external modulators. As numerical example, a PAPR of 10 dB means that for the transmission of 2mW, the transmitter should be able to handle peaks of 20mW.

Hard clipping is a simple technique to limit the excursion of the OFDM signal by doing:

$$x[m] = \begin{cases} x[m], \text{ if } |x[m]| < A_{Clip} \\ A{\cdot}exp(j{\cdot}\varphi_{x[m]}), \text{ otherwise} \end{cases} \tag{2.20}$$

where the value of A_{Clip} is an important system parameter in optical OOFDM systems: the smaller its value, the smaller the amplitude excursion of the electrical OFDM signal, and therefore less stringent conditions on the design of electronics in the transceiver and higher optical modulation efficiency, but the higher the distortion introduced by such nonlinear operation.

A_{Clip} is usually given in relation to the clipping level, define as:

$$CL = \frac{A_{Clip}^2}{\langle|x[m]|^2\rangle} \tag{2.21}$$

The optimum value for the clipping level depends on several system parameters, such as digital-to-analog conversion resolution, the desired system bit-error-rate (BER) or the modulation format employed [59–61].

2.2.2.3 Subcarrier granularity

The generation and detection of OFDM signals transform the whole frequency transmission channel into a joint of N narrowband parallel channels. This division into multiple channels reports significant advantages, such as channel adaptability and differentiated service provisioning.

If one works under the hypothesis that a feedback link from the receiver to the transmitter is feasible, the transmitter can adapt the information transmission conditions to those present in the channel. Power or bit loading, as well as the combination of both are efficient strategies

to realize this adaptation [1]. The signal-to-noise ratio (SNR) in Fig. 2.7 is the figure of merit used to illustrate the concept of power allocation and bit loading techniques.

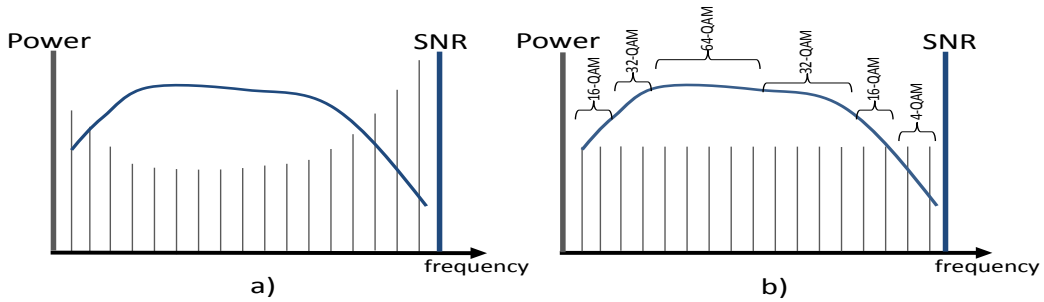

Figure 2.7: a) Power loading and b) bit loading techniques

Power loading allows the optimization of information transmission according to the water-filling principle by increasing (decreasing) the power of each subcarrier as the channel transmission characteristics are worse (better); similarly for bit loading, in which the constellation size of the modulation format employed on each subcarrier is varied as the channel transmission characteristics. Note that when bit loading is used, the transmission information rate changes:

$$R(bits/s) = \frac{No.\ bits/OFDM\ symbol}{Total\ OFDM\ symbol\ duration}$$

$$= \begin{cases} \dfrac{\sum_{k=1}^{N} log_2(M[k])}{T/FS \cdot (FS + N_{pre})}, & \text{with pre-fix} \quad (2.22) \\ \dfrac{\sum_{k=1}^{N} log_2(M[k])}{T/FS \cdot (FS + N_{pre} + N_{pos})}, & \text{with pre- and post-fix} \quad (2.23) \end{cases}$$

where $M[k]$ stands for the constellation size of the QAM format used at the kth subcarrier.

On the other hand, the availability of multiple and independent channels make possible the simultaneous provision of different services to the same user and the coexistence of several users by sharing the available number of subcarriers, access technique referred as OFDM-Access (OFDMA) [58]. Provided that proper signaling information for the delivery and reception of the composing OFDM signal subcarriers, the subcarriers can play as information tubes and provide virtual point-to-point connections.

2.3 Application to Optical Communications

Traditionally time-division multiplexing based schemes (Fig. 2.8(a)) employed in optical communications become more and more challenging as the transmission rate increases: its non-rate-scalability nature forces to the employment of shorter pulses as the transmission rate increases, with its consequent narrower receiver time window and wider optical bandwidths, making necessary precisely engineering dispersion compensation [62]. Alternatively, OOFDM makes a more efficient usage of the optical spectrum and performs a parallel transmission of lower rates channels/subcarriers (Fig. 2.8(b)).

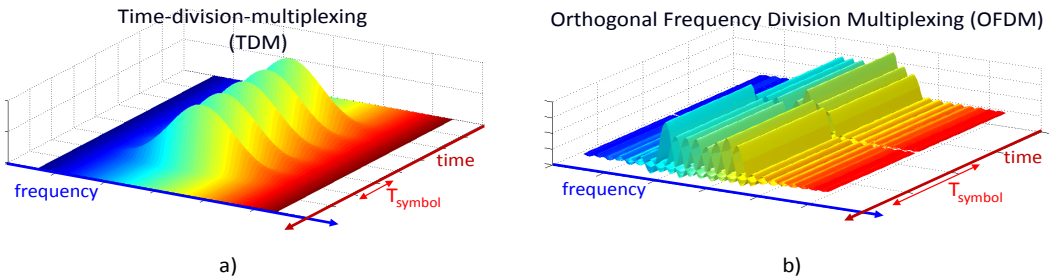

Figure 2.8: Comparison of multiplexing schemes.

The main concept behind OFDM such as the bandwidth division into orthogonal channels has become very popular and has found its room into multiple optical scenarios with different variants. Fig. 2.9 aims to show an overview of the different variants of optical communication systems

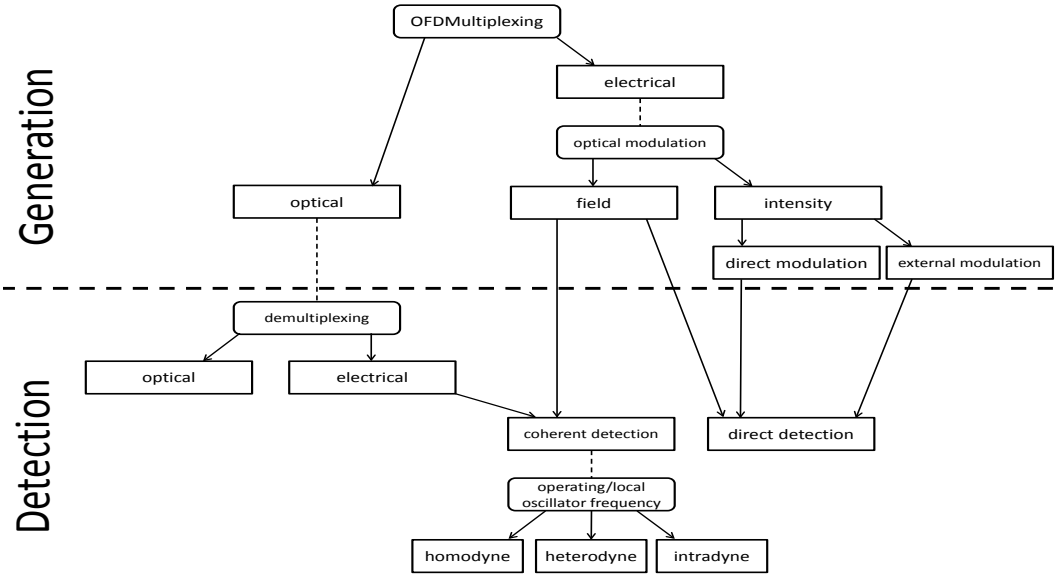

Figure 2.9: Overview of OOFDM schemes.

The first level of decision in Fig. 2.9 appears when one must decide how the different orthogonal channels are multiplexed and demultiplexed. An optical implementation of the multiplexing and demultiplexing stages of an OOFDM system is advantageous in terms of power consumption [63] compared to the electrical implementation. The multiplexing is essentially accomplished by combining the different orthogonal channels, and it is the demultiplexing stage where attention has focused: the overlapping spectra contents of the different channels must be separated with no-crosstalk. The FFT operation required for such requirement has been realized using concatenated delay-interferometers [62] or modified designs of arrayed-waveguide grating routers [64]. Electrically demultiplexing of optically-multiplexed OFDM signals after coherent detection is also an alternative [62].

On the other hand, an electrical implementation employs much more mature technology for the processing of the signals as well as more widely studied techniques for the handling of the optical signals. We explain next the different electrically generated schemes shown in Fig. 2.9, emphasizing directly-modulated/detected systems, optical communication scheme with which we deal in next chapters.

2.3.1 Directly-modulated/detected systems

In DM/DD systems, the electrically generated information signal drives the intensity of a laser source. The semiconductor laser is composed of n-type and p-type basic materials that form a p-n juncture as shown in Fig. 2.10(a). When a sufficiently high value of forward

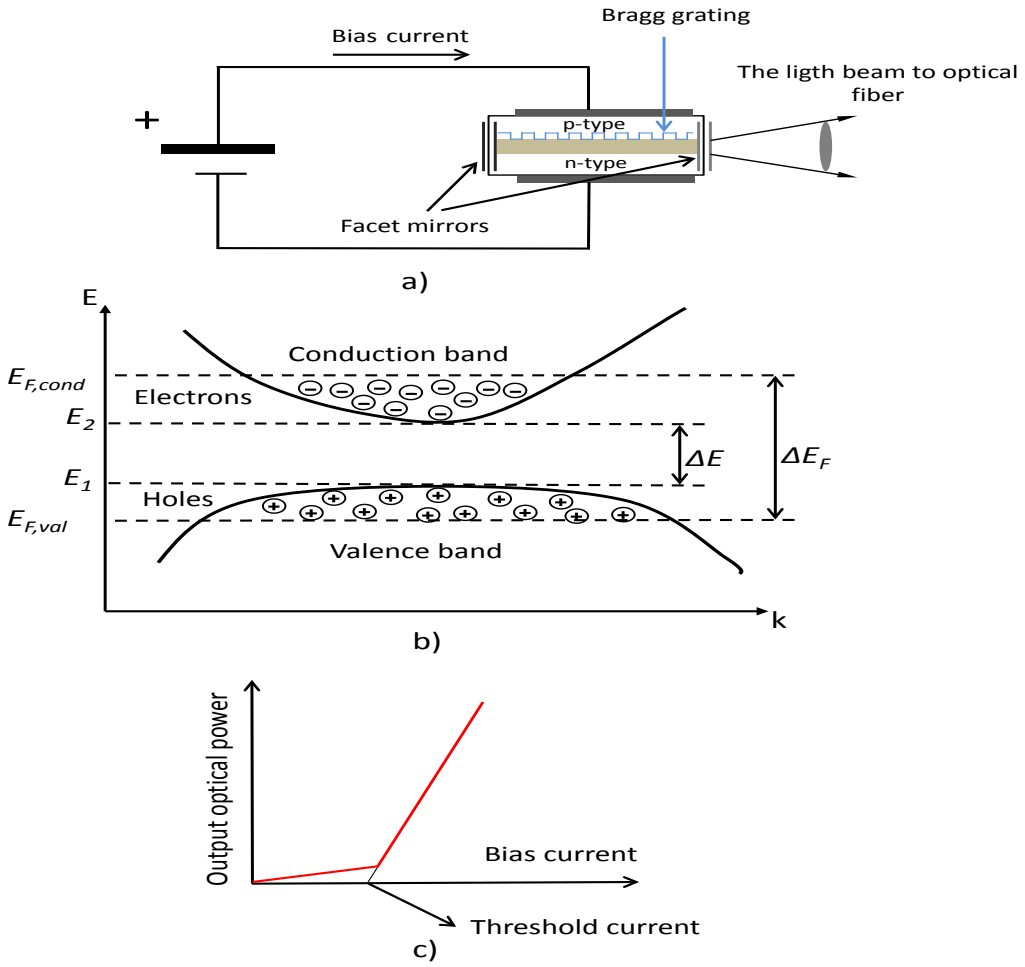

Figure 2.10: a) Basic structure of a distributed-feedback laser, b) energy diagram and population inversion in semiconductors, and c) output optical power versus bias current curve.

bias is applied to the structure, inversion population occurs and the population of electrons corresponding to the energy level E_2 is higher than that to the energy level E_1. The condition for inversion population such that the rate of stimulated emission is higher than that of spontaneous emission is that the difference of energy of the quasi-Fermi levels, $E_{F,cond} -$

$E_{F,val}$, must be higher than the energy difference $E_2 - E_1$, as illustrated in Fig. 2.10(b). The electrons in the conduction band can potentially recombine with the holes in the valence band in a radiative process, resulting, thus, in the generation of photons. The generated light in the cavity make multiple paths between the facet mirrors located at the edges of the structure, coming out from the structure. The bias current threshold, where the laser's output is dominated by stimulated emission rather than by spontaneous emission, can be easily recognized by a sharp slope increase at the functional curve presenting output light power versus bias current as illustrated in Fig. 2.10(c).

The light radiation from semiconductor lasers can be characterized through the rate equations which describe the electrons and photon density in the laser cavity [65, 66]:

$$\begin{array}{ll} \frac{dn(t)}{dt} & = \frac{i(t)}{e \cdot V} - \gamma_e(n) \cdot n(t) - G(n,p) \cdot p(t) \\ \frac{dp(t)}{dt} & = \big(\Gamma \cdot G(n,p) - \gamma\big) \cdot p(t) + R_{sp}(n) \end{array} \tag{2.24}$$

where $i(t)$ is the injected current, V is the laser cavity volume, γ_e and γ are the electron and photon recombination rate, respectively, $G(n,p)$ is the gain related to the stimulated emission, Γ is the cavity confinement factor, $R_{sp}(n)$ is the spontaneous emission rate, $p(t)$ and $n(t)$ are the photon and electron densities. The total optical power emitted by the laser can be calculated as $P(t) = C_p \cdot p(t)$, where C_p is the photon density to optical power conversion factor.

Despite of its simplicity, the direct modulation of a laser entails also an optical phase modulation or frequency chirp, which can be expressed as:

$$\frac{d\phi}{dt} = \frac{1}{2}\alpha\Gamma v_g a_g (n(t) - n_t) \tag{2.25}$$

The resulting optical signal fed into the optical fiber is given thus by $E(t) = \sqrt{P(t)} \cdot exp\big(j\phi(t)\big) \cdot exp\big(j\omega_0(t)\big)$. In a back-to-back configuration, and assuming no other nonlinear distortion source is introduced, a linear operation is achieved; however, once the optical signal is propagated through the fiber, fiber linear effects such as the chromatic dispersion interact with the optical field, resulting in nonlinear distortions upon intensity detection, as depicted in Fig. 2.11, and is studied throughout this thesis.

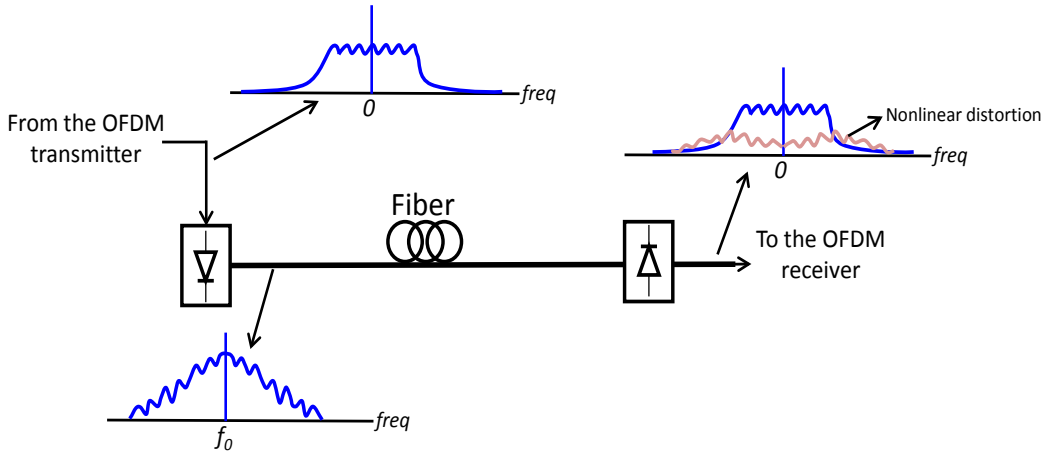

Figure 2.11: DM/DD system.

Direct modulation of a laser source is a cost-effective solution able to achieve transmission information bit rates in the order of Gbits/s and a suitable scheme for metro and access

optical networks (an optical transport network is shown in Fig. 2.12) where the link reach is in the order of tens of kilometers.

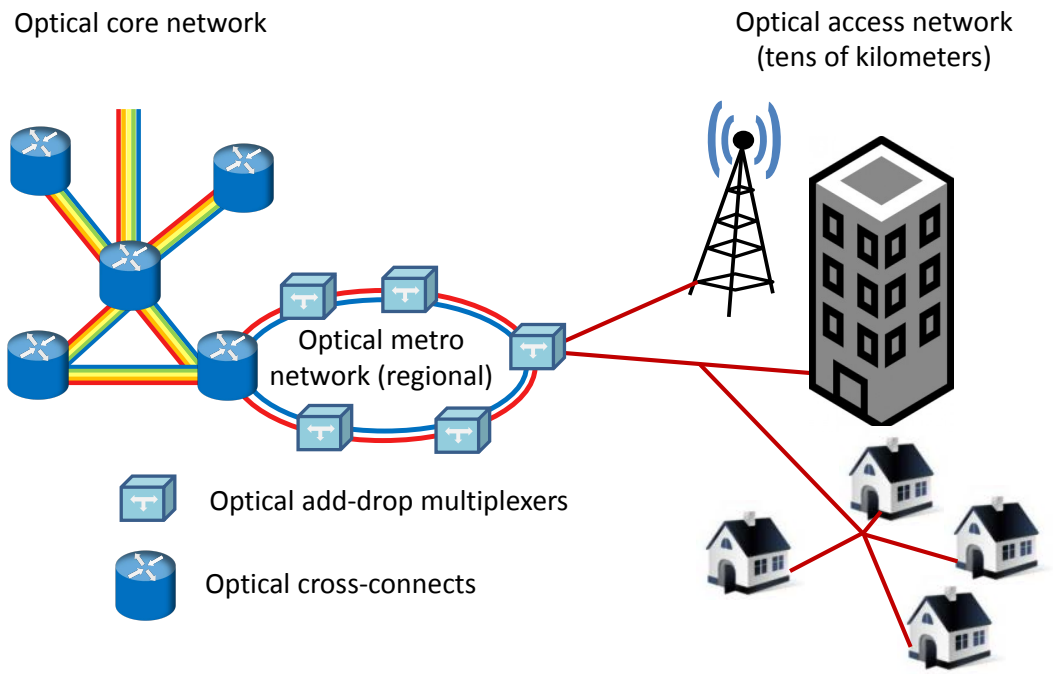

Figure 2.12: Optical transport network.

2.3.2 Externally-modulated systems

For linear-field modulation and externally intensity modulation based-systems, the Mach-Zehnder modulator (MZM) is usually used for optical modulation. Based on the electro-optic effect, such as the refractive index of the crystal changes as a consequence of the applied external field, both amplitude and phase modulation can be performed. Some of the materials typically used for electro-optical effect employment are lithium niobate ($LiNbO_3$), indium phosphate (InP), gallium arsenate (GaAs), and some polymer materials [56].

The electrical field output E_{out} in MZM from Fig. 2.13(a) is related to the field input E_{in} as:

$$E_{out}(t) = \frac{1}{2}\left(exp\left(j\frac{\pi}{V_\pi}\left(V_{rf1}(t) + V_{b1}\right)\right) + exp\left(j\frac{\pi}{V_\pi}\left(V_{rf2}(t) + V_{b2}\right)\right)\right) \cdot E_{in} \tag{2.26}$$

where V_π is the differential drive voltage required to introduce a phase shift of π radians between two waveguide arms. $V_1(t)$ and $V_2(t)$ are the electrical dive signals applied to upper and lower electrodes, respectively. For zero-chirp operation, the modulation signals are equal but with opposite sign ($V_1(t) = -V_2(t) = m \cdot V_{rf}(t)$) and the relation between the output and input fields of the MZM can be expressed as:

$$\frac{E_{out}(t)}{E_{in}} = exp\left(j\frac{\pi}{V_\pi}\frac{V_{b1} + V_{b2}}{2}\right) \cdot cos\left(\frac{\pi}{V_\pi}\left(m \cdot V_{rf}(t) + \frac{V_{b1} - V_{b2}}{2}\right)\right) \cdot E_{in} \tag{2.27}$$

In Fig. 2.13(b) are shown the field transfer function $E_{out}(t)/E_{in}$ and the intensity transfer function $|E_{out}(t)/E_{in}|^2$. For linear field modulation, the MZM must be operated at the null point (NP) by setting $V_b = \frac{V_{b1}-V_{b2}}{2} = (2k+1)V_\pi,\ k \in \mathbb{Z}$, whilst the quadrature-point (QP) is selected for operation when intensity modulation is performed, $V_b = \frac{V_{b1}-V_{b2}}{2} = (2k+1)V_\pi/2,\ k \in \mathbb{Z}$.

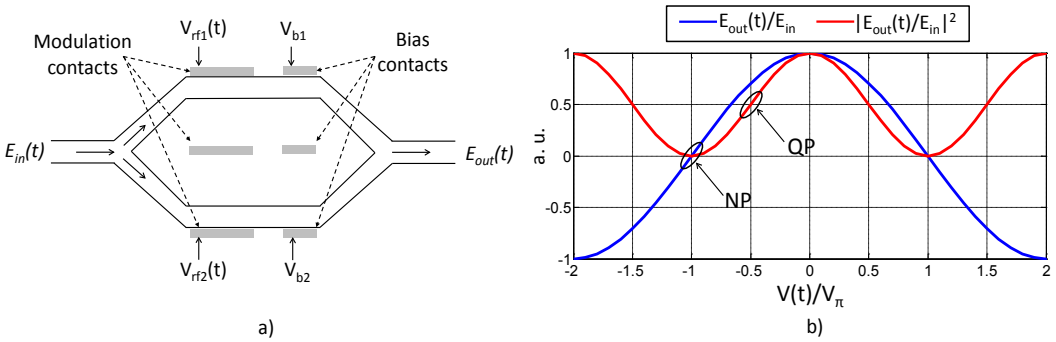

Figure 2.13: a) Mach Zehnder modulator. b) Field and intensity transfer functions of a MZM modulation.

In linear field modulation based-systems, the modulating signal is generally given by a frequency-upconverted OFDM signal, such as that in Eq. (2.9), as shown in Fig. 2.14(a). Another option is the employment of an IQ optical modulator which comprises two MZMs to up convert the real/imaginary parts of the signal [67, 68], as shown in Fig. 2.14(b) .

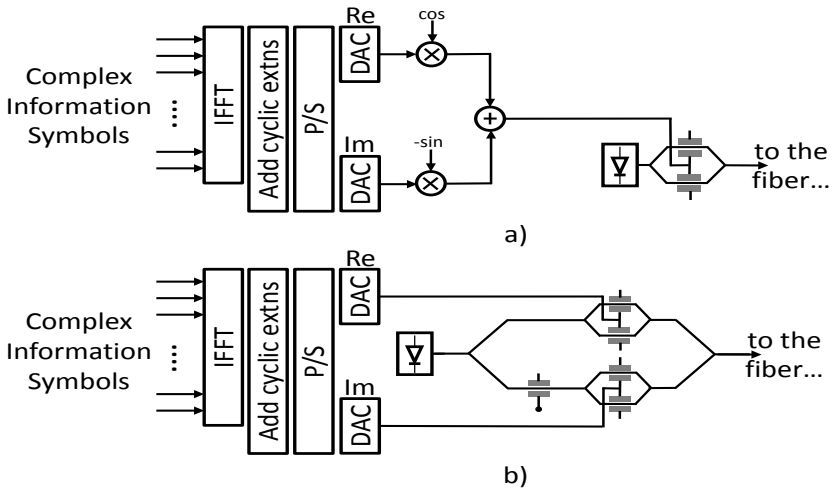

Figure 2.14: OOFDM System with a) electrical frequency up-conversion. b) optical frequency up-conversion.

Unlike intensity modulated systems, where direct detection is the logical choice, both direct [67] and coherent detection [69] can be used when the field is modulated.

2.3.2.1 *Directly-detected systems*

When direct detection is employed, an optical carrier is transmitted together with the information signal, of which generally only one of the sidebands from the field modulation is transmitted in order to overcome chromatic dispersion-induced fading. Such single-sideband modulation can be carried out by using an optical filter at the output of the modulator, as indicated in Fig. 2.15. The photodetector output is proportional to the incident power, which means that only information carried by the amplitude change can be correctly detected, while the phase information is lost. The beat between the optical carrier and the signal sideband as result of the intensity detection gives us the desired information sideband in the electrical domain, together with signal×signal beat interference terms. This is also known as a self-coherent receiver, and has advantages in terms of phase noise, though the spectral efficiency is not as high as a coherent receiver [18].

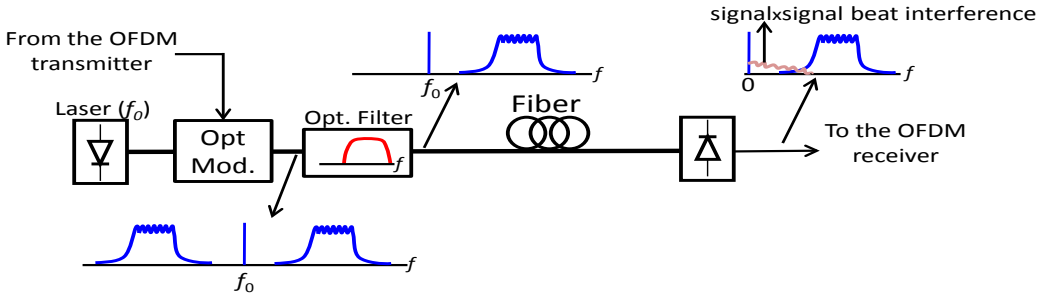

Figure 2.15: Directly-detected system.

2.3.2.2 *Coherently-detected systems*

Unlinke directly-detected systems, coherent detection allows the recovery of the full electric field, which contains both amplitude and phase information, and, thus, the information can be enconded in both the in-phase and quadrature components of the field. Moreover, compared to systems with direct detection [45], the employment of both field polarizations for information enconding is straightforward. Coherent detection represents the most promising detection technique for achieving high spectral efficiencies while maximizing signal-to-noise ratio efficiency [70].

The optical signal at the output of the fiber is mixed with an optical signal coming from a local oscillator which serves as absolute phase reference, as indicated in Fig. 2.16. In Fig. 2.16(a) the heterodyne design of the detector is shown, in which the optical angular frequency of the signal ω_s is not equal to optical angular frequency of the local laser oscillator ω_{LO}, whilst in Fig. 2.16(b) its homodyne version is shown, in which $\omega_s = \omega_{LO}$.

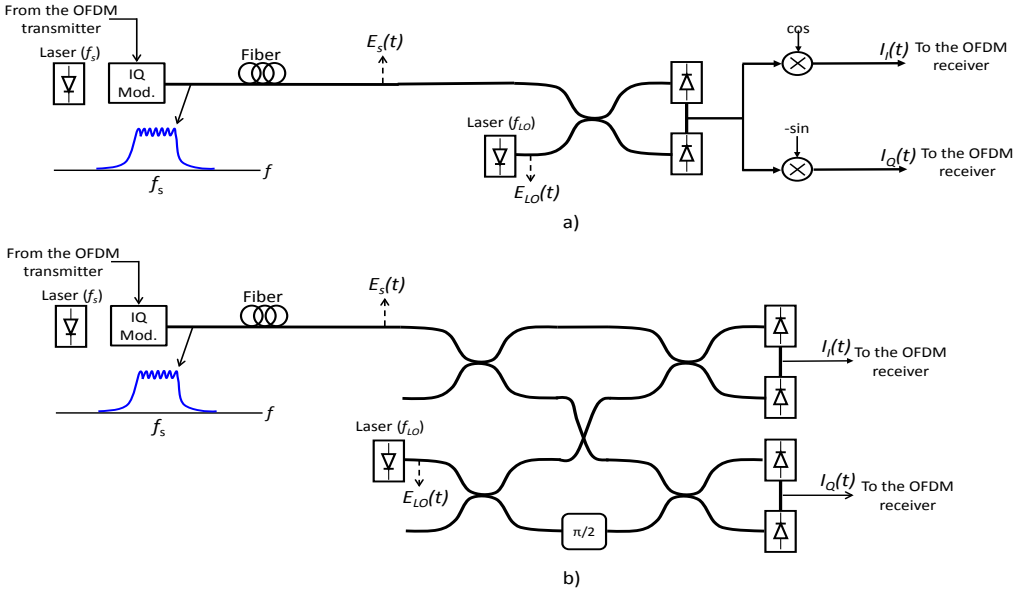

Figure 2.16: System with a) heterodyne and b) homodyne coherent detection.

The signals at the output of the detectors in Fig. 2.16(a) can be expressed as:

$$\begin{aligned} I_1(t) &\propto \frac{1}{2}\Re\cdot|E_s(t)+E_{LO}(t)|^2 \\ &= \frac{1}{2}\Re\cdot|E_s|^2+\frac{1}{2}R\cdot|E_{LO}|^2+\Re\cdot Re\Big\{E_s(t)\cdot E_{LO}^*(t)\Big\} \end{aligned} \tag{2.28}$$

$$\begin{aligned} I_2(t) &\propto \frac{1}{2}\Re\cdot|E_s(t)-E_{LO}(t)|^2 \\ &= \frac{1}{2}\Re\cdot|E_s|^2+\frac{1}{2}R\cdot|E_{LO}|^2-\Re\cdot Re\Big\{E_s(t)\cdot E_{LO}^*(t)\Big\} \end{aligned} \tag{2.29}$$

where $E_s(t) = A_s(t)\cdot exp\Big(\omega_s\cdot t+\phi_s(t)\Big)$ and $E_{LO}(t) = A_{LO}(t)\cdot exp\Big(\omega_{LO}\cdot t+\phi_{LO}(t)\Big)$ are the transmitted information and the local oscillator optical signals, and $\Re$ is the responsivity of the photodetector. The output of the balanced detector is thus given by

$$I(t) = I_1(t) - I_2(t) = 2\Re\cdot Re\Big\{E_s(t)\cdot E_{LO}^*(t)\Big\} \tag{2.30}$$

$$= 2\Re\cdot A_s(t)\cdot A_{LO}(t)\cdot cos\Big(\omega_{IF}\cdot t+\phi_s(t)-\phi_{LO}(t)\Big) \tag{2.31}$$

where $\omega_{IF} = \omega_s - \omega_{LO}$. An electrical oscillator is then employed to down-convert the signal at the intermediate frequency ω_{IF} to baseband, as shown Fig. 2.16(a). Similarly, the photocurrents at the output of the balanced detectors in the homodyne design are given by:

$$\begin{aligned} I_I(t) &= I_1(t) - I_2(t) = 2\Re\cdot Re\Big\{E_s(t)\cdot E_{LO}^*(t)\Big\} \\ &= 2\Re\cdot A_s(t)\cdot A_{LO}(t)\cdot cos\Big(\Delta\omega\cdot t+\phi_s(t)-\phi_{LO}(t)\Big) \end{aligned} \tag{2.32}$$

$$\begin{aligned} I_Q(t) &= I_3(t) - I_4(t) = 2\Re\cdot Im\Big\{E_s(t)\cdot E_{LO}^*(t)\Big\} \\ &= 2\Re\cdot A_s(t)\cdot A_{LO}(t)\cdot sin\Big(\Delta\omega\cdot t+\phi_s(t)-\phi_{LO}(t)\Big) \end{aligned} \tag{2.33}$$

Optical phase lock-loops or signal processing algorithms must be used to correct mismatches between the transmitter laser and the local oscillator frequencies, apart from the processing needed for the recovery of the phase information $\phi_s(t)$ [56, 70, 71]. Both aspects are of great importance in OOFDM systems due to the sensitivity of OFDM to frequency offsets and phase noise, which destroy the orthogonality between subcarriers.

2.4 Summary

We have reviewed the basic concepts on OFDM for the understanding of the work presented in next Chapters. In short,

- OFDM is a multiplexing technique with which the information data is transmitted in parallel at lower rates than in a serial fashion and over the transmitted signal's frequency content.
- The IDFT realizes the assignation of data to an orthogonal basis function at the transmitter, and the DFT its corresponding detection at the receiver side.
- Both operations also determine the points where the signal is translated from frequency to time domain and from time to frequency domain, respectively.
- Linear effects which affect to the signal, $x[m], m = 0, 1, ...FS - 1$, can be easily compensated at the receiver end side if proper values of the cyclic extensions are used.
- The amplitude values of the OFDM signal is random, and they can achieve unexpected high values, which imposes stringent conditions on the transceiver design.
- The main advantages OFDM brings to optical communications come from the division of the available transmission bandwidth into independent channels (scalability, adaptability and subcarrier granularity), as well as its ease equalization of linear filtering effects.
- Manifold and different architecture designs have been proposed for the transmission of OOFDM signals for optical communications, being the result of the many trade-offs involved: link reach, cost, transmission rate, signal quality, power efficiency,...
- In metro and access optical networks, where the cost is of main concern and the link reach is limited to a tens of kilometers, direct modulation/detection is a suitable scheme for the provision of Gbits/s communication services.

Chapter 3

Theoretical Analysis of DM/DD OOFDM Systems

3.1 Introduction

As we have pointed out in Chapter 1, impressive experimental results in terms of signal line rates in OOFDM systems with direct modulation have been achieved. Nevertheless, there is an obvious lack of theoretical results which enlighten the physics behind the performance of such systems. A deep understanding of such physics is necessary for a proper design of DM/DD OOFDM systems leading to higher transmission bit rates.

We can find in the literature some IM/DD OOFDM analysis which study the system performance. However, they focus on the influence of the transceiver electronics design parameters but not on the direct modulation process and fiber transmission effects [60], or based on not general mathematical assumptions on the optical direct modulation process [43]. In [41], a small-signal analysis which includes the laser rate equations is performed, but, consequently, laser nonlinear distortion is neglected in the analysis. In [72], they neglect the influence of laser chirp when OOFDM is compared with on-off keying format. In [73] they report a significant performance improvement when OOFDM signals are propagated through negative dispersion fibers, but a clear and explicit explanation of this phenomenon for directly modulated OOFDM signals propagation is needed in order to find out the conditions which make possible this improvement, what can only be achieved through a rigorous mathematical description of the physical mechanisms involved.

In this chapter, we present a theoretical analysis using a detailed mathematical treatment to study the effects of the laser nonlinearity and the global impact of the laser chirp and chromatic dispersion with regard to the system performance. Our approach allows the evaluation of an IM/DD OOFDM SMF link under different conditions and the separate computation of the different intermodulation distortion (IMD) penalties. The chapter is

structured as follows: in Section 3.2 we describe the DM/DD OOFDM system and present the mathematical formulation derived to obtain an analytical expression of the detected photocurrent. Section 3.3 presents the results obtained by evaluating the previous expression and we compare them to those provided by commercial software simulations for different system parameter values with the aim of theoretical validation. In Sections 3.4 and 3.5 the analytical formulation allows us to isolate and study the useful term for the information signal detection at the receiver-end side and the nonlinear distortion which impairs the system performance. Finally, in Section 3.6, the contents of the chapter are summarized.

3.2 Analytical Formulation

As we saw in Chapter 2, after calculating the IFFT of the information symbols block, with Hermitian symmetry and digital-to-analog conversion, the OFDM symbol starting at t=0 and with duration T can be expressed as:

$$s(t) = \sum_{k=1}^{N} |X_k| \cdot cos(\Omega_k t + \varphi_{X_k}) * h_{trx}(t) + n_{trx}(t), \;\; 0 \leq t \leq T \tag{3.1}$$

where $X_k = |X_k| e^{j \cdot \varphi_{X_k}}$ are the information complex symbols, Ω_k is the angular frequency value of the k-th subcarrier, N the number of subcarriers, and $n_{trx}(t)$ is a noisy term due to quantization and clipping [60]. The value of the discrete frequency Ω_k is given by $k \cdot \Delta\Omega$, where $\Delta\Omega$ is the spacing angular frequency between consecutive subcarriers. The analog OFDM signal is then scaled to yield a certain value of peak current and a dc value is added to operate the optical source. The input current to the laser is then given by:

$$\begin{aligned} i(t) =& i_0 + i_m(t) = i_0 + m \cdot \Big(\sum_{k=1}^{N} |X_k| \cdot cos(\Omega_k t + \varphi_{X_k}) * h_{trx}(t) + n_{trx}(t) \Big) \\ =& i_0 + \sum_{k=1}^{N} 2 i_k \cdot cos(\Omega_k t + \varphi_{i_k}) * h_{trx}(t) + n'_{trx}(t), \;\; 0 \leq t \leq T \end{aligned} \tag{3.2}$$

where i_0 represents the dc-offset added just before the laser, m is the scaling factor determined by the electrical attenuation to operate the laser within a certain region ($|i_m(t)| \leq \Delta i$), and $i_k \cdot exp((-)j\varphi_{i_k})$ is the driving current coefficient at frequency $(-)\Omega_k$. The directly modulated laser model employed for simulations is governed by the following equations [65, 66]:

$$\begin{array}{ll} \frac{dp(t)}{dt} & = [\Gamma \cdot v_g a \frac{n(t)-n_t}{1+\varepsilon_{nl} \cdot p(t)} - \frac{1}{\tau_p}] p(t) + \zeta \Gamma \cdot n^2(t) \\ \frac{dn(t)}{dt} & = \frac{i(t)}{e \cdot V} - An - Bn^2 - Cn^3 - v_g a \frac{n(t)-n_t}{1+\varepsilon_{nl} \cdot p(t)} \cdot p(t) \\ \frac{d\phi}{dt} & = \frac{1}{2} \alpha \Gamma v_g a_g (n(t) - n_t) \end{array} \tag{3.3}$$

where $p(t)$, $n(t)$ are the photon and carrier densities in the laser active region, respectively, $\phi(t)$ is the phase of the output optical signal, Γ is the confinement factor, v_g is the group velocity, a_g is the linear material gain coefficient, n_t is the transparency carrier density, ε_{nl} is the nonlinear gain coefficient, τ_p is the photon lifetime, ζ determines the fraction of spontaneous emission that is emitted into the fundamental mode of the laser, V is the volume of the active region, $i(t)$ is the driving current fed into the laser, e is the electron charge, A is the non radiative-recombination coefficient, B is the radiative-recombination coefficient and C is the Auger recombination coefficient. This DML model takes into account longitudinal

mode spatial hole burning, linear and nonlinear carrier recombination, and nonlinear gain effects. Although Langevin source noises are not included, this lumped DML model has proved to provide sufficiently accuracy when compared to experimental results [41, 74].

The optical field at the output of the DML laser is given by:

$$E(t, z = 0) = \sqrt{P(t)} \cdot exp\big(j \cdot \phi(t)\big) \cdot exp\big(j \cdot \omega_0 t\big) \tag{3.4}$$

where $P(t)$ and $\phi(t)$ are the output optical intensity and phase, respectively, and ω_0 is the laser central wavelength. The optical intensity is related to the photon density by:

$$P(t) = \frac{1}{2}\alpha_m \eta_{opt} v_g h f_0 \frac{V}{\Gamma} \cdot p(t) = C_p \cdot p(t) \tag{3.5}$$

being η_{opt} the coupling efficiency, hf_0 the photon energy at the emission frequency f_0, and α_m the mirror loss. The output optical phase, $\phi(t)$, is determined by Eq. (3.3).

The transfer function of the SMF is given by:

$$H_{fib}(\omega) = exp\big(j \cdot (\beta_0 + \beta_1 \cdot (\omega - \omega_0) + \frac{1}{2}\beta_2 \cdot (\omega - \omega_0)^2) \cdot L\big) \tag{3.6}$$

where $\beta(\omega)$ is the propagation constant of the fiber, β_0 its value at $\omega = \omega_0$, β_1 and β_2 are its first and second derivatives evaluated at ω_0 and L is the length of the fiber. β_2 is related to the dispersion parameter D of the fiber through $\beta_2 = -D\frac{\lambda_0^2}{2\pi \cdot c_0}$, where c_0 denotes the speed of light in vacuum. Therefore, the mathematical analysis performed is applicable to OOFDM systems operating in the third window where the second order dispersion parameter dominates and the coefficient of the third order dispersion is small. Once the optical signal is propagated through the fiber, the optical intensity is detected by means of a square-law photodetector:

$$I_{ph}(t) = \Re \cdot |E(t, z = L)|^2 \tag{3.7}$$

where $\Re$ is the responsivity of the photodetector. The described OOFDM system is depicted in Fig. 3.1.

Our goal is to obtain a mathematical expression of Eq. (3.7), since it will be a much more useful tool for the understanding of directly modulated OOFDM systems than the observation of the final results in numerical simulations.

In order to derive an approximated mathematical expression of the detected photocurrent which faithfully describes the laser nonlinearity and the conversion of laser chirp to optical intensity as result of the chromatic dispersion, we make several assumptions. First of all, noises generated at the transmitter electronic stage, such as quantization and clipping noises, are ignored. Besides, transmitter filtering effects are neglected as well, and the OFDM symbol duration extends to $-\infty$ to ∞, so we can write:

$$i(t) = i_0 + \sum_{k=1}^{N} 2i_k \cdot cos(\Omega_k t + \varphi_{i_k}) \tag{3.8}$$

Given the fact that the optical fiber transfer function operates in the field domain, we need to get rid out of the square root in Eq. (3.4) in order to determine a mathematical expression of the ouput fiber optical field. We approximate the optical intensity $|E(t, z = 0)|^2$ by:

$$P(t) \approx P_0 + P_1(t) + P_2(t) + P_{11}(t) \tag{3.9}$$

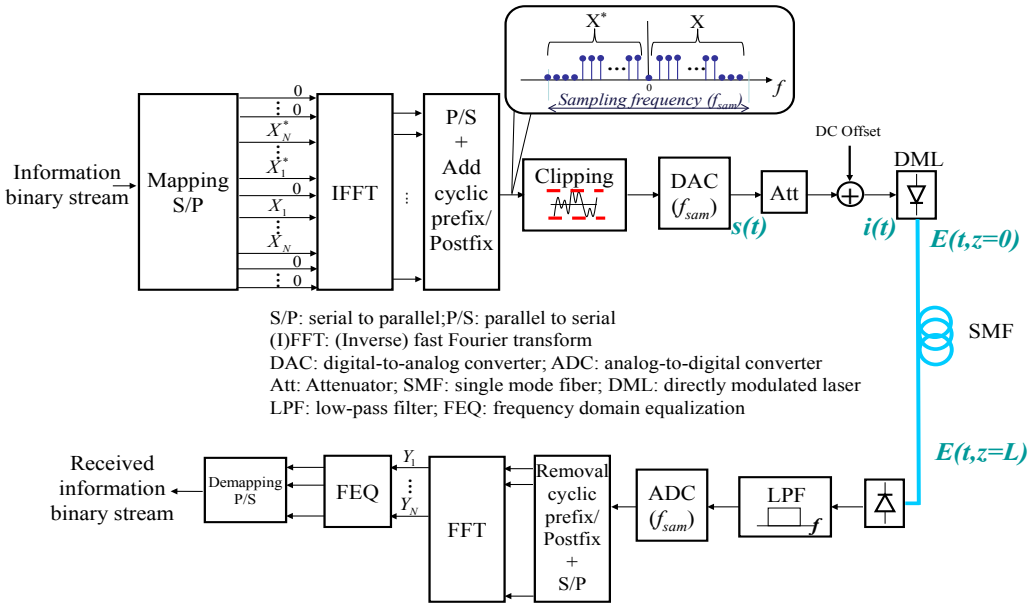

Figure 3.1: Schematic illustration of the simulated OOFDM system. Inset: OFDM signal power spectrum

where P_0 is the mean optical power and

$$\begin{aligned}
P_1(t) &= \sum_{k=1}^{N} 2p_k \cdot cos\big(\Omega_k t + \varphi_{p_k}\big) \\
P_2(t) &= \sum_{k=1}^{N} 2p_{2k} \cdot cos\big(2\Omega_k t + \varphi_{p_{2k}}\big) \\
P_{11}(t) &= \sum_{k=1}^{N}\sum_{l=1}^{k-1} 2p_{kl} \cdot cos\big((\Omega_k + \Omega_l)t + \varphi_{p_{kl}}\big) + \\
&\quad \sum_{k=1}^{N}\sum_{l=1}^{k-1} 2p_{k_l} \cdot cos\big(((\Omega_k - \Omega_l) + \varphi_{p_{k_l}})\big)
\end{aligned} \tag{3.10}$$

where $p_k \cdot e^{j\cdot\varphi_{p_k}}$, $p_{2k} \cdot e^{j\cdot\varphi_{p_{2k}}}$, $p_{kl} \cdot e^{j\cdot\varphi_{p_{kl}}}$ and $p_{k\_l} e^{j\cdot\varphi_{p_{k\_l}}}$ are the first and second order complex coefficients of the intensity at frequencies $\Omega_k, 2\Omega_k, (\Omega_k + \Omega_l)$ and $(\Omega_k - \Omega_l)$, respectively, whose values are determined by the transfer functions $H_{p1}(\Omega_k)$, $H_{p2}(\Omega_k)$, $H_{p11}(\Omega_k, \Omega_l)$ and the input driving current:

$$\begin{aligned}
p_k \cdot exp\big(j \cdot \varphi_{p_k}\big) &= H_{p_1}\big(\Omega_k\big) \cdot i_k \cdot exp\big(j \cdot \varphi_{i_k}\big) \\
p_{2k} \cdot exp\big(\varphi_{p_{2k}}\big) &= H_{p_2}\big(\Omega_k\big) \cdot i_k^2 \cdot exp\big(j \cdot 2 \cdot \varphi_{i_k}\big) \\
p_{kl} \cdot exp\big(j \cdot \varphi_{p_{kl}}\big) &= H_{p_{11}}\big((\Omega_k, \Omega_l)\big) \cdot i_k \cdot i_l \cdot exp\big(j \cdot (\varphi_{i_k} + \varphi_{i_l})\big) \\
p_{k_l} \cdot exp\big(j \cdot \varphi_{p_{k_l}}\big) &= H_{p_{11}}\big((\Omega_k, -\Omega_l)\big) \cdot i_k \cdot i_l \cdot exp\big(j \cdot (\varphi_{i_k} - \varphi_{i_l})\big)
\end{aligned} \tag{3.11}$$

The first and second order intensity/driving current transfer functions, $H_{p1}(\Omega_k)$, $H_{p2}(\Omega_k)$ and $H_{p11}(\Omega_k, \Omega_l)$ have been derived by doing a perturbative analysis of Eqs. (3.3), and whose

details can be consulted in Appendix A. Using the approximation $\sqrt{1+x} \approx 1 + \frac{x}{2} - \frac{x^2}{8}$, the modulus of the optical field is approximated by:

$$
\begin{aligned}
|E(t)| \approx \frac{1}{P_0^{\frac{1}{2}}} \cdot \big(1 + \frac{P_1(t)+P_2(t)+P_{11}(t)}{2} - \frac{P_1^2(t)}{8 \cdot P_0}\big) = \\
a + b \cdot P_1(t) + c \cdot P_2(t) + c \cdot P_{11}(t) + d \cdot \sum_{k=1}^{N} \sum_{\substack{l=1 \\ l \neq k}}^{N} 2 p_k \cdot p_l \cdot cos\big((\Omega_k + \Omega_l)t + \varphi_{p_k} + \varphi_{p_l}\big) \\
+ d \cdot \sum_{k=1}^{N} \sum_{\substack{l=1 \\ l \neq k}}^{N} 2 p_k \cdot p_l \cdot cos\big((\Omega_k - \Omega_l)t + \varphi_{p_k} - \varphi_{p_l}\big) + d \sum_{k=1}^{N} 2 p_k^2 \cdot cos\big(2(\Omega_k t + \varphi_{p_k})\big)
\end{aligned}
\tag{3.12}
$$

where the constants

$$
a = P_0^{\frac{1}{2}},\ b = c = \frac{1}{2 P_0^{\frac{1}{2}}},\ d = -\frac{1}{8 P_0^{\frac{3}{2}}}
\tag{3.13}
$$

have been introduced merely because of nomenclature simplification. To describe completely the optical signal in Eq. (3.4), we need to find a mathematical approximation for the optical phase $\phi(t)$. Preliminary results have shown the convenience of adding also the laser nonlinearity into the mathematical expression of optical phase $\phi(t)$. For that reason, the optical phase is approximated by:

$$
\phi(t) \approx \sum_{k=1}^{N} m_k \cdot sin(\Omega_k t + \varphi_{m_k})
\tag{3.14}
$$

where m_k is the frequency modulation index at the k-th subcarrier and φ_{m_k} its corresponding phase, which values are given by:

$$
\begin{aligned}
m_k \cdot exp\big(j \cdot \varphi_{m_k}\big) = & 2j \cdot H_{\phi_1}\big(\Omega_k\big) \cdot i_k \cdot exp\big(j \cdot \varphi_{i_k}\big) + \\
& 2j \cdot H_{\phi_2}\big(\Omega_r\big) \cdot i_r \cdot exp\big(j \cdot 2 \cdot \varphi_{i_r}\big) + \\
& 2j \cdot H_{\phi_{11}}\big(\Omega_m, \Omega_n\big) \cdot i_m \cdot exp\big(j \cdot \varphi_{i_m}\big) \cdot i_n \cdot exp\big(j \cdot \varphi_{i_n}\big) + \\
& 2j \cdot H_{\phi_{11}}\big(\Omega_p, \Omega_q\big) \cdot i_p \cdot exp\big(j \cdot \varphi_{i_p}\big) \cdot i_q \cdot exp\big(-j \cdot \varphi_{i_q}\big)
\end{aligned}
\tag{3.15}
$$

where the different indices must satisfy:

$$
\begin{aligned}
k &= 1, 2, ...N \\
2 \cdot r &= k \\
m + n &= k, m > n \\
p - q &= k, p > q
\end{aligned}
$$

That is, we have included in $m_k \cdot exp\big(j \cdot \varphi_{m_k}\big)$ the second harmonic and intermodulation products which fall at the discrete subcarrier frequency Ω_k. The mathematical approximation of the complex electric field we obtain for subsequent mathematical analysis is given by:

$$
E(t) = |E(t)| \cdot exp\big(j \cdot \sum_{k=1}^{N} m_k \cdot sin(\Omega_k t + \varphi_{m_k})\big)
\tag{3.16}
$$

Complex exponential functions are usually handled using a small argument approximation, as done in [43] and [41] to study the time-varying output phase from the laser. Nevertheless,

at the aim of carrying out a rigorous theoretical analysis, we use the Jacobi-Anger identity to deal with the approximated output optical phase $\phi(t)$:

$$\begin{aligned} &exp\big(j\cdot\sum_{k=1}^{N} m_k\cdot sin(\Omega_k t+\varphi_{m_k})\big) \\ &=\prod_{k=1}^{N}\Big(\sum_{n_k=-\infty}^{\infty} J_{n_k}\big(m_k\big)\Big)\cdot exp\Big(\sum_{k=1}^{N} n_k\big(\Omega_k\cdot t+\varphi_{m_k}\big)\Big) \end{aligned} \tag{3.17}$$

In this way we obtain an expression with which each spectral component of the optical signal is completely determined. The effects of the propagation through the dispersive fiber can be taken into account by multiplying the signal's spectral content with the fiber transfer function in Eq. (3.6), and going back to the time-domain by calculating the inverse Fourier transform [75]:

$$E(t,z=L)=FT^{-1}\{FT\{E(t,z=0)\}\cdot H_{fib}(\Omega)\} \tag{3.18}$$

Using the Graf's theorem for the summation of Bessel functions [76], as done in [77], and neglecting some higher order terms, the final expression of the photocurrent calculated as Eq. (3.7) can be simplified up to a point. Because of its length, we separate the photocurrent expression in different terms:

$$\begin{aligned} I_{ph}(t)\approx\Re\cdot\sum_{n_1\ldots n_N=-\infty}^{\infty}\Bigg(&T0_{(n_1\ldots n_N)}+T1_{(n_1\ldots n_N)}+T2_{(n_1\ldots n_N)}+ \\ &T3_{(n_1\ldots n_N)}+T4_{(n_1\ldots n_N)}+T5_{(n_1\ldots n_N)}\Bigg)\cdot exp\Bigg(j\Big(\Omega_{imp}t+\sum_{k=1}^{N} n_k\big(\varphi_{m_k}+\frac{\pi}{2}\big)\Big)\Bigg) \end{aligned} \tag{3.19}$$

where $\theta_k=-\frac{\beta_2}{2}\Omega_{imp}\Omega_k L$, with $\Omega_{imp}=\sum_{k=1}^{N} n_k\cdot\Omega_k$. By particularizing for different combinations of values of $n_1,\quad n_2,...,\quad n_N$, the different components which fall at Ω_{imp} can be easily found. The expressions of $T0$, $T1$, $T2$, $T3$, $T4$ and $T5$ are:

$$T0_{(n_1\ldots n_N)}=J_{n_1}(\mu_1)\cdot\cdot J_{n_N}(\mu_N)\cdot\Big(a^2+2\cdot b^2\sum_{k=1}^{N} p_k^2\cdot cos(2\theta_k)\Big) \tag{3.20}$$

being $\mu_k=2m_k\cdot sin(\theta_k)$. The term $T0$ is due to the laser phase/frequency modulation and its conversion to intensity after propagation: as result of the spectral imbalance due to chromatic dispersion, the coefficients μ begin to be different to zero; as result nonlinear distortion products start to appear at Ω_{imp}, but also a linear information signal component, as we will see in Section 3.4.

$$\begin{aligned} &T1_{(n_1\ldots n_N)}= \\ &J_{n_1}(\mu_1)\cdot\cdot J_{n_N}(\mu_N)\cdot\Bigg(2ab\sum_{k=1}^{N}\frac{p_k\cdot cos(\theta_k)}{J_{n_k}(\mu_k)}\cdot\Big(J_{n_k+1}(\mu_k)\cdot exp\big(j(\varphi_{m_k}-\varphi_{p_k}+\frac{\pi}{2})\big)+ \\ &\qquad J_{n_k-1}(\mu_k)\cdot exp\big(-j(\varphi_{m_k}-\varphi_{p_k}+\frac{\pi}{2})\big)\Big)\Bigg) \end{aligned} \tag{3.21}$$

$T1$ contains the useful part of the intensity modulated information signal. By setting an index n_r to 1 at once, the information modulated into the intensity may be found for

frequencies $\Omega_{imp} = \Omega_1, \Omega_2, .., \Omega_N$. It is the result of the beating betwen the optical carrier and the information sideband, as we can see from the fact that it is directly proportional to $a \cdot b$. The expression of $T1$ allows us to determine the different intermodulation products which arise because of the interplay of laser chirp and chromatic dispersion at Ω_{imp} as result of the propagation of $P_1(t)$ through the fiber.

$$T2_{(n_1 \ldots n_N)} = \\ J_{n_1}(\mu_1) \cdot\cdot J_{n_N}(\mu_N) \cdot \Bigg(2ac \sum_{k=1}^{N} \frac{p_{2k} \cdot cos(2\theta_k)}{J_{n_k}(\mu_k)} \Big(J_{n_k+2}(\mu_k) \cdot exp\big(j(2\varphi_{m_k} - \varphi_{p_{2k}} + \pi)\big) + \\ J_{n_k-2}(\mu_k) \cdot exp\big(-j(2\varphi_{m_k} - \varphi_{p_{2k}} + \pi)\big) \Big) \Bigg) \tag{3.22}$$

$$T3_{(n_1 \ldots n_N)} = J_{n_1}(\mu_1) \cdot\cdot J_{n_N}(\mu_N) \cdot \\ \Bigg(2ac \sum_{k=1}^{N} \sum_{l=1}^{k-1} \frac{p_{kl} \cdot cos(\theta_k + \theta_l)}{J_{n_k}(\mu_k) J_{n_l}(\mu_l)} \Big(J_{n_k+1}(\mu_k) \cdot J_{n_l+1}(\mu_l) \cdot exp\big(j(\varphi_{m_k} + \varphi_{m_l} - \varphi_{p_{kl}} + \pi)\big) + \\ J_{n_k-1}(\mu_k) \cdot J_{n_l-1}(\mu_l) \cdot exp\big(-j(\varphi_{m_k} + \varphi_{m_l} - \varphi_{p_{kl}} + \pi)\big) \Big) + \\ 2ac \sum_{k=1}^{N} \sum_{l=1}^{k-1} \frac{p_{k\_l} \cdot cos(\theta_k - \theta_l)}{J_{n_k}(\mu_k) J_{n_l}(\mu_l)} \Big(J_{n_k+1}(\mu_k) \cdot J_{n_l-1}(\mu_l) \cdot exp\big(j(\varphi_{m_k} - \varphi_{m_l} - \varphi_{p_{k\_l}})\big) + \\ J_{n_k-1}(\mu_k) \cdot J_{n_l+1}(\mu_l) \cdot exp\big(-j(\varphi_{m_k} - \varphi_{m_l} - \varphi_{p_{k\_l}})\big) \Big) \Bigg) \tag{3.23}$$

The origin of $T2$ and $T3$ is the laser second order nonlinear distortion represented by $P_2(t)$ and $P_{11}(t)$ in Eq. (3.10). This nonlinear distortion is affected by the laser chirp and its consequent conversion to intensity due to chromatic dispersion. When intensity detection occurs, its beat with the optical carrier generates $T2$ and $T3$.

$$
\begin{aligned}
T4_{(n_1 \ldots n_N)} &= J_{n_1}(\mu_1) \cdot\cdot J_{n_N}(\mu_N) \cdot \\
&\left(\sum_{k=1}^{N} \sum_{\substack{l=1 \\ l \neq k}}^{N} \frac{p_k \cdot p_l}{J_{n_k}(\mu_k) J_{n_l}(\mu_l)} \Big(-J_{n_k+1}(\mu_k) \cdot J_{n_l+1}(\mu_l) \cdot exp\Big(j(\varphi_{m_k} - \varphi_{p_k} + \varphi_{m_l} - \varphi_{p_l}) \Big) \cdot \right. \\
&\qquad \Big(2ad \cdot cos(\theta_k + \theta_l) + b^2 \cdot exp\big(j(\theta_k - \theta_l) \big) \Big) - \\
&\qquad J_{n_k-1}(\mu_k) \cdot J_{n_l-1}(\mu_l) \cdot exp\Big(-j(\varphi_{m_k} - \varphi_{p_k} + \varphi_{m_l} - \varphi_{p_l}) \Big) \cdot \\
&\qquad \left. \Big(2ad \cdot cos(\theta_k + \theta_l) + b^2 exp\big(-j(\theta_k - \theta_l) \big) \Big) \right) + \\
&\sum_{k=1}^{N} \sum_{\substack{l=1 \\ l \neq k}}^{N} \frac{p_k \cdot p_l}{J_{n_k}(\mu_k) J_{n_l}(\mu_l)} \Big(J_{n_k+1}(\mu_k) \cdot J_{n_l-1}(\mu_l) \cdot exp\Big(j(\varphi_{m_k} - \varphi_{p_k} - \varphi_{m_l} + \varphi_{p_l}) \Big) \cdot \\
&\qquad \Big(2ad \cdot cos(\theta_k - \theta_l) + b^2 \cdot exp\big(j(\theta_k + \theta_l) \big) \Big) + \\
&\qquad J_{n_k-1}(\mu_k) \cdot J_{n_l+1}(\mu_l) \cdot exp\Big(-j(\varphi_{m_k} - \varphi_{p_k} - \varphi_{m_l} + \varphi_{p_l}) \Big) \cdot \\
&\qquad \left. \Big(2ad \cdot cos(\theta_k - \theta_l) + b^2 \cdot exp\big(-j(\theta_k + \theta_l) \big) \Big) \right) \Big)
\end{aligned}
\tag{3.24}
$$

$$
\begin{aligned}
T5_{(n_1 \ldots n_N)} &= J_{n_1}(\mu_1) \cdot\cdot J_{n_N}(\mu_N) \cdot \\
&\left(\sum_{k=1}^{N} p_k^2 \frac{2ad \cdot cos(2\theta_k) + b^2}{J_{n_k}(\mu_k)} \Big(J_{n_k+2}(\mu_k) \cdot exp\big(j2(\varphi_{m_k} - \varphi_{p_k} + \frac{\pi}{2}) \big) + \right. \\
&\qquad \left. J_{n_k-2}(\mu_k) \cdot exp\big(-j2(\varphi_{m_k} - \varphi_{p_k} + \frac{\pi}{2}) \big) \Big) \right)
\end{aligned}
\tag{3.25}
$$

Finally, terms $T4$ and $T5$ are due to the nonlinear mapping inherent to intensity modulation [1] between the electrical OFDM signal and the optical field. In our mathematical treatment we have considered the term $P_1^2(t)$ in Eq. (3.12), and $T4$ and $T5$ are the result of its propagation through the dispersive link and subsequent intensity detection.

The mathematical treatment performed to deal with the laser chirp using the Jacobi-Anger identity allows us to calculate any order of intermodulation which results of the conversion of the laser chirp to intensity. Effectively, the different intensity terms in Eq. (3.9) and transmitted through the dispersive link interfere with those due to the laser chirp, which causes different nonlinear distortion products in the detected photocurrent. The particular contribution of each term ($T0$, $T1$,...$T5$) at different frequencies is obtained by particularizing for different values of $n_1, n_2, ..., n_N$, being its order equals to $n = \sum_{i=1}^{N} |n_i|$ [77]. As example, the contribution of $T0$ at $\Omega = \Omega_4$ can be calculated for an order equals to $n = 2$ by imposing $n_2 = 2$, $n_k = 0$ with $k \in [1, 3...N]$, or $n_1 = 1$, $n_3 = 1$, $n_k = 0$ with $k \in [2, 4, 5, ...N]$, or $n_5 = 1$, $n_1 = -1$, $n_k = 0$ with $k \in [2, 3, 4, 6, 7, ...N]$. Proceeding in this way, we can calculate the contribution of $T0$, $T1$,...$T5$ for different combinations of values for $n_1, n_2, ..., n_N$.

Please note that the derived expression for the photocurrent can be easily adapted to a directly modulated OOFDM system with RF-upconversion, since, in that case, the driving

modulating signal can be written as:

$$i(t) = i_0 + \sum_{k=-N/2}^{N/2-1} i_k \cdot cos\Big(\big(\Omega_c + \Omega_k\big)\cdot t + \varphi_{i_k}\Big) \tag{3.26}$$

and, thus, its mathematical treatment is very similar to that explained for Eq. (3.8).

3.3 Accuracy of the analytical model

Given the complex derivation procedure of the analytical formulation, one is left with the uneasy question of whether it may be correct and accurate. Moreover, the analytical formulation just presented is the basis of the next chapters, and, therefore, it is mandatory to validate it and explore its possible limitations. In order to validate it we have compared the results provided by Eq. (3.19), with those provided by commercial simulation packages based on the numerical integration of the laser rate equations. After all, in order to derive Eq. (3.19), we have done several assumptions:

- We have assumed that the analog electrical OFDM signal can be expressed as a sum of infinite time duration tones in Eq. (3.8). In the frequency domain, infinite-time tones are represented by Delta's dirac, but, as we saw in Chapter 2, OFDM signal's power spectrum is better represented by $sinc^2$ functions, with their corresponding non-zero bandwidth.
- We have considered up to a second order laser nonlinearity in Eq. (3.9). Depending on the laser parameters, its operation point and the number of tones of the laser modulating signal, it may be convenient to consider third order laser nonlinearity as well.
- The modulus of the optical signal has been approximated by using a series expansion of $\sqrt{1+x} \approx 1 + \frac{x}{2} - \frac{x^2}{8}$ where $x << 1$: the smaller is the value of the modulating signal i_m compared to the dc-offset i_0, the more accurate this approach is.
- Finally, after photodection, we retain the most significant beats: those generated by the optical carrier, and the signal $\times$ signal beat.

In order to demonstrate the validity of the analytical formulation performed in the previous sections, we carry out a series of comparison tests with the simulations results obtained by using Matlab and VPI software packages. In order to quantify how close the theoretical formulation is to the simulation results, we calculate the next figure of merit:

$$Err_y[r] = \sqrt{\frac{\Big\langle |Y_{rec_{sim}}[r] - Y_{rec_{theo}}[r]|^2 \Big\rangle}{\Big\langle |Y_{rec_{sim}}[r]|^2 \Big\rangle}} \times 100, \qquad r = 1, 2, ...N \tag{3.27}$$

where $Y_{rec_{sim}}[r]$ and $Y_{rec_{theo}}[r]$ are the received complex symbols before equalization at the *r-th* subcarrier from simulations and from the evaluation of 3.19, respectively. Since we are also interested on the validity of the model to measure the IMD which impairs the recovery

of the signal at the receiver-end side, we also calculate numerically the total IMD with the aim of comparison:

$$IMD[r] = \langle |\hat{Y}[r] - X[r]|^2 \rangle, \qquad r = 1, 2, ...N \tag{3.28}$$

where $\hat{Y}[r]$ is the equalized complex symbol of the *r-th* subcarrier.

Amongst the great variety of system parameters which can be varied, we perform our comparisons by changing:

- OOFDM modulation parameters: cyclic pre/post fix lengths (T_{pre} and T_{pos}), signal's bandwidth (BW), and the number of subcarriers the OFDM signal is composed (N).
- Laser modulation: bias point, i_0, and the laser driving signal amplitude swing, Δi.
- Laser internal parameters: the nonlinear gain coefficient, ε_{nl}, the linewidth enhancement factor, α and the photon lifetime, τ_p (through the laser cavity loss, α_{int}).

Given the large number of parameters involved, the comparisons are done by varying just one of the parameters at once. The default number of subcarriers N is 26 and the default values for i_0 and Δi are *60mA* and *5mA*, respectively, whilst the next default laser parameters are used: $\varepsilon_{nl} = 3 \times 10^{-23} m^3$, $\alpha = 4$ and $\tau_p(\alpha_{int} = 2873 m^{-1}) = 1.9375 ps$.

On other hand, as it can be noted from Eqs. (6.8)-(6.13), we need to truncate their computational evaluation to a certain limit of intermodulation order $n = \sum_{i=1}^{N} |n_i|$: $T0$ and $T1$ are evaluated up to an order equal to $n = \sum_{i=1}^{N} |n_i| = 3$, whilst $T2$, $T4$ and $T5$ are evaluated up to an order equal $n = \sum_{i=1}^{N} |n_i| = 2$. Such different treatment is easily explained by the different origin of $T0$ and $T1$ with respect to $T2$, $T4$ and $T5$: as explained in Section 3.2, $T0$ and $T1$ find their origin in the first order laser frequency/phase and intensity modulations, respectively, whilst $T2$, $T4$ and $T5$ are intrinsically nonlinear terms, and, therefore, of smaller magnitude.

3.3.1 OOFDM modulation parameters

The next parameter values are used: a sampling rate f_{sam} equal to 4GHz, which gives us an electrical bandwidth BW equal to 2GHz. This electrical bandwidth is divided into 32 bins, which means a spacing frequency Δf equal to 62.5 MHz. From these 32 bins, $N = 26$ are used for the transmission of information data; 32-QAM is used as modulation format, and the electrical transmitter and receiver filters are square root raised cosine type. A cyclic pre/posfix of 50% the original OFDM symbol duration are appended to each OFDM symbol and a CL, defined as in Eq. (2.21), of 13.8dB is set. The laser operation point is 60mA. The default laser parameters used for the DML model are those shown in Table 3.1

The time waveform and the power spectral density of the laser driving modulating signal (with no bias offset) is shown in Fig. 3.2.

We can observe that the peak-to-peak driving current amplitude is approximately 10mA and the signal bandwidth is approximately 1.6GHz (26×62.5MHz=1.625GHz). For a back-to-back transmission, the received complex symbols, the defined error measurement Err_y and the intermodulation distortion are shown in Fig. 3.3.

Table 3.1: Laser Parameters

Parameter	Value
Cavity length, width and thickness	300, 2 and 0.2 μm
Confinement factor	0.3
Group refractive index	4
Linear gain coefficient	4 x 10^{-20} m^2
Nonlinear gain coefficient	3 x 10^{-23} m^3
Transparency carrier density	1.5 x 10^{24} m^{-3}
Nonradiative recombination rate	0.1 x 10^{8} s^{-1}
Biomolecular recombination coefficient	1.0 x 10^{-16} m^3
Auger recombination coefficient	3 x 10^{-41} m^6/s
Internal loss	2873 m^{-1}
Mirror loss	2990.9 m^{-1}
Coupling factor	1x10^{-5}
Optical efficiency	1
Facet reflectivities	0.3

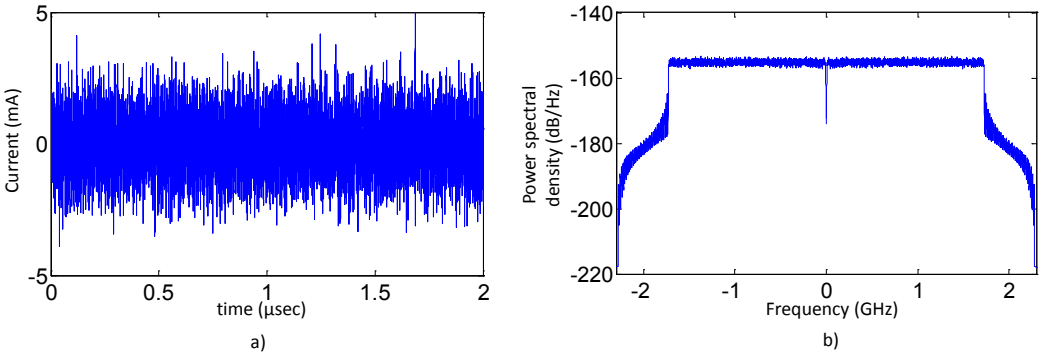

Figure 3.2: a) OFDM waveform and b) calculated power spectral density

From the constellation diagram, we can see that the received complex symbols are very close, and the error quantification through Err_y gives excellent results. Concretely, the relative error Err_y adopt values below 0.3%. For the indicated working conditions, the theoretical formulation is able to accurately describe the physic phenomena which affect the detected information signal. In Fig. 3.3(c) we have compared the IMD obtained from simulations and the analytical formulation, showing also very good agreements.

The same results have been obtained when the OOFDM signal propagates through a dispersive fiber span of 140km in order to check whether the theoretical model still gives accurate results.

As shown in Fig. 3.4 the obtained theory is able to accurately describe the effects of the accumulated dispersion: the complex symbols received obtained through the analytical formulation follow very precisely those obtained through simulations (Fig. 3.4(a)), giving values

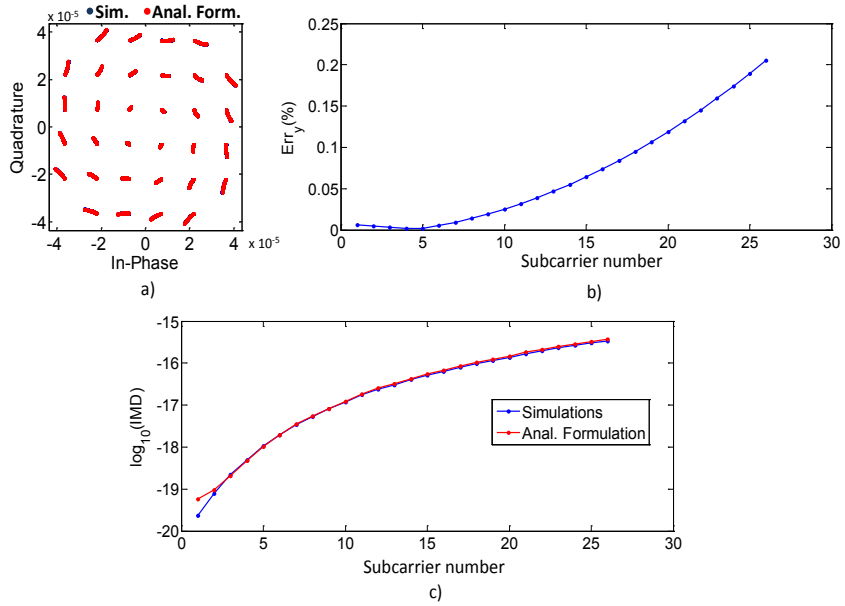

Figure 3.3: (a) Received symbols $Y_{rec_{sim}}$ (blue points) and $Y_{rec_{theo}}$ (red points), (b) relative error Err_y, and (c) IMD calculated from simulations and the analytical formulation.

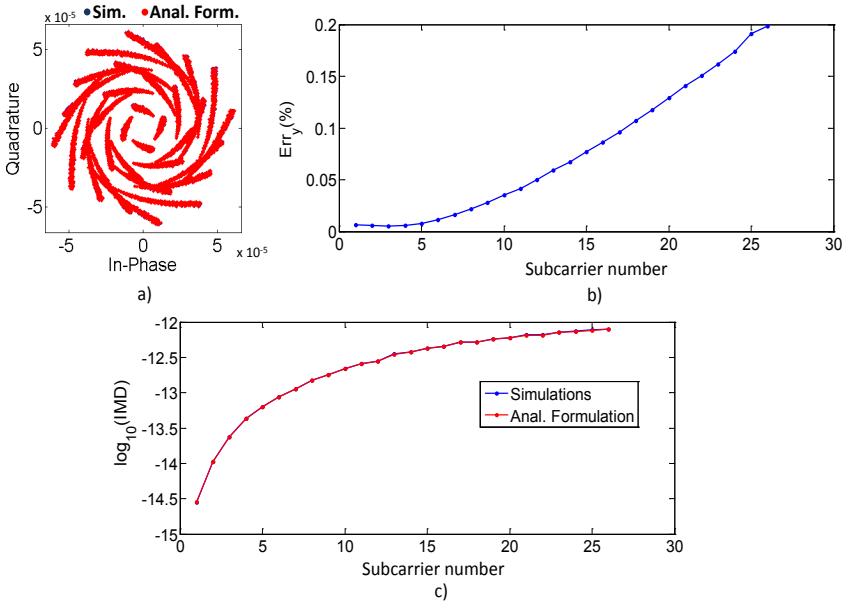

Figure 3.4: (a) $Y_{rec_{sim}}$ (blue points) and $Y_{rec_{theo}}$ (red points), (b) Err_y, and (c) IMD calculated from simulations and the analytical formulation.

of relative error Err_y below 0.2% (Fig. 3.4(b)), and providing an accurate description of the IMD (Fig. 3.4(c)).

3.3.1.1 *Variation of cyclic pre/post-fix lengths*

The setting of the prefix and postfix lengths to 50% the symbol duration yields to a waste of transmission capacity and such high values are not usual in literature on OOFDM systems. As we commented in Chapter 2, the purpose of the cyclic pre/postfix is to cancel out or mitigate the ISI and ICI effects due to the propagation of the signal through the communication channel. In Fig. 3.5 we show the relative error Err_y and the IMD values obtained when the length of the pre/postfix is equal to 1/4, 1/8 and 1/16 the OFDM symbol duration. The fiber length is equal to 140km.

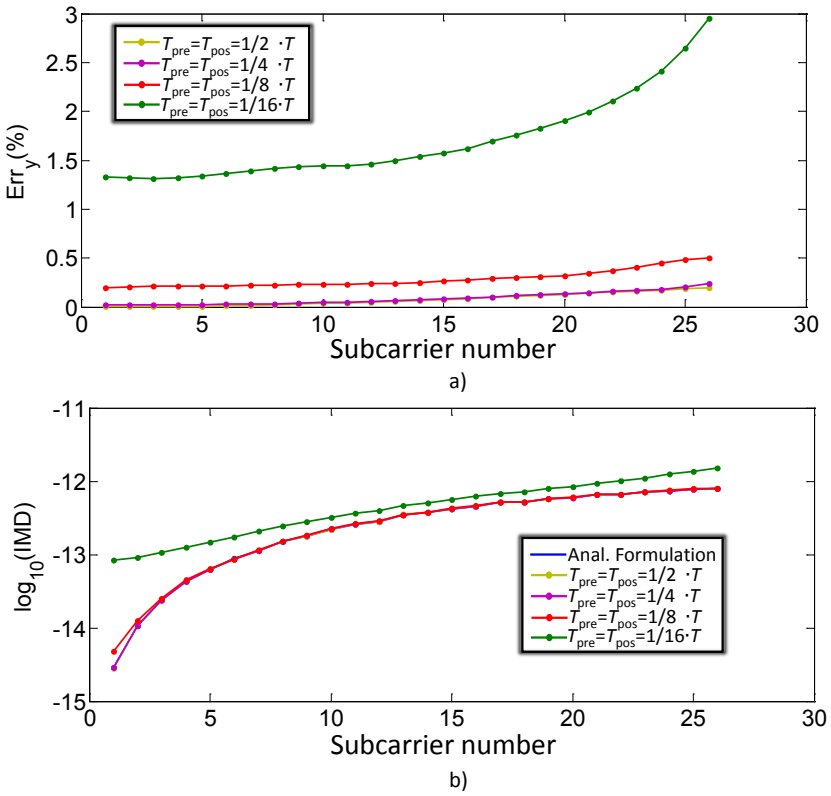

Figure 3.5: Results obtained for several cyclic extension length values. (a) relative error Err_y, (b) IMD calculated from simulations and the analytical formulation.

We can see from Fig. 3.5(a) that reasonably good matching is obtained for all values of $T_{pre} = T_{pos}$ shown, but the relative error increases rapidly when $T_{pre} = T_{pos}$ is changed from a value of $1/8 \cdot T$ to a value of $1/16 \cdot T$. In Fig. 3.5(b) we show the obtained IMD values, and we can observe that there is also a difference in the IMD values provided by the analytical model and those obtained through simulations when $T_{pre} = T_{pos} = 1/16 \cdot T$. We can conclude that the the analytical formulation gives accurate results provided that the impairment due to ISI and ICI effects is kept low. The reason for such discrepancy is simple: the ISI and ICI effects find their origin essentially in the finite duration of the OOFDM symbols sent and their mixture due to filtering effects, whilst the analytical treatment we have presented is based on the assumption that rf-waves in Eq. (3.8) time-infinite. In Chapter 4 expressions to account for the ISI and ICI effects will be presented.

3.3.1.2 Variation of the signal bandwidth

In order to achieve information rates beyond 10Gb/s with high order modulation formats able to provide spectral efficiencies larger than 2bits/Hz, signal bandwidths on the order of several gigahertzs must be used. The question is whether the analytical formulation still gives accurate results when the bandwidth of the electrical laser driving signal is increased. In Fig. 3.6 we show the values obtained for Err_y and IMD when the electrical bandwidth BW is changed. The fiber length is equal to 100km.

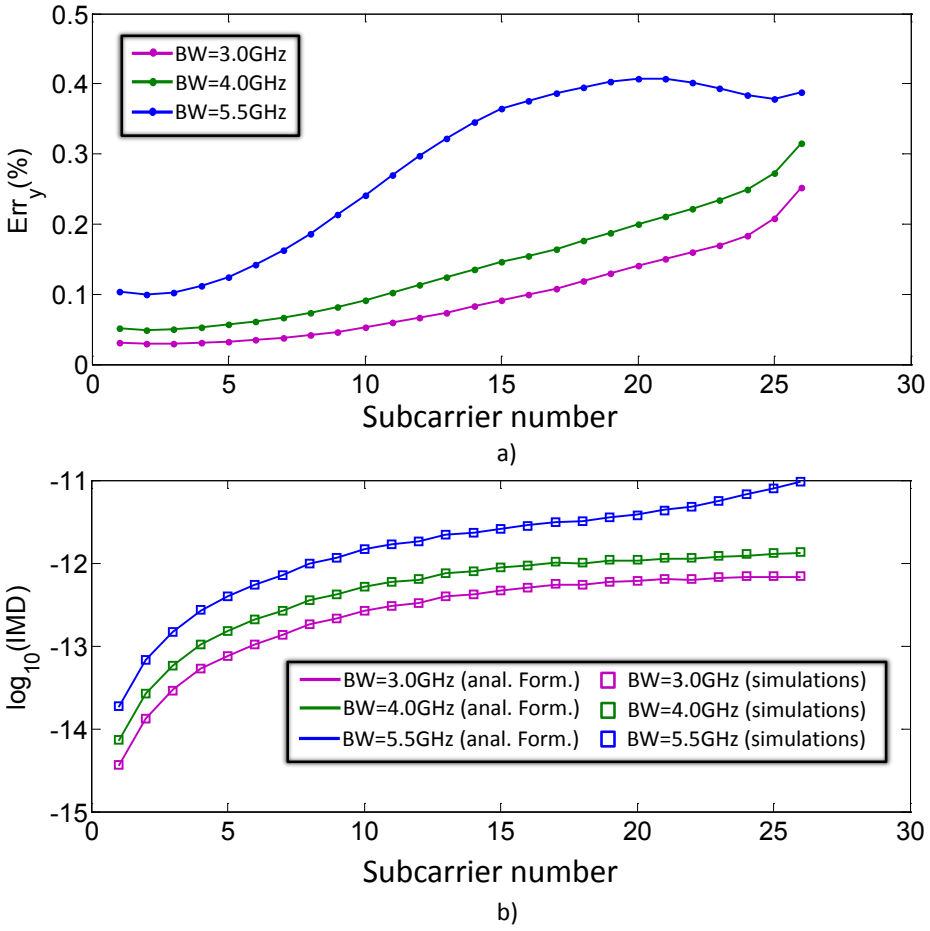

Figure 3.6: Results obtained for several electrical bandwidth values. (a) relative error Err_y, (c) IMD calculated from simulations and the analytical formulation.

Fig. 3.6 demonstrates that the theoretical treatment presented in this chapter includes the different filtering effects due to the direct modulation laser as a result of a higher occupied bandwidth and can be used for the study of broadband communications for the provision of high bit rates: the relative error for $BW = 5.5$GHz is still below 0.45%, and the nonlinear distortion matches very precisely with that obtained through simulations. The slight increase in the relative error observed when the electrical signal bandwidth is increased may be due to manifold reasons. At the view of the great matching obtained when the IMD is compared in Fig. 3.6(b), it may be due to some misalignment between the first order transfer functions predicted by the theory and those effectively obtained in simulations (e.g., due to inaccuracies

in the carrier and photon densities at steady state); stronger laser nonlinearities as result of a working operation closer to the laser resonance frequency may be also contributing to this error.

3.3.1.3 Variation of the number of subcarriers

The increase on the number of subcarriers on OFDM systems may yield advantageous features such as a lower % of the OFDM symbol duration dedicated to the transmission of the cyclic extensions. The number of subcarriers effectively used in literature is diverse, ranging from tens to thousands of them. Given the high computational load for the evaluation of the photocurrent expression and its exponential dependence with the number of subcarriers, the evaluation we carry out here is limited to 110. The results for different number of subcarriers are shown in Fig. 3.7 for an electrical bandwidth BW equal to 5.5GHz, a fiber length equal to 100km, a peak driving current equal to 5mA and a bias point equal to 60mA.

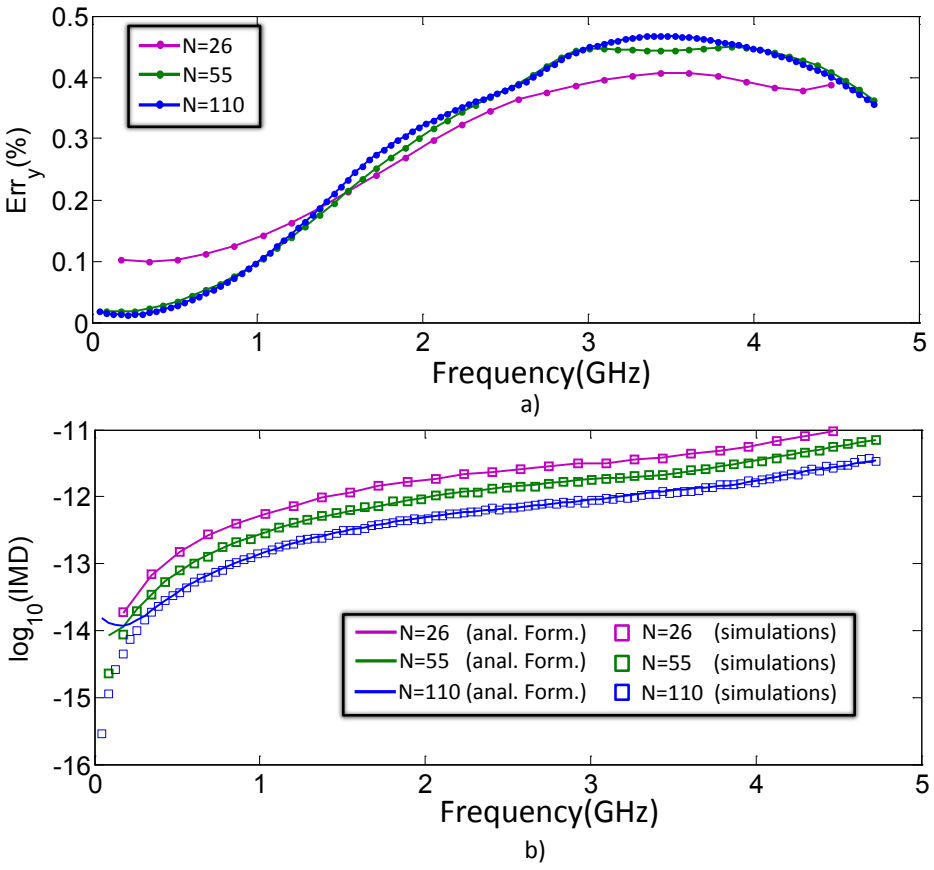

Figure 3.7: Results obtained for several values of number of subcarriers. (a) relative error Err_y, (c) IMD calculated from simulations and the analytical formulation.

From Fig. 3.7, it is demonstrated that the analytical formulation is also applicable to OOFDM signals with different number of subcarriers, since the theory calculates accurately the different intermodulation combinations. The relative error Err_y is smaller than

0.5% for the three cases shown, and the theoretically calculated nonlinear distortion matches perfectly with that calculated through simulations.

3.3.2 Laser operation

The choice of the laser operation point and its modulation depth is one of the most important factors which affect the performance of DM/DD OOFDM systems: it affects the laser modulation bandwidth, the dynamics of the intensity and phase modulations, the nonlinearities introduced by the laser and the nonlinearity as result of the signal propagation through the dispersive link.

In Fig. 3.8 we have changed the value of the laser driving signal amplitude swing Δi from 5mA to 15mA for a laser bias set to 60mA. The fiber length is equal to 100km and the electrical bandwidth is equal to 5.5GHz.

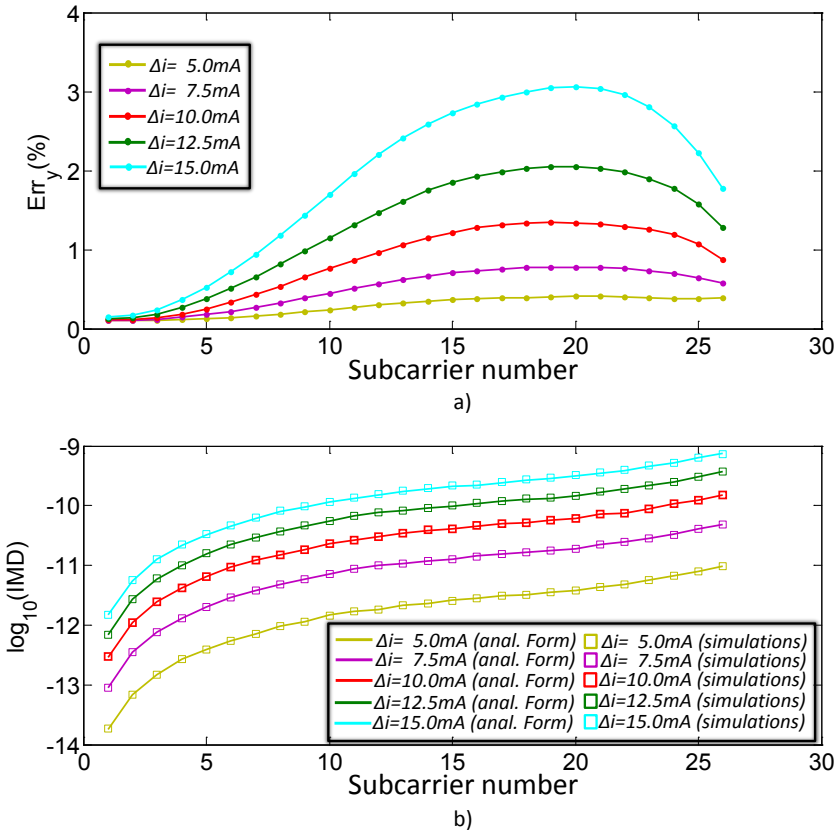

Figure 3.8: Results obtained for several values of the laser driving signal amplitude swing. (a) relative error Err_y, (c) IMD calculated from simulations and the analytical formulation.

It can be observed that the analytical model is rather sensitive to the variation of the laser modulation depth. However, even for the maximum value $\Delta i = 15mA$, the theory provided give us an error smaller than 4% as we can see from Fig. 3.8(a) and the nonlinear distortion is still precisely described (Fig. 3.8(b)). We can observe that the nonlinear distortion increases in the same quantity when Δi is doubled: there is 12dB of difference between the curves

corresponding to $\Delta i = 5mA$ and $\Delta i = 10mA$, which is exactly the same difference between the curves corresponding to $\Delta i = 7.5mA$ and $\Delta i = 15mA$.

A variation of the bias point induces a change of the dynamics of the laser because of the different value of the steady-state photon density value. In Fig. 3.9 the laser operation point is varied from 40mA to 100mA, the fiber length is equal to 100km and the electrical bandwidth is equal to 5.5GHz.

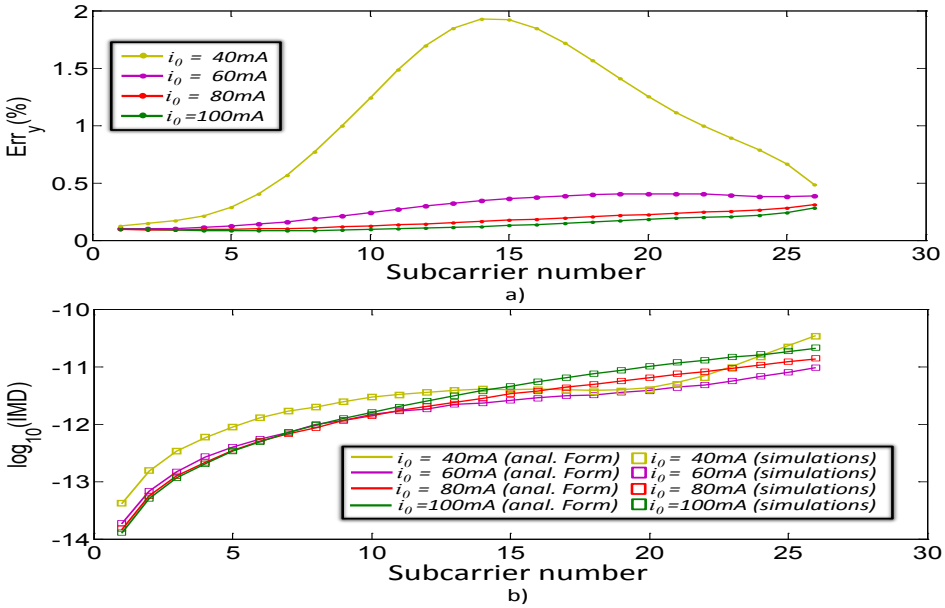

Figure 3.9: Results obtained for several laser operation points. (a) relative error Err_y, (c) IMD calculated from simulations and the analytical formulation.

As expected from the assumption on the small magnitude of the laser modulating signal i_m with respect to its average value i_0, the relative error increases substantially when the laser point is closer to the laser threshold. However, the consideration of the laser nonlinearity through the terms $P_{11}(t)$ and $P_2(t)$ in Eq. (3.9) and in the laser phase modulation through Eqs. (3.14)-(3.15) help to obtain still very low values of relative error (smaller than 2% for the conditions in Fig. 3.9(a)) and an accurate description of the nonlinear distortion (Fig. 3.9(b)).

3.3.3 Laser intrinsic parameters

The nonlinear gain coefficient ε_{nl}, the linewidth enhancement factor α and the photon lifetime τ_p are chosen as variable laser parameters to carry out the next comparison tests because of their influence on the laser intensity and phase modulations [78]. The nonlinear gain coefficient ε_{nl} models the gain compression which occurs at large current biases as result of the depletion in the number of carriers available. In Fig. 3.10 we show the results when ε_{nl} is varied from $7 \times 10^{-24} m^3$ to $1 \times 10^{-22} m^3$. The fiber length is equal to 100km and the electrical bandwidth is equal to 5.5GHz.

It is worthy to remark from Fig. 3.10(a) that low values of ε_{nl}, $7 \times 10^{-24} m^3$ and $1 \times 10^{-23} m^3$ yield higher values for the relative error, which seems to be contradictory to the fact that

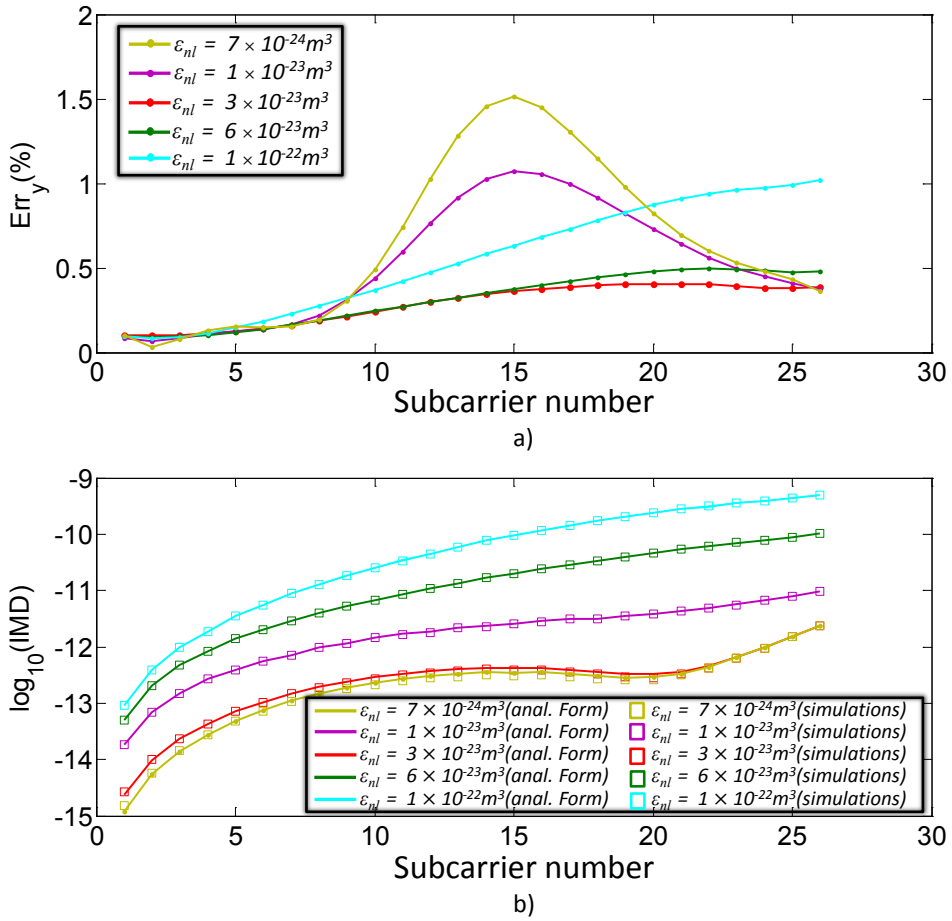

Figure 3.10: Results obtained for several values of nonlinear gain coefficient. (a) relative error Err_y, (c) IMD calculated from simulations and the analytical formulation.

smaller laser nonlinearity is introduced. However, as it is seen in the next sections, firstly, laser nonlinearity has not be necessarily and completely detrimental and can, up to a point, mitigate the nonlinear distortion due to the signal propagation through the dispersive fiber and subsequent intensity detection, and, secondly, ε_{nl} has a great influence on the laser phase modulation and, under particular cases, it may interfere with the detected component due to the laser intensity modulation causing dips in the transfer function of the communication system; these dips in the transfer function may be behind of this increase of the relative error. As result of higher values of $\varepsilon_{nl} = 1 \times 10^{-22} m^3$, laser nonlinearity increases and so the relative error Err_y (smaller than 1.5%), as it can be also observed in Fig. 3.10(b), where a great matching between the results obtained through the evaluation of the analytical formulation and those obtained through simulations is observed.

As Eq. (3.3) indicates, the laser frequency/phase modulation is directly proportional to the linewidth enhancement factor and has its origin in the carrier-induced index change. Since we can find in the market lasers with diverse values of α, it is interesting to check whether the analytical formulation provided is able to describe different laser phase modulation effects. In Fig. 3.11 we show the results obtained when α is varied in an OOFDM system with a fiber link of 100km and an electrical bandwidth of 5.5GHz. Note that we have included a

case in which α is negative for the sake of validation, though is not possible with a laser diode source,.

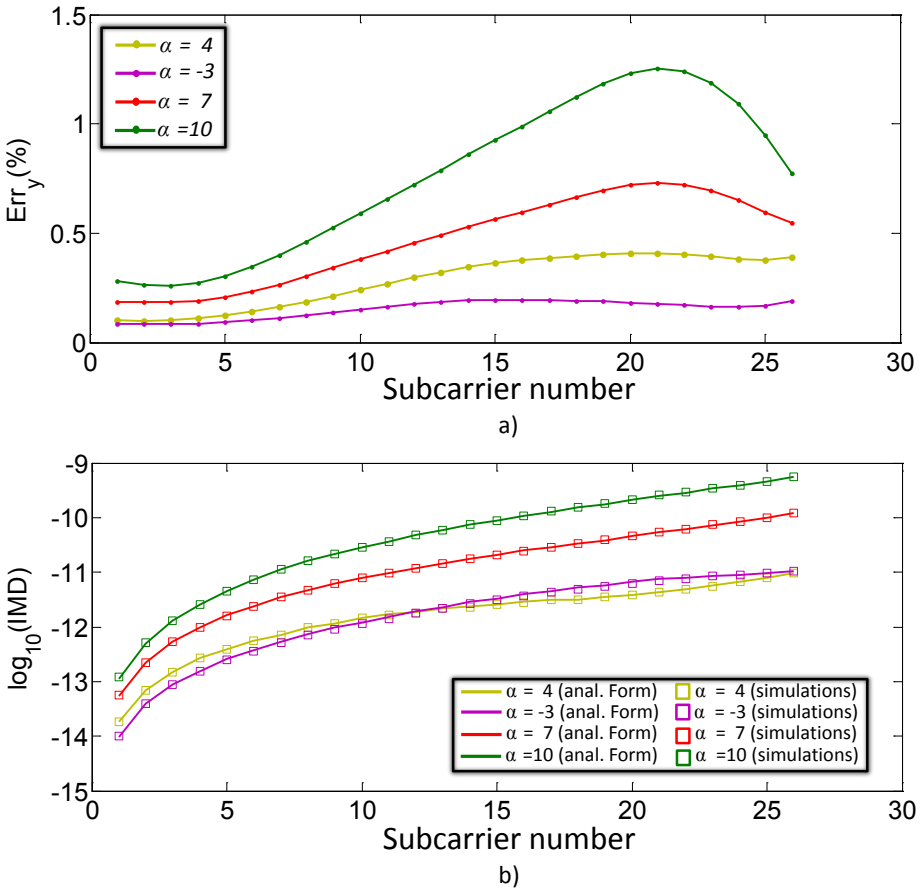

Figure 3.11: Results obtained for several values of linewidth enhancement factor. (a) relative error Err_y, (c) IMD calculated from simulations and the analytical formulation.

The results observed confirm the validity of the theory provided and values for Err_y smaller than 1.5% are obtained, as we can observe in Fig. 3.11(a), and an accurate description of the distortion due to the laser frequecy modulation, as we can observe in Fig. 3.11(b).

Finally, we evaluate the obtained analytical formulation when faced to changes in the value of the photon lifetime. In Fig. 3.12 we show the results obtained when the photon lifetime is varied from $\tau_p = 1.5319ps$ to $\tau_p = 2.2188ps$. As in the previous cases, the fiber length is equal to 100km, and the electrical bandwidth is equal to 5.5GHz.

The relative error Err_y is once again within acceptable values and increases just slightly with the decrease of τ_p. A smaller value for Err_y than 0.5% in Fig. 3.12(a), together with the accurate description of the nonlinear distortion observed in Fig. 3.12(b) lead us to conclude that the analytical formulation can be used to describe DM/DD OOFDM systems with variable laser intrinsic parameters.

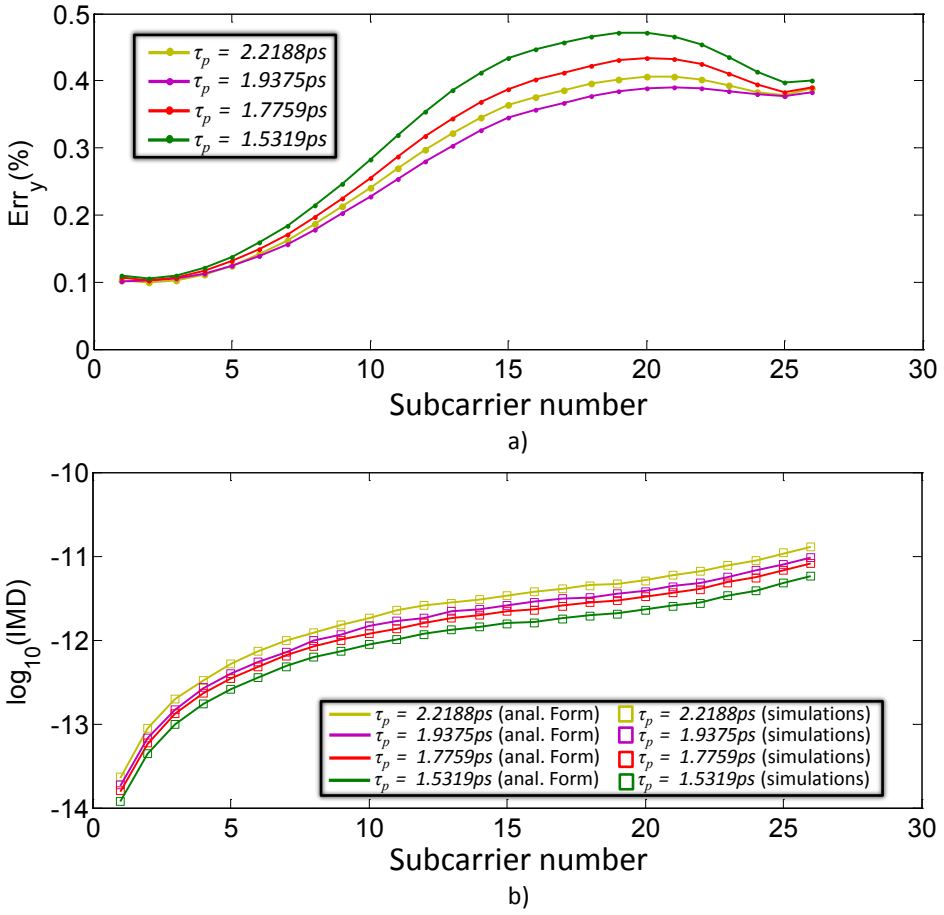

Figure 3.12: Results obtained for several values of photon lifetime. (a) relative error Err_y, (c) IMD calculated from simulations and the analytical formulation.

3.4 Intensity and Phase modulated optical signals

At the receiver end, after propagation through the dispersive fiber, the detected information signal is due to both the laser intensity and phase modulated signal components. Analytically, the detected signal can be determined by setting a certain index n_r, with $r \in [0, 1, ...N]$,

to 1, and the rest of indices to 0 in the expressions for $T0$ and $T1$, Eqs.(6.8)-(6.9):

$$\Big(T0|_{n_r=1}+T1|_{n_r=1}\Big)\cdot exp\Big(j\Big(\Omega_r\cdot t+(\varphi_{m_r}+\frac{\pi}{2})\Big)\Big)\approx\prod_{\substack{k=1\\k\neq r}}^{N}J_0(\mu_k)\cdot$$

$$\Big(\overbrace{P_0\cdot J_1(\mu_r)}^{PM}\cdot+\overbrace{p_r\cdot cos(\theta_r)}^{IM}\cdot\Big(-J_2(\mu_r)\cdot exp\big(j(2\varphi_{m_r}-\varphi_{p_r})\big)+J_0(\mu_r)\cdot exp\big(j\varphi_{p_r}\big)\Big)$$

$$+\sum_{\substack{k=1\\k\neq r}}^{N}\frac{p_k\cdot cos(\theta_k)}{J_0(\mu_k)}\cdot\Big(-J_1(\mu_r)\cdot J_1(\mu_k)\cdot exp\big(j(\varphi_{m_k}+\varphi_{m_r}-\varphi_{p_k})\big)+$$

$$J_1(\mu_r)\cdot J_{-1}(\mu_k)\cdot exp\big(-j(\varphi_{m_k}-\varphi_{m_r}-\varphi_{p_k})\big)\Big)\Big)exp\Big(j\Omega_r\cdot t\Big) \tag{3.29}$$

Both intensity and phase modulated components contribute to the transmission and detection of the information signal through their corresponding laser transfer functions, H_{p_1} and H_{ϕ_1}, respectively. Nevertheless, the phase modulated part of the transmitted optical signal has surprisingly not received much attention in research on DM/DD OOFDM systems. Moreover, as Eq. (3.29) indicates, this part of the detected signal is proportional to the average optical power P_0, and, thus, statements on the power inefficiency of IM OOFDM signals [72] must be, at least, refined when dealing with directly modulated schemes.

In Fig. 3.13 we show the calculated constellation diagrams of the received symbols from the evaluation of expressions for $T0|_{n_r=1}$ and $T1|_{n_r=1}$, as well as the comparison with the received symbols obtained from the simulations for the sake of validity. The results have been obtained for a back-to-back configuration and a fiber length equal to 100km. As expected,

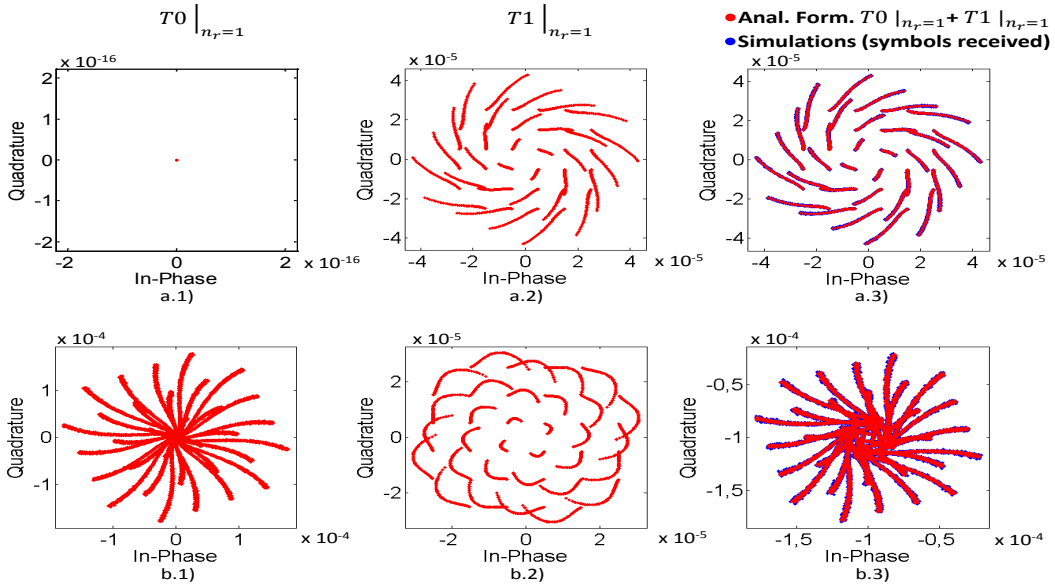

Figure 3.13: Constellation diagrams of the received symbols corresponding to $T0|_{n_r=1}$ and $T1|_{n_r=1}$ and $T0|_{n_r=1}+T1|_{n_r=1}$ for a) L=0km and b) L=100km.

for a back-to-back configuration, the symbols detected due to the laser phase modulation ($T0|_{n_r=1}$, Fig. 3.13(a.1)) are null, because no conversion to intensity due to the chromatic

dispersion has taken place. Therefore, the final symbols shown in Fig. 3.13(a.3)) are due only to the intensity modulated part of the optical signal, ($T1|_{n_r=1}$, Fig. 3.13(a.2)). However, once the 100km span of dispersive fiber is inserted, the information transmitted on the phase modulated part of the optical signal start to spring up, as observed in Fig. 3.13(b.1); this part of the detected information signal combines with that due to the laser intensity modulation Fig. 3.13(b.2), in order to finally produce the final detected symbols, Fig. 3.13(b.3).

We can observe from Fig. 3.13(b.1) and Fig. 3.13(b.2) that some of the symbols due to the laser phase modulation are even greater than those due to the laser intensity modulation, predictably those on highest frequencies because the accumulated chromatic dispersion effect is higher. Since the magnitude of the part of the detected optical signal due to the laser phase modulation can be of the same order than that due to the intensity modulation, it is straightforward to wonder on how these two signal detected terms are combined: if the phase difference between them is null, they are summed up “in phase", and, on the contrary, if the phase difference is π rads, they cancel one to another. It is clear that the system performance is better when the former situation occurs.

The phase difference between the intensity and phase modulated parts of the optical signal depend on the intrinsic laser parameters involved in the optical modulation and the sign of the dispersion parameter. In Fig. 3.14, we show the constellation diagrams of the calculated transfer functions corresponding to the intensity and phase modulated parts of the optical signal and the total transfer function when the sign of D and the value of the nonlinear gain coefficient ε_{nl} are changed.

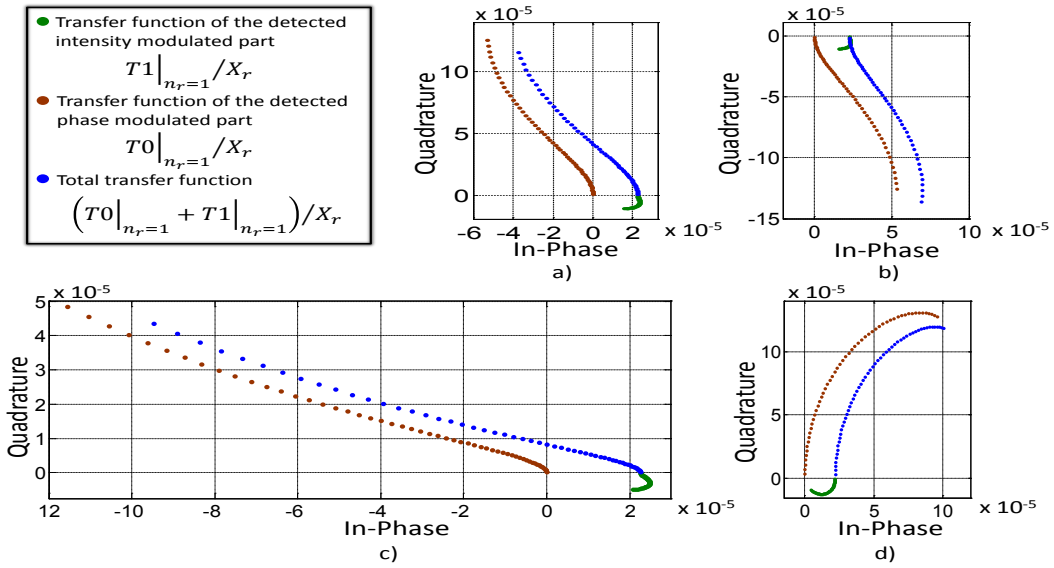

Figure 3.14: Constellation diagrams of the transfer functions of the detected intensity and phase modulated parts of the optical signal, and the total transfer function for a fiber length equal to 100km. a) $D = 17 \times 10^{-6} ps/(km \cdot nm)$ and $\varepsilon_{nl} = 3 \times 10^{-23} m^3$, b) $D = -17 \times 10^{-6} ps/(km \cdot nm)$ and $\varepsilon_{nl} = 3 \times 10^{-23} m^3$, c) $D = 17 \times 10^{-6} ps/(km \cdot nm)$ and $\varepsilon_{nl} = 7 \times 10^{-24} m^3$, and d) $D = 17 \times 10^{-6} ps/(km \cdot nm)$ and $\varepsilon_{nl} = 1 \times 10^{-22} m^3$.

As we can see from Fig. 3.14, the magnitude of the transfer function due to the laser phase modulation gets higher values than that due to the laser intensity modulation as the frequency increases, whilst at low frequencies the total transfer function is mainly due to the

intensity modulated part of the optical signal. The first case, shown in Fig. 3.14(a), corresponds to that with a typical value for the nonlinear gain coefficient and a dispersive fiber with normal dispersion. Except for the lowest frequencies, the magnitude of the resulting total transfer function is slightly smaller than that due to the laser phase modulation. Just the opposite occurs for a dispersive fiber with anomalous dispersion (Fig. 3.14(b)), where the values due to laser phase modulation rotates π and get similar phase values to those due to $T1|_{n_r=1}$, resulting in a constructive interference and thus in a higher total transfer function. As we can see from Fig. 3.14(c) and Fig. 3.14(d) the nonlinear gain coefficient ε_{nl} has a great influence on the phase difference between both kind of detected signal components. For low values, Fig. 3.14(c), their phases are approximately opposite, which may produce a significant fading at determined frequencies. A more favourable situation seems to occur in Fig. 3.14(d) where both components are added more constructively; however, a higher value of ε_{nl} leads to higher laser nonlinearities, and, thus, a proper choice of its value is not conditioned only by the first order/linear effects shown in Fig. 3.14.

In order to see more clearly the effects of the phase mismatch between $T0|_{n_r=1}$ and $T1|_{n_r=1}$, we calculate the next power ratio:

$$\eta_{\mathrm{DML},\beta 2}(r) = \frac{\left|T0|_{n_r=1} + T1|_{n_r=1}\right|^2}{\left|T0|_{n_r=1}\right|^2 + \left|T1|_{n_r=1}\right|^2 + 2\left|T0|_{n_r=1}\right| \cdot \left|T1|_{n_r=1}\right|}, \; r = 1, 2...N \tag{3.30}$$

That is, $\eta_{\mathrm{DML},\beta 2}$ is the ratio between the actual signal power at the rth subcarrier and that obtained in the case $T0|_{n_r=1}$ and $T1|_{n_r=1}$ are summed up with the same phase. In Fig. 3.15 we show the obtained ratio $\eta_{\mathrm{DML},\beta 2}$ for the four different cases. It is clear that the the higher

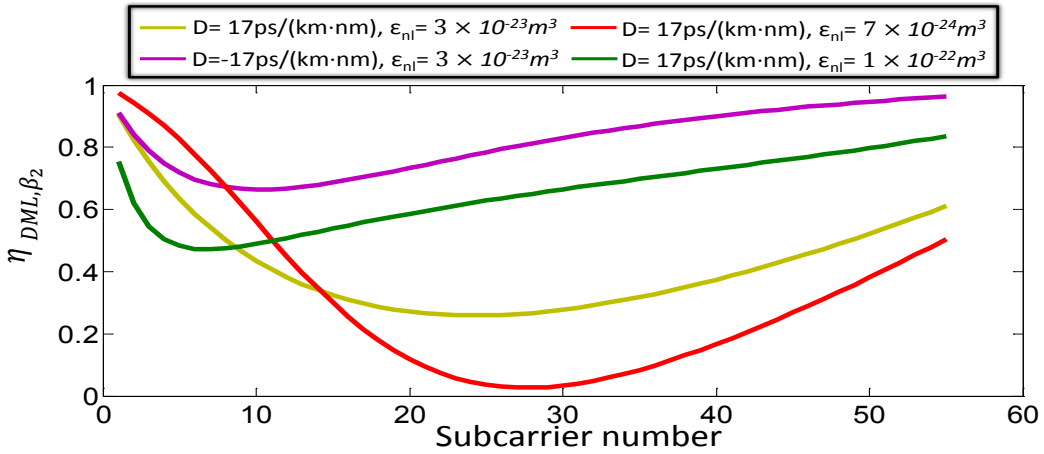

Figure 3.15: Power ratio $\eta_{\mathrm{DML},\beta 2}(r)$ for a fiber length equal to 100km.

the value of $\eta_{\mathrm{DML},\beta 2}$, higher is the power efficiency of the signal information transmission. The most advantageous situation occurs for the fiber with anomalous dispersion; these high values of efficiency explain the improvement observed in previous works when fibers with negative dispersion are employed [73]. It is also worthy to remark the small values of $\eta_{\mathrm{DML},\beta 2}$ obtained for $\varepsilon_{nl} = 7 \times 10^{-24}$: values smaller than 0.2 are obtained within the frequency band $\left[18 \times \Delta f = 1.54GHz,\ 41 \times \Delta f = 3.52GHz\right]$, which severely affect the final system peformance.

3.5 Carrier to interference power ratio and nonlinearity description

The analytical model presented in Section 3.2 allows to extend Eq. (2.15) in order to take into account the nonlinear distortion which impairs the received complex symbol $Y[r]$:

$$Y[r] = H[r] \cdot X[r] + I[r],\ r = 1, ...N \tag{3.31}$$

where $H[r]$ and $I[r]$ represent the channel transfer function and interference components of the r-th output of the receiver FFT.

Nonlinear distortion due to the direct modulation of the laser has been identified as one of the limiting system performance factors in DM/DD OOFDM systems [74]. In the context of wireless OFDM communications systems, nonlinear distortion effects have been subject of extensive study due to the significant impact on system performance [79, 80]. For the correct design of nonlinear distortion impairment mitigation techniques (pre- and post-compensation strategies) in optical communications, we need to know the mechanisms that generate the nonlinear distortion, as well as its power in comparison with that of the signal. The analytical formulation here presented is an useful tool for such purpose, since it allows us to isolate the different sources of nonlinear distortion and get a more detailed comprehension of them than by merely observing the compound effect into the detected signal.

In our model, at the absence of receiver noise, the only effect which impairs significantly the signal is the nonlinear distortion due to the DML and the subsequent propagation of the chirped signal through the optical fiber, since ISI & ICI effects are overcome with a proper choice of the cyclic prefix length and clipping noise is negligible. Thus, $I[r]$ is appropriately characterized by Eqs. (3.19)-(6.13). The system performance can be then characterized through the carrier-to-interference power ratio (CIPR):

$$CIPR(r) = \frac{|H[r]|^2}{\langle |I[r]|^2 \rangle},\ r = 1, 2, ...N \tag{3.32}$$

assuming that $\sigma_x^2 = 1$. A reasonable estimation of $CIPR(r)$ is given by:

$$CIPR(r) = \tag{3.33}$$

$$\frac{\left| T0|_{n_r=1} + T1|_{n_r=1} \right|^2}{|T0|_{n=2}+T1|_{n=2}+T2|_{n=2}+T3|_{n=2}+T4|_{n=2}+T5|_{n=2}+T0|_{n=3}+T1|_{n=3}|^2} \tag{3.34}$$

In Fig. 3.16 we show the estimated CIPR, together with that obtained through simulation with the aim of validation. Unlike simulations, the analytical formulation also allows us to determine the ratio between the power information signal and isolated interfering terms, which are determined by imposing different combinations for the indexes n_1, n_2,...n_N, as explained in Section 3.2. The laser parameters used for the DML model are those shown in Table 3.1 whilst f_{sam}=11GHz (BW=5.5GHz), FS=128, N=55, i_0=60mA and Δi=10mA.

We can observe that the total $CIPR$ of both the simulated and theoretical models agree for $L = 20km$ and $L = 100km$. For the studied conditions, the second order intermodulation is the dominant source of nonlinear distortion, whose determination is done by imposing $n_p = 1$, $n_q = \pm 1$, $n_k = 0$, p, q and $k \in [1, 2, ...N]$ with $l > p$, $k \neq l$ and $k \neq p$. We can observe that for $L = 20km$ in Fig. 3.16(a), most of the distortion comes from $T1$, and more concretely, when it is particularized to $n_p = 1$, $n_q = -1$. As the frequency increases, $T1$

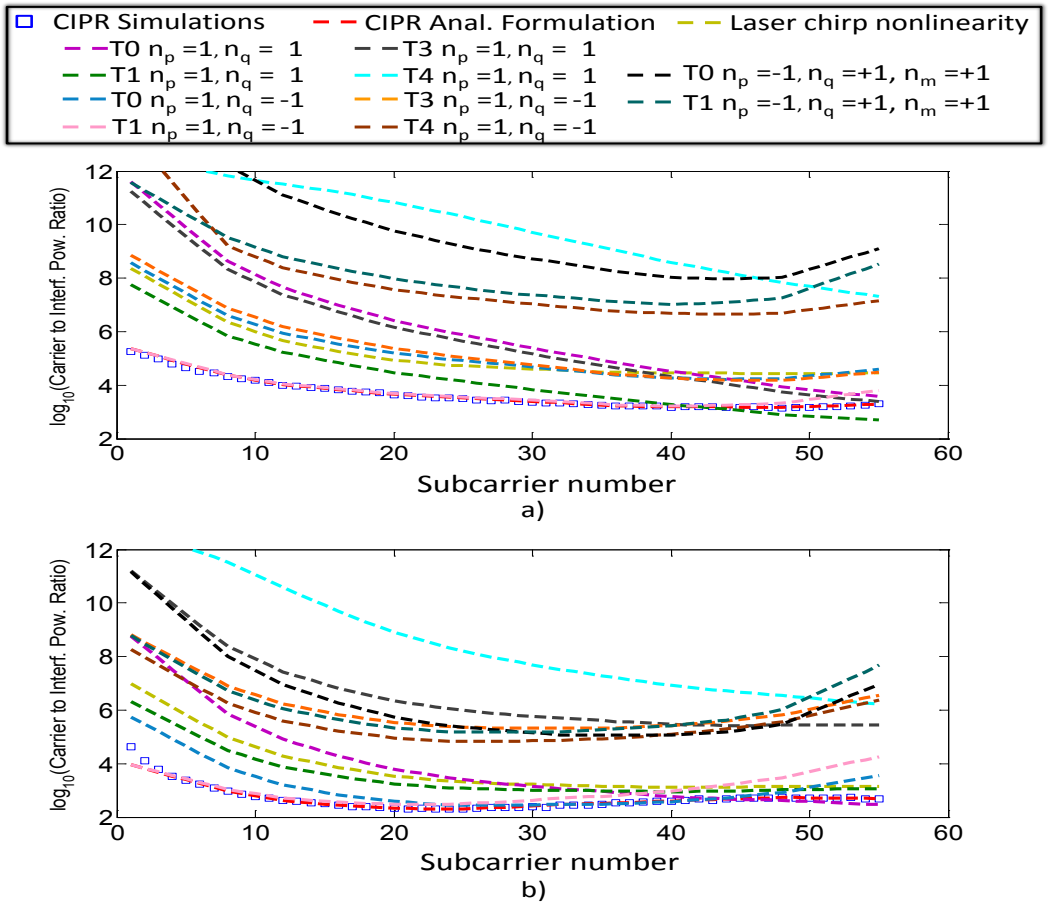

Figure 3.16: Comparison of the carrier to interference power ratio obtained through simulation of a DM/DD OOFDM system and that obtained through evaluation of Eqs. (6.8)-(6.13), power ratio between carrier and different interfering terms. (a) L=20km, and (b) L=100km.

with $n_p = 1$, $n_q = 1$ becomes more detrimental, as expected because of the higher number of nonlinear products of this type which fall on the signal subcarriers.

We can also observe that as the distance increases to $L = 100km$, the distortion imposed by $T0$ increases, which is due exclusively to the beat between different phase-to-intensity converted components. The high power allocated on the optical carrier (given by a in Eq. (3.13)), yields a significant value of $T0$, and thus the interplay between laser phase modulation and chromatic dispersion may degrade considerably the signal quality.

The nonlinear distortion caused by terms $T3$, $T4$ as well as that caused by the laser chirp nonlinearities are of secondary importance with respect to the system performance limitation, since their corresponding ratios are several dBs higher than those corresponding to $T0$ and $T1$. Similarly with the third order intermodulation distortion, we show the product calculated by imposing n_p=-1, n_q=1 n_m=1 in the expressions for $T0$ and $T1$; thus, for baseband DM/DD OOFDM systems, the limitation imposed by second order distortion should be in a first step overcome to enhance its system performance, and mainly that coming from the transmission of the optical carrier and the information signal.

Finally, note that the total $CIPR$ gets value higher than 20dB, but, even with so high values, nonlinear distortion affects the bit-error-rate when high order modulation formats (16-QAM, 32-QAM,..512QAM) are employed, since the detected information symbols at the receiver end side must be weakly impaired in order to correctly decide which symbol has been transmitted.

3.6 Summary

In this chapter an analytical model to describe the effects of laser direct modulation and chromatic dispersion in an DM/DD OOFDM system has been reported. The optical signal at the laser output was analytically characterized by using an accurate second order perturbative analysis of the rate equations which describe the photon and carrier densities as well as the output optical phase.

The results obtained by the evaluation of the analytical formulation have been validated by comparing them with commercial software simulated results and have demonstrated that the analytical formulation offers a great versatility and accuracy for the description of OOFDM systems with different transmission conditions. In order to demonstrate this point, determining parameters of the generation of the laser driving OFDM signal, the laser operation as well as the dynamics of the optical modulation have been varied. It has been found that the analytical formulation is able to account for the main effects in DM/DD OOFDM systems, providing us huge quantity for their characterization and potential technique for their improvement.

We have observed that the detected information signal is due to two linear terms which come from the laser intensity and phase modulations, being the latter, under particular conditions, of higher magnitude than the former. Their phase difference, determined by the laser modulation and the propagation of the signal through the dispersive fiber, affect significantly the power efficiency of the system and, therefore, determines the system performance. The proposed analytical formulation also gives us an accurate description of the nonlinear distortion which impairs the detected information signal through the separation of the different interfering terms, which makes possible their analysis and penalty quantification as well as a better design of techniques for its overcoming. The results reported in this chapter have demonstrated that second order intermodulation distortion caused by the beat between the information signal and phase-to-intensity converted components have an important degradation effect on the quality signal. For the studied conditions, values of CIPR slightly higher than 20dB have been obtained, which are unacceptable when high modulation formats are employed at the aim of increasing the transmission spectral efficiency. As we will see, both the mixing of the laser intensity and phase modulate parts of the optical signal and the nonlinear distortion are focus of study in the next chapters when optimization of the system is performed, a nonlinear distortion mitigation technique is proposed, or optical filtering is proposed for the enhancement of the information signal term upon photodetection. Additional effects, such as the effects of ISI & ICI due to the transmitter, channel and receiver filtering effects, as well as clipping of the signal at the transmitter must also be included to get a better description of the DM/DD OOFDM system.

Chapter 4

Design of DM/DD OOFDM Systems

4.1 Introduction

In Chapter 3 we provided an analytical formulation aimed to describe the dynamics of a DM/DD OOFDM signal which passes through an optical dispersive fiber. However, OFDM is a technique which heavily relies on signal processing at both end-sides of the communication system, transmitter and receiver. For this reason, it is of primary importance to pay attention to some of the main parameters which affect the received signal quality and the proposal of analytical models which account for the end-to-end performance of OOFDM systems.

DML OOFDM signals present several characteristics which make their understanding and design rather challenging. In particular, these demanding characteristics have their origin in its multi-carrier nature and the random amplitude of the electrical OFDM signal generated at the transmitter. The literature on wireless OFDM systems aimed to study the influence of diverse system parameters is more than extensive (see, e.g., [81–83]), but, due to the relatively short period of time since OFDM started to attract attention for its use in optical communications, the research on OOFDM systems is not so rich.

At the aim of giving an analytical description more comprehensive, we study in this chapter two important design parameters: the clipping level (Chapter 2, Eq. (2.21)) used when the generated electrical OFDM signal is deliberately clipped at the transmitter, and the length of the cyclic extensions added to avoid ISI and the loss of the orthogonality between subcarriers due to filtering effects. Moreover, simplified expressions of the nonlinear distortion in DM/DD OOFDM systems are also provided. The interest of such simplified expressions is motivated by the greater understanding we can get from a clearer mathematical formulation and the possibility of exploring the capabilities and pushing further the potentiality of

DM/DD OOFDM systems. Moreover, potential future equalization and nonlinear cancellation techniques may take advantage of such expressions, as it is demonstrated in Chapter 5.

4.2 OOFDM system description

The OOFDM system object of study in this Chapter is depicted in Fig. 4.1.

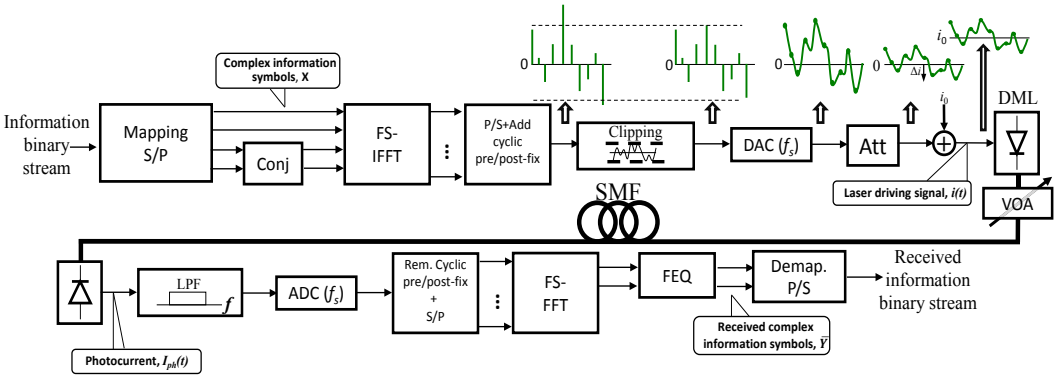

S/P: serial to parallel; **P/S**: parallel to serial; **(I)FFT**: (Inverse) fast Fourier transform; **DAC**: digital-to-analog converter; **ADC**: analog-to-digital converter
Att: Attenuator; **VOA**: Variable optical attenuator; **SMF**: single mode fiber; **DML**: directly modulated laser;
LPF: low-pass filter; **FEQ**: frequency domain equalization

Figure 4.1: Schematic illustration of the OOFDM system.

As we remember, the IFFT operation and subsequent digital-to-analog conversion maps the incoming block of data X_1, X_2,...X_N into a comb of squally spaced tones. After propering operations at the receiver, analog-to-digital conversion and FFT reverse these operations and the information symbols X_1, X_2,...X_N are detected.

The amplitude of the discrete OFDM signal after the transmitter IFFT is limited with a hard-clipping, which operation is described by:

$$x[n] = \begin{cases} x[n], \text{ if } |x[n]| < A_{Clip} \\ A{\cdot}exp(j{\cdot}\varphi_{x[n]}), \text{ otherwise} \end{cases} \tag{4.1}$$

where the amplitude value A_{Clip} is related to the clipping level CL by $A_{Clip} = \sqrt{CL \cdot \langle |x[n]|^2 \rangle}$. At the transmitter side each OFDM symbol is also cyclically extended by copying a certain number of samples of the original OFDM symbol and appendying them to the beginning and end.

As we remember from Chapters 2 and 3, the received complex symbol at the r-th subcarrier, $Y[r]$, can be then expressed as:

$$Y[r] = H[r] \cdot X[r] + N[r] + I[r], \ r = 1, ...N \tag{4.2}$$

where $X[r]$, $H[r]$, $N[r]$ and $I[r]$ represent the information symbol, the channel transfer function coefficient, the noise and interference components of the r-th output of the receiver FFT. For the particular case studied in this work, we have included in the definition of $H[r]$, $N[r]$ and $I[r]$ the next factors:

- $H[r]$: determined by the electronic stage of the transmitter and receiver, as well as the optical channel.
- $\sigma_N^2[r]$: the noise due to clipping, that due to ISI & ICI effects and receiver thermal and shot noises are included in this magnitude.
- $I[r]$: the nonlinear distortion caused by laser nonlinearities, the chromatic dispersion and the laser chirp, as described in Chapter 3.

In the following, we give a mathematical description of each of these effects in order to finally quantify the performance through Eq. (4.2).

4.3 Analytical formulation

4.3.1 Transfer function

A simple expression of the transfer function for a dispersive link when a directly-modulated signal is propagated and detected by means of a PIN detector was derived in Chapter 3, Eq. (3.29). By approximating the Bessel functions of first kind involved in Eq. (3.29) using their Maclaurin series expansion:

$$J_n(\mu) = \begin{cases} 1 & \text{if } n = 0 \\ \frac{n\mu}{2} & \text{if } n = \pm 1 \end{cases} \tag{4.3}$$

and neglecting contributions of higher order, the contributions due to the laser phase and intensity modulations can be expressed as:

$$T0|_{n_r=1} = 2jP_0 \cdot H_{\phi_1}(\Omega_r) \cdot sin(\theta_r) \cdot i_r \cdot e^{j\varphi_{i_r}} \tag{4.4}$$

$$T1|_{n_r=1} = H_{p_1}(\Omega_r) \cdot cos(\theta_r) \cdot i_r \cdot e^{j\varphi_{i_r}} \tag{4.5}$$

and, thus, the transfer function from the laser input to the PIN output (H_o in Fig. 4.1) is given by:

$$H_0(\Omega_r) = 2jP_0 \cdot H_{\phi_1}(\Omega_r) \cdot sin(\theta_r) + H_{p_1}(\Omega_r) \cdot cos(\theta_r) \tag{4.6}$$

In order to find the expression for the transfer function which describes the end-to-end filtering effects, $H_e(\Omega_r)$, the filtering of the electronic stages at the transmitter and receiver sides are included:

$$H_e(\Omega_r) = H_{trx}(\Omega_r) \cdot H_0(\Omega_r) \cdot H_{rx}(\Omega_r) \tag{4.7}$$

However, we assume that the filtering effects are negligible and we account only for a scaling factor at the transmitter. Therefore, the discrete transfer function from the input of the DAC at transmitter to the output of the ADC at the receiver is given by:

$$H_e(e^{j\Omega_r}) = m \cdot H_0(e^{j\Omega_r}) \tag{4.8}$$

The IFFT-to-FFT transfer function, $H[r]$ in Eq. (4.2) can be then approximated by:

$$H[r] = m \cdot \left(2jP_0 \cdot H_{\phi_1}(\Omega_r) \cdot sin(\theta_r) + H_{p_1}(\Omega_r) \cdot cos(\theta_r)\right) \tag{4.9}$$

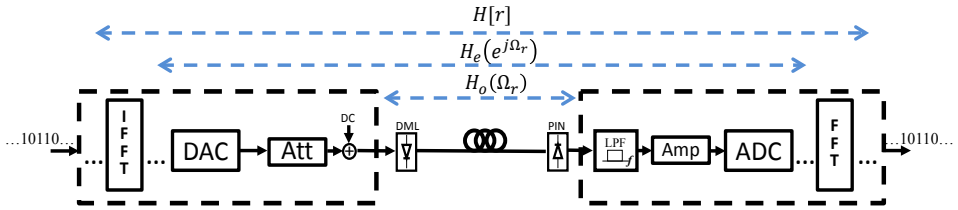

Figure 4.2: Schematic illustration of the OOFDM system showing the linear transfer functions $H_0(\Omega)$, $H_e(e^{j\Omega})$ and $H[r]$, $r = 1, ..., N$.

4.3.2 Clipping

After arranging the QAM symbols X_1, X_2,...X_N with Hermitian symmetry at the IFFT input, the signal at the input of the clipping device is given by:

$$x[n] = 2Re\left\{\sum_{k=1}^{N} X_k \cdot exp\left(j \cdot 2\pi \cdot k \cdot \frac{n}{FS}\right)\right\} \tag{4.10}$$

where $Re\{\cdot\}$ stands for the real part of a complex quantity. As the central limit theorem, for a sufficiently high value of N, $x[n]$ follows a Gaussian distribution with zero mean ($\langle X_k \rangle = 0$) and variance equal to $2N\sigma_x^2$ ($\sigma_x^2 = \langle |X_k|^2 \rangle$).

The Bussgang's theorem [84] can be used to analytically describe the memoryless nonlinear operation performed by the clipping device, and the output signal can be expressed as the sum of an undistorted signal part and a noisy term:

$$x_{clip}[n] = \chi \cdot x[n] + n_{\bar{p},clip}[n] \tag{4.11}$$

where the attenuation constant χ is given by [60]:

$$\chi = 1 - erfc\left(\sqrt{CL/2}\right) \tag{4.12}$$

and the noisy term $n_{\bar{p},clip}[n]$ is not correlated to the undistorted signal $x[n]$ and $erfc(\cdot)$ is the complementary error function. Note that we have included the subindex $\bar{p}$ in the noisy term $n_{\bar{p},clip}[n]$; such notation is explained later.

In order to evaluate the effects of the clipping noise $n_{\bar{p},clip}[n]$ at the receiver, the noise power at the kth subcarrier is calculated as:

$$\sigma^2_{\bar{p},clip}[k] = n_{\bar{p},clip}(e^{j\Omega_k}) \cdot |H_e(e^{j\Omega_k})|^2 \cdot \Delta\Omega \tag{4.13}$$

where $H_e(e^{j\Omega})$ is given in Eq. (4.8), $\Delta\Omega$ is the angular frequency separation between the OFDM subcarriers, and $n_{\bar{p},clip}(e^{j\Omega_k})$ is the PSD of clipping noise $n_{\bar{p},clip}[n]$, which can be calculated from its autocorrelation. In [85], an expression for the autocorrelation of the clipped signal is given:

$$\begin{aligned} R_{\bar{p},x_{clip}}[\varsigma] &= \langle x_{clip}[n] \cdot x_{clip}[n+\varsigma] \rangle = R_x[0]\left(\chi^2 \cdot R_x[\varsigma] + \sum_{q=2,4,6...}^{\infty} C_q \cdot \left(r_x[\varsigma]\right)^{q+1}\right) \\ &= R_x[0]\left(\chi^2 \cdot R_x[\varsigma] + R_{\bar{p},clip}[\varsigma]\right) \end{aligned} \tag{4.14}$$

where the coefficients C_q are:

$$C_q = \frac{4 \cdot H_{q-1}^2\left(\sqrt{CL/2}\right)}{\pi \cdot 2^q \cdot (q+1)!} \tag{4.15}$$

being H_q an Hermite polynomial of order q [76], $R_x[\varsigma]$ is the autocorrelation of the discrete OFDM signal, Eq. (4.10), $r_x[\varsigma]$ is the autocorrelation coefficient ($r_x[\varsigma] = R_x[\varsigma]/R_x[0]$) and $R_{\bar{p},clip}[\varsigma]$ is the autocorrelation of the clipping noise. Now the PSD of $n_{\bar{p},clip}[n]$ can be calculated as:

$$n_{\bar{p},clip}(e^{j\Omega}) = R_x[0] \cdot \sum_{q=2,4,6\ldots}^{\infty} C_q \cdot \left(\underbrace{r_x(e^{j\Omega})}_{1} * \cdots * \underbrace{r_x(e^{j\Omega})}_{q+1}\right) \tag{4.16}$$

where

$$r_x[\varsigma] \overset{\text{FT}}{\longleftrightarrow} r_x(e^{j\Omega}) \tag{4.17}$$

For the computation of $n_{\bar{p},clip}(e^{j\Omega})$, it can be assumed that $r_x(e^{j\Omega})$ has a rectangular shape, as depicted in Fig. 4.3(a). Note that the $q+1$ multiplication in Eq. (4.14) becomes a $q+1$ fold convolution in the frequency domain, as shown in Fig. 4.3(b).

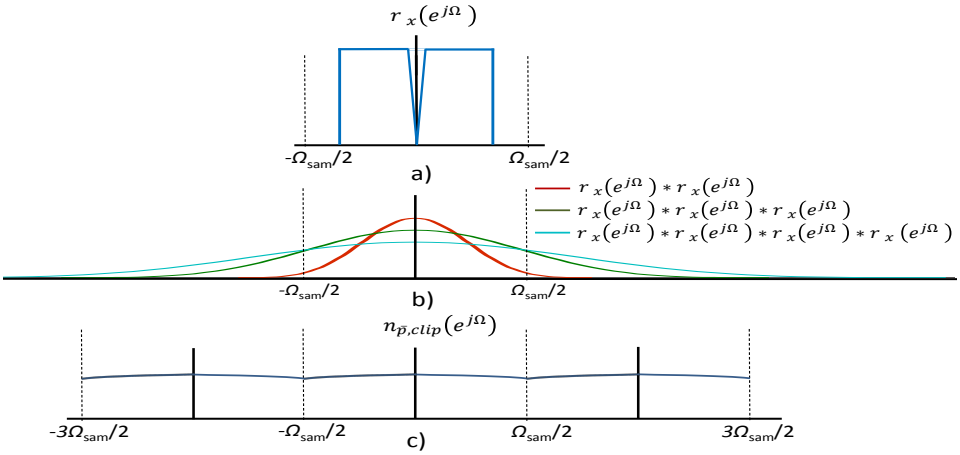

Figure 4.3: a) PSD of the OFDM input signal, b) two, three and four-fold convolution of the input signal's PSD, c) PSD of clipping noise.

The $q+1$ fold convolutions leads to the smearing of clipping noise with frequency, which spreads over a wider bandwidth than the signal, causing aliasing on the discrete signal $x[n] = x(n \cdot T_{sam})$, being T_{sam} the sampling period, Fig. 4.3(c).

In Fig. 4.4 we compare the normalized power spectral density of the clipping noise for different values of CL and for $N = 110$ and $N = 60$, being $FS = 256$.

As expected, the smaller the value of CL, higher is the clipping noise introduced, and its spectral density ranges from values around -40dB/Hz for $CL = 10$dB to values around -20dB/Hz for $CL = 5$dB. We observe from Fig. 4.4 that comparisons between the PSDs obtained through simulations and that obtained through the evaluation of Eq. (4.16) are in good agreement. When no-oversampling ($FS/(2N+1) = 1$) or a sufficiently small value is used (Fig. 4.4(a)), most of clipping noise power falls into the signal band, and the flat

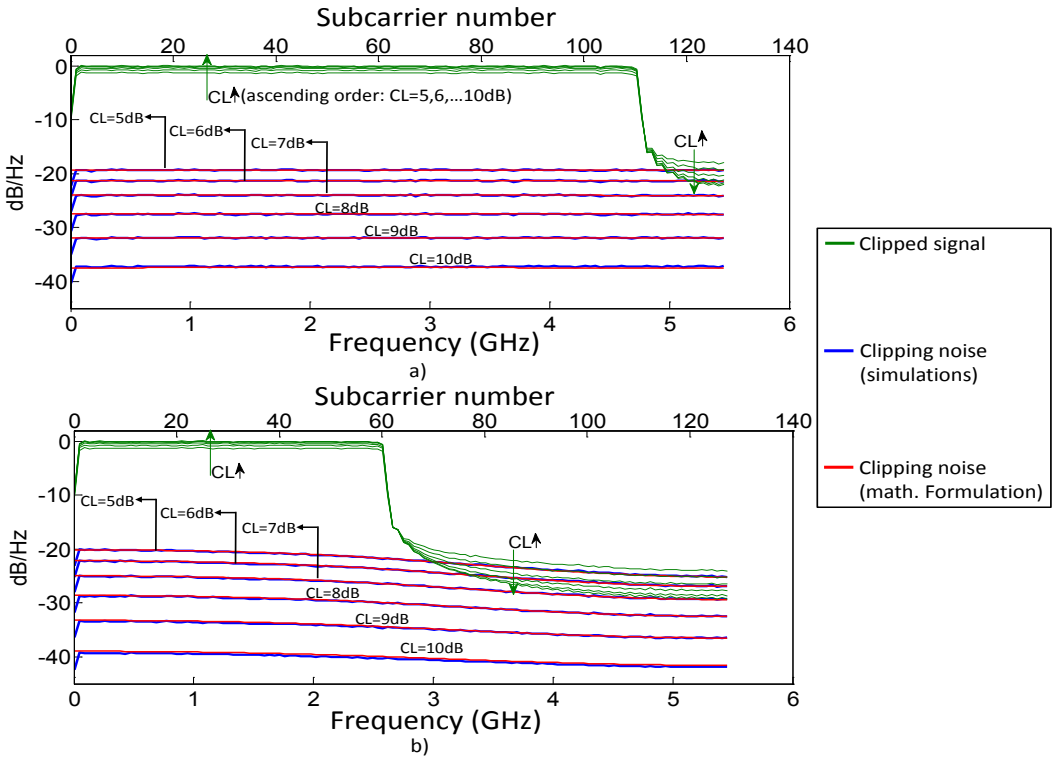

Figure 4.4: Power spectral density of the clipped signal and the clipping noise for $FS = 256$ a) $N = 110$, and b) $N = 60$.

spectrum approximation [60] is a valid assumption. The power spectrum description given by Eq. (4.16) is a more general expression, which may also be employed for systems with deliberate clipping using any value of oversampling ratio. In the case of $N = 60$, Fig. 4.4(b), the clipping noise is not uniformly distributed, but we can observe a roll-off with frequency which must be taken into account in order to appropriately describe the clipping noise effects on each subcarrier.

4.3.3 Clipping revisited

The spectral estimation given by Eq. (4.16) involves a statistical averaging and the clipping noise is assumed to be uniformly distributed with time. However, CL is usually set to a high value and the clipping noise forms a kind of impulsive noise rather than a continual background noise [86]. As a consequence, the spectral averaging may lead to an underestimation of the bit error probability.

In order to get a better approach in these situations, we propose to divide the whole clipping process into a finite number of processes, which are given by the joint of the OFDM symbols with the same number of clips, Fig. 4.5.

The problem now is to find out the expression for the power spectral density of each of these composing random processes with different average sampling rates.

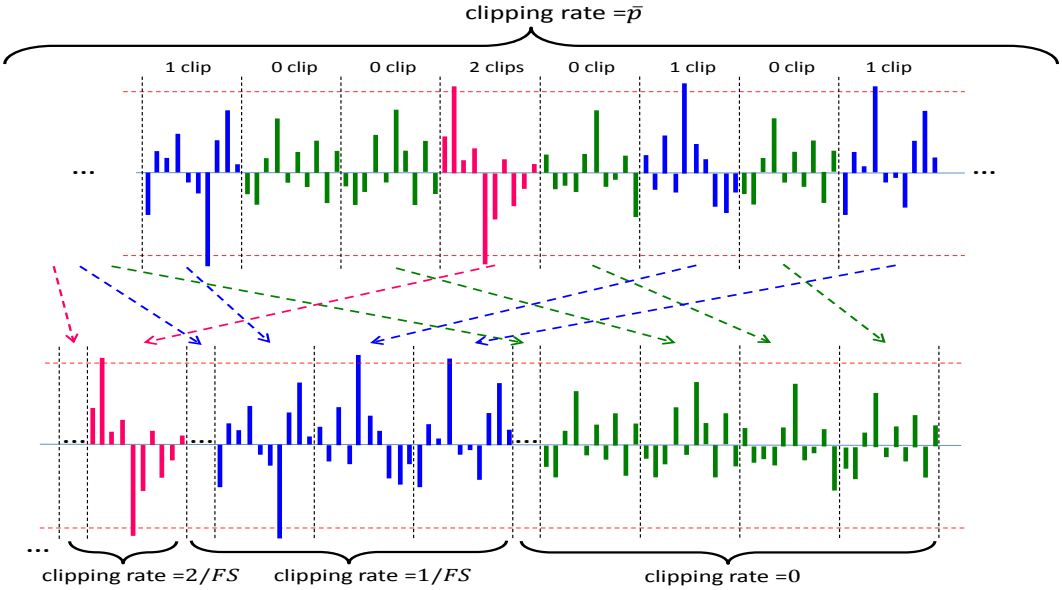

Figure 4.5: Re-ordering of the clipping process.

We have denoted as $\bar{p}$ the "default" average sampling rate, which is calculated as the mean value of the binomial distribution:

$$p_i = \binom{FS}{i} \Big(erfc\big(\sqrt{(CL/2)}\big) \Big)^i \Big(1 - erfc\big(\sqrt{(CL/2)}\big) \Big)^{FS-i} \tag{4.18}$$

which gives the probability of finding i discrete samples above or below the amplitude threshold A_{clip} within FS samples under the Gaussian assumption for the amplitude of the OFDM signal.

The derivation presented in Appendix B is based on the separation of the random process which describes the probability distribution of the clipping noise and the sampling function which describes its occurrence. Being $\hat{n}_{clip}(e^{j\Omega})$ the power spectral density of the random process, once it is sampled with an average sampling rate $\bar{p}$, their power spectral densities are related through:

$$\hat{n}_{\bar{p},clip}(e^{j\Omega}) = \bar{p} \cdot R_{clip}[0] + \bar{p}^2 \big(\hat{n}_{clip}(e^{j\Omega}) - R_{clip}[0] \big) \tag{4.19}$$

The first term of the right hand side corresponds to the white noise, whilst the second one is the coloured (correlated) noise.

Observing Eq. (4.19), the power spectral density of the random process with an average clipping rate equal to i/FS, can be expressed as a function of $\hat{n}_{\bar{p},clip}(e^{j\Omega})$ by (des)normalizing its white and coloured components appropriately:

$$\begin{aligned} & n_{i,clip}(e^{j\Omega}) \approx \\ & \frac{i}{FS}\frac{1}{\bar{p}} R_{\bar{p},clip}[0] + \frac{i-1}{FS-1}\frac{i}{FS}\frac{1}{\bar{p}^2} \Big(n_{\bar{p},clip}(e^{j\Omega}) - R_{\bar{p},clip}[0] \Big) \end{aligned} \tag{4.20}$$

where $R_{\bar{p},clip}[0]$ and $n_{\bar{p},clip}(e^{j\Omega})$ are given by Eqs. 4.14 and 4.16.

The corresponding variance is calculated as:

$$\sigma^2_{i,clip}[k] = n_{i,clip}(e^{j\Omega_k}) \cdot |H(e^{j\Omega_k})|^2 \cdot \Delta\Omega \tag{4.21}$$

Once obtained $\sigma^2_{i,clip}$, we can refine the error probability by separating the different OFDM symbols featuring respectively 0, 1, 2,...i_{max} clips:

$$Pr(bit\ error) = \sum_{i=0}^{i_{max}} Pr(bit\ error|i\ clips) \cdot p_i \tag{4.22}$$

where we use the variance $\sigma^2_{i,clip}$ for the calculation of $Pr(bit\ error|i\ clips)$.

4.3.4 Cyclic extensions-linear filtering effects

As it was said in Chapter 2, a certain number of guard samples is appended to each original OFDM symbol in order to avoid ISI and ICI effects. Since the transmission information rate is reduced because of the transmission of redundant samples, it is essential to evaluate the penalty due ISI & ICI effects as a function of the number of these redundant samples. Fig. 4.6 shows two different possible situations.

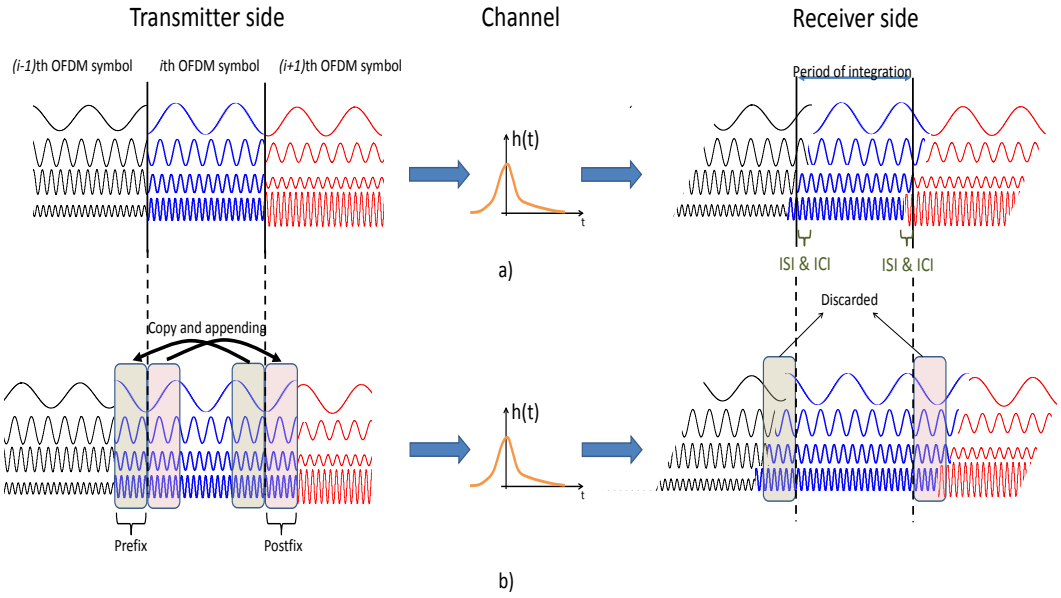

Figure 4.6: a) OOFDM signal without cyclic extensions passing through a dispersive channel, b) OOFDM signal with cyclic extensions passing through a dispersive channel.

In Fig. 4.6(a) a null number of samples for the cyclic pre- and post-fixes is appended, whilst in Fig. 4.6(b) the ISI & ICI effects due to the system impulse response are completely canceled out thanks to the appending of a sufficiently high number of samples for the cyclic pre- and post-fixes. Both are extreme situations, and a number of samples for the cyclic extensions sufficiently high to reduce the ISI & ICI effects without sacrificing considerably the transmission information rate must be found.

The theoretical expressions aimed to evaluate the penalty due to ISI & ICI effects are deduced from similar analysis to those reported in [87] and [88], but we take into account the correlation between the discrete samples of the generated OFDM signal and we employ

the transfer function given by Eq. (4.9) to include laser intensity and phase modulations as well as the propagation of the signal through the dispersive fiber.

$N_{pre} = \eta_{pre} \cdot FS$ and $N_{pos} = \eta_{pos} \cdot FS$ samples are used as pre- and post-fix for each OFDM symbol. We consider a channel impulse response with a positive tail extending to $T_{sam} \cdot L_+$ and a negative tail extending to $-T_{sam} \cdot L_-$ ($L+$ and $L-$ represent a certain number of samples, and T_{sam} is the sampling period), and we assume that ISI occurs only due to the adjacent OFDM symbols. Apart from ISI, ICI also occurs due to the loss of orthogonality between subcarriers, and the variance characterizing this process has the same value as that due to ISI. The total variance due to ISI & ICI on the k-th subcarrier can be obtained as (see Appendix D):

$$\begin{aligned}
&\sigma^2_{ISI}[k]+\sigma^2_{ICI}[k] = \\
&2R_x[0] \sum_{q=N_{pre}+1}^{L_+} H_{q,pos_tail}[k] \cdot H^*_{q,pos_tail}[k] + \\
&2R_x[0] \cdot \sum_{q=N_{pos}}^{L_--1} H_{q,neg_tail}[k] \cdot H^*_{q,neg_tail}[k] + \\
&2 \sum_{\substack{p= \\ N_{pre}+1}}^{L_+} \sum_{\substack{q= \\ N_{pre}+1 \\ q \neq p}}^{L_+} R_x[|p-q|] \cdot e^{j2\pi \cdot k \frac{p-q}{FS}} \cdot H_{p,pos_tail}[k] \cdot H^*_{q,pos_tail}[k] + \\
&2 \sum_{\substack{p= \\ N_{pos}}}^{L_--1} \sum_{\substack{q= \\ N_{pos} \\ q \neq p}}^{L_--1} R_x[|p-q|] \cdot e^{-j2\pi \cdot k \frac{p-q}{FS}} \cdot H_{p,neg_tail}[k] \cdot H^*_{q,neg_tail}[k]
\end{aligned} \tag{4.23}$$

where H_{q,pos_tail} and H_{q,neg_tail} represent the FS-point discrete Fourier Transform of the positive and negative tails of the channel impulse response:

$$H_{q,pos\_tail}[k] = H[k] \circledast DFT\{[\underbrace{0 \ldots 0}_{q} \ \underbrace{1 \ldots 1}_{FS-L_--q} \ \underbrace{0 \ldots 0}_{L_-}]\} \tag{4.24}$$

$$H_{q,neg\_tail}[k] = H[k] \circledast DFT\{[\underbrace{0 \ldots 0}_{L_+} \ \underbrace{1 \ldots 1}_{FS-L_+-q} \ \underbrace{0 \ldots 0}_{q}]\} \tag{4.25}$$

where $\circledast$ represents circular convolution and $H[k]$ is given by Eq. (4.9). Note that the two last terms in Eq. (4.23) include the contribution due to the non-zero correlation between the OFDM signal samples for $\varsigma \neq 0$. The expression for the autocorrelation of the generated OFDM signal is given by (see Appendix C):

$$R_x[\varsigma] = \sigma^2_x \left(\frac{sin\left(2\pi(2N+1)\frac{\varsigma}{FS}\right)}{sin\left(2\pi\frac{\varsigma}{FS}\right)} - 1 \right) \tag{4.26}$$

Equation (4.23) provides the expression for the variance due to ISI and ICI effects from the signal parameters (number of subcarriers N, size of the (I)FFT FS and length of the cyclic extensions), as well from the communication system link parameters through the transfer function $H[k]$, $k = 1, 2, ...N$.

We evaluate Eq. (4.23) for an OFDM signal with $FS = 256$ and $N = 110$. Its autocorrelation function, obtained through the evaluation of Eq. (4.26) and simulations, is depicted

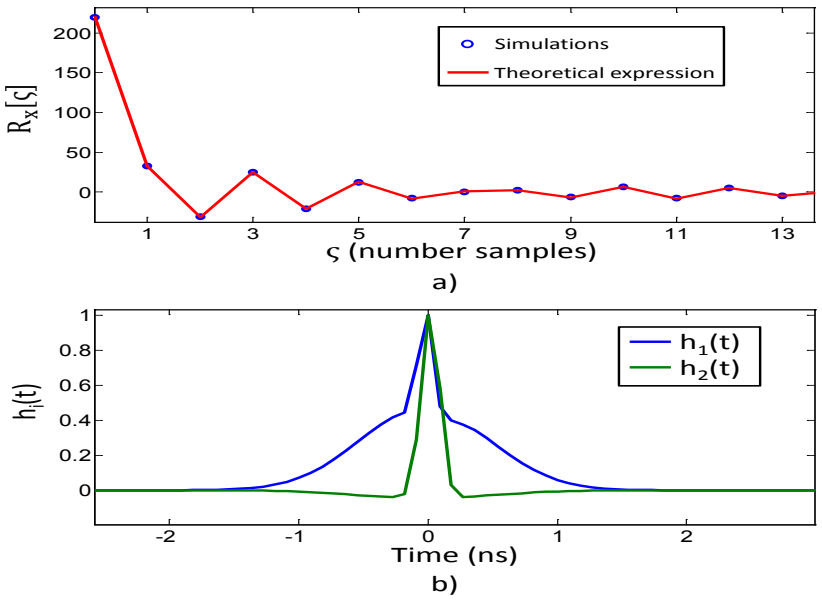

Figure 4.7: a) Autocorrelation function $R_x[\varsigma]$ for $FS = 256$ and $N = 110$. b) Arbitrary time-dispersive impulse responses.

in Fig. 4.7(a). The two impulse reponses employed to evaluate Eq. (4.23) are shown in Fig. 4.7(b).

As it can be observed in Fig. 4.7(a), though $R_x[\varsigma]$ decays rapidly, $R_x[\varsigma]$ adopts values for $\varsigma = 1,\ 2, ...5$ which can affect the accuracy of the computed penalty due to the ISI & ICI effects as Eq. (4.23). Both impulse responses in Fig. 4.7(b) present positive and negative tails around their maximum values at $t = 0$. In Fig. 4.8 the normalized variance $\sigma_x^2/(\sigma_{ISI}^2[k] + \sigma_{ICI}^2[k]),\ k = 1, 2, ...N$ is shown for several values of $N_{pre} = N_{pos}$ for both impulse responses.

As we can observe in Fig. 4.8 for both channel impulses responses, the results obtained through the evaluation of the analytical expressions are in good agreement with the results obtained through simulations, which demonstrates the validity of the expressions for different channel impulses responses provided that the channel length does not spreads for longer than a OFDM symbol. As expected, the variance of ISI & ICI is reduced as the number of samples $N_{pre} = N_{pos}$ increases. Since $h_1(t)$ is wider than the impulse response $h_2(t)$, the ISI & ICI effects are stronger for $h_1(t)$ than for $h_2(t)$, as we can observe comparing Figs. 4.8(a) and 4.8(b) for the same value of $N_{pre} = N_{pos}$. Remarkably, the subcarriers are not equally impaired by the ISI & ICI effects, as we can observe from the non-uniform distribution of its variance with the frequency.

In linearly field modulation based-systems, the length of the cyclic extension is designed to be higher than the delay difference between the fastest and lowest subcarrier when the OOFDM signal passes through the dispersive channel [1, 69], which in the case of chromatic dispersion is given by $\Delta t = |\beta_2| \cdot L \cdot N \cdot \Delta\Omega$. For DM/DD systems, the effects of ISI and ICI can not be accounted in a straight manner as in linearly field modulation-based systems, and, for this reason, it is of great interest to have available expressions such as Eq. (4.6) for its determination. In Fig. 4.9 we show the the normalized variance $\sigma_x^2/(\sigma_{ISI}^2[k] + \sigma_{ICI}^2[k]),\ k =$

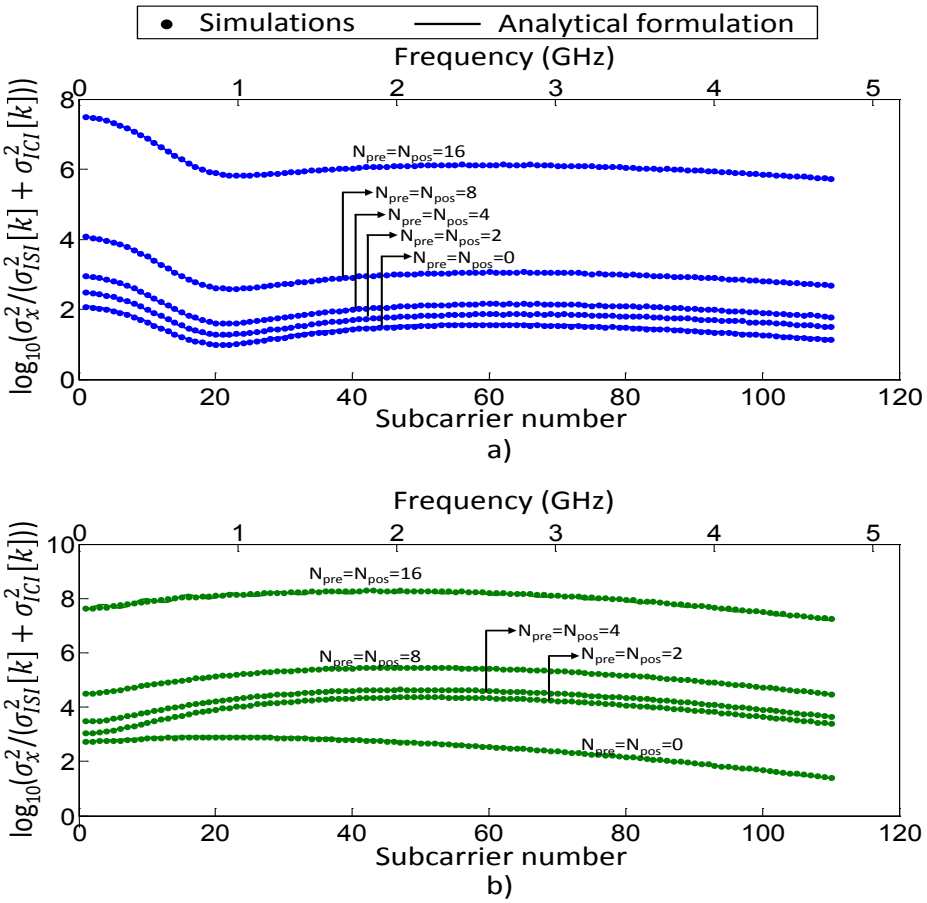

Figure 4.8: Ratio $\sigma_x^2/(\sigma_{ISI}^2[k]+\sigma_{ICI}^2[k])$, $k=1,2,...N$ for a) $h_1(t)$ and b) $h_2(t)$.

$1,2,...N$ for different fiber lengths when the system parameters specified in Table 4.1 are used in a DM/DD OOFDM system. The number of subcarriers N is equal to 110 and $N_{pre}=N_{pos}=0$.

Table 4.1: System Parameters

Opt. Modulation	i_0	60 mA
	Δi	10 mA
	Input power	0 dBm
Laser Parameters	Emission wavelength	1552.52 nm
	Length, width and thickness	300, 2 and 0.2 μm
	Transparency carrier density	1.5 x 10^{24} m^{-3}
	Confinement factor	0.3
	Linear gain coefficient	4 x 10^{-20} m^2
	Nonlinear gain coefficient	3 x 10^{-23} m^{-3}
	Linewidth enhancement factor	4

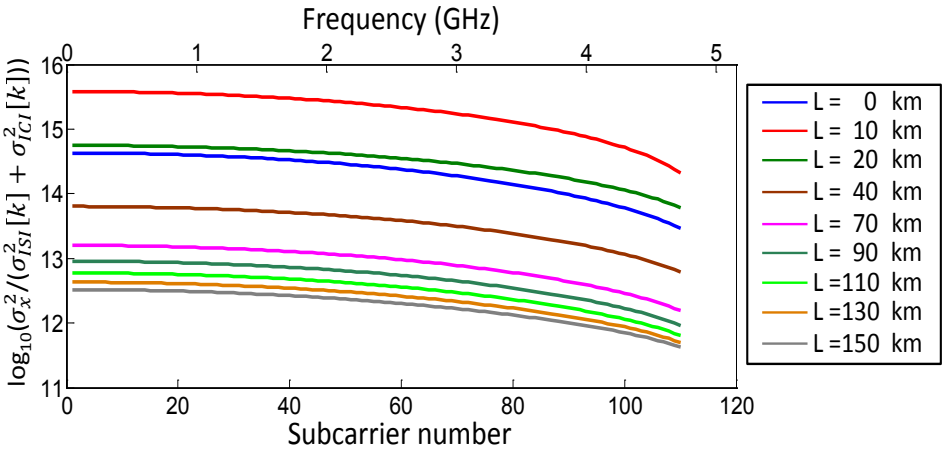

Figure 4.9: Ratio $\sigma_x^2/(\sigma_{ISI}^2[k]+\sigma_{ICI}^2[k]),\ k=1,2,...N$ for different fiber lengths.

In general, the value of $\sigma_{ISI}^2+\sigma_{ICI}^2$ increases with the distance, although for short distances the trend is different: the penalty due to ISI & ICI effects is higher for $L=0$ km than for $L=10$ km, and the penalty for $L=20$ is of similar value than for $L=0$ km.

4.3.5 Nonlinear distortion

Using the same approximations as in the subsection 4.3.1 to obtain the expression for the transfer function in Eq. (4.9), we can now derive simplified expressions of the nonlinear distortion given by Eqs. (3.21)-(3.25). With this approximation, the evaluation of the nonlinear distortion is rather direct and still accurate for typical parameter values employed in DM/DD OOFDM systems in short/medium haul links.

The resulting nonlinear distortion expressions are given next:

Intensity modulation nonlinearity

$$I_{p,DML}[k] = \sum_{l=1}^{\lceil k/2\rceil-1} H_{p_{11}}\left(\Omega_l,\Omega_{k-l}\right)\cdot cos(\theta_k)\cdot i_l\cdot i_{k-l}\cdot e^{j(\varphi_{i_l}+\varphi_{i_{k-l}})}+ \sum_{l=k+1}^{N} H_{p_{11}}\left(\Omega_l,-\Omega_{l-k}\right)\cdot cos(\theta_k)\cdot i_l\cdot i_{l-k}\cdot e^{j(\varphi_{i_l}-\varphi_{i_{l-k}})} \quad (4.27)$$

Phase modulation nonlinearity

$$
\begin{aligned}
&I_{\phi,DML}[k] = \\
&-2\sum_{l=1}^{\lceil k/2\rceil-1} P_0 \cdot H_{\phi_{11}}\big(\Omega_l, \Omega_{k-l}\big) \cdot sin(\theta_k) \cdot i_l \cdot i_{k-l} \cdot e^{j(\varphi_{i_l}+\varphi_{i_{k-l}})} + \\
&(-2)\sum_{\substack{l=\\ k+1}}^{N} P_0 \cdot H_{\phi_{11}}\big(\Omega_l, -\Omega_{l-k}\big) \cdot sin(\theta_k) \cdot i_l \cdot i_{l-k} \cdot e^{j(\varphi_{i_l}-\varphi_{i_{l-k}})}
\end{aligned} \tag{4.28}
$$

Dispersion-imbalanced intensity/phase components

$$
\begin{aligned}
&I_{p/\phi,\beta_2}[k] = (-2)\cdot \\
&\Big(\sum_{l=1}^{\lceil k/2\rceil-1} H_{p_1}\big(\Omega_l\big) H_{\phi_1}\big(\Omega_{k-l}\big) cos(\theta_l) sin(\theta_{k-l}) \cdot i_l \cdot i_{k-l} \cdot e^{j(\varphi_{i_l}+\varphi_{i_{k-l}})} \\
&+ H_{p_1}\big(\Omega_{k-l}\big) H_{\phi_1}\big(\Omega_l\big) cos(\theta_{k-l}) sin(\theta_l) \cdot i_l \cdot i_{k-l} \cdot e^{j(\varphi_{i_l}+\varphi_{i_{k-l}})} - \\
&\sum_{\substack{l=\\ k+1}}^{N} H_{p_1}\big(\Omega_l\big) H^*_{\phi_1}\big(\Omega_{l-k}\big) cos(\theta_l) sin(\theta_{l-k}) \cdot i_l \cdot i_{l-k} \cdot e^{j(\varphi_{i_l}-\varphi_{i_{l-k}})} \\
&+ H^*_{p_1}\big(\Omega_{l-k}\big) H_{\phi_1}\big(\Omega_l\big) cos(\theta_{l-k}) sin(\theta_l) \cdot i_l \cdot i_{l-k} \cdot e^{j(\varphi_{i_l}-\varphi_{i_{l-k}})} \Big)
\end{aligned} \tag{4.29}
$$

Dispersion-imbalanced phase components

$$
\begin{aligned}
I_{\phi,\beta_2}[k] = 4 &\sum_{l=1}^{\lceil k/2\rceil-1} P_0 \cdot H_{\phi_1}\big(\Omega_l\big) H_{\phi_1}\big(\Omega_{k-l}\big) sin(\theta_l) sin(\theta_{k-l}) \cdot \\
&i_l \cdot i_{k-l} \cdot e^{j(\varphi_{i_l}+\varphi_{i_{k-l}})} - 4 \sum_{l=k+1}^{N} P_0 \cdot H_{\phi_1}\big(\Omega_l\big) H^*_{\phi_1}\big(\Omega_{l-k}\big) \cdot \\
&sin(\theta_l) sin(\theta_{l-k}) \cdot i_l \cdot i_{l-k} \cdot e^{j\cdot(\varphi_{i_l}-\varphi_{i_{l-k}})}
\end{aligned} \tag{4.30}
$$

Dispersion-imbalanced intensity components

$$
\begin{aligned}
&I_{p,\beta_2}[k] = \\
&\sum_{l=1}^{\lceil k/2\rceil-1} \frac{1}{2P_0} \cdot H_{p_1}\big(\Omega_l\big) H_{p_1}\big(\Omega_{k-l}\big) \Big(cos\big(\frac{\beta_2}{2}\Omega_k(\Omega_l - \Omega_{k-l})L\big) \\
&- cos\big(\frac{\beta_2}{2}\Omega_k(\Omega_l + \Omega_{k-l})L\big)\Big) \cdot i_l \cdot i_{k-l} \cdot e^{j(\varphi_{i_l}+\varphi_{i_{k-l}})} + \\
&\sum_{l=k+1}^{N} \frac{1}{2P_0} \cdot H_{p_1}\big(\Omega_l\big) H^*_{p_1}\big(\Omega_{l-k}\big) \Big(cos\big(\frac{\beta_2}{2}\Omega_k(\Omega_l + \Omega_{l-k})L\big) \\
&- cos\big(\frac{\beta_2}{2}\Omega_k(\Omega_l - \Omega_{l-k})L\big)\Big) \cdot i_l \cdot i_{l-k} \cdot e^{j\cdot(\varphi_{i_l}-\varphi_{i_{l-k}})}
\end{aligned} \tag{4.31}
$$

The total nonlinear distortion, $I[k]$, is given by the sum of these terms:

$$
I[k] = I_{p,DML}[k] + I_{\phi,DML}[k] + I_{p/\phi,\beta_2}[k] + I_{\phi,\beta_2}[k] + I_{p,\beta_2}[k] \tag{4.32}
$$

and the variance due to nonlinear distortion is calculated as:

$$\sigma^2_{IMD}[k] = \langle |I[k]|^2 \rangle = \\ \langle |I_{p,DML}[k] + I_{\phi,DML}[k] + I_{p/\phi,\beta_2}[k] + I_{\phi,\beta_2}[k] + I_{p,\beta_2}[k]|^2 \rangle \quad (4.33)$$

With respect to Eqs. (4.27)-(4.31) we would like to make note that (i) the amplitude of the intermodulation distortion is proportional to m^2 through the product of the two intensity coefficients, as expected from the second order nonlinear distortion, and (ii) $\sigma^2_I[k]$ has been computed by summing up in amplitude the different nonlinear distortion terms since their phases are not independent.

The nonlinear distortion variance σ^2_{IMD} determined by numerical simulations of the system and the evaluation of Eqs. (4.27)-(4.31) is compared in Fig. 4.10. The size of the (I)FFT, FS, as well as the number of information subcarriers, N, are changed. On each plot, several curves have been obtained for different transmission distances, L. The clipping level, CL, as well as the number of samples N_{pre} and N_{pos} are set to a sufficiently high value to make clipping noise and $\sigma^2_{ISI}[k] + \sigma^2_{ICI}[k]$ negligible. The dispersion parameter D is set to $17ps/(km \cdot nm)$, the responsivity is equal to $1A/W$, and the rest of parameters are the same as those specified in Table 4.1.

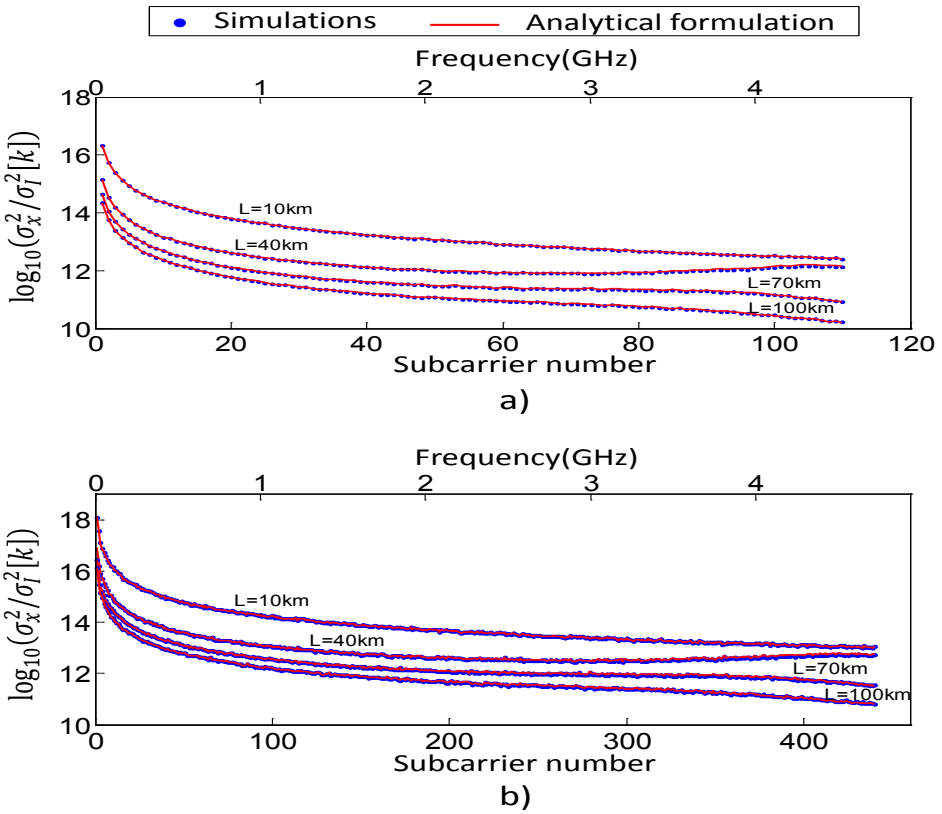

Figure 4.10: Signal to nonlinear distortion power ratio. a) $FS = 256$, $N = 110$, b) $FS = 1024$, $N = 440$.

Once again, the theory provided offers us similar results to those obtained through simulations. As expected, for higher accumulated dispersion values, the nonlinear distortion

increases as a result of a stronger imbalance of the spectral components. It is interesting to note that it seems that an increase in the number of subcarriers from $N = 110$ to $N = 440$, leads to a lower nonlinear distortion, as observed when we compare the values of both figures. However, this effect is only due to the decrease of the laser modulation index as result of the increase in the number of subcarriers: the higher the number of subcarriers, the higher is also the amplitude swing of the analog signal which is fed into the electrical attenuator (see Fig. 4.1), and also higher the attenuation needed to adapt the laser driving signal within a certain region of laser operation (Δi).

The analytical expressions provided offer us an accurate description on the nature of the nonlinear distortion and hence, on the possible techniques to combat it. The separation of the nonlinear distortion components as that in Eqs. (4.27)-(4.31) allows us to consider different design strategies focusing on a particular source of distortion, or the simplification of equalization techniques by processing those subcarriers which are more strongly impaired by nonlinear distortion.

4.3.6 Signal to noise-interference ratio as figure of merit

Due to the unique algorithm used to demultiplex the received OFDM signal through the use of a FFT, the different impairment effects which add to the received complex symbol, $H[k] \cdot X[k]$, can be approximated to a Gaussian distribution [17] provided a sufficiently high number of data subcarriers N is used. Thus, the system performance evaluation can be accomplished through a simple figure of merit which accounts for the power of the undistorted part of the received information signal and the variance of the impairment effects on each subcarrier [60]:

$$SNR[k] = \frac{|H[k]|^2 \cdot \sigma_x^2}{\sigma^2_{\bar{p},clip}[k] + \sigma^2_{ISI\&ICI}[k] + \sigma^2_{s\&t} + \sigma^2_{IMD}[k]}, \; k = 1, 2, ...N \tag{4.34}$$

Equation (4.34) can be easily determined since we already know all the magnitudes involved: $H[k]$ is given by Eq. (4.9), $\sigma^2_{\bar{p},clip}$ is calculated as Eq. (4.13), $\sigma^2_{ISI\&ICI}$ is given by Eq. (4.23), the expressions for the thermal and shot noises can be found in [89], and σ^2_{IMD} is given by Eq. (4.33).

In order to calculate the BER of each subcarrier ($BER[k]$), due to the analytical treatment to study the clipping noise explained in the subsection 4.3.3, a signal-to-noise ratio conditioned to the number of clips i is calculated:

$$SNR_{i,clips}[k] = \frac{|H[k]|^2 \cdot \sigma_x^2}{\sigma^2_{i,clips}[k] + \sigma^2_{ISI\&ICI}[k] + \sigma^2_{s\&t} + \sigma^2_{IMD}[k]}, \; k = 1, 2, ...N \tag{4.35}$$

Once determined $SNR_{i,clips}[k]$, $BER[k]$ with $k = 1, ...N$ is easily determined with the help of BER evaluation formulas [55, 90] and making use of Eq. (4.36):

$$BER[k] = \sum_{i=0}^{i_{max}} Pr(bit\ error | i\ clips) \cdot p_i = \sum_{i=0}^{i_{max}} Pr(SNR_{i,clips}[k]) \cdot p_i \tag{4.36}$$

Finally, the total BER, BER_T, can be easily computed as:

$$BER_T = \frac{\sum_{k=1}^{N} log_2(M[k]) \cdot BER[k]}{\sum_{k=1}^{N} log_2(M[k])} \tag{4.37}$$

where $M[k]$ stands for the constellation size of the QAM format used at the kth subcarrier. The transmission information bit rate depends on the particular modulation format employed, and can be expressed in a general way as:

$$R(bits/s) = \frac{No.\ bits/OFDM\ symbol}{Total\ OFDM\ symbol\ duration} = \frac{\sum_{k=1}^{N} log_2(M[k])}{(BW/(FS/2))^{-1} \cdot (1 + \eta_{pre} + \eta_{pos})} \tag{4.38}$$

In Fig. 4.11 we show the estimated SNR through the evaluation of Eq. (4.35) and that obtained through simulations for different values of cyclic extensions length, clipping level and number of subcarriers transmitted N, being the optical fiber length equal to 20 km, $\beta_2 = 17ps/(km \cdot nm)$. The rest of parameters are the same as those specified in Table 4.1. Thermal and shot noises are not included in order to not mask the impairments studied. For certain conditions, we also show the analytically estimated values for $BER[k]$ when 128-QAM is used as modulation format.

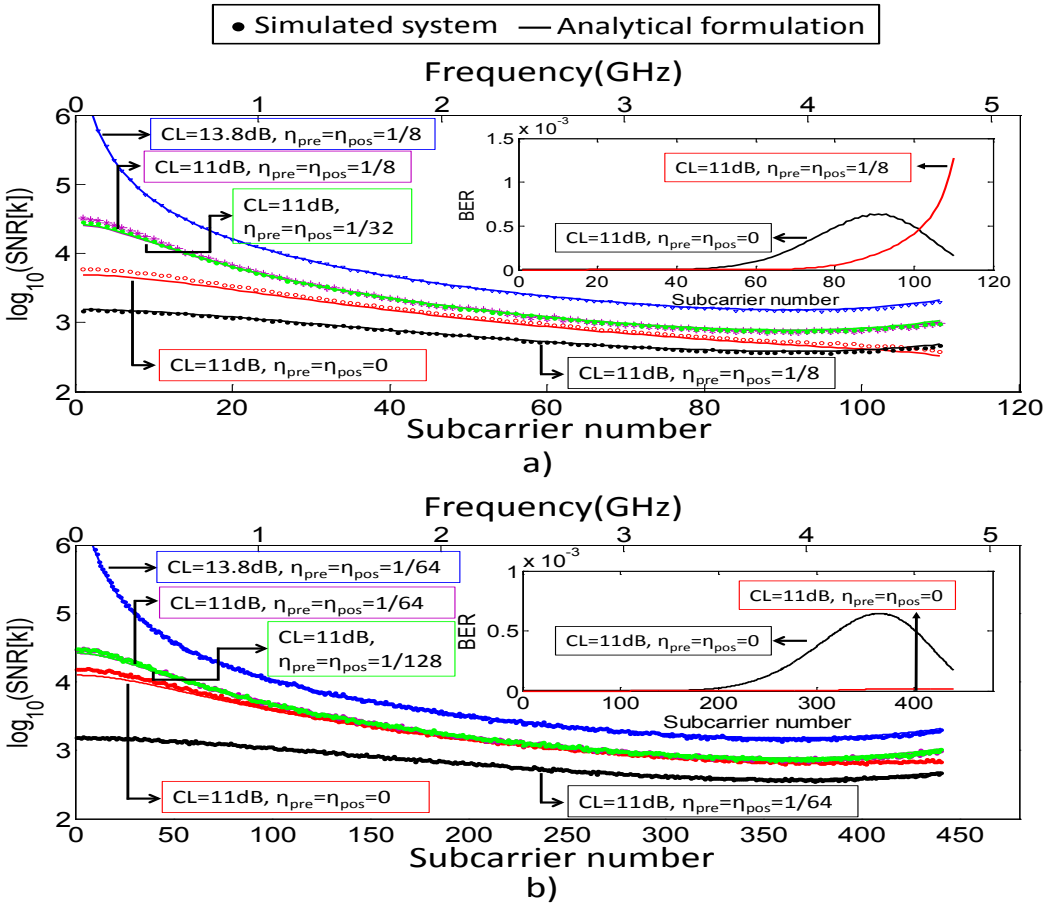

Figure 4.11: SNR vs subcarrier number for L=20 km. Insets: analitically estimated BER values. a) $FS = 64$, $N = 55$, and b) $FS = 1024$, $N = 440$.

The evolution of $SNR[k]$ when the clipping level is changed is similar for both values of N and it increases as a result of a higher value of CL as expected. There is a significant

decrease of the $SNR[k]$ for low frequency values when the value of CL is decreased (for example, when CL changes from a value equal to 13.8dB to a value equal to 9dB) as a result of the clipping noise at these frequencies.

When N is increased, the % of samples dedicated to the pre- and post-fixes on each OFDM symbol, $\eta_{pre} + \eta_{pos}$, for which there is not a significant improvement decreases: for $N = 55$, we can observe how $SNR[k]$ increases substantially when $\eta_{pre} = \eta_{pos}$ changes from 0 to 1/32, but a small improvement is observed when it changes from 1/32 to 1/8; for $N = 440$, there is a significant improvement when we change from $\eta_{pre} = \eta_{pos} = 0$ to a value equal to 1/128, getting similar values when $\eta_{pre} = \eta_{pos}$ is equal to 1/64.

With respect to the BER values shown in the insets, we obtain similar values when clipping is the main source of impairment (CL is equal to 9dB) for both values of N. Nevertheless, when $\eta_{pre} = \eta_{pos} = 0$ the BER reduces considerably when $N = 440$. A higher value of N is thus advantageous to decrease the value of η_{pre} and η_{pos}, but it yields more stringent conditions with respect to the amplitude dynamic range A_{clip}.

The excellent matching of the results derived from the analytical method and those provided by simulation validate the applicability of our derived expressions. Furthermore, our equations can be applied to test various strategies for improving the systems performance such as adaptive modulation and power allocation algorithms.

4.4 Results

4.4.1 Variation of CL, cyclic extensions length and laser modulation depth

The set of analytical expressions derived in previous sections are used to study the described sources of impairment in DM/DD OOFDM systems. As in the previous sections, in the transmission of the optical signal through the fiber only the group velocity dispersion is considered, ignoring higher dispersion terms and fiber nonlinearities. The optical modulation and laser parameters are those in Table 4.1, whilst the group dispersion velocity is set to $17ps/(km{\cdot}nm)$, the intensity fiber attenuation coefficient is set to 0.2dB/km, and the thermal noise spectral density is equal to 10 pA/$\sqrt{Hz}$.

We start by discussing the value of CL which should be adopted at the transmitter, though the final choice of one value or another is a subject of specific electronics requirements. First of all, it must be clear that clipping also affects the mapping efficiency of the information carried by the laser driving signal and finally detected at the receiver-end side through the laser modulation.

We show in Fig. 4.12 the BER obtained for different values of CL and different values of fiber length. In order to maintain the BER values around $10^{-3} - 10^{-4}$, the modulation format is varied accordingly from 128-QAM to 16-QAM. Both approaches for the quantification of the clipping noise, referred as classical and proposed, are shown: in the classical approach, Eq. (4.13) and Eq. (4.34) are used for the calculation of the variance of the clipping noise and the SNR, respectively; instead, in the proposed approach, Eq. (4.21) and Eq. (4.35) are used, whilst the BER is evaluated through Eq. (4.36). Time consuming simulation BER values based on error counting have been also included for the sake of validation.

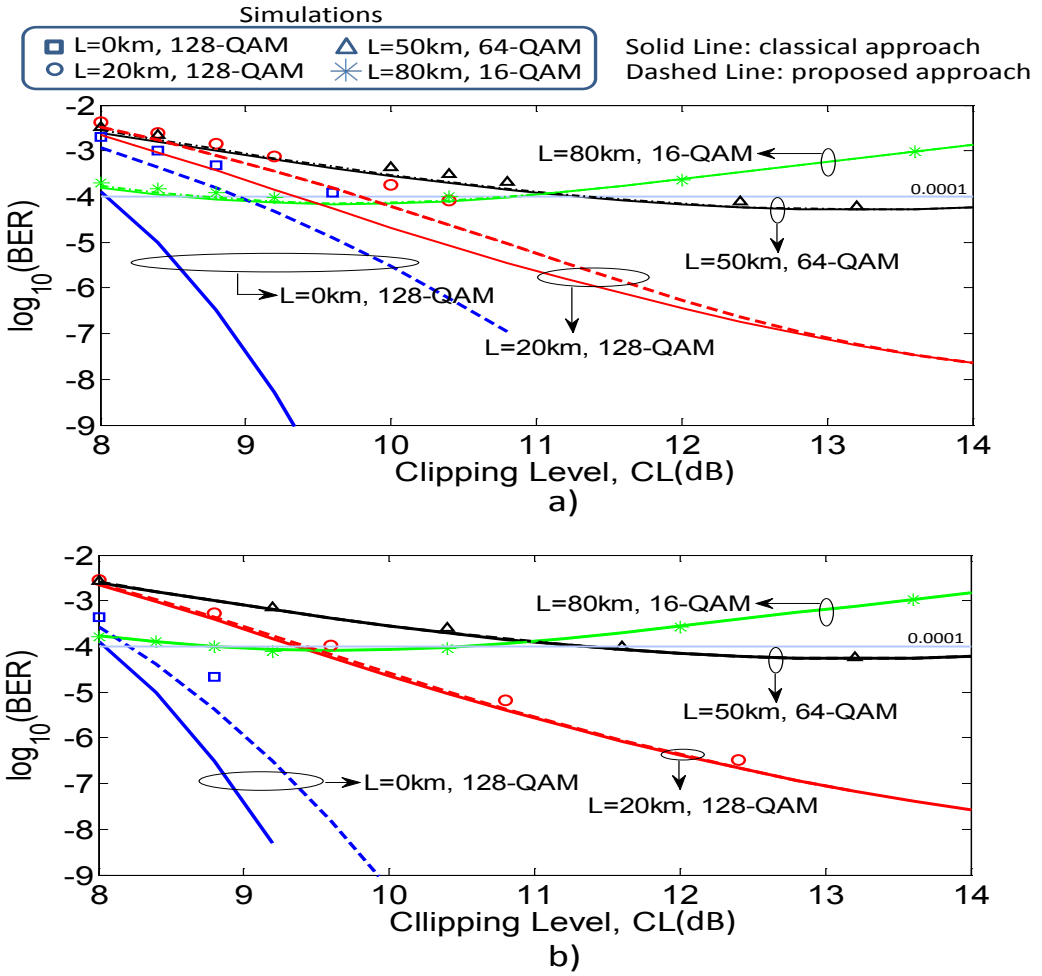

Figure 4.12: BER values in function of the clipping level for different distances. a) $FS = 128$, $N = 55$, and b) $FS = 1024$, $N = 440$.

Since the performance is affected by all the impairments studied in the previous sections (ICI & ISI, nonlinear distortion and receiver noise), and how strongly these impairments affect the signal quality depend on the fiber length (through the accumulated dispersion and the fiber attenuation), the choice of one value of CL or another depends on the particular operating conditions of the communication system.

In order to ease the electronics transmitter design by limiting as much as possible the amplitude value of the OFDM signal, the value of CL is chosen in such a way a BER of 10^{-4} is obtained, which lets some margin until the 7% overhead FEC limit of 2.3×10^{-3}.

With regard to the matching with simulation results, the error is higher for 0 and 20 km, being the classical approach for the clipping noise more inaccurate. The simple approach proposed in this work allows to reduce the error considerably in these cases, specially when $N = 55$. At a BER equal to 10^{-4}, for $N = 55$ and L=0 km, the CL must be set to a value equal to 8dB and 9dB as the classical and proposed approaches, respectively. The latter is

much closer to the value given by the simulations, equal to 9.6dB. For $N = 440$, the couple of values are [8.25dB,8.5dB], respectively.

We can observe that for L=20 km and with the same modulation format, 128-QAM, the value of CL to obtain a BER equal to 10^{-4} must be increased, independently of the number of subcarriers. Our approach gives values of CL equal to 9.8dB and 9.45dB for $N = 55$ and 440, respectively. From the rapid descending trend of the red curves, we can conclude that clipping has a great impact on the system performance obtained for these particular conditions.

As the distance increases to L=50 km and L=80 km, both approaches, the classical and the proposed ones, give similar results and very close to those provided by simulations. For L=50 km, the CL should be set to a value around 11.35dB, and for L=80 km the CL should be set to value around 8.7dB, independently of the number of subcarriers. For L=50 km, we can observe that the BER starts to increase for values higher than 13dB: as the distance increases, the other impairment sources begin to be dominant, and an increase on the CL yields to a laser modulation inefficiency, which is detrimental to the information recovery at the presence of receiver noise and nonlinear distortion. This effect is more important when L=80km, and the value of CL from which there is not an important improvement is around 9.5dB.

Once a value of CL is set accordingly to the BER we want to achieve, BER values for different number redundant samples $N_{pre} = N_{pos}$ are also obtained to choose an appropriate value. Fig. 4.13 shows the results obtained.

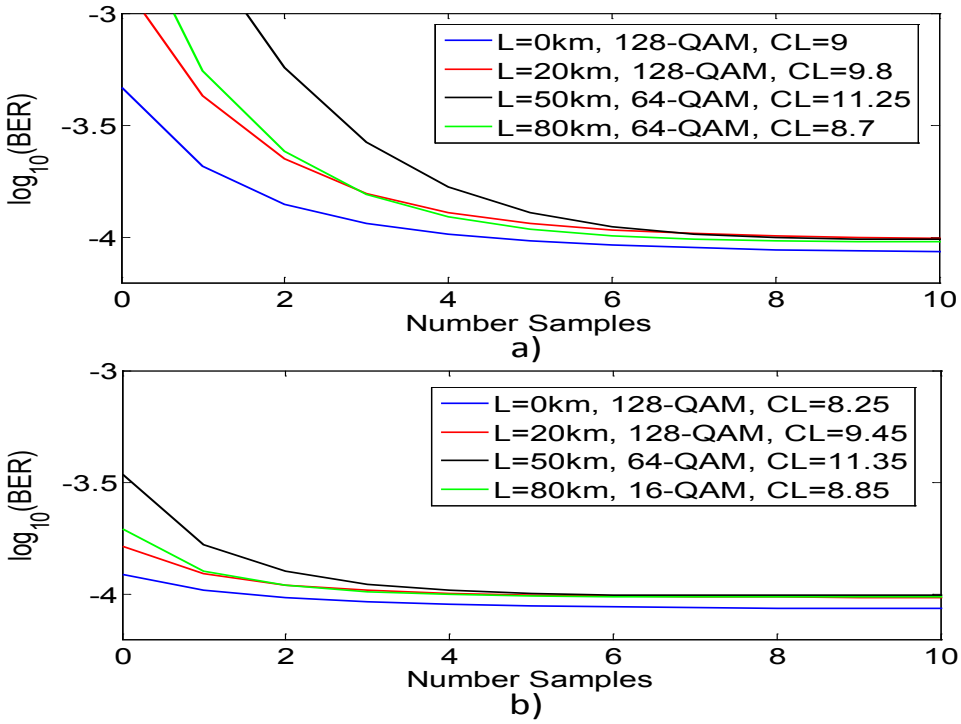

Figure 4.13: BER values vs $N_{pre} = N_{pos}$ value for different distances. a) $FS = 128$ and b) $FS = 1024$, $N = 440$.

Depending on the distance and on the specified CL, an appropriate value of $N_{pre} = N_{pos}$ is selected in order to obtain a) a BER equal to 10^{-4} or b) a BER almost equal to 10^{-4}, but not equal because the small improvement that an increase of $N_{pre} = N_{pos}$ does not compensate the resulting transmission rate and power penalties, may be adopted. For example, for $N = 55$ (Fig. 4.13(a)), $L = 80$ km, we can choose a value of $N_{pre} = N_{pos}$ equal to 8 samples, which would give us a transmission rate (R in Eq. (4.38)) of $16.8Gbits/s$ and a BER of 10^{-4}, or $N_{pre} = N_{pos}$ equal to 4 samples, with which we obtain $R = 17.8Gbits/s$ with a BER of 1.23×10^{-4}. With the increasing of number of subcarriers, the length of the pre/post-fix becomes a matter of secondary concern and the transmission information rate suffers smaller penalties with its increase: for $N = 440$ (Fig. 4.13(b)), $L = 50$ km, 64-QAM and $N_{pre} = N_{pos} = 2$, we obtain $R = 28.25Gbits/s$, whilst for $N_{pre} = N_{pos} = 6$ we obtain $R = 28.03Gbits/s$.

It is also worth mentioning that, in the case the BER may be reduced by increasing the value of CL (Fig. 4.12), it may be convenient to increase it slightly in order to reduce the number of redundant samples. For example, for L=20km, an increase of the CL yields a smaller BER, which might be interesting to reduce the values of N_{pre} and N_{pos}. At short distances, where the improvement with an increase of CL is higher, and for low values of FS and N, where proportionally more samples are wasted into the cyclic pre/postfix (higher values of η_{pre} and η_{pos}), an slight increase of CL could be more convenient to achieve a determined BER.

If we introduce another degree of freedom by playing with the value of laser operation region, Δi, we can further reduce the BER value, or reduce the value of CL in order to ease the electronics, or we can make use of adaptive modulation format in order to increase the transmission information rate. The results obtained for $N = 440$, $L = 50$ km and $N_{pre} = N_{pos} = 6$ are shown in Fig. 4.14.

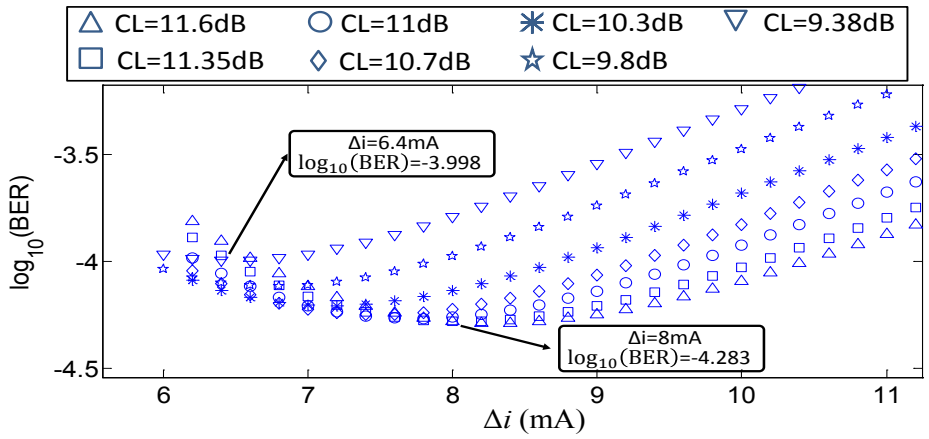

Figure 4.14: System performance for $N = 440$ and L=50km. BER in function of the swing of the laser operation region (all subcarriers employ 64-QAM).

From Fig. 4.14, we can conclude that with the default value $\Delta i = 0.01$ the system performance was severely affected by nonlinearities, and a decrease of its value leads to a system performance increase. If we maintain the value of CL at the previous value, 11.35 dB, the optimum value is $\Delta i = 0.008$ A. With this pair of values, we achieve a BER of 5.2×10^{-5}. In the case we were interested on a decrease of the clipping level, we could decrease it to a value

of 9.38dB and use a value of Δi equal to 0.0064 A, with which we obtain a BER of 1×10^{-4}. Finally, we could set $CL = 11.35$ dB and $\Delta i = 0.008$ A, but changing the modulation format of certain subcarriers (those with lowest BER) in order to increase the transmission information rate. The resulting modulation formats and BER of each subcarrier is shown in Fig. 4.15(b).

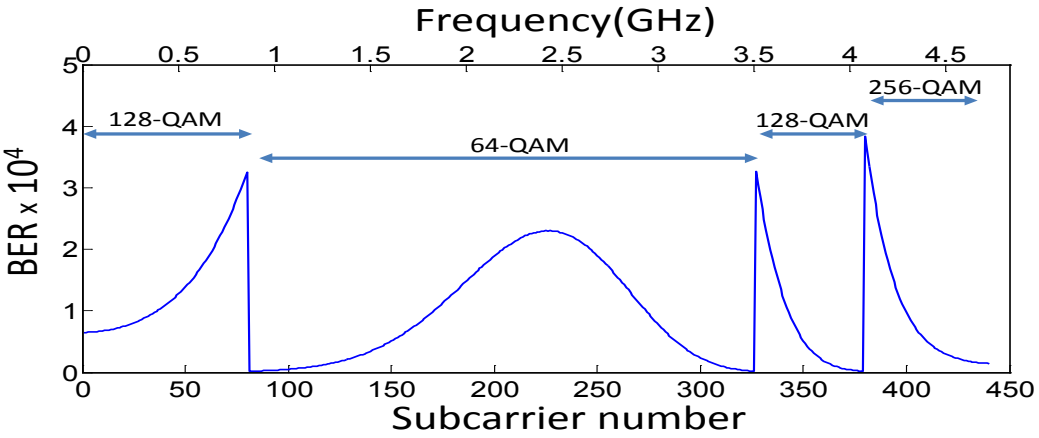

Figure 4.15: System performance for $N = 440$ and L=50km. BER and modulation format employed on each subcarrier to obtain a BER equal to 1×10^{-4} with CL=11.35dB and $\Delta i = 8mA$.

The resulting transmission information rate is 30.74 Gbits/s, which means an increase of 2.44Gbits/s, and a BER of 1×10^{-4}. Note that under the particular conditions used, a modulation format of 256-QAM is used at highest frequencies, which is due to the absence of bandwidth limited devices at the transmitter and receiver which would attenuate these frequencies. The addition of linear filtering effects does not represent any problem since they can be easily incorporated into Eq. (4.7).

4.4.2 Influence of laser modulation dynamics

Apart from the parameters studied in the previous sections and which can be easily varied in the electronic part of the transceiver, we need to pay some attention to those that, though not variable in a easy fashion, play a crucial role into the achieved system performance. The system performance is affected by two factors related with the laser modulation: the power of the useful information term at the receiver, represented by the total transfer function in Eq. (4.6), and the power of the nonlinear distortion, represented by Eqs. (4.27)-(4.31). The results and conclusions obtained are useful to get some insight into the limiting system performance factors, guidelines on choosing laser sources for optical modulation, as well as the influence of the variation on the laser modulation dynamics (e.g., those due to thermal effects) in a DM/DD OOFDM system.

In order to quantify the obtained performance, we employ the achievable transmission information rate in Eq. (4.38), obtained as result of applying bit loading. Therefore, a feedback-path from the transmitter to the receiver is assumed to make the transmitter able to adapt the transmission information rate to the communication system conditions. The decision on using a format for a certain subcarrier is based on the calculated BER of that particular subcarrier, $BER[k]$. Under the Gaussian assumption for the noise distribution, the BER is

directly determined once we have calculated SNR[k]. The modulation format of the subcarrier with the minimum value of BER is increased provided that the total BER_T does not exceed a certain threshold. The number of subcarriers is set to $N = 110$, and, thus, the (I)FFT size is equal to 256.

4.4.2.1 Optical fiber length equal to 40km

For a fiber length equal to 40km, $N_{pre} = N_{pos} = 32$, $CL = 11$dB, $\tau_p = 1.5$ps and an amplitude swing $\Delta i = 8$mA the obtained information transmission rate values when α and ε_{nl} are varied simultaneously and two different values of i_0 are shown in Fig. 4.16.

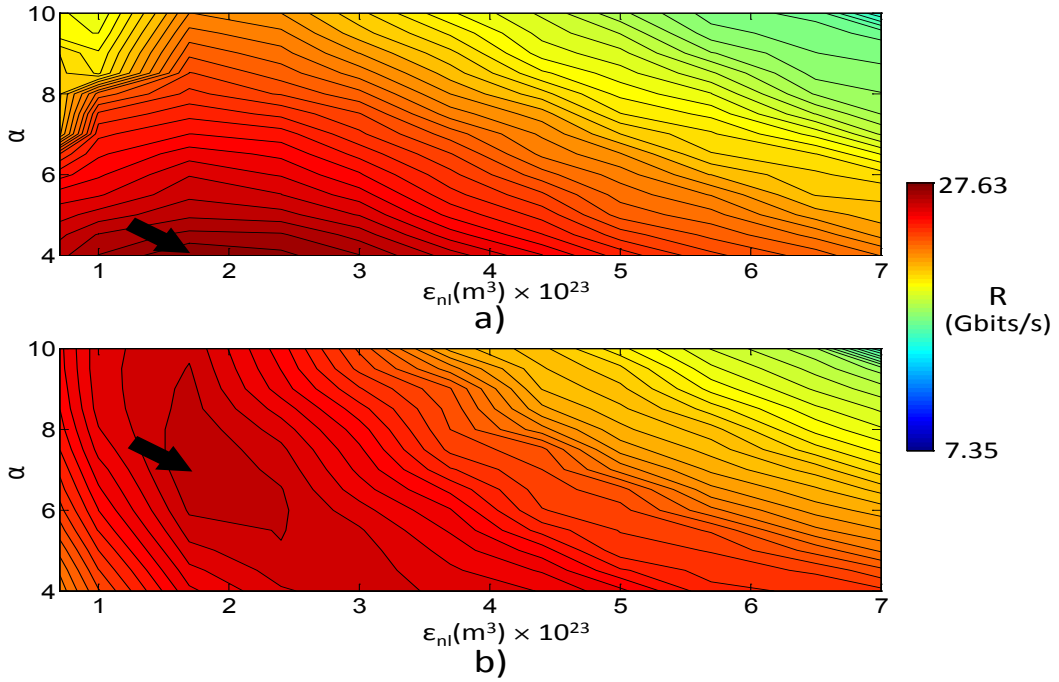

Figure 4.16: Information transmission rate for a) $i_0 = 46mA$ and b) $i_0 = 78mA$.

The arrows in Fig. 4.16 indicate at which point the maximum value of transmission information rate is achieved, being 27.63Gbits/s for $i_0 = 46$mA, $\alpha = 4$ and $\varepsilon_{nl} = 1.7 \times 10^{-23} m^3$, and 26.606Gbits/s for $i_0 = 78$mA, $\alpha = 7$ and $\varepsilon = 1.7 \times 10^{-23} m^3$. From Fig. 4.16(a) we can observe that the system performance is clearly limited by the laser chirp and the information transmission rate decreases with α, whereas for $i_0 = 78$mA, a higher value of α is beneficial because of the linear contribution due to the laser chirp, as expressed in Eq. (4.6). The variation of the achievable information transmission rate with ε_{nl} is due to two counteracting factors: at small values, frequency dips may appear as result of the opposite phases between the two terms in Eq. (4.6), and at higher values, laser nonlinearity becomes more significant. In Fig. 4.17 we plot the ratios $\sigma^2_{s\&t}[k]/|H[k]|^2$ and $\sigma^2_{IMD}[k]/|H[k]|^2$, $k = 1, 2, ...N$, for $i_0 = 46$mA and $\alpha = 4$.

We can observe that for low values of ε_{nl}, the receiver noise impairs more significantly than the nonlinear distortion, specially at frequencies around $2\pi \cdot 3.74 \times 10^9$rads/s ($\approx 87 \cdot \Delta\Omega$),

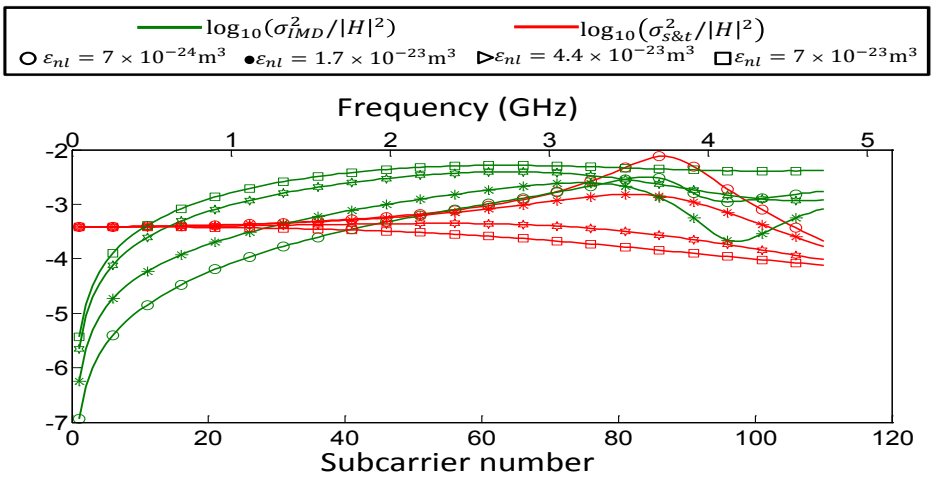

Figure 4.17: Nonlinear distortion and receiver noise variances to signal power for different values of ε_{nl}.

where a dip in $H(\Omega)$ enhances the detrimental effect of the receiver noise, assumed to be uniformly distributed along the receiver bandwidth. As ε_{nl} increases, $\sigma^2_{s\&t}[k]/|H[k]|^2$ gets smaller values as result of the increase in $H(\Omega)$, and the nonlinear distortion becomes the main limiting system performance factor, as we can observe from the increase of $\sigma^2_{IMD}[k]/|H[k]|^2$.

In Fig. 4.18, we set $i_0 = 46\text{mA}$, $\Delta i = 8\text{mA}$ and change the value of the photon lifetime. The maximum achievable information transmission rates are 27.64Gbits/s for $\tau_p = 2.2ps$, 27.46Gbits/s for $\tau_p = 1.83ps$ and 26.94Gbits/s for $\tau_p = 1.5ps$, the three of them with $\alpha = 4$ and $\varepsilon_{nl} = 1.7 \times 10^{-23}m^3$. Therefore, variations of the value of the photon lifetime around a reasonable value does not seem to lead to significant changes in the information transmission rate obtained for the particular conditions studied here. The bit loading technique, provided that the monitoring and adaptive mechanism are able to track the changes in the transmission conditions, is proven to be an useful tool for the variation of laser parameters, e.g. due to thermal effects [91]. In Fig. 4.19(a), we show the obtained BER and the modulation format employed for each subcarrier for the three different values of τ_p. We can observe that the BER profile are very similar and thus the modulation formats employed along the signal bandwidth. In order to understand the BER values obtained, we need to study the ratios $\sigma^2_{s\&t}[k]/|H[k]|^2$ and $\sigma^2_{IMD}[k]/|H[k]|^2$, which are shown in Fig. 4.19(b). Besides, given the fact that the 3-dB bandwidth of the intensity modulation is approximately inversely proportional to the square root of the photon lifetime [66], it is worth getting more insight on why an increase of the photon lifetime seems to be beneficial.

From Fig. 4.19(b) we can observe that the variation of BER follows that due to the intermodulation distribution with the frequency. When τ_p decreases, the laser transfer function $H_{p_1}(\Omega)$ increases, and so may the system performance. However, the intermodulation distortion increases at a faster rate because it is a function of the product $H_{p_1}(\Omega)$ with itself, as pointed out by Eqs. (4.27)-(4.31). Since the system is severely limited by nonlinearities, the decrease of τ_p causes the increase of the nonlinear distortion (Fig.4.19(b)), which results in an increase of the BER, Fig. 4.19(a).

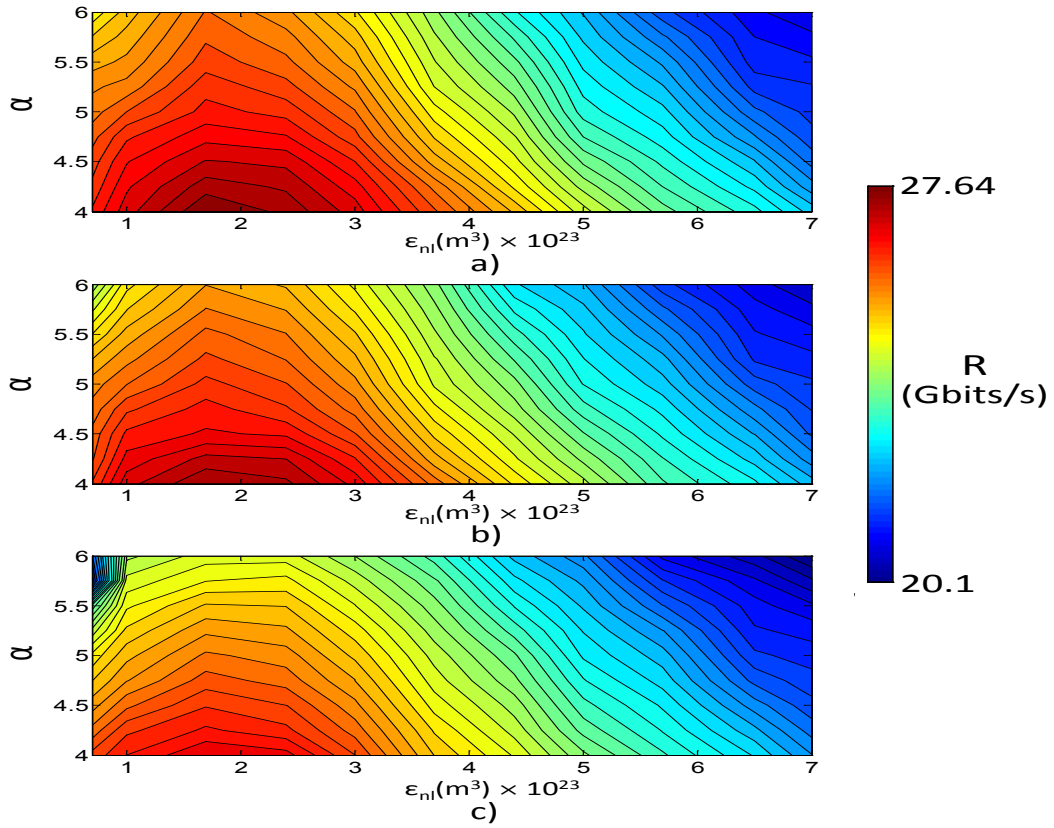

Figure 4.18: Information transmission rate for a) $\tau_p = 2.2$ps, b) $\tau_p = 1.83$ps, and c) $\tau_p = 1.5$ps.

In the following simulations, at the view of the marginal influence of the photon lifetime into the system performance and the adaptability of the system thanks to the bit loading technique, we set τ_p to a default value equal to 1.83ps.

Next we change simultaneously the amplitude swing of the laser driving signal, Δi, and the clipping level CL. It is very interesting to vary these two parameters simultaneously, because both have influence on the optical modulation efficiency, but the former is directly related to the nonlinear distortion, whilst the latter controls how much clipping noise is introduced. For these simulations, we set $\alpha = 4$, $\varepsilon = 1.7 \times 10^{-23} m^3$ and $\tau_p = 1.83$ps. The results are shown in Fig. 4.20.

The black dashed lines in Fig. 4.20, labeled with numbers "1" and "2" aim to delimit different regions in which the limiting system performance factor is different: above the line "1", an increase of CL must with a fixed value of Δi yields a reduction of the transmission information rate, which indicate us that the system performance is limited by the modulation efficiency (or, in other words, by the receiver noise power); below the line "2", an increase of Δi with a fixed value of CL yields also a reduction of the transmission information rate due to the system nonlinearities; between the two lines, the system performance is limited by the clipping noise, and, consequently, a decrease of CL yields a reduction of the system performance. The maximum achievable transmission rate is around 24.34Gbits/s, which is achieved for values of Δi higher than 9mA and values of CL higher than 12.5dB. In the presence of quantization noise, a smaller value of CL may be more convenient.

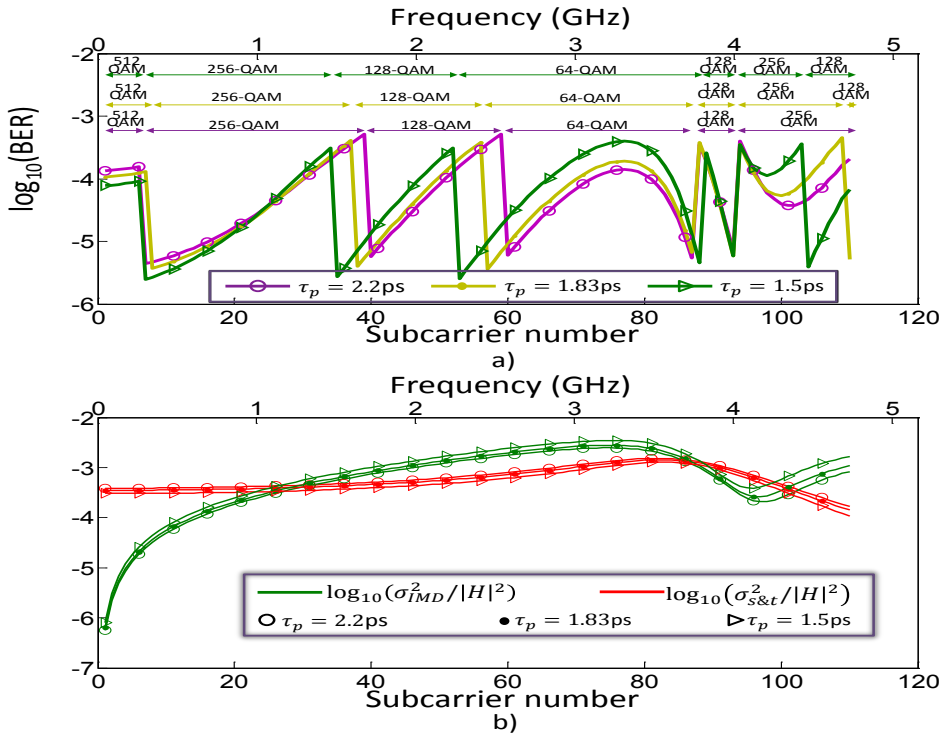

Figure 4.19: a) BER of each subcarrier and corresponding modulation format. b) Nonlinear distortion and receiver noise variances to signal power.

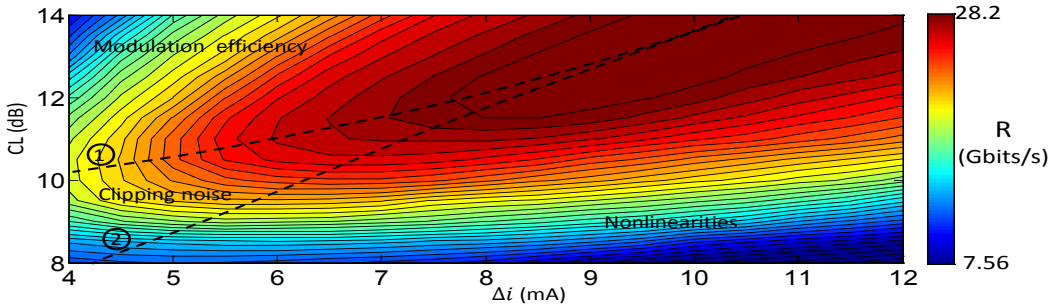

Figure 4.20: Information transmission rate as a function of CL and Δi.

Finally, we determine the performance achieved with different lengths of cyclic extensions. The results obtained for $i_0 = 46mA$, $\alpha = 4$, $\varepsilon_{nl} = 1.7 \times 10^{-23} m^3$, $\tau_p = 1.83$ps, $\Delta i = 8.5$mA and $CL = 12$dB are shown in Fig. 4.21.

From Fig. 4.21 it is clear than smaller values for N_{pre} and N_{pos} can be used without falling into a penalty due to ISI & ICI effects. It is worth mentioning that bit loading may be also helping to overcome ISI & ICI effects by allocating more bits into those subcarrier more weakly impaired [92], given that, as it was observed in previous sections, the variance of ISI & ICI is not uniformly distributed with the frequency. From Fig. 4.21, a value of $N_{pre} = N_{pos} = 8$ can be used, leading to a transmission information rate equal to 32.83Gbits/s. Taking into account that we are generating a double-sideband OOFDM signal with a bandwidth around 4.73GHz, it means a spectral efficiency of approximately 3.47bits/s/Hz.

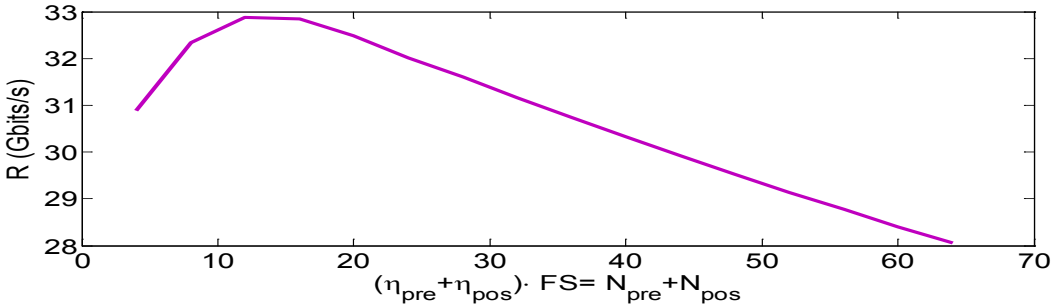

Figure 4.21: Information transmission rate as a function of $N_{pre} + N_{pos}$.

4.4.2.2 Optical fiber length equal to 100km

The obvious effect of the increase on the fiber length up to 100km is the higher attenuation of the optical signal, and, consequently, a greater influence of the receiver noise. In Fig. 4.22 we show the results obtained for L=100km.

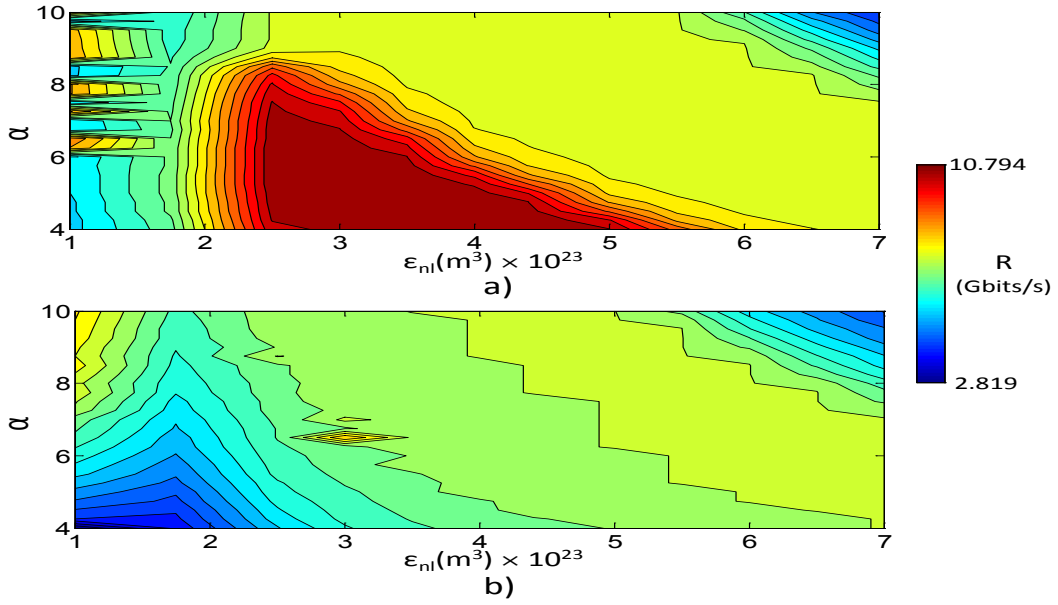

Figure 4.22: Information transmission rate. a) i_0=50mA, $\Delta i = 10mA$, CL = 11dB; b) i_0=75mA, $\Delta i = 10mA$, CL = 11dB.

We can see that, as expected, the achievable transmission information rates are greatly reduced when compared to L=40km, and the maximum value for R is around 10.8Gbits/s. This maximum value for R is obtained when i_0=50mA (Fig. 4.22(a)), $\varepsilon_{nl} = 3.5 \times 10^{-23} m^3$ and $\alpha = 4.5$. An increase of the laser bias point to 75mA (Fig. 4.22(b)) yields a considerable information transmission rate penalty due to the higher optical attenuation needed to adjust the input power to 0dBm.

The simultaneous variation of the amplitude swing Δi and the clipping level does not help to the increase of R, as we can observe from Fig. 4.23(a). The great dominant influence of

the receiver noise is behind the wide area for which values for R close the maximum value are obtained. After varying the cyclic extension lengths, Fig. 4.23(b), we can achieve a transmission information rate around 13.12Gbits/s for $N_{pre} + N_{pos} = 4$, which implies a spectral efficiency of 1.37bits/s/Hz.

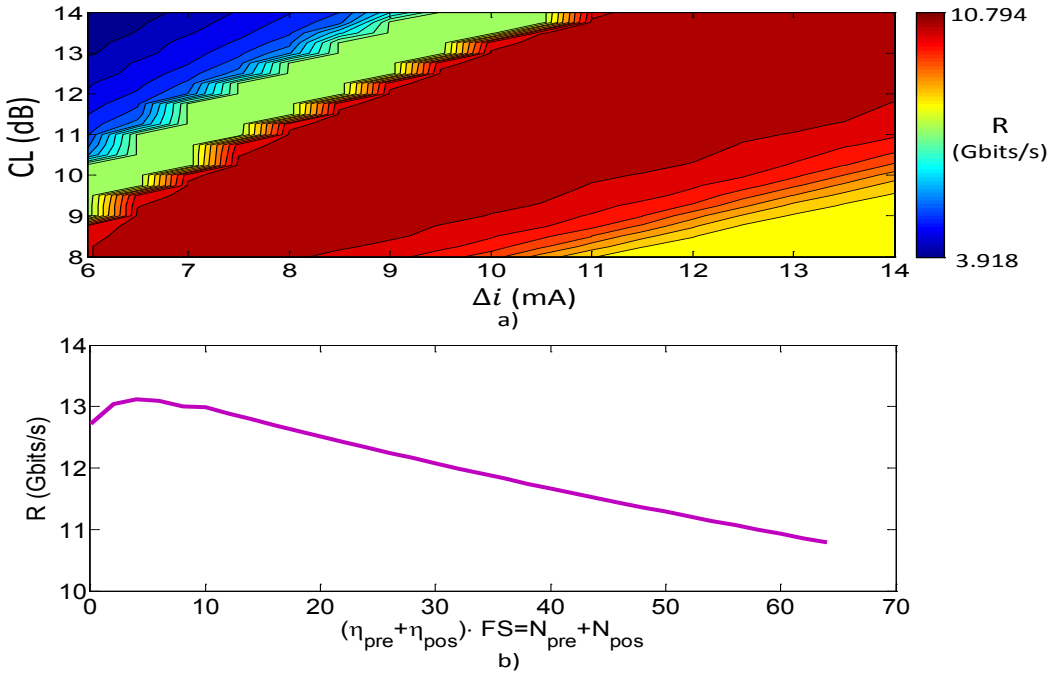

Figure 4.23: Information transmission rate. a) i_0=50mA, $\varepsilon_{nl} = 3.5 \times 10^{-23} m^3$, $\alpha = 4.5$; b) i_0=50mA, $\varepsilon_{nl} = 3.5 \times 10^{-23} m^3$, $\alpha = 4.5$, CL=12dB, $\Delta i = 11mA$.

4.5 Summary

We have developed analytical expressions which provide a combined description of the manifold impairments which affect the quality of the detected OOFDM signal in a DM/DD system.

The clipping noise at the receiver side has been derived by means of its power spectral density, for which a slight modification has been proposed to account for the non-uniform temporal ocurrence of clipping. For systems operating at BER values around $10^{-3} - 10^{-4}$, a reasonable estimation of the appropriate value for the clipping level can be obtained with the theory provided. The results given demonstrate that for the clipping level, rather than choosing an unique value, it should be tailored to the operating conditions, which include a great variety of factors, and, thus, the theory provided constitutes a very useful tool for a fast estimation and understanding of the system performance.

We have also given an expression of the penalty imposed by the channel impulse response length, including the laser modulation and signal propagation through the optical fiber, and the correlation between the time OFDM signal samples. The study on the length of cyclic pre/postfix length is of great importance in systems with low number of subcarriers, where a

significant proportion of the transmitted signal is in the form of cyclic guards. Provided that quantization noise is negligible, both, the values of cyclic prefix/postfix length and clipping level, can be adjusted in order to get a particular value of BER. For the particular conditions studied in Subsection 4.4.1, for short distances ($\approx 20km$) the increase of CL leads to an increase of the system performance, and to achieve a BER equal to 10^{-4} a CL around 10dB is enough; on the other hand for longer distances and due to the effects of the receiver noise, the increase of CL leads reduced marginal system performance improvements: for $L = 50km$, a CL around [11dB,12dB] seems the most appropriate choice, and for $L = 80$km, the value of CL is substantially reduced to around 9dB.

We have taken a step forward into the study of the main nonlinear distortion in a DM/DD OOFDM system by giving detailed and comprehensive equations which offers great accuracy when compared to simulation results and allows us to find an optimum value of the laser operation region. The flexibility of the theory provided allows us to estimate the system performance at a subcarrier level, and, thus, use them in combination with adaptive modulation format techniques. By appropriate tuning of the system parameters and using adaptive modulation format, for $N = 440$ and a laser bias point i_0=60mA, an information transmission rate of 30.7 Gbits/s through 50 km of optical fiber and with an OFDM signal bandwidth of 4.73GHz can be obtained by setting $CL = 11.35$dB and Δi=8mA.

We have also quantified the system performance through the information transmission rate achieved as figure of merit when bit loading is employed. System parameters such as the laser bias point/modulation depth/linewidth enhancement factor/nonlinear gain coefficient and the clipping level have been varied to explore the potentiality of DM/DD OOFDM systems. As expected, the laser nonlinear gain coefficient and the linewidth enhancement factor are determining parameters in the system performance. For a distance $L = 40$km, the most appropriate values are $\varepsilon_{nl} = 1.7 \times 10^{-23}\text{m}^3$ and $\alpha = 4$ with a laser bias point equal to 46mA; clear and distinguished operating regions impaired by different effects (clipping noise, nonlinear distortion, and receiver noise) have been found as result of changing the value for CL within [8dB,14dB] and the value for Δi within [4mA,12mA], giving as most appropriate values $CL = 12dB$ and $\Delta i = 8.5$mA. For $L = 100$km, the most appropriate values are $\varepsilon_{nl} = 1.7 \times 10^{-23}\text{m}^3$, $\alpha = 4.5$ and $i_0 = 50$mA; due to the longer distance and thus the higher attenuation, the receiver noise is the pre-dominant effect, and a broad area for which Δi and CL can be varied without significant changes in the achieved transmission information rate is obtained. After setting appropriately the length of the cyclic extensions, transmission information rates equal to 32.87Gbits/s and 13.12Gbits/s for $L = 40$km and $L = 100$km, respectively, have been achieved.

Chapter 5

Performance enhancement with pre-distorted signal waveforms

5.1 Introduction

As it is was mentioned in Chapters 1 and 2, OFDM is a widespread modulation format in wireless communication systems. In these systems, unlike for optical communication systems, the transmitted signal does not undergo any nonlinearity due to the channel [1] and equalization techniques have focused on the interference imposed by signals coming from different sources. For the efficient design of optical communication systems, solutions adapted to the peculiarities of optical communication channels are needed, and, in the case of DM/DD communication systems, techniques which focus on the nonlinearity due to the laser modulation, the propagation of the intensity modulated signal through the dispersive link and the photodetection process. These nonlinearities have been subject of study in Chapters 3 and 4.

Several solutions have been proposed in order to overcome the system performance limitations imposed by nonlinear distortion in intensity modulated optical systems [41, 42, 93–98]. For example, digital pre-distortion (DPD) technique was used to mitigate the nonlinearity of an externally modulated reflective semiconductor optical amplifier in [93], of a DML [94], and electro-absorption modulated lasers and Mach-Zehnder modulators [95]. In [96] a multi-stage digital postprocessing linearization technique based on the iterative substraction of distortion due to the Mach-Zehnder modulation and fiber propagation is proposed. In [41], an analytical model for the characterization of the nonlinear distortion in a DML-based OOFDM system is proposed and it is employed at the receiver-end side for the reconstruction of the interference terms and subsequent substraction using a decision-feedback equalizer; in [42] this technique is adapted to an electro-absorption modulated laser and the laser chirp analytical model is improved to achieve higher nonlinear distortion efficiency values in a

100km-haul link. In [97, 98] the employment of a nonlinear adaptive Volterra equalizer at the receiver-end side with low-cost optical modulators is investigated for short-reach links.

In this chapter, a pre-distortion technique which aims to mitigate the nonlinear distortion in DM/DD OOFDM systems is presented. This pre-distortion technique operates in the frequency domain (before the transmitter inverse Fourier transform), is based on the analytical model reported in Chapter 4 for the reconstruction of the interference, and takes advantage of the channel state information provided by the feedback link. Unlike the previously mentioned references about digital pre-distortion, the technique here proposed aims to mitigate the nonlinear distortion with an end-to-end perspective, rather than only that originated by the optical modulator. The system performance of the OOFDM system with the pre-distortion technique is evaluated for different operating conditions (clipping ratio, laser bias point and laser modulation depth).

The chapter is structured as follows: in Section 5.2, we provide a description of the proposed pre-distortion technique. Section 5.3 presents the results of extensive simulations using the analytical model of the system reported in Chapter 4 and employing the proposed pre-distortion technique. The system performance of a conventional DM/DD OOFDM system, that with the proposed technique and that obtained with nonlinear equalization at the receiver are compared. Finally, in Section 5.4, the contents of the chapter are summarized.

5.2 Proposed pre-distortion technique

The principle of the pre-distortion technique proposed in this chapter to outperform the performance of the basic DM/DD OOFDM system is rather simple and is based on the reconstruction of the interference $I[k]$ with $k = 1, 2...N$ and proper substraction at the transmitter. The motivation for such strategy relies on the potential knowledge available at the transmitter of the interference impairing the detected signal at the receiver end-side and, therefore, the possibility of achieving the capacity of the Gaussian channel without interference under a proper design [99]. The conventional DM/DD system is modified as illustrated in Fig. 5.1 when the proposed technique is employed. The OOFDM transmitter is exactly the same as that in previous chapters (mapping, IFFT, cyclic extensions, clipping and DAC). The same applies to the OOFDM receiver at the other end-side of the SMF, where the process is essentially the inverse to that in the transmitter. Once the optical modulated signal is generated through the direct laser modulation, and its average optical power has been adjusted, the signal is divided in two signals by means of an optical splitter with constant κ: one is transmitted through the optical fiber in order to extract the information from the received signal, and the other is directly fed-back to an OFDM receiver. The purpose of such division and the detection of the fed-back signal is explained next.

5.2.1 Interference reconstruction

The reconstruction of the interfering term $I[k] = I_{p,DML}[k] + I_{\phi,DML}[k] + I_{p/\phi,\beta_2}[k] + I_{\phi,\beta_2}[k] + I_{p,\beta_2}[k]$ with $k = 1, 2, ...N$ is based on the expressions reported in Chapter 4, Eqs. (4.27)-(4.31). We remember that $I_{p/\phi,\beta_2}$, I_{ϕ,β_2} and I_{p,β_2} are functions of the first order laser transfer functions $H_{p_1}(\Omega_k)$ and $H_{\phi_1}(\Omega_k)$, whilst $I_{p,DML}$ and $I_{\phi,DML}$ find their origin in the laser nonlinearities, and, thus, are functions of the second order transfer functions $H_{p_{11}}(\Omega_k, \Omega_l)$ and $H_{\phi_{11}}(\Omega_k, \Omega_l)$. Thereby, in order to reconstruct $I[k]$, we need to know

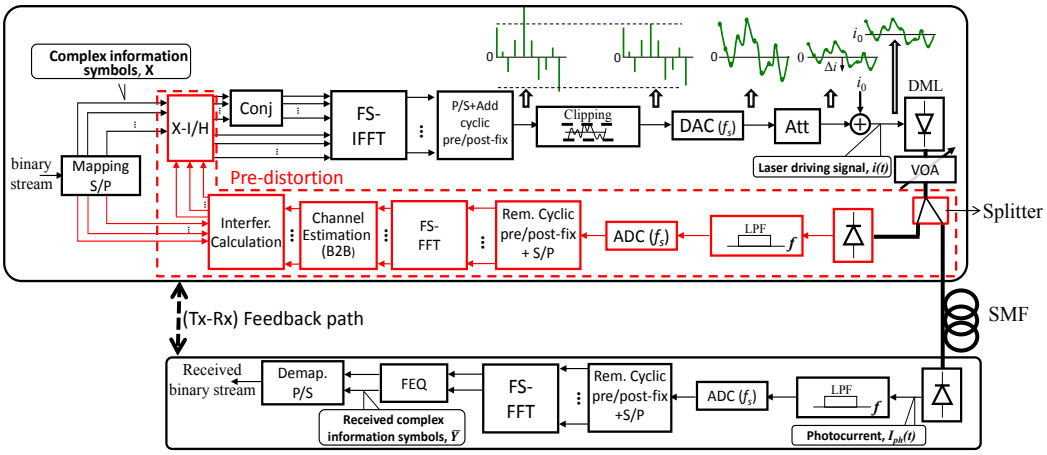

S/P: serial to parallel; **P/S**: parallel to serial; **(I)FFT**: (Inverse) fast Fourier transform;
DAC: digital-to-analog converter; **ADC**: analog-to-digital converter; **Att**: Attenuator; **VOA**: Variable optical attenuator;
SMF: single mode fiber; **DML**: directly modulated laser; **LPF**: low-pass filter; **FEQ**: frequency domain equalization

Figure 5.1: OOFDM system. Blocks in red: parts due to the proposed pre-distortion technique.

the fiber length L, the fiber group velocity dispersion parameter β_2, the fiber intensity attenuation coefficient α_{fib}, the average optical power P_0, and the laser intensity and phase modulation transfer functions $H_{p_1}(\Omega_k)$, $H_{p_{11}}(\Omega_k, \Omega_l)$ and $H_{\phi_1}(\Omega_k)$, $H_{\phi_{11}}(\Omega_k, \Omega_l)$, respectively.

Similarly to previous works [41, 42, 50], it is assumed that the transmitter has previous knowledge on the optical link parameters, such as L, β_2, and α_{fib}. From the feedback signal, the average optical power P_0 [50] and $H_{p_1}(\Omega_k)$ $k = 1, 2...N$ can be determined.

Once P_0 and $H_{p_1}(\Omega_k)$ $k = 1, 2...N$ are known, using the optical link attenuation and the accumulated dispersion, $H_{\phi_1}(\Omega_k)$ $k = 1, 2...N$ can be estimated from the total transfer function $H(\Omega_k)$ $k = 1, 2...N$:

$$H_e(e^{j\Omega_r}) = m \cdot e^{-\frac{\alpha_{fib}}{2}} \cdot \Big(2jP_0 \cdot H_{\phi_1}(\Omega_r) \cdot sin(\theta_r) + H_{p_1}(\Omega_r) \cdot cos(\theta_r)\Big) \tag{5.1}$$

Then, we can reconstruct the nonlinear distortion due to chromatic dispersion on the intensity and frequency modulated parts of the transmitted optical signal, $I_{p/\phi,\beta_2}[k]$, $I_{\phi,\beta_2}[k]$ and $I_{p,\beta_2}[k]$ with $k = 1, 2, ...N$ (see Eqs. (4.29)-(4.31)).

Moreover, the interfering terms caused by second order laser nonlinearity, $I_{p,DML}$ and $I_{\phi,DML}$, can be also partially mitigated. As previously said, they depend on the second order laser transfer functions $H_{p_{11}}(\Omega_k, \Omega_l)$ and $H_{\phi_{11}}(\Omega_k, \Omega_l)$. A possible approach for their calculation is the probing of the system with all the possible pairs of tones, though this approach would be time consuming and inefficient [100]. However, the second order laser intensity transfer function can be expressed as (see Appendix A):

$$H_{p_{11}}(\Omega_l, \Omega_{k-l}) = H'_{p_{11}}(\Omega_k) \cdot H_{p_1}(\Omega_l) H_{p_1}(\Omega_{k-l}) \tag{5.2}$$

$$H_{p_{11}}(\Omega_l, -\Omega_{l-k}) = H'_{p_{11}}(\Omega_k) \cdot H_{p_1}(\Omega_l) H^*_{p_1}(\Omega_{l-k}) \tag{5.3}$$

and therefore the nonlinear distortion term $I_{p,DML}$ (Eq. (4.27)) can be written as:

$$I_{p,DML}[k] = H'_{p_{11}}(\Omega_k)\cdot cos(\theta_k)\cdot\Big(\sum_{l=1}^{\lceil k/2\rceil-1} H_{p_1}(\Omega_l)H_{p_1}(\Omega_{k-l})\cdot i_l\cdot i_{k-l}\cdot e^{j(\varphi_{i_l}+\varphi_{i_{k-l}})}+ \sum_{l=k+1}^{N} H_{p_1}(\Omega_l)\cdot H^*_{p_1}(\Omega_{l-k})\cdot i_l\cdot i_{l-k}\cdot e^{j(\varphi_{i_l}-\varphi_{i_{l-k}})}\Big) \tag{5.4}$$

from which a estimation of $H'_{p_{11}}(\Omega_k)$, $k = 1,2...N$ can be obtained from the back-to-back feedback path, and, thus, of the second order nonlinear distortion transfer function $H_{p_{11}}(\Omega_l,\Omega_{k-l})$, $k = 1,2...N$. Finally, from Eq. (A.21) the second order transfer function $H_{\phi_{11}}(\Omega_k,\Omega_l)$ can be written as:

$$H_{\phi_{11}}(\Omega_l,\Omega_{k-l}) = \left(\frac{H_{\phi_1}(\Omega_k)}{H_{p_1}(\Omega_k)}\cdot H'_{p_{11}}(\Omega_k) - \frac{\frac{1}{2}\alpha\Gamma v_g a_g\cdot\Gamma\cdot G_n(n_0,p_0)\cdot\left(\frac{\delta_1 n(\Omega_l)}{\delta_1 p(\Omega_l)}+\frac{\delta_1 n(\Omega_{k-l})}{\delta_1 p(\Omega_{k-l})}\right)}{\left(\Gamma\cdot p_0\cdot G_n(n_0,p_0)+R_{sp}(n_0)+n_0\cdot\frac{dR_{sp}(n)}{dn}|_{n=n_0}\right)}\right)\cdot H_{p_1}(\Omega_l)H_{p_1}(\Omega_{k-l}) \tag{5.5}$$

being n_0 and p_0 the carrier and photon density steady-state values, respectively, $G_n(n,p) = \frac{\partial G(n,p)}{\partial n}$ and $G_p(n,p) = \frac{\partial G(n,p)}{\partial p}$ and $\frac{\delta_1 n(\Omega_r)}{\delta_1 p(\Omega_r)}$ denotes the first order transfer function of the carrier density modulation versus the photon density. The first term of the right hand side in Eq. (5.5) can be already determined, since we have estimated all the magnitudes involved, and the second one is considered as unknown. Thus, the pre-distortion technique is designed to perform a partial mitigation of the nonlinear distortion $I_{\phi,DML}[k]$, $k = 1,2...N$. For the sake of clarity, Fig. 5.2 depicts the way the different parameters involved in the reconstruction of the interference terms have been determined.

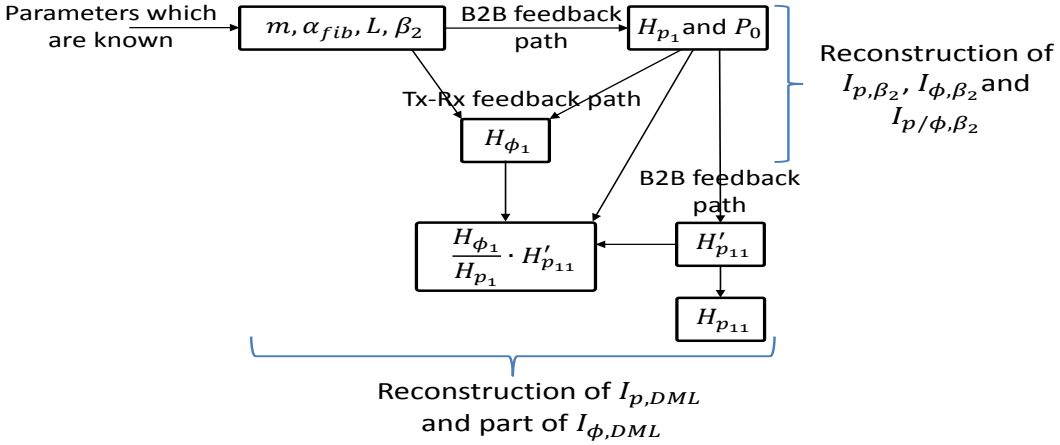

Figure 5.2: Parameter estimation for interference reconstruction.

5.2.2 Processing at the transmitter

Once the magnitudes involved in the expressions of the interference terms have been estimated, the reconstructed interference is substracted from the original information complex

symbols to generate the pre-distorted symbols to be transmitted on each OFDM subcarrier. Fig. 5.3 shows a block diagram of the proposed pre-distortion technique in order to clarify the steps followed. The part at the right side of Fig. 5.3 aims to provide updated estimations

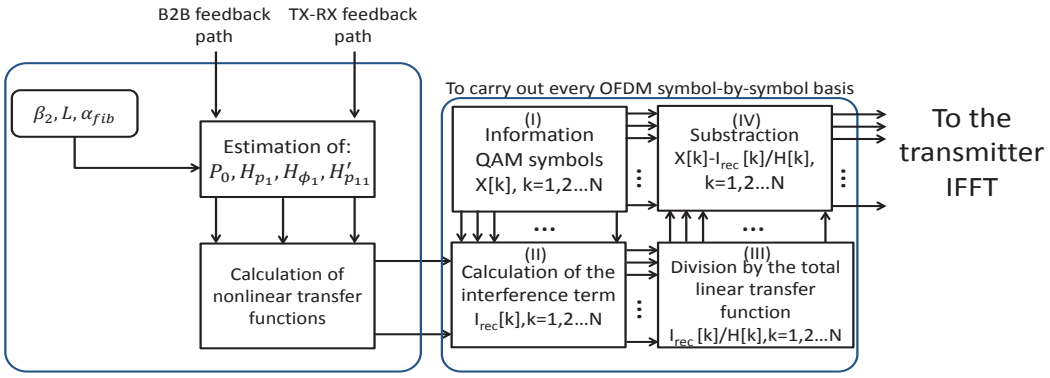

Figure 5.3: Block diagram of the proposed pre-distortion technique.

of the nonlinear transfer function coefficients for the reconstruction of the interference term. Denoting as X_k^0 the original information symbols X_k, once the symbols X_k^0, $k = 1, 2, ...N$ are generated (block (I) in Fig. 5.3), the interference term $I_{rec}^0[k]$, $k = 1, 2, ...N$ is reconstructed (block (II) in Fig. 5.3) as:

$$
\begin{aligned}
&I_{rec}^0[k] = \\
&\sum_{l=1}^{\lceil k/2 \rceil - 1} \Big(H_{p/\phi,\beta_2\{1,1\}}(\Omega_l) \cdot H_{p/\phi,\beta_2\{1,1\}}(\Omega_{k-l}) + H_{\phi,\beta_2\{1,1\}}(\Omega_l) \cdot H_{\phi,\beta_2\{1,1\}}(\Omega_{k-l}) + \\
&H_{p,\beta_2\{1,1\}}(\Omega_k) \cdot H_{p,\beta_2\{1,1\}}(\Omega_{k-l}) + H'_{p,DML}(\Omega_k) \cdot H_{p,DML\{1,1\}}(\Omega_l) \cdot \\
&H_{p,DML\{1,1\}}(\Omega_{k-l}) + H'_{\phi,DML}(\Omega_k) \cdot H_{\phi,DML\{1,1\}}(\Omega_l) \cdot H_{\phi,DML\{1,1\}}(\Omega_{k-l}) \Big) \cdot \\
&X_l^0 \cdot X_{k-l}^0 + \sum_{l=k+1}^{N} \Big(H_{p/\phi,\beta_2\{1,-1\}}(\Omega_l) \cdot H_{p/\phi,\beta_2\{1,-1\}}(\Omega_{l-k}) + H_{\phi,\beta_2\{1,-1\}}(\Omega_l) \cdot \\
&H_{\phi,\beta_2\{1,-1\}}(\Omega_{l-k}) + H_{p,\beta_2\{1,-1\}}(\Omega_k) \cdot H_{p,\beta_2\{1,-1\}}(\Omega_{l-k}) + H'_{p,DML}(\Omega_k) \cdot \\
&H_{p,DML\{1,-1\}}(\Omega_l) \cdot H_{p,DML\{1,-1\}}(\Omega_{l-k}) + H'_{\phi,DML}(\Omega_k) \cdot \\
&H_{\phi,DML\{1,-1\}}(\Omega_l) \cdot H_{\phi,DML}(\Omega_{l-k}) \Big) \cdot X_l^0 \cdot (X_{l-k}^0)^*, \; k = 1, 2, ...N
\end{aligned}
\tag{5.6}
$$

where the nonlinear transfer function coefficients in Eq. (5.6) account for the effects of the electrical and optical (chromatic dispersion and fiber attenuation) parts of the communication system. $H_{p/\phi,\beta_2\{1,\pm1\}}$ are the coefficients for the reconstruction of $I_{p/\phi,\beta_2}$, and similarly for the rest of coefficients $H_{\phi,\beta_2\{1,\pm1\}}$, $H_{p,\beta_2\{1,\pm1\}}$, $H_{\phi,DML\{1,\pm1\}}$, $H'_{\phi,DML\{1,\pm1\}}$, $H_{p,DML\{1,\pm1\}}$ and $H'_{p,DML\{1,\pm1\}}$.

The interference term just computed, $I_{rec}^0[k]$, is divided by the total linear transfer function (block (III) in Fig. 5.3). Finally, the values $I_{rec}^0[k]/H[k]$, $k = 1, 2, ...N$ are subtracted from the information complex symbols (block (IV) in Fig. 5.3):

$$
X_k^1 = X_k^0 - I_{rec}^0[k]/H[k], \; k = 1, 2, ...N \tag{5.7}
$$

Next, we denote as $I^0[k]$ the nonlinear distortion which actually impairs the information signal in the DM/DD OOFDM system when X_k^0 are transmitted. As result of the transmi-

ssion of X_k^1 instead of X_k^0, we have at the output of the communication system (neglecting the noisy term):

$$Y[k] = H[k] \cdot X_k^1 + I^1[k] = H[k] \cdot X_k^0 - I_{rec}^0[k] + I^1[k] \tag{5.8}$$

where the interference $I^1[k]$ can be expressed in function of $I^0[k]$ as $I^1[k] = I^0[k] + \chi_1[k]$, where $\chi_1[k]$ is a difference term due to the transmission of $X_k^1,\ k = 1,..N$ instead of $X_k^0,\ k = 1, 2, ...N$ through the nonlinear communication system.

With this technique, the system performance increases provided that the reconstructed interference $I_{rec}^0[k]$ is sufficiently close to the actual interference $I^0[k]$ and the magnitude of the additional nonlinear term $\chi_1[k]$ is smaller than $I^0[k]$, which is a reasonable assumption in a communication system using high order QAM modulation formats and the symbols must be weakly impaired in order to assure a certain performance (e.g., $BER_T \leq 10^{-4}$). Under the first assumption:

$$Y[k] = H[k] \cdot X_k^0 - I_{rec}^0[k] + I^0[k] + \chi_1[k] \approx H[k] \cdot X_k^0 + \chi_1[k] \tag{5.9}$$

Provided that the reconstruction of the interference is sufficiently accurate and $I_{rec}^0[k] \approx I^0[k]$, it may be convenient to go further and proceed iteratively. By doing so, we can transmit $X_k^1 = X_k^0 - I_{rec}^1[k]$, where $I_{rec}^1[k]$ is now the reconstructed interference when X_k^1 are sent, and calculated by substituting X_k^0 by X_k^1, $k = 1, 2, ...N$ in Eq. (5.6).

The process could be repeated over and over again, but the nonlinear distortion is considerably reduced after the first iteration, and the remaining distortion is hardly reduced without a further refinement of the algorithm aimed to increase its efficiency. The limitation on the efficiency comes from the assumptions made for the simplification of the analytical model for the reconstruction of the nonlinear distortion and the transfer function estimations. In a real scenario, we should also add the tolerances and deviations of a practical implementation as another reason more for not going beyond in the iterative process.

Before the pre-distortion technique, the signal-to-noise ratio of the k-th subcarrier $SNR[k]$ is given by Eq. (4.34). The signal-to-noise ratio of the k-th subcarrier after application of the pre-distortion is denoted as $SNR_{prd}[k]$ and is given by:

$$SNR_{prd}[k] = \frac{\kappa^2 \cdot |H[k]|^2 \cdot \langle |X[k]|^2 \rangle}{\kappa^2 \cdot \left(\sigma_{clip}^2[k] + \sigma_{ISI\&ICI}^2[k] + \sigma_{shot}^2\right) + \eta_{canc}[k] \cdot \sigma_{IMD}^2[k] + \sigma_{ther}^2}$$
$$k = 1, 2, ...N \tag{5.10}$$

where $\eta_{canc}[k],\ k = 1, 2...N$ is the ratio between the nonlinear distortion power with and without using the pre-distortion technique:

$$\eta_{canc}[k] = \sigma_{IMD}^2|_{prd}[k] / \sigma_{IMD}^2[k],\ k = 1, 2...N \tag{5.11}$$

5.2.3 Complexity of the proposed technique

Digital techniques aimed to the mitigation of nonlinear distortion in OOFDM systems are rather complex due to the mixing of the information transmitted in parallel by multiple information channels. Regarding the technique proposed in this work, we have two differentiated parts, as shown in Fig. 5.3: the right side aims to provide updated nonlinear transfer coefficients, and the left side aims to reconstruct the interference term.

The update of the nonlinear transfer function coefficients in Eq. (5.6) may be performed every certain number of OFDM symbols, and, thus, the added complexity is less important compared to that added by the part at the left side of Fig. 5.3.

Since the interference term depends on the information symbols to be transmitted, it must be calculated for each OFDM symbol. The calculation of $I^0_{rec}[k]$, with $k = 1, 2, ...N$ represents the more complex part of the pre-distortion technique: its direct calculation as Eq. (5.6) would require a number of complex multiplications proportional to N^2:

$$\begin{aligned}\text{Number of complex multiplications} \approx 7(\text{inner products}) \cdot \Big(\frac{1}{2}\frac{N^2}{2}(\text{first sum}) \\ + \frac{N^2}{2}(\text{second sum})\Big) + 2 \cdot N(\text{outer products, first sum}) \\ + 2 \cdot N(\text{outer products, second sum}).\end{aligned} \tag{5.12}$$

Once obtained the reconstructed interference terms, N complex divisions further are needed to calculate $I^0_{rec}[k]/H[k]$, $k = 1, 2, ...N$.

Being the complexity of the algorithm of $\mathcal{O}(N^2)$ the practical application of the algorithm, even for a modest number of subcarriers N, is limited. Simplification of the algorithm must be carried out to achieve a reasonable applicability of the technique in a real-time transmission:

- By applying the pre-distortion technique selectively: in the previous subsection, we have pointed out the possibility of reducing interference terms of different nature, but, their impact is not necessarily equal and depends on the particular conditions of the communication system. If the pre-distortion is applied only for those with stronger power, some complexity reduction can be achieved. Moreover, the interference is not uniformly distributed with frequency [41, 101], which allows us to further reduce the complexity by applying the pre-distortion technique to those subcarriers more strongly impaired.

- As suggested in [41], the convolution of subcarriers in the frequency domain, such as that in expression Eq. (5.6), can be efficiently computed by means of discrete Fourier transform processing [102]. Each forward and inverse Fourier transform would require $\bar{N} \cdot log_2(\bar{N})$ complex multiplications (where $log_2(\bar{N})$ is the minimum integer such that $2N \leq \bar{N}$)). Since each of the two sums contains 5 inner terms, we would require to compute 10 forward and inverse Fourier transforms. However, the change of the complexity order from N^2 to $\bar{N} \cdot log_2(\bar{N})$ means a significant complexity reduction compared to its direct calculation for high and moderate values of N. Besides, as commented in the previous point, it may not be necessary to cancel all the interference terms in Eq. (5.6), which would reduce the number of forward and inverse Fourier transforms.

5.3 Results

5.3.1 System parameter values

The sampling rate f_{sam} is equal to 11Gsam/s, being the electrical bandwidth BW equal to 5.5GHz; the IFFT processor has a size of $FS = 256$; $N = 110$ subcarriers are used for information transmission; a cyclic pre- and post-fix of 32 samples ($N_{pre} = N_{pos} = 32$, $\eta_{pre} = \eta_{pos} = 32/256 = 1/8$) are appended to each OFDM symbol; after digital-to-analog conversion, the obtained analog signal is adapted for laser driving by scaling it to yield a peak-to-peak value of Δi and adding a dc-offset i_0. The laser model is the same as that employed in previous chapters (Eq. (2.24)), being the laser parameters employed for simulations those shown in Table 5.1.

Table 5.1: Laser parameters

f_0	193.1 THz
V	120×10^{-18} m^3
n_g	4
a_g	4×10^{-20} m^2
n_t	1.5×10^{24} m^{-3}
v_g	7.49×10^7 m/s
$\gamma_e(n)$	$A[s^{-1}] + B[m^3 s^{-1}] \cdot n + C[m^6 s^{-1}] \cdot n^2 =$ $0.1 \times 10^8 + 1.0 \times 10^{-16} \cdot n + 3 \times 10^{-41} \cdot n^2$
α	5
Γ	0.3
$R_{sp}(n)$	$\zeta \cdot \Gamma \cdot B \cdot n^2 =$ $10^{-4} \cdot 0.3 \cdot 1.0 \times 10^{-16} \cdot n^2$
$G(n,p)$	$a_g/(1 + \varepsilon_{nl}[m^3] \cdot p) =$ $4 \times 10^{-20}/(1 + 7 \times 10^{-23} \cdot p)$

The fiber chromatic dispersion D is set to 17ps/(km · nm) and the loss parameter to 0.2dB/km. The responsivity of the photodiode R is set to $1 A/W$. After photodetection, shot and thermal noises [89] have been considered, being 10pA/$\sqrt{\text{Hz}}$ the thermal noise spectral density.

5.3.2 Nonlinear distortion ratio

In order to evaluate the system performance of the OOFDM system through Eq. (5.10), the nonlinear distortion cancellation ratio of the pre-distortion technique, $\eta_{canc}[k]$, $k = 1, 2...N$, must be calculated. It is worthy to remark that for its computation one must turn to computationally time exhausting numerical simulations of the DM/DD OOFDM system in Fig. 5.1. The nonlinear distortion cancellation ratio depends greatly on the signal quality of both the back-to-back and Tx-Rx feedback paths, being the quality of the signals affected by the laser bias point i_0, the clipping introduced at the transmitter CL, and the amplitude swing of the laser modulating signal Δi. In Fig. 5.4 we show the value of $\eta_{canc}[k]$ for a

fiber length equal to 40km and three different laser bias points ($i_0 = 45$mA, $i_0 = 65$mA and $i_0 = 85$mA). Within each figure, CL and Δi are changed.

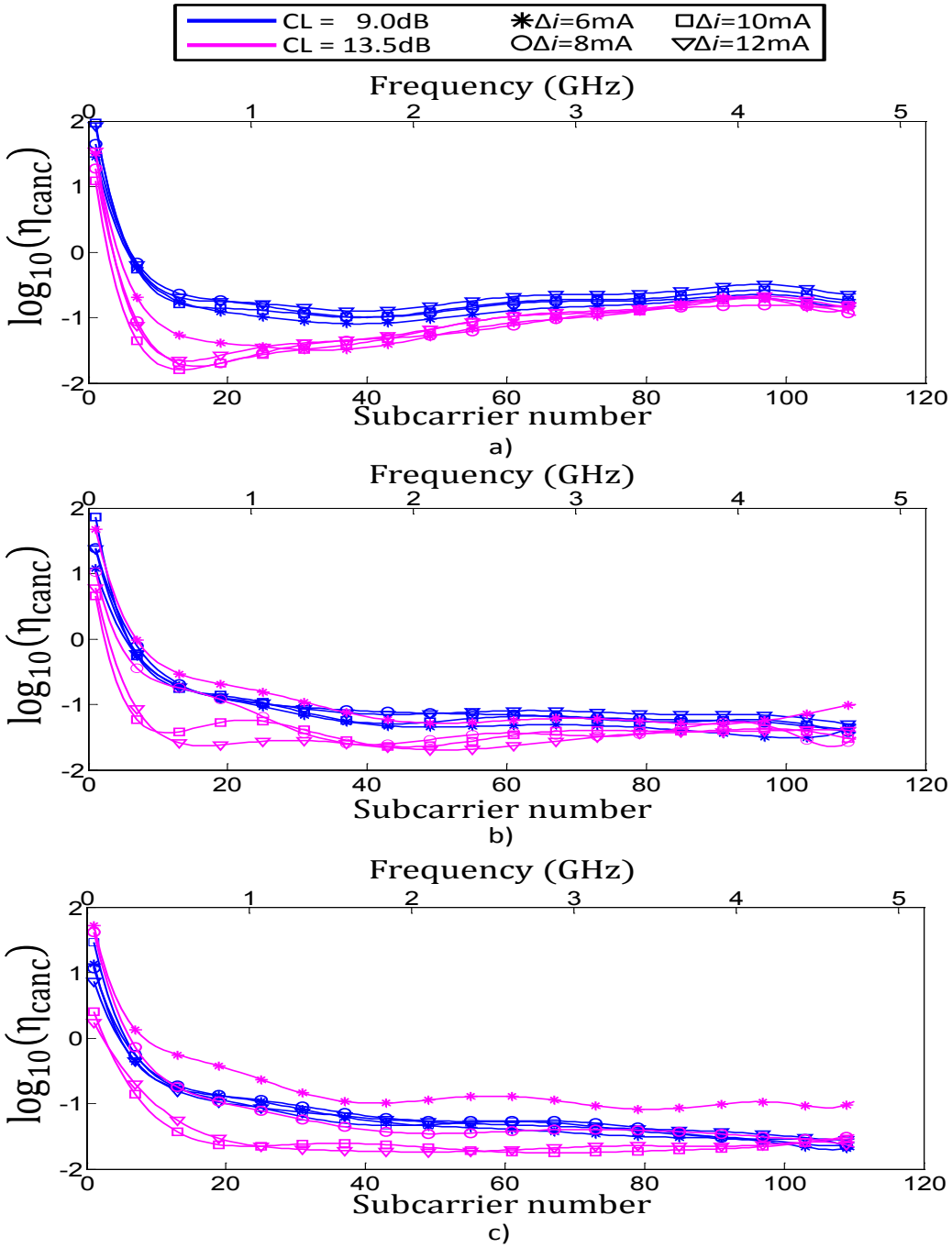

Figure 5.4: Nonlinear distortion cancellation ratio η_{canc} for a) $i_0 = 45mA$, b) $i_0 = 65mA$ and c) $i_0 = 85mA$. Optical fiber length equal to 40km.

In general, we can observe that the pre-distortion technique does not work appropriately at low frequencies, but this incorrect behavior is limited to a few number of the lowest

subcarriers, where the nonlinear distortion is typically low [101]. A poor laser modulation efficiency, as result of high values for i_0 and CL and a small value of Δi, leads to higher values of η_{canc}, as observed in Fig. 5.4(c) for $CL = 13.5dB$ and $\Delta i = 6$mA; from the same figure, we can also observe that an increase of Δi to 8, 10 and 12 mA, or the decrease of CL to 9dB gives us smaller values for η_{canc}. On the other hand, we must remember that the proposed pre-distortion technique relies on an approximated analytical model which is less accurate as the laser modulation efficiency increases. For example, in Fig. 5.4(a) for $CL = 9$dB, the increase of Δi leads to the increase of η_{canc}.

The nonlinear cancellation ratio of the proposed technique depends on the clipping introduced at the transmitter. The reduction of CL leads to a stronger influence of the clipping noise (which impairs the estimation of the transfer functions H_{p_1} and $H_{p_{11}}$) and a lower accuracy of the analytical model. This can be clearly observed In Fig. 5.4(a), where a value for CL equal to 9dB yields higher values for η_{canc} than for $CL = 13.5$dB. In particular, values around 0.1585 ($10^{-0.8}$) are obtained for $CL = 9dB$, and values within a range of $[0.025, 0.1259]$ ($[10^{-1.6}, 10^{-0.9}]$) are obtained for $CL = 13.5$dB. Apart from these aspects, the proposed technique achieves a considerable reduction of the nonlinear distortion, ranging from (Fig. 5.4(a)) $\eta_{canc} = 10^{-1.7} = 0.02$ to $\eta_{canc} = 10^{-0.9} = 0.126$ for $CL = 13.5$dB and $i_0 = 45$mA, values lower than (Fig. 5.4(b)) $\eta_{canc} = 10^{-1} = 0.1$ for $CL = 13.5$dB and $i_0 = 65$mA, and values around (Fig. 5.4(c)) $\eta_{canc} = 10^{-1.5} = 0.031$ for most of the subcarriers for $CL = 13.5$dB and $i_0 = 85$mA.

5.3.3 OOFDM system with bit-loading and pre-distortion

Once calculated η_{canc} for a set of system parameter values ($i_0 = 45$, 65, 75, 85mA, $CL =$ 9, 10.5, 12, 13.5dB, $\Delta i = 6$, 8, 10, 12mA and $L = 40$, 100km), a more exhaustive search for the optimum conditions is carried out using the simplified analytical model and the computation of the signal-to-noise ratio in Eq. (5.10). As it was done in the previous chapter, bit-loading is used, leading to different values of transmission information rate according to the channel conditions. Setting an objective BER_T equal to 10^{-4}, the results obtained when CL and Δi are changed for both the conventional DM/DD OOFDM system and that with pre-distortion are shown in Fig. 5.5.

The first aspect which calls our attention is the difference in transmission information rate values and in the optimum operation conditions between the systems with and without pre-distortion. The performance of the DM/DD OOFDM system with pre-distortion increases when the laser bias point is increased to $i_0 = 65$mA and $i_0 = 85$mA as compared to $i_0 = 45$mA, as we can observe by comparing Fig. 5.5(b.1) and (c.1) with Fig. 5.5(a.1). The amplitude swing of the laser modulating signal Δi ranges from 6mA to 12mA, and in the particular cases of $i_0 = 65$mA (Fig. 5.5(b.1)) and $i_0 = 85$mA (Fig. 5.5(c.1)), the higher transmission information rates are found for values of Δi higher than 10mA. Concretely, as indicated in Fig. 5.5(c.1), a maximum value equal to R=34.781Gbits/s is found for $i_0 =$ 85mA, $\Delta i = 11.5$mA and $CL = 12.5$dB. On the contrary, the decrease of the laser bias point is beneficial in the conventional DM/DD OOFDM system, and a value for $i_0 = 45$mA (Fig. 5.5(a.2)) gives us a transmission information rate $R = 25.781$Gbits/s when $\Delta i = 4$mA and $CL = 12$dB.

Regarding the system with pre-distortion, it can be observed that a reduction of the value for CL is detrimental due to the clipping noise. This is clearly observed in Figs. 5.5(b.1) and (c.1) by the fact that a reduction of CL from 11dB to 9dB leads to smaller values of

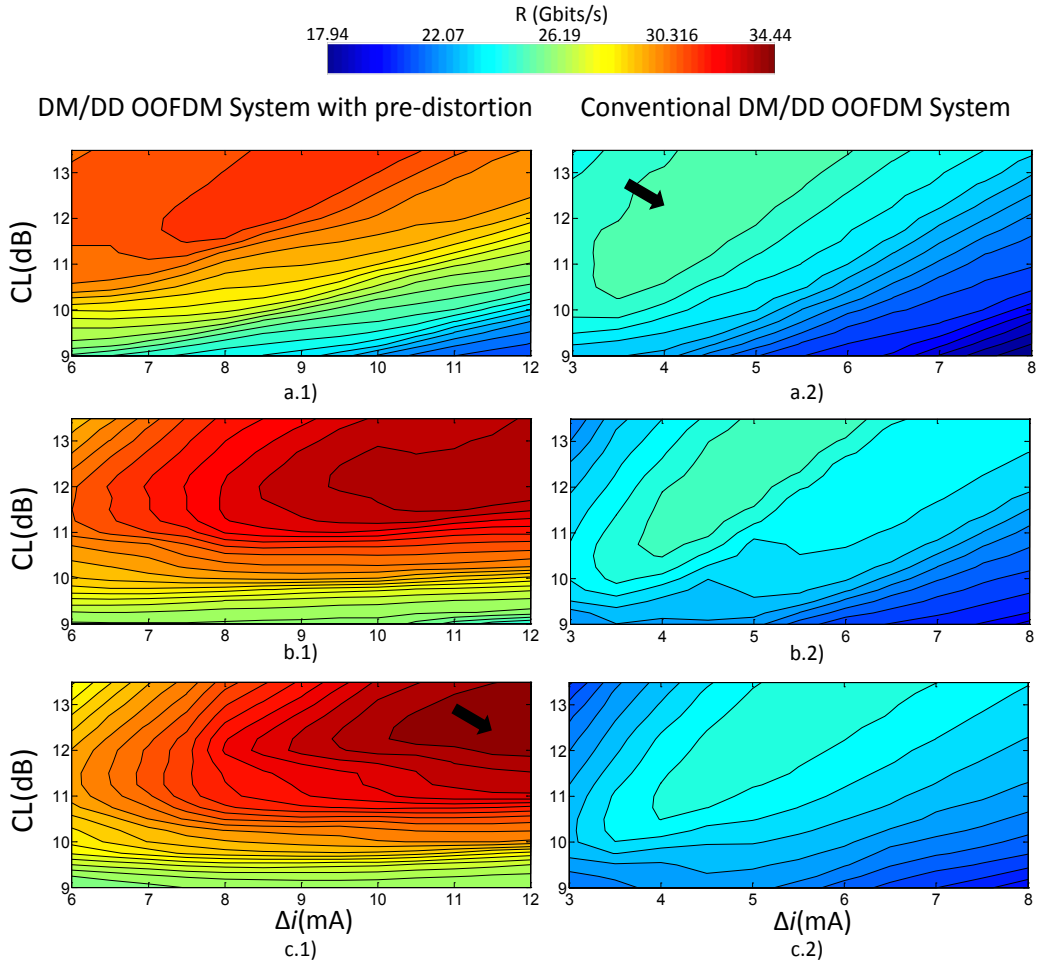

Figure 5.5: Transmission information rate as a function of CL and Δi for the DM/DD OOFDM system with pre-distortion (left side) and the conventional DM/DD OOFDM system (right side) for $L = 40$km a) $i_0 = 45mA$, b) $i_0 = 65mA$ and c) $i_0 = 85mA$.

R, but an increase of the amplitude swing of the laser modulating signal, Δi, has marginal effects. The increase of Δi and the consequent higher impact of nonlinearities is evident for $i_0 = 45$mA (Fig. 5.5(a.1)). An increase of the laser bias point to 65mA (Fig. 5.5(b.1)), and 85mA (Fig. 5.5(c)) seems to be beneficial and results in higher values of transmission information rate than for $i_0 = 45$mA. A reasonable value for the clipping level equal to 12dB, $i_0 = 65$mA and $\Delta i = 10$mA can provide us a transmission information rate around 34.4Gbits/s.

The results obtained for $L = 100$km and the DM/DD OOFDM system with pre-distortion are shown in Fig. 5.6. As we can observe, an increase of the value of CL leads generally to a reduction of the obtained transmission information rate because of the optical modulation efficiency loss. Remarkably, in Fig. 5.6(a) we can observe two different regions which lead to transmission information rates around 14Gbits/s, which is the result of the trade-offs between modulation effiency/receiver noise/nonlinear distortion/nonlinear distortion cancellation efficiency obtained the proposed pre-distortion technique. Similarly to $L = 40km$,

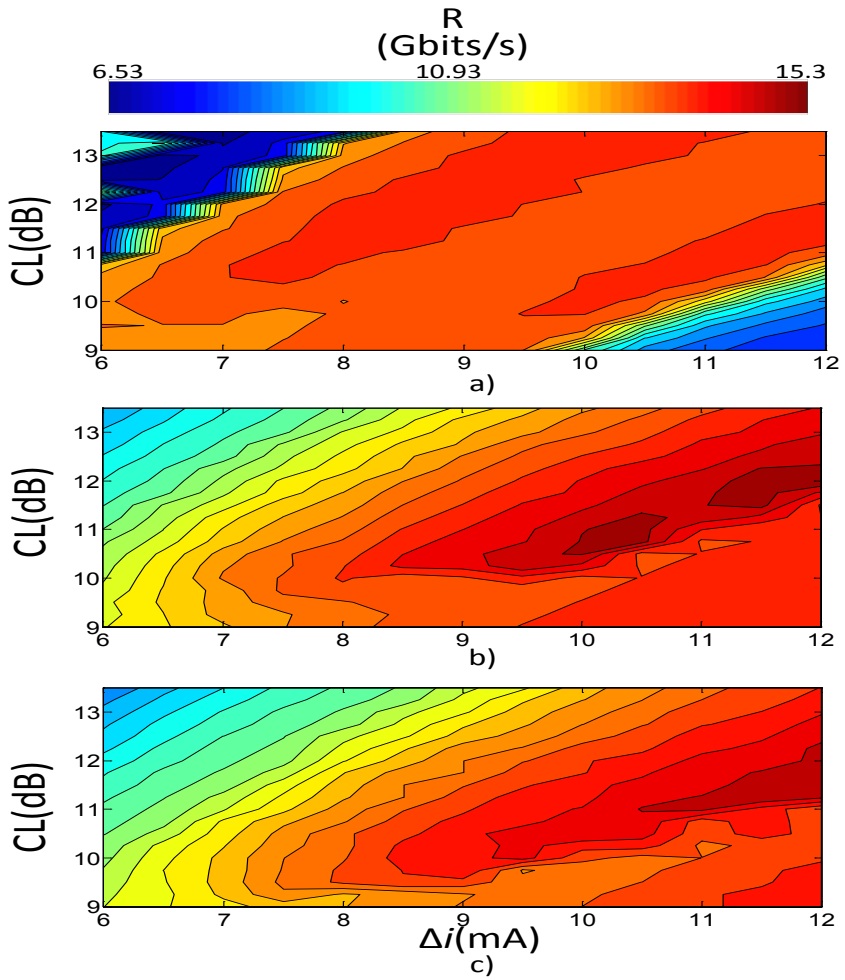

Figure 5.6: Transmission information rate as a function of CL and Δi for the DM/DD OOFDM system with pre-distortion for $L = 100$km a) $i_0 = 45mA$, b) $i_0 = 65mA$ and c) $i_0 = 85mA$.

an increase of the laser bias point to 65mA (Fig. 5.6(b)), and 85mA (Fig. 5.6(c)) gives us higher values of transmission information rate. By setting $i_0 = 65mA$, $CL = 12dB$ and $\Delta i = 12$mA, one can theoretically achieves a transmission information rate around 15.3Gbits/s.

In order to fully obtain the maximum system performance in terms of transmission rate, we study the obtained values for R when the length of the cyclic extensions N_{pre} and N_{pos} is changed in order to reduce as much as possible the number of redundant samples. With the values for i_0, CL and Δi set to the previously selected values ($i_0 = 65$mA, $CL = 12$dB, and $\Delta i = 10$mA for L=40km; $i_0 = 65$mA, $CL = 12$dB, and $\Delta i = 12$mA for L=100km), the obtained results are shown in Fig. 5.7 for both optical fiber lengths, $L = 40$km and $L = 100$km.

From Fig. 5.7(a) it is clear than smaller values for N_{pre} and N_{pos} can be used without falling into a penalty due to ISI & ICI effects. It is worth mentioning that bit loading may be also helping to overcome ISI & ICI effects by allocating more bits into those subcarrier more weakly impaired. Concretely, a value of $N_{pre} = N_{pos} = 4$ can be used, leading to a

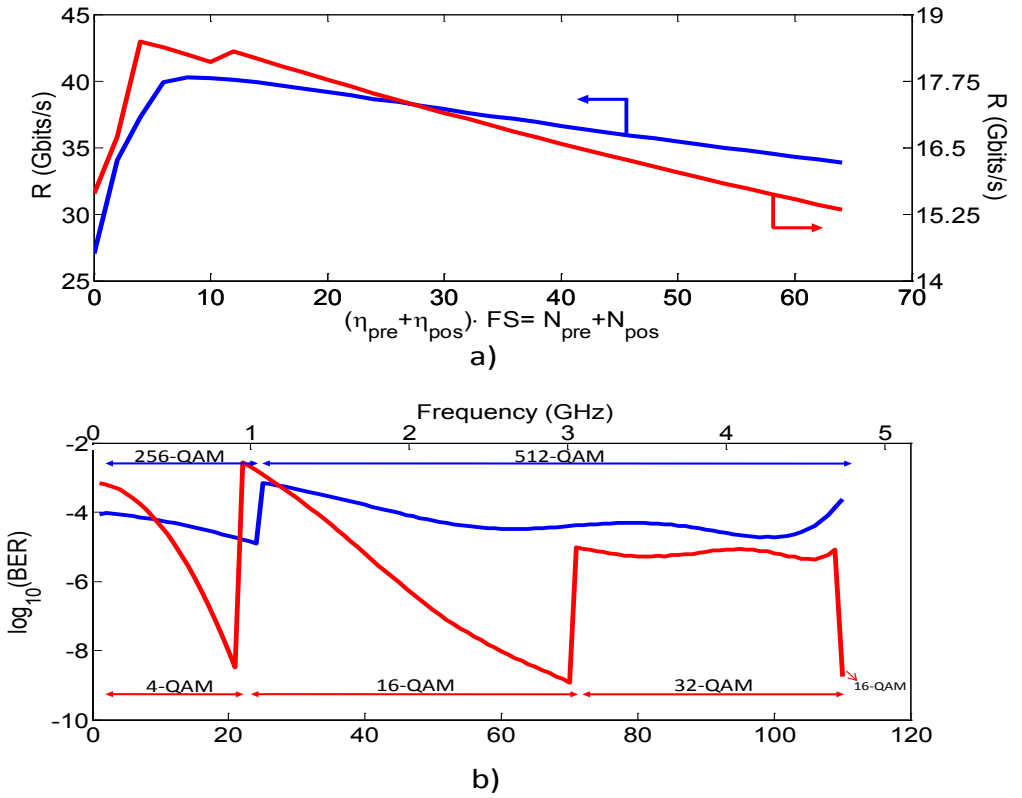

Figure 5.7: a) Information transmission rate achieved in function of the number of samples for the cyclic extensions, b) BER of each subcarrier and corresponding modulation format. Blue: optical fiber length equal to 40km. Red: optical fiber lengths equal to 100km.

transmission information rate equal to 40Gbits/s for $L = 40$km, whilst a value of $N_{pre} = N_{pos} = 2$ leads to a transmission information rate equals to 18.5Gbits/s for $L = 100$km. Using these cyclic extension lengths, the obtained BER and the modulation format employed of each subcarrier is shown in Fig. 5.7(b). For $L = 40$km, a modulation format as high as 512-QAM can be used in most of the signal bandwidth, and for $L = 100$km, 4-QAM, 16-QAM and 32-QAM are used for the information transmission.

5.3.4 Comparison with brute force simulations

In previous sections we have performed extensive simulations using the approximated and simplified model of the OOFDM system, which has allowed us to save time in the computation of the system performance. Now we compute the resulting BER through brute force simulations of the system in Fig. 5.1 and bit error counting with the final system parameters obtained in subsection 5.3.3.

For the conventional DM/DD OOFDM system, using $CL = 12dB$, $i_0 = 45$mA and $\Delta i = 4$mA, $N_{pre} = N_{pos} = 3$ for $L = 40km$ a transmission information rate equal to 31Gbits/s can be theoretically achieved, whilst the values found in the previous subsection are employed in the pre-distorted system. The conventional system and that with pre-distortion do not have

the same optimum operation conditions because of the mitigation of the nonlinear distortion and the change of the different system trade-offs involved in the performance of the two systems. The transfer functions and the obtained signal-to-noise ratio of the conventional system and that with pre-distortion are shown in Fig. 5.8 for L=40km. As expected, the

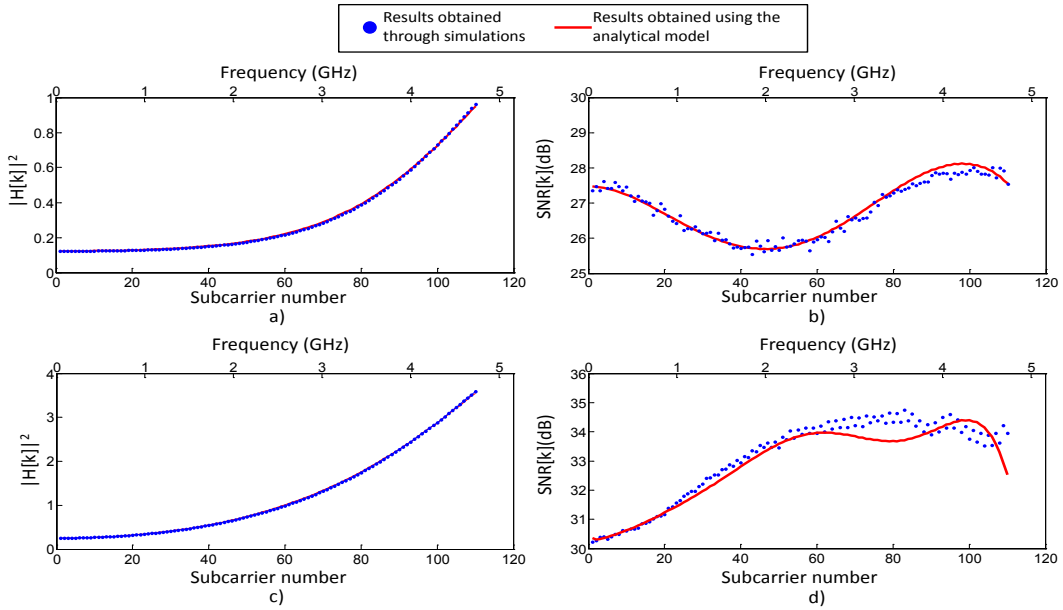

Figure 5.8: a) System transfer function of the conventional system, b) SNR of the conventional system, c) System transfer function of the system with pre-distortion technique, d) SNR of the system with pre-distortion technique (SNR_{prd}).

results obtained through simulations are in good agreement with those obtained using the analytical model. The magnitude of the transfer function of the system with pre-distortion (Fig. 5.8(c)) reach higher values than that obtained in the conventional system (Fig. 5.8(a)) due to the higher laser modulation efficiency. However, the increase on the value of Δi does not lead to a reduction of the signal-to-noise ratio due to nonlinear distortion (Fig. 5.8(d)) thanks to the pre-distortion technique.

The improvement on several dBs on the SNR when using the proposed technique (Fig. 5.8(d)) compared to the conventional system (Fig. 5.8(b)) allows us to increase significantly the transmission information rate, as we see next. Before, apart from these two systems, the system performance of a DM/DD OOFDM system with the non-equalizer receiver reported in [41] is also studied. The schematic of such non-equalizer is shown in Fig. 5.9. After passing the received signal into the frequency domain through the FFT operation, the complex symbols are linearly equalized, making decisions afterward on them. Note that these decisions may be right or wrong, depending on the quality of the received signal. The decided complex symbols are used to reconstruct the nonlinear distortion, in the same way as we did in our proposed technique at the transmitter. Once the interference terms are reconstructed, these are weighted by means of weighting coefficients previously calculated in a training stage. Finally, the weighted interference terms are subtracted from the received complex symbols at the output of the FFT. The process can be repeated iteratively, but only one iteration is recommended because of the computation complexity and the marginal improvement of further iterations [41].

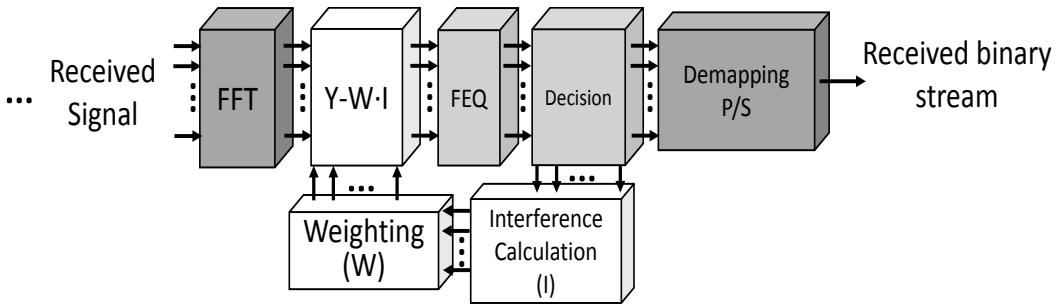

Figure 5.9: Decision-feedback equalizer at the receiver and proposed in [41].

The transmission information rate of the three systems is shown in Fig. 5.10 for L=40km and L=100km. For $L = 100$km, the conventional OOFDM system achieves a transmission information rate equal to 10Gbits/s with the optimized values $i_0 = 45$mA, $\Delta i = 7$mA, $CL = 12dB$ and $N_{pre} = N_{pos} = 3$ whilst the values found in the previous section are employed in the pre-distorted system. In the DM/DD OOFDM system with non-equalization at the receiver, our analytical model is used for the reconstruction of the interference. A high number of trials have been done to adjust the amplitude swing Δi and the laser bias current i_0 as well as the modulation format profile across the OFDM subcarriers in order to maximize the transmission information rate.

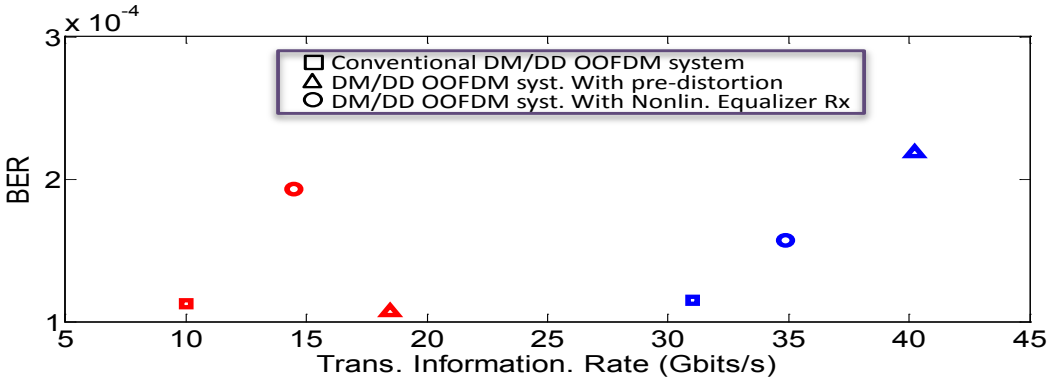

Figure 5.10: Obtained BER values obtained through brute force simulations.

We observe from Fig. 5.10 that the obtained BER values are close to the objective $BER = 10^{-4}$. As predicted by the simulations with the simplified model, the achieved transmission information rates when the pre-distortion technique is used are considerably higher. With the nonlinear equalizer at the receiver, the transmission information rates are equal to 33.08Gbits/s and 14.49Gbits/s for L=40km and L=100km, respectively. Though the values obtained with the nonlinear equalizer at the receiver are not the result of a so exhaustive system parameter optimization, the values presented in Fig. 5.10 show an intuitively clear issue: a nonlinear equalization at the receiver can improve the quality of the detected signal, but, since the interference reconstruction depend on decisions about the received information signal, the obtained performance will eventually depend on the signal quality of the conventional DM/DD OOFDM system.

In Fig. 5.11 we show the constellation diagrams of the 62th-110th subcarriers in order to get a visual impression of the improvement achieved by means of the proposed pre-distortion technique.

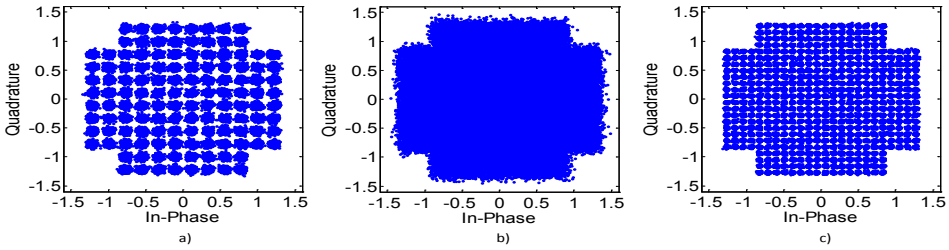

Figure 5.11: Constellation diagrams of the 62th to 110th subcarriers for $L = 40$km. a) Conventional DM/DD OOFDM system (128-QAM), b) DM/DD OOFDM system without pre-distortion technique (512-QAM), and c) DM/DD OOFDM system with pre-distortion technique (512-QAM).

The conventional DM/DD OOFDM system, with the same system parameters as those used to obtain the results in Fig. 5.10, employs 128-QAM in the subcarriers ranging from 62 to 110, and the received symbols after equalization are shown in Fig. 5.11(a). Using this modulation format guarantees that the obtained BER does not exceed considerably the objective $BER_T = 10^{-4}$, situation which would occur if the modulation format order is increased to 512-QAM. The aim of the constellation diagrams Figs. 5.11(b)–5.11(c) is to show the effects of the proposed pre-distortion technique. Both of them show the constellation diagram for the same subcarriers (62 to 110), using 512-QAM as modulation format and employing the same system parameters as those used to obtain the results in Fig. 5.10 for the system with pre-distortion, but in Fig. 5.11(b) the pre-distortion technique is not used at all. It is clear that the quality of the received signal is ruined and it would lead to an unacceptable value of BER_T. The use of the pre-distortion technique, Fig. 5.11(c), offers us a much clearer constellation diagram, and, similarly to Fig. 5.11(a), an appropriate quality of the received symbols is achieved and the value of the obtained BER_T does not increase significantly. Evidently, the transmission information rate achieved with the proposed technique is higher than that in the conventional system as result of using higher modulation format orders.

5.3.5 Tolerance to dispersion and optical link attenuation mismatches

As explained in the subsection 5.2.1, we start the interference reconstruction from the assumption that some parameters are known, such as the optical attenuation ($10^{-\alpha_{fib} \cdot L/10}$) or the accumulated dispersion ($D \cdot L$). In this subsection we explore the nonlinear distortion cancellation efficiency in front of mismatches in α_{fib} and D. In Fig. 5.12 we show the values obtained for η_{canc} when a value 0.2dB/km of intensity fiber attenuation is assumed, and the actual value is varied for $L = 40$km. As expected, the nonlinear distortion cancellation efficiency is deteriorated as we get away from the assumed value 0.2dB/km. In order to get similar values of η_{canc} to those obtained when the actual and the assumed values are equal, the total attenuation must not deviate beyond 3% from the assumed value. We can observe that errors of 7.6% may lead to values of η_{canc} higher than 0.2, reaching values up to 0.4, whilst errors of 9.6% may lead to values up to 0.6. The system performance improvements obtained with such poor cancellation distortion efficiencies may not be of sufficiently magnitude to pay the prize of the higher complexity the proposed technique requires.

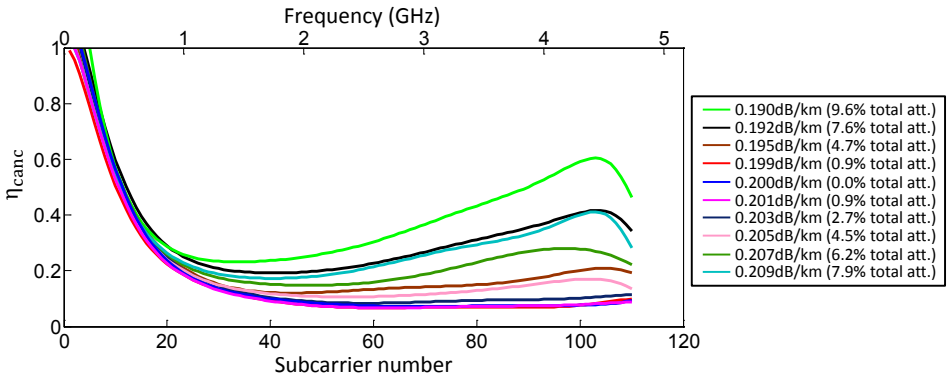

Figure 5.12: Nonlinear distortion cancellation ratio in front of attenuation estimation mistmaches. Optical fiber length equal to 40km.

In Fig. 5.13 we show the values obtained for η_{canc} when a value for the dispersion parameter equal to $17ps/(km \cdot nm)$ is assumed, and the actual value is varied for $L = 40$km. Surprisingly, the nonlinear distortion cancellation efficiency is not significantly affected, or

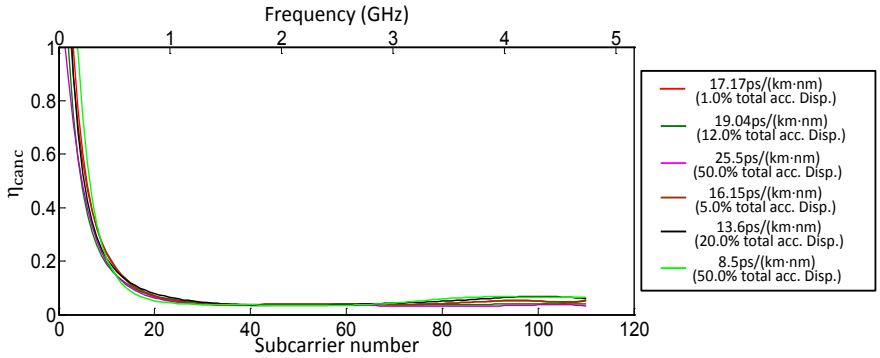

Figure 5.13: Nonlinear distortion cancellation ratio in front of accumulated dispersion estimation mistmaches. Optical fiber length equal to 40km.

not affected at all. The explanation for this is that the change on the dispersion parameter changes the total transfer function, and therefore the estimated value of the laser transfer function H_{ϕ_1}. Such change of the value of H_{ϕ_1}, may be, surprisingly, compensating for the deviations in the reconstruction of the interference terms.

5.4 Summary

We have proposed a novel pre-distortion technique which takes advantage of the relatively stable conditions in a DM/DD system, in such a way the transmitter may know a priori the impairing nonlinear distortion at the transmitter. Its operation conditions have been studied in order to explore its potential performance and make comparisons with that obtained in a conventional DM/DD OOFDM system. Significant nonlinear distortion reduction ratio values have been obtained, arriving up to values equal to [0.02,0.13]. The system performance has been greatly improved for different distances, allowing to employ higher modulation

QAM formats on the OFDM subcarriers. Transmission information rates equal to 40Gbits/s and 18.5Gbits/s have been obtained for L=40km and L=100km, respectively, with a BER in the order of 10^{-4}.

We have also compared the results obtained with those from brute force simulations, demonstrating the feasibility of the simplified analytical model to predict the final system performance in front of varying system parameters. The results also show that the performance obtained with the pre-distortion technique proposed in this work outperforms that obtained with a nonlinear distortion canceller at the receiver: the pre-distorted waveform may be considered as a special modulation format, with particular optimum operating conditions, whilst the performance with a nonlinear distortion canceler at the receiver is unavoidably linked to the operating conditions/performance of the conventional OOFDM system to assure a certain level quality of the received signal. The transmission information rates obtained when a nonlinear equalizer at the receiver is used are equal to 33.08Gbits/s and 14.49Gbits/s for L=40km and L=100km, respectively. Furthermore, apart from the substantial improvement compared to the nonlinear equalization at the receiver, the proposed pre-distortion technique would allow us to locate the more complex electrical parts in the optical line terminal instead of in the optical network unit for downlink transmission, which is advantageous in optical access networks.

Finally, we have studied the obtained nonlinear distortion cancellation efficiency in front of mismatches in the optical link attenuation and dispersion: the proposed technique is significantly sensitive to errors in the estimated optical attenuation, making necessary to precisely determine this magnitude; on the other hand, the proposed technique is very robust to errors in the estimated accumulated dispersion, and the nonlinear distortion cancellation efficiency remains practically equal even for important deviations in the accumulated dispersion. The latter aspect requires more study, and may open an interesting line for the simplification of the proposed technique.

The pre-distortion technique here proposed represents a valuable technique for its employment in optical metro/access networks, where the two-way end-to-end communications is a reasonable assumption, and, thus, the transmitter can extract information on the transmission channel. The proposed dedicated receiver added for monitoring purposes may be that used for communications in a bi-directional communication system: the receiver is used most of the time for communications (uplink direction), and, only, in some intervals of time, it may perform monitoring to update the parameters involved in the reconstruction of the interference.

Chapter 6

Optically filtered DM/DD OOFDM Systems

6.1 Introduction

In previous chapters we have seen that, despite of the advantages brought by the direct modulation of a laser in the OFDM transmitter in terms of cost reduction, compactness, low power consumption and high optical output power, its performance is severely limited by distortions arising from the laser, the optical intensity detection process and the propagation of the chirped signal through the dispersive link. To overcome these one can rely, for instance, on electronic techniques for the cancellation of the nonlinear distortions, such as that presented in Chapter 5. Another interesting alternative is the use of an optical filter to improve the system performance by suitable conversion of the inherent frequency modulation at the laser transmitter output into additional intensity modulation at the end of the link [103].

The optical filtering technique is only qualitatively understood and further work is necessary to grasp the theoretical foundations which can provide the design criteria for optimum operation. For instance a 7dB improvement of power budget has been reported in [104] but neither a thorough explanation for this improvement nor the directions for further exploit the potential of this technique are well understood [105].

This chapter addresses precisely this point by providing an end-to-end analytical model to describe the operation of a DM/DD OOFDM system when an arbitrary optical filter is inserted in the dispersive link. This is done by extending the analysis presented in Chapter 3 for the description of DM/DD OOFDM systems. The chapter is structured as follows: in Section 6.2, we provide a theoretical description of the optically filtered OOFDM system which includes the derivation of the mathematical formulae. We also describe mathematically the transfer functions of the different optical filtering structures which are later employed in

the simulation and analytical results. Section 6.3 presents the results obtained by evaluating the expressions derived and those obtained through numerical simulations for the sake of validation. We then illustrate the optimization of the filter parameters by computing the effective signal-to-noise ratio and the power budget improvements are evaluated, paying special attention to the impact of the clipping level.

6.2 Optically filtered DM/DD multicarrier signals: theory

6.2.1 Analytical formulation

The optically filtered DM/DD OOFDM system considered in this paper consists of an OFDM transmitter, the DML, the dispersive fiber link, the optical filter, the photodetection stage, and, finally, the OFDM receiver, as shown in Fig. 6.1.

The main operations in the OFDM transmitter include data mapping using 16-QAM, IFFT, cyclic prefix insertion, OFDM symbol serialization, clipping and DAC.

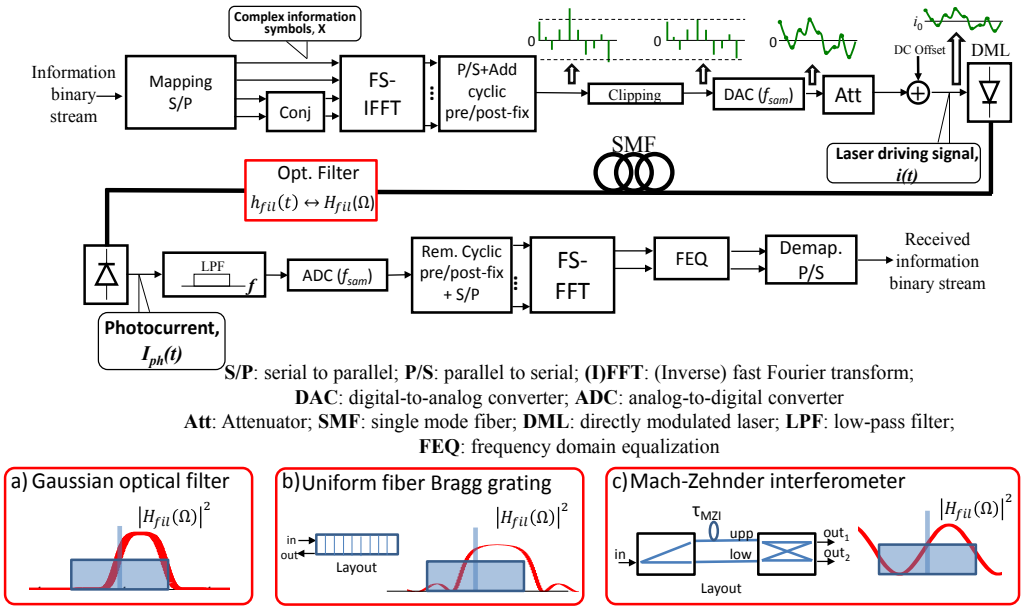

Figure 6.1: Schematic illustration of the optically filtered OOFDM system.

As we did in Chapter 3, the complex electrical field at the output of the laser source is approximated as:

$$E(t, z{=}0){=}$$
$$\left(\sqrt{P_0}{+}\frac{P_1(t)}{2\sqrt{P_0}}{+}\frac{P_2(t)}{2\sqrt{P_0}}{+}\frac{P_{11}(t)}{2\sqrt{P_0}}{-}\frac{P_1(t){\cdot}P_1(t)}{8P_0^{\frac{3}{2}}}\right){\cdot}exp\left(j{\cdot}\sum_{k=1}^{N} m_k{\cdot}sin(\Omega_k t{+}\varphi_{m_k})\right) \qquad (6.1)$$

where P_0 is the average optical power and

$$P_1(t) = \sum_{k=1}^{N} 2p_k \cdot cos\big(\Omega_k t + \varphi_{p_k}\big);\ P_2(t) = \sum_{k=1}^{N} 2p_{2k} \cdot cos\big(2\Omega_k t + \varphi_{p_{2k}}\big)$$
$$P_{11}(t) = \sum_{k=1}^{N}\sum_{l=1}^{k-1} 2p_{kl} \cdot cos\big((\Omega_k + \Omega_l)t + \varphi_{p_{kl}}\big)$$
$$+ \sum_{k=1}^{N}\sum_{l=1}^{k-1} 2p_{k\_l} \cdot cos\big(((\Omega_k - \Omega_l)t + \varphi_{p_{k\_l}})\big) \tag{6.2}$$

being $p_k \cdot exp(j\varphi_{p_k})$ the first order complex coefficient and $p_{2k} \cdot exp(j\varphi_{p_{2k}})$, $p_{kl} \cdot exp(j\varphi_{p_{kl}})$, $p_{k\_l} \cdot exp(j\varphi_{p_{k\_l}})$ the second order complex coefficients of the optical intensity, given by Eq. (3.11), whereas m_k is the frequency modulation index at the k-th subcarrier and φ_{m_k} its corresponding phase, which values are given by Eq. (3.15). As in previous chapters, the SMF is assumed to be a linear medium, whose transfer function is given by Eq. (3.6), and the field at its output is calculated through the inverse Fourier transform of the product of the spectra of the signal in Eq. (6.1) and the fiber transfer function:

$$E(t, z = L) = FT^{-1}\{E(\Omega, z = 0) \cdot H_{fib}(\Omega = \omega - \omega_0)\} =$$
$$\sum_{n_1,\ldots,n_N=-\infty}^{\infty} E_{(n_1,\ldots,n_N)}(z = L) \cdot e^{j\left(-\beta_0 \cdot L + \Omega_{imp} \cdot (t - \beta_1 \cdot L) + \sum_{i=1}^{N} n_i \cdot \varphi_{m_i} - \frac{\beta_2}{2}\Omega_{imp}^2 \cdot L\right)} \tag{6.3}$$

being $\Omega_{imp} = \sum_{k=1}^{N} n_k \cdot \Omega_k$. Note that the constant phase shift $e^{-j\beta_0 \cdot L}$ is cancelled out upon square-law detection and the time shift $\beta_1 \cdot L$ is not of importance under proper time synchronization at the receiver, such that $t' = t - \beta_1 \cdot L$. The effects of the optical filtering onto the optical signal can be easily taken into account using the well-known digital filtering theory [106, 107]. The impulse response and corresponding transfer function of the optical filter are given by:

$$h_{fil}(t') = \sum_{\kappa=0}^{Ord-1} h_\kappa \cdot \delta(t' - \tau_\kappa) \overset{\text{FT}}{\longleftrightarrow} H_{fil}(\Omega) = \sum_{\kappa=0}^{Ord-1} h_\kappa \cdot e^{-j \cdot \tau_\kappa \cdot \Omega} \tag{6.4}$$

where Ord is the order of the filter. Equation (6.4) is obviously valid for optical filters with finite impulse responses, and gives reasonably accurate results in the case of optical filters with infinite impulse responses provided that the value of Ord is set to a sufficiently high value. The field at its output is calculated as

$$E_{fil}(t', z = L) = \sum_{\kappa=0}^{Ord-1} h_\kappa \cdot E(t' - \tau_\kappa, z = L) \tag{6.5}$$

Finally, the photocurrent is calculated as the squared modulus of the field

$$I_{ph}(t') = \Re \cdot |E_{fil}(t', z = L)|^2 \tag{6.6}$$

being $\Re$ the responsivity of the photodetector. For the sake of simplification, we only consider the most relevant beats and we use the Graf's theorem for the sum of Bessel functions [76].

After a lengthy mathematical manipulation, $I_{ph}(t')$ can be expressed as:

$$I_{ph}(t') \approx \Re \cdot \sum_{\kappa=0}^{Ord-1} \sum_{\varepsilon=0}^{Ord-1} h_\kappa h_\varepsilon^* \cdot \sum_{n_1 \ldots n_N=-\infty}^{\infty} \Big(T0_{(n_1,\ldots,n_N)}(\kappa,\varepsilon) + T1_{(n_1,\ldots,n_N)}(\kappa,\varepsilon) + T2_{(n_1,\ldots,n_N)}(\kappa,\varepsilon) + T3_{(n_1,\ldots,n_N)}(\kappa,\varepsilon) + T4_{(n_1,\ldots,n_N)}(\kappa,\varepsilon) + T5_{(n_1,\ldots,n_N)}(\kappa,\varepsilon) \Big) \cdot exp\left(j \left(\Omega_{imp} t' + \sum_{i=1}^{N} n_i \left(\frac{\tau_\kappa + \tau_\varepsilon}{2} + \varphi_{m_i} + \frac{\pi}{2} \right) \right) \right) \tag{6.7}$$

$T0$ and $T1$ contain the information component, which can be extracted by setting one of the indices n_1, n_2,...n_N to 1, and the rest to 0, as well as nonlinear distortion due to the laser chirp, the expressions of which are obtained by particularizing the indices n_1, n_2,...n_N such that $\sum_1^N |n_k| > 1$. $T2$, $T3$, $T4$ and $T5$ are essentially terms due to nonlinear distortion which stem from the laser nonlinearities ($T2$ and $T3$) and the imbalance caused by the chromatic dispersion and optical filtering on the optical field ($T4$ and $T5$). The expressions of $T0$, $T1$, $T2$, $T3$, $T4$ and $T5$ are:

$$T0_{(n_1,\ldots,n_N)}(\kappa,\varepsilon) = J_{n_1}(\mu_{1,\kappa,\varepsilon}) \cdot\cdot J_{n_N}(\mu_{N,\kappa,\varepsilon}) \Big(P0 + \frac{1}{2P0} \sum_{k=1}^{N} p_k^2 \cdot cos(2\theta_{k,\kappa,\varepsilon}) \Big) \tag{6.8}$$

$$T1_{(n_1,\ldots,n_N)}(\kappa,\varepsilon) = J_{n_1}(\mu_{1,\kappa,\varepsilon}) \cdot\cdot J_{n_N}(\mu_{N,\kappa,\varepsilon}) \left(\sum_{k=1}^{N} \frac{p_k}{J_{n_k}(\mu_{k,\kappa,\varepsilon})} \cdot cos(\theta_{k,\kappa,\varepsilon}) \cdot \Big(J_{n_k+1}(\mu_{k,\kappa,\varepsilon}) \cdot e^{j(\varphi_{m_k} - \varphi_{p_k} + \frac{\pi}{2})} + J_{n_k-1}(\mu_{k,\kappa,\varepsilon}) \cdot e^{-j(\varphi_{m_k} - \varphi_{p_k} + \frac{\pi}{2})} \Big) \right) \tag{6.9}$$

$$T2_{(n_1,\ldots,n_N)}(\kappa,\varepsilon) = J_{n_1}(\mu_{1,\kappa,\varepsilon}) \cdot\cdot J_{n_N}(\mu_{N,\kappa,\varepsilon}) \left(\sum_{k=1}^{N} \frac{p_{2k} \cdot cos(2\theta_{k,\kappa,\varepsilon})}{J_{n_k}(\mu_{k,\kappa,\varepsilon})} \Big(J_{n_k+2}(\mu_{k,\kappa,\varepsilon}) \cdot e^{j(2\varphi_{m_k} - \varphi_{p_{2k}} + \pi)} + J_{n_k-2}(\mu_{k,\kappa,\varepsilon}) \cdot e^{-j(2\varphi_{m_k} - \varphi_{p_{2k}} + \pi)} \Big) \right) \tag{6.10}$$

$$T3_{(n_1,\,...,\,n_N)}(\kappa,\varepsilon) = J_{n_1}(\mu_{1,\kappa,\varepsilon})\cdot\cdot J_{n_N}(\mu_{N,\kappa,\varepsilon})\Bigg(\sum_{k=1}^{N}\sum_{l=1}^{k-1}\frac{p_{kl}}{J_{n_k}(\mu_{k,\kappa,\varepsilon})J_{n_l}(\mu_{l,\kappa,\varepsilon})}$$
$$cos(\theta_{k,\kappa,\varepsilon}+\theta_{l,\kappa,\varepsilon})\Big(J_{n_k+1}(\mu_{k,\kappa,\varepsilon})\cdot J_{n_l+1}(\mu_{l,\kappa,\varepsilon})\cdot e^{j(\varphi_{m_k}+\varphi_{m_l}-\varphi_{p_{kl}}+\pi)}+$$
$$J_{n_k-1}(\mu_{k,\kappa,\varepsilon})\cdot J_{n_l-1}(\mu_{l,\kappa,\varepsilon})\cdot e^{-j(\varphi_{m_k}+\varphi_{m_l}-\varphi_{p_{kl}}+\pi)}\Big)$$
$$+\sum_{k=1}^{N}\sum_{l=1}^{k-1}\frac{p_{k\_l}}{J_{n_k}(\mu_{k,\kappa,\varepsilon})J_{n_l}(\mu_{l,\kappa,\varepsilon})}$$
$$cos(\theta_{k,\kappa,\varepsilon}-\theta_{l,\kappa,\varepsilon})\Big(J_{n_k+1}(\mu_{k,\kappa,\varepsilon})\cdot J_{n_l-1}(\mu_{l,\kappa,\varepsilon})\cdot e^{j(\varphi_{m_k}-\varphi_{m_l}-\varphi_{p_{k\_l}})}+$$
$$J_{n_k-1}(\mu_{k,\kappa,\varepsilon})\cdot J_{n_l+1}(\mu_{l,\kappa,\varepsilon})\cdot e^{-j(\varphi_{m_k}-\varphi_{m_l}-\varphi_{p_{k\_l}})}\Big)\Bigg) \tag{6.11}$$

$$T4_{(n_1,\,...,\,n_N)}(\kappa,\varepsilon) = \frac{J_{n_1}(\mu_{1,\kappa,\varepsilon})\cdot\cdot J_{n_N}(\mu_{N,\kappa,\varepsilon})}{4\cdot P0}\Bigg(\sum_{k=1}^{N}\sum_{\substack{l=1\\l\neq k}}^{N}\frac{p_k\cdot p_l}{J_{n_k}(\mu_{k,\kappa,\varepsilon})J_{n_l}(\mu_{l,\kappa,\varepsilon})}$$
$$\Big(J_{n_k+1}(\mu_{k,\kappa,\varepsilon})\cdot J_{n_l+1}(\mu_{l,\kappa,\varepsilon})\cdot e^{j(\varphi_{m_k}-\varphi_{p_k}+\varphi_{m_l}-\varphi_{p_l}+\pi)}\begin{pmatrix}-cos(\theta_{k,\kappa,\varepsilon}+\theta_{l,\kappa,\varepsilon})+\\ e^{j(\theta_{k,\kappa,\varepsilon}-\theta_{l,\kappa,\varepsilon})}\end{pmatrix}$$
$$+J_{n_k-1}(\mu_{k,\kappa,\varepsilon})\cdot J_{n_l-1}(\mu_{l,\kappa,\varepsilon})\cdot e^{-j(\varphi_{m_k}-\varphi_{p_k}+\varphi_{m_l}-\varphi_{p_l}+\pi)}\begin{pmatrix}-cos(\theta_{k,\kappa,\varepsilon}+\theta_{l,\kappa,\varepsilon})+\\ e^{-j(\theta_{k,\kappa,\varepsilon}-\theta_{l,\kappa,\varepsilon})}\end{pmatrix}\Big)+$$
$$\sum_{k=1}^{N}\sum_{\substack{l=1\\l\neq k}}^{N}\frac{p_k\cdot p_l}{J_{n_k}(\mu_{k,\kappa,\varepsilon})J_{n_l}(\mu_{l,\kappa,\varepsilon})}$$
$$\Big(J_{n_k+1}(\mu_{k,\kappa,\varepsilon})\cdot J_{n_l-1}(\mu_{l,\kappa,\varepsilon})\cdot e^{j(\varphi_{m_k}-\varphi_{p_k}-\varphi_{m_l}+\varphi_{p_l})}\begin{pmatrix}-cos(\theta_{k,\kappa,\varepsilon}-\theta_{l,\kappa,\varepsilon})+\\ e^{j(\theta_{k,\kappa,\varepsilon}+\theta_{l,\kappa,\varepsilon})}\end{pmatrix}$$
$$+J_{n_k-1}(\mu_{k,\kappa,\varepsilon})\cdot J_{n_l+1}(\mu_{l,\kappa,\varepsilon})\cdot e^{-j(\varphi_{m_k}-\varphi_{p_k}-\varphi_{m_l}+\varphi_{p_l})}\Big)\begin{pmatrix}-cos(\theta_{k,\kappa,\varepsilon}-\theta_{l,\kappa,\varepsilon})+\\ e^{-j(\theta_{k,\kappa,\varepsilon}+\theta_{l,\kappa,\varepsilon})}\end{pmatrix}\Bigg) \tag{6.12}$$

$$T5_{(n_1,\,...,\,n_N)}(\kappa,\varepsilon) = J_{n_1}(\mu_{1,\kappa,\varepsilon})\cdot\cdot J_{n_N}(\mu_{N,\kappa,\varepsilon})\frac{1}{4\cdot P0}\Bigg(\sum_{k=1}^{N}p_k^2\frac{1-cos(2\theta_{k,\kappa,\varepsilon})}{J_{n_k}(\mu_{k,\kappa,\varepsilon})}$$
$$\Big(J_{n_k+2}(\mu_{k,\kappa,\varepsilon})\cdot e^{j2(\varphi_{m_k}-\varphi_{p_k}+\frac{\pi}{2})}+J_{n_k-2}(\mu_{k,\kappa,\varepsilon})\cdot e^{-j2(\varphi_{m_k}-\varphi_{p_k}+\frac{\pi}{2})}\Big)\Bigg) \tag{6.13}$$

where $\theta_{k,\kappa,\varepsilon} = -\big(\frac{\tau_\kappa-\tau_\varepsilon}{2}+\frac{\beta_2}{2}\Omega_{imp}\Omega_k L\big)$, and $\mu_k = 2m_k\cdot sin(\theta_{k,\kappa,\varepsilon})$. We can see that the dispersion-induced phase delay at Ω_r, equal to $-\beta_2/2\cdot\Omega_r^2\cdot L$, is increased by that due to the optical filter to result in $\theta_{r,\kappa,\varepsilon} = -\big(\frac{\tau_\kappa-\tau_\varepsilon}{2}+\frac{\beta_2}{2}\Omega_r^2 L\big)$. Moreover, from Eq. (6.7), the different spectra components are weighted by the product of the filter coefficients $h_\kappa\cdot h_\varepsilon^*$ and are also affected by the average phase delay $(\tau_\kappa+\tau_\varepsilon)/2$.

Because of the complexity of the expressions provided, we have proceeded as in Chapter 4 and we have obtained a simplified version of Eqs. (6.8)-(6.13) which gives reasonable good results: provided that the argument of the Bessel functions is sufficiently small, they can be approximated by the first term of their series expansion [76]; besides, within each sum, only the most significant contribution at the rth subcarrier is retained. With these simplifications

and making use of the transfer function of the optical filter Eq. (6.4), the expression for the signal information component can be expressed as:

$$\begin{aligned}&T0|_{n_r=1}+T1|_{n_r=1}=\\&\left(\frac{H^*_{fil}(0)\cdot H_{fil}(\Omega_r)}{2}\Big(H_{p1}\big(\Omega_r\big)\cdot e^{-j\cdot\Omega_r^2\frac{\beta_2}{2}L}+2\cdot P_0\cdot H_{\phi_1}\big(\Omega_r\big)\cdot e^{-j\cdot\Omega_r^2\frac{\beta_2}{2}L}\Big)+\right.\\&\left.\frac{H_{fil}(0)\cdot H^*_{fil}(-\Omega_r)}{2}\Big(H_{p1}\big(\Omega_r\big)\cdot e^{j\cdot\Omega_r^2\frac{\beta_2}{2}L}-2\cdot P_0\cdot H_{\phi_1}\big(\Omega_r\big)\cdot e^{j\cdot\Omega_r^2\frac{\beta_2}{2}L}\Big)\right)\cdot\frac{m}{2}\cdot X_r\end{aligned}\tag{6.14}$$

whilst the expressions obtained for the second order intermodulation falling on the rth subcarrier of the type $A+B$ and $A-B$, where A and B stand for two arbitrary subcarriers, are:

Intensity modulation nonlinearity

$$I^{A+B}_{p,DML}[r]=\sum_{l=1}^{\lceil r/2\rceil-1}H_{p_{11}}\big(\Omega_l,\Omega_{r-l}\big)\cdot\frac{1}{2}\begin{pmatrix}H_{fil}(0)\cdot H^*_{fil}(-\Omega_r)\cdot e^{-j\theta_r}\\+H_{fil}(\Omega_r)\cdot H^*_{fil}(0)\cdot e^{j\theta_r}\end{pmatrix}\cdot i_l\cdot i_{r-l}\cdot e^{j(\varphi_{i_l}+\varphi_{i_{r-l}})}\tag{6.15}$$

$$I^{A-B}_{p,DML}[r]=\sum_{l=r+1}^{N}H_{p_{11}}\big(\Omega_l,-\Omega_{l-r}\big)\cdot\frac{1}{2}\begin{pmatrix}H_{fil}(0)\cdot H^*_{fil}(-\Omega_r)\cdot e^{-j\theta_r}\\+H_{fil}(\Omega_r)\cdot H^*_{fil}(0)\cdot e^{j\theta_r}\end{pmatrix}\cdot i_l\cdot i_{l-r}\cdot e^{j(\varphi_{i_l}-\varphi_{i_{l-r}})}\tag{6.16}$$

Phase modulation nonlinearity

$$\begin{aligned}&I^{A+B}_{\phi,DML}[r]=\\&P_0\cdot 2j\sum_{l=1}^{\lceil r/2\rceil-1}\cdot H_{\phi_{11}}\big(\Omega_l,\Omega_{r-l}\big)\cdot\frac{1}{2}\begin{pmatrix}H_{fil}(0)\cdot H^*_{fil}(-\Omega_r)\cdot e^{-j\theta_r}\\-H_{fil}(\Omega_r)\cdot H^*_{fil}(0)\cdot e^{j\theta_r}\end{pmatrix}\cdot i_l\cdot i_{r-l}\cdot e^{j(\varphi_{i_l}+\varphi_{i_{r-l}})}\end{aligned}\tag{6.17}$$

$$\begin{aligned}&I^{A-B}_{\phi,DML}[r]=\\&P_0\cdot 2j\sum_{\substack{l=\\r+1}}^{N}P_0\cdot H_{\phi_{11}}\big(\Omega_l,-\Omega_{l-r}\big)\cdot\frac{1}{2}\begin{pmatrix}H_{fil}(0)\cdot H^*_{fil}(-\Omega_r)\cdot e^{-j\theta_r}\\-H_{fil}(\Omega_r)\cdot H^*_{fil}(0)\cdot e^{j\theta_r}\end{pmatrix}\cdot i_l\cdot i_{l-r}\cdot e^{j(\varphi_{i_l}-\varphi_{i_{l-r}})}\end{aligned}\tag{6.18}$$

Dispersion-imbalanced intensity/phase components

$$\begin{aligned}I^{A+B}_{p/\phi,\beta_2}[r]=(-2j)\cdot\Bigg[&\sum_{l=1}^{\lceil r/2\rceil-1}\frac{H_{p_1}\big(\Omega_l\big)H_{\phi_1}\big(\Omega_{r-l}\big)}{4}\cdot\\&\begin{pmatrix}H_{fil}(0)\cdot H^*_{fil}(-\Omega_r)\cdot e^{-j\theta_r}-H_{fil}(\Omega_r)\cdot H^*_{fil}(0)\cdot e^{j\theta_r}\\-H_{fil}(\Omega_{r-l})\cdot H^*_{fil}(-\Omega_l)\cdot e^{j(\theta_{r-l}-\theta_l)}+H_{fil}(\Omega_l)\cdot H^*_{fil}(-\Omega_{r-l})\cdot e^{-j(\theta_{r-l}-\theta_l)}\end{pmatrix}\\&\cdot i_l\cdot i_{r-l}\cdot e^{j(\varphi_{i_l}+\varphi_{i_{r-l}})}+\frac{H_{p_1}\big(\Omega_{r-l}\big)H_{\phi_1}\big(\Omega_l\big)}{4}\cdot\\&\begin{pmatrix}H_{fil}(0)\cdot H^*_{fil}(-\Omega_r)\cdot e^{-j\theta_r}-H_{fil}(\Omega_r)\cdot H^*_{fil}(0)\cdot e^{j\theta_r}\\+H_{fil}(\Omega_{r-l})\cdot H^*_{fil}(-\Omega_l)\cdot e^{j(\theta_{r-l}-\theta_l)}-H_{fil}(\Omega_l)\cdot H^*_{fil}(-\Omega_{r-l})\cdot e^{-j(\theta_{r-l}-\theta_l)}\end{pmatrix}\\&\cdot i_l\cdot i_{r-l}\cdot e^{j(\varphi_{i_l}+\varphi_{i_{r-l}})}\Bigg]\end{aligned}\tag{6.19}$$

$$I^{A-B}_{p/\phi,\beta_2}[r] = (-2j)\cdot\left[\sum_{\substack{l=\\ r+1}}^{N}\frac{H_{p_1}(\Omega_l)H^*_{\phi_1}(\Omega_{l-r})}{4}\cdot\right.$$
$$\begin{pmatrix} H_{fil}(0)\cdot H^*_{fil}(-\Omega_r)\cdot e^{-j\theta_r} - H_{fil}(\Omega_r)\cdot H^*_{fil}(0)\cdot e^{j\theta_r} \\ -H_{fil}(-\Omega_{l-r})\cdot H^*_{fil}(-\Omega_l)\cdot e^{-j(\theta_{l-r}+\theta_l)} + H_{fil}(\Omega_l)\cdot H^*_{fil}(\Omega_{l-r})\cdot e^{j(\theta_{l-r}+\theta_l)} \end{pmatrix}$$
$$\cdot i_l\cdot i_{l-r}\cdot e^{j(\varphi_{i_l}-\varphi_{i_{l-r}})} + \frac{H^*_{p_1}(\Omega_{l-r})H_{\phi_1}(\Omega_l)}{4}\cdot$$
$$\begin{pmatrix} H_{fil}(0)\cdot H^*_{fil}(-\Omega_r)\cdot e^{-j\theta_r} - H_{fil}(\Omega_r)\cdot H^*_{fil}(0)\cdot e^{j\theta_r} \\ +H_{fil}(-\Omega_{l-r})\cdot H^*_{fil}(-\Omega_l)\cdot e^{-j(\theta_{l-r}+\theta_l)} - H_{fil}(\Omega_l)\cdot H^*_{fil}(\Omega_{l-r})\cdot e^{j(\theta_{l-r}+\theta_l)} \end{pmatrix}$$
$$\left.\cdot i_l\cdot i_{l-r}\cdot e^{j(\varphi_{i_l}-\varphi_{i_{l-r}})}\right] \tag{6.20}$$

Dispersion-imbalanced phase components

$$I^{A+B}_{\phi,\beta_2}[r] = -4P_0\cdot\sum_{l=1}^{\lceil r/2\rceil-1}\frac{H_{\phi_1}(\Omega_l)H_{\phi_1}(\Omega_{r-l})}{4}\cdot$$
$$\begin{pmatrix} H_{fil}(0)\cdot H^*_{fil}(-\Omega_r)\cdot e^{-j\theta_r} + H_{fil}(\Omega_r)\cdot H^*_{fil}(0)\cdot e^{j\theta_r} \\ -H_{fil}(\Omega_{r-l})\cdot H^*_{fil}(-\Omega_l)\cdot e^{j(\theta_{r-l}-\theta_l)} - H_{fil}(\Omega_l)\cdot H^*_{fil}(-\Omega_{r-l})\cdot e^{-j(\theta_{r-l}-\theta_l)} \end{pmatrix}$$
$$\cdot i_l\cdot i_{r-l}\cdot e^{j(\varphi_{i_l}+\varphi_{i_{r-l}})} \tag{6.21}$$
$$I^{A-B}_{\phi,\beta_2}[r] = -4P_0\cdot\sum_{l=r+1}^{N}\frac{H_{\phi_1}(\Omega_l)H^*_{\phi_1}(\Omega_{l-r})}{4}\cdot$$
$$\begin{pmatrix} H_{fil}(0)\cdot H^*_{fil}(-\Omega_r)\cdot e^{-j\theta_r} + H_{fil}(\Omega_r)\cdot H^*_{fil}(0)\cdot e^{j\theta_r} \\ -H_{fil}(-\Omega_{l-r})\cdot H^*_{fil}(-\Omega_l)\cdot e^{-j(\theta_{l-r}+\theta_l)} - H_{fil}(\Omega_l)\cdot H^*_{fil}(\Omega_{l-r})\cdot e^{j(\theta_{l-r}+\theta_l)} \end{pmatrix}$$
$$\cdot i_l\cdot i_{l-r}\cdot e^{j\cdot(\varphi_{i_l}-\varphi_{i_{l-r}})} \tag{6.22}$$

Dispersion-imbalanced intensity components

$$I^{A+B}_{p,\beta_2}[r] = -\frac{1}{P_0}\cdot\sum_{l=1}^{\lceil r/2\rceil-1}\frac{H_{p_1}(\Omega_l)H_{p_1}(\Omega_{r-l})}{4}\cdot$$
$$\begin{pmatrix} H_{fil}(0)\cdot H^*_{fil}(-\Omega_r)\cdot e^{-j\theta_r} + H_{fil}(\Omega_r)\cdot H^*_{fil}(0)\cdot e^{j\theta_r} \\ -H_{fil}(\Omega_{r-l})\cdot H^*_{fil}(-\Omega_l)\cdot e^{j(\theta_{r-l}-\theta_l)} - H_{fil}(\Omega_l)\cdot H^*_{fil}(-\Omega_{r-l})\cdot e^{-j(\theta_{r-l}-\theta_l)} \end{pmatrix}$$
$$\cdot i_l\cdot i_{r-l}\cdot e^{j(\varphi_{i_l}+\varphi_{i_{r-l}})} \tag{6.23}$$
$$I^{A-B}_{p,\beta_2}[r] = -\frac{1}{P_0}\cdot\sum_{l=r+1}^{N}\frac{H_{p_1}(\Omega_l)H^*_{p_1}(\Omega_{l-r})}{4}\cdot$$
$$\begin{pmatrix} H_{fil}(0)\cdot H^*_{fil}(-\Omega_r)\cdot e^{-j\theta_r} + H_{fil}(\Omega_r)\cdot H^*_{fil}(0)\cdot e^{j\theta_r} \\ -H_{fil}(-\Omega_{l-r})\cdot H^*_{fil}(-\Omega_l)\cdot e^{-j(\theta_{l-r}+\theta_l)} - H_{fil}(\Omega_l)\cdot H^*_{fil}(\Omega_{l-r})\cdot e^{j(\theta_{l-r}+\theta_l)} \end{pmatrix}$$
$$\cdot i_l\cdot i_{l-r}\cdot e^{j\cdot(\varphi_{i_l}-\varphi_{i_{l-r}})} \tag{6.24}$$

where $\theta_k = \theta_{k,0,0} = -\frac{\beta_2}{2}\Omega_{imp}\Omega_k L$.

From expression Eq. (6.14) we note that:

- Since we have only considered the photocurrent terms due to the beat with the optical carrier, the photocurrent is null when the optical carrier vanishes, which occurs when $H_{fil}(0) = 0$.
- When no optical filter is used ($H_{fil}(\Omega) = 1$), the expression reduces to that reported in Chapter 3. Similar results are obtained when a symmetrical filtering with respect to the optical carrier ($H_{fil}(\Omega) = H_{fil}(-\Omega)$) is employed.
- In the case some asymmetry is introduced, information components that otherwise would be counteracted, start to spring up, increasing thus the signal information detected at the receiver and the system performance. This is the working principle of optical filtering techniques aimed to increase the system performance.
- Note that we have not taken into account ICI & ISI effects due to the impulse response of the channel once the optical filter is inserted. The previous analysis can not account for these effects, since it begins from the assumption that the RF-waves in Eq. (3.2) are non-finite. However, ICI and ISI effects can be easily quantified once the linear channel transfer function of the whole system Eq. (6.14) is obtained and can be used in Eq. (4.23).

6.2.2 Optical filtering approaches

6.2.2.1 Supergaussian filter

Optical filters with Supergaussian profiles are used as a first-step approximation to real filters (e.g., in [108]). The transfer function modulus is given by:

$$|H_{fil}(\Omega = \omega - \omega_0)| = exp\left(ln\left(\frac{1}{\sqrt{2}}\right) \cdot \left(\frac{\Omega - \Omega_c}{(\Delta\Omega_{3dB}/2)}\right)^{2 \cdot q}\right) \tag{6.25}$$

where Ω_c is the central angular frequency, $\Delta\Omega_{3dB}$ is the 3-dB bandwidth and q is the order of the Supergaussian filter. Its phase response is approximated by the finite summation [105]:

$$\phi^*_{fil}(\omega_i) = \frac{\Delta\omega}{\pi} \sum_{r=-R}^{R} \frac{\omega_i}{\omega_i^2 - \omega_r^2} \cdot ln\left(|H_{fil}(\omega_r)|\right) \tag{6.26}$$

which is based on the assumption that the optical filter satifies the causality condition and, thus, the real and imaginary parts of $H_{fil}(\Omega)$ are related by the Hilbert's transform [109]. In Eq. (6.26) R is an integer value for the truncation of the spectra calculation, $\Delta\omega$ the frequency step and $\omega_r = r \cdot \Delta\omega$.

6.2.2.2 Mach-Zehnder interferometer (MZI)

A simple implementable optical filter is given by the MZI, constructed simply by connecting the two output ports of a coupler to the two input ports of another coupler by means of two

delay lines with different lengths, as depicted in the inset (c) of Fig. 6.1. Depending on the output port, its impulse response is given by:

$$h_{fil,1}(t) = j{\cdot}\frac{1}{2}\big(exp(j\cdot\phi_{low}) + exp(j\cdot\phi_{upp}){\cdot}\delta(t-\tau_{MZI})\big) \tag{6.27}$$

if the output port 1 is selected, and:

$$h_{fil,2}(t) = \frac{1}{2}\big(exp(j\cdot\phi_{low}) - exp(j\cdot\phi_{upp}){\cdot}\delta(t-\tau_{MZI})\big) \tag{6.28}$$

if the output port 2 is selected.

6.2.2.3 Uniform fiber-Bragg grating (UFBG)

For the case of a UFBG, the coupled mode differential equations describing the evolution of the two counter-propagating modes in the periodically perturbed refractive index structure can be solved analytically. For a FBG with grating period Λ, effective modal index n_{eff} and zero-to-peak amplitude of the refractive index modulation δn, the amplitude reflection and transmission coefficients can be expressed as [110]:

$$r(f) = \frac{-j\cdot\frac{\kappa}{\gamma}\cdot sinh(\gamma\cdot L_{FBG})}{cosh(\gamma\cdot L_{FBG}) + j\frac{\delta}{\gamma}\cdot sinh(\gamma\cdot L_{FBG})} \tag{6.29}$$

$$t(f) = \frac{1}{cosh(\gamma\cdot L_{FBG}) + j\frac{\delta}{\gamma}\cdot sinh(\gamma\cdot L_{FBG})} \tag{6.30}$$

where L_{FBG} is the length of the grating, $\kappa = \pi/(2\cdot n_{eff}\cdot\Lambda)\cdot\delta n$ is the coupling coefficient, $\delta = 2\pi\cdot n_{eff}\cdot f/c - \pi/\Lambda$ is the detuning from the grating resonance and $\gamma^2 = \kappa^2 - \delta^2$. The grating bandwidth $\Delta\lambda_{FBG}$, defined as the wavelength range between the first zeros at each side of the Bragg peak is given by [110]:

$$\Delta\lambda_{FBG} = \lambda_b\frac{\delta n}{n_{eff}}\left(1 + \left(\frac{\lambda_b}{\delta n{\cdot}L_{FBG}}\right)^2\right)^{\frac{1}{2}} \tag{6.31}$$

where $\lambda_b = 2{\cdot}n_{eff}{\cdot}\Lambda$ is the Bragg wavelength.

6.2.2.4 Balanced configurations

There are two interesting aspects that deserve consideration: (i) the transmitted optical signal is composed of two sidebands which are conjugated one another, that is, it presents some information redundancy, condition which is needed to obtain a real-valued signal to drive the laser intensity at the transmitter, and (ii) the improvement observed when an optical filter is used is not due to the elimination of some spectral signal content, but from introducing some degree of imbalance in such a way the spectral information components are mixed in a more efficient way upon photo-detection. These two aspects lead us to propose the balanced configurations shown in Fig. 6.2.

In both configurations, the reciprocal transfer function is used to detect the otherwise wasted sideband and the OFDM receiver processing on each branch is performed as usual. The

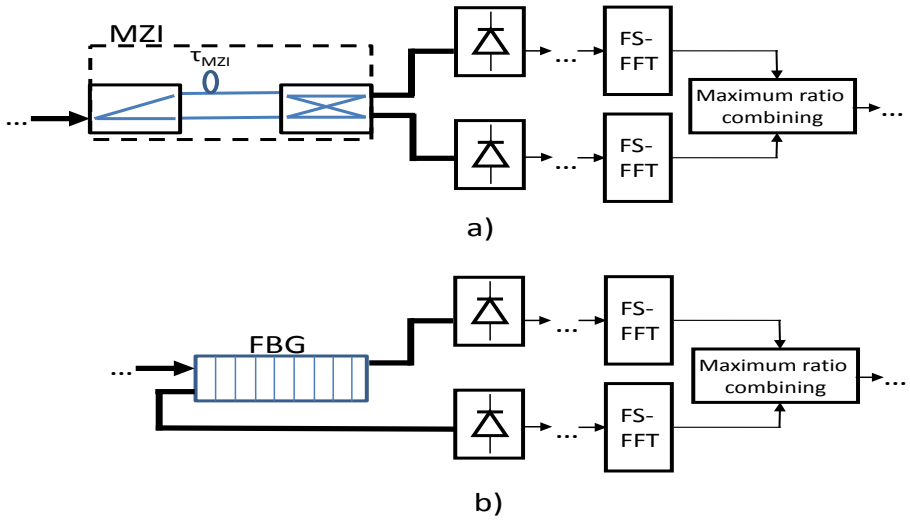

Figure 6.2: Balanced filtered configurations. a) both output ports of a MZI are used and b) both reflected and transmitted optical signals are used for information detection.

information symbols from the two branches after FFT are combined by using a maximum ratio combiner:

$$\bar{Y}[r] = \frac{H^*_{upper}[r]\cdot Y_{upper}[r] + H^*_{lower}[r]\cdot Y_{lower}[r]}{|H_{upper}[r]|^2 + |H_{lower}[r]|^2},\ r = 1, 2, ...N \tag{6.32}$$

where $Y_{upper}[r]$ and $Y_{lower}[r]$ are the received complex symbols at the r-th subcarrier of the upper and lower branch, respectively, $H_{upper}[r]$ and $H_{lower}[r]$ are the rth coefficient of the estimated transfer function corresponding to the upper and lower branch, respectively, and $Y[r]$ is the resulting equalized symbol.

In the balanced configuration with a MZI, signals from both output ports are used, rather than only one of them, Fig. 6.2(a), and with a FBG, both the reflected and transmitted signals from the grating, Fig. 6.2(b), are detected. Furthermore, the proper combination of the two signals leads to some improvement, as shown in the following section.

6.3 Results

6.3.1 Default system parameters

The next default system parameters are used to obtain the presented results: the sampling rate f_{sam} is equal to 11Gsam/s, being the electrical bandwidth BW equal to 5.5GHz; the information binary stream is mapped into 16-QAM complex symbols, which are arranged with a Hermmitian symmetry at the input of the IFFT processor of size $FS = 256$; $N = 110$ subcarriers are used for information transmission; a cyclic pre- and a post-fix of 16 samples ($N_{pre} = N_{pos} = 16$) are appended for the mitigation of ICI and ISI effects; the resulting transmission information rate, R, is equal to 16.8Gbits/s; a high clipping level ($CL = 13.8dB$) is used in order to limit the amplitude swing of the OFDM signal. For the modeling of the digital-to-analog conversion, quantization noise due to a limited bit

resolution is not taken into account and a square-root raised-cosine filter is employed. The obtained analog signal is adapted for laser driving by scaling the analog signal to yield a peak-to-peak value of $\Delta i = 10mA$ and adding a DC-offset $i_0 = 60mA$. Note that we have set the clipping level to a relatively high value, though the employment of a smaller value may lead to some system performance improvement because of a higher modulation efficiency even at the expense of some clipping noise [60]. Nevertheless, in subsection 6.3.4 we study the impact of different clipping level values used at the transmitter in order to give power budget curves closer to those obtained in a practical scenario.

The fiber chromatic dispersion D is set to $17ps/(km{\cdot}nm)$, the fiber-loss parameters is set to 0.2dB/km and its length is equal to 25 km. After photodetection, shot and thermal noises have been considered, being $10\text{pA}/\sqrt{Hz}$ the thermal noise spectral density. Training symbols are used to obtain a channel estimation and perform one-tap equalization of the detected information symbols.

6.3.2 Supergaussian filter approach

The analysis of the system performance starts with the study of the linear effects on the detected information signal, given by the expression Eq. (6.14). In Fig. 6.3 we show some results obtained when a Supergaussian optical filter is inserted, but without considering its phase response. The transfer function of the optical filter obtained through evaluation of Eq. (6.25) is shown in Fig. 6.3(a) to illustrate the influence of the change of its parameters ($\Delta\Omega_{3dB}$, Ω_c and q). The modulus of the OOFDM system transfer function ($|H(\Omega_r)| = \left|T0|_{n_r=1} + T1|_{n_r=1}\right|/|X_r|$) calculated through Eq. (6.14) for different values of Ω_c, $\Delta\Omega_{3dB}$ and q is shown in Fig. 6.3(b), (c) and (d), respectively. Simulation results are also shown for the sake of validation.

With respect to the OOFDM system transfer function, the theory provided gives reasonably accurate results when the central frequency, the optical bandwidth or the Gaussian order is varied as shown in Fig. 6.3 (b), (c) and (d), respectively. The variation of these parameters allows to control the degree of imbalance introduced between both sidebands and how much the optical carrier is attenuated. Both factors finally determine the system total transfer function. The results show that Eq. (6.14) gives us accurate results for the evaluation of the linear effects on the transmitted complex symbols in an DM/DD OOFDM system.

In Fig. 6.4 we compare the optical power budget obtained when a) a Supergaussian filter is employed, but without taking into account its phase, and b) when a Supergaussian filter is employed, and its phase is given by Eq. (6.26). In both figures we have included the power budget curve obtained when no optical filter is employed for comparison purposes. The parameters of the Supergaussian filters used to obtain the results shown are listed in Table 6.1.

Table 6.1: Supergaussian filter parameters

	q	$\Delta\Omega_{3dB}/(2\pi)$(GHz)	$\Omega_c/(2\pi)$(GHz)
$H_{gauss,1}$	1	5.5	2.5
$H_{gauss,2}$	2	5.5	2.5
$H_{gauss,3}$	3	5.5	2.5
$H_{gauss,4}$	2	10	4.6

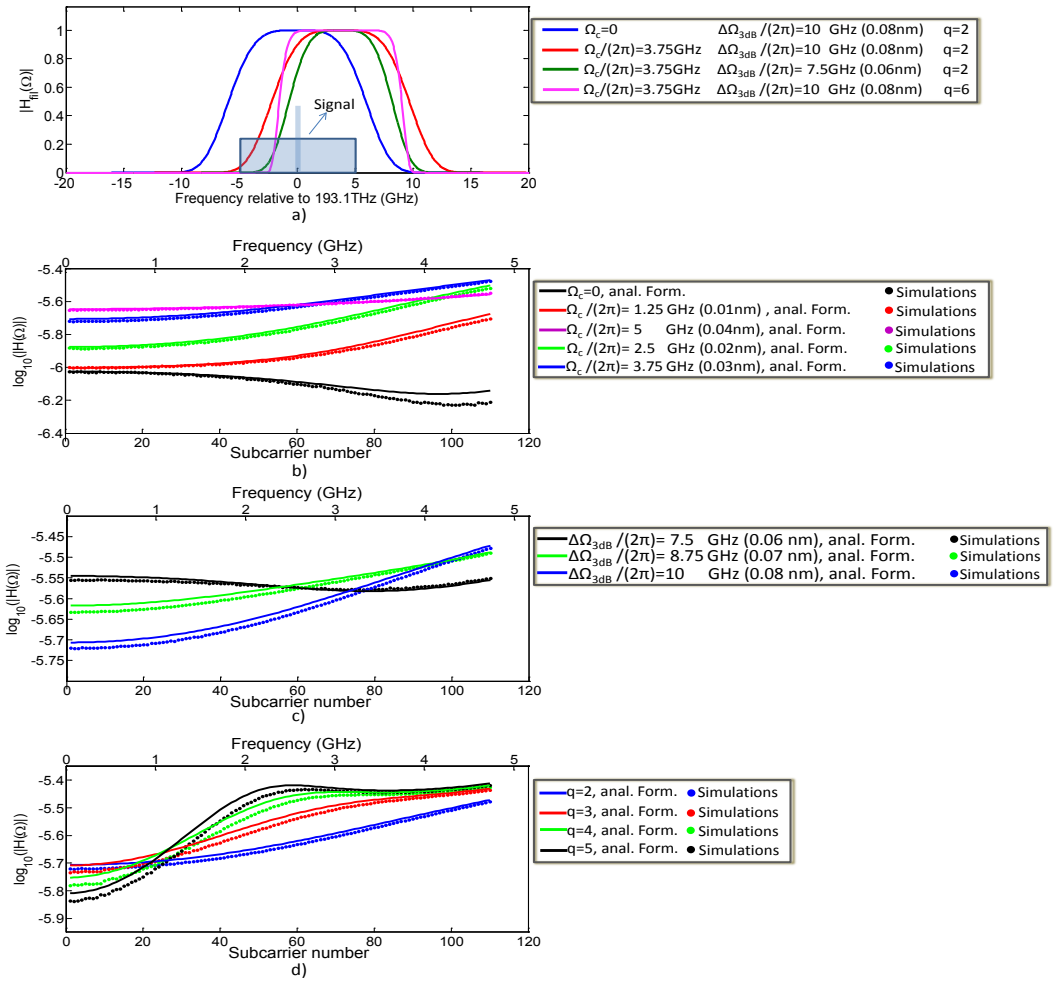

Figure 6.3: a) Optical filter transfer function. OOFDM system transfer function with b) $q = 2$, $\Delta\Omega_{3dB}/(2\pi) = 10$GHz (0.08nm), c) $q = 2$, $\Omega_c/(2\pi) = 3.75$GHz (0.03nm), and d) $\Delta\Omega_{3dB}/(2\pi) = 10$GHz (0.08nm), $\Omega_c/(2\pi) = 3.75$GHz (0.03nm).

The optical bandwidths corresponding to those indicated in Table 6.1 are equal to 0.044 nm ($\Omega_{3dB}/(2\pi) = 5.5$GHz) and 0.08 nm ($\Omega_{3dB}/(2\pi) = 10$GHz). Simulation results and those derived from the analytical formulation are shown in Fig. 6.4 for the sake of validation.

First of all, we must remark the reasonably good accuracy provided by the analytical formulation. The values from the analytical formulation match greatly with those from simulations for the optical filters $H_{gauss,1}$ and H_{gauss_4}, as we can observe from Figs. 6.4(a) and 6.4(b). When the optical filters $H_{gauss,2}$ and H_{gauss_3} are employed, the BER values obtained from the analytical formulation are slightly undervalued compared to those from simulations. The reason for such difference seems to be the assumptions made for the simplification of the theory: the Bessel functions were approximated by the first term of its series expansion in order to derive Eq. (6.14) and Eqs. (6.16)-(6.24). Since the argument of the Bessel functions is affected by the optical filtering, this approximation may be misleading. In order to achieve more accurate results from the mathematical expressions at the expense of little

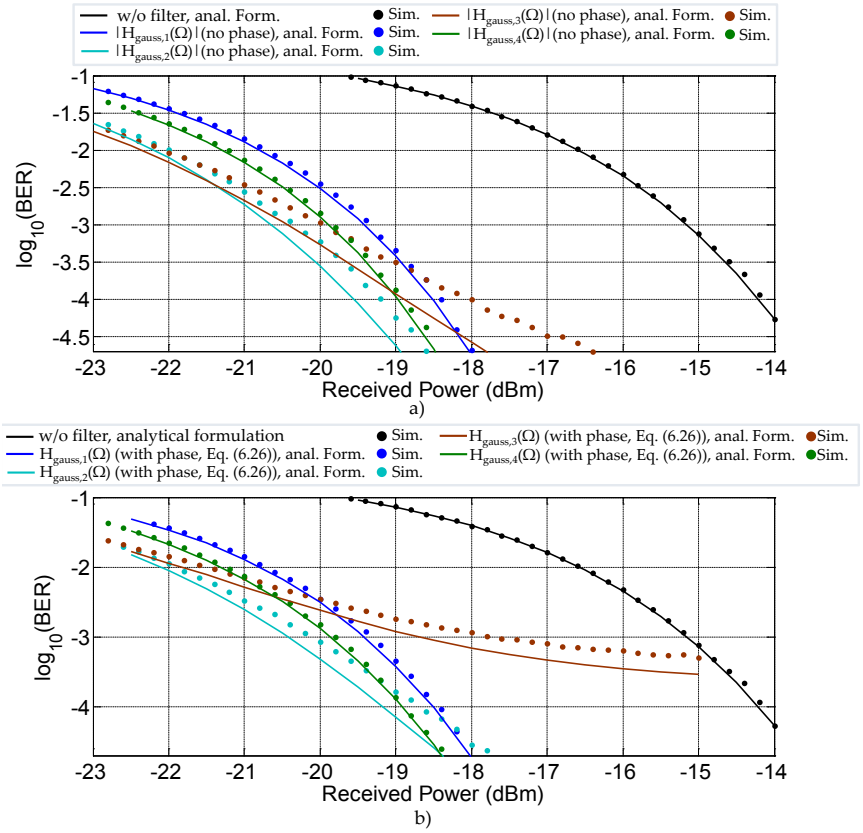

Figure 6.4: BER as a function of the received average optical power. a) Only the modulus of the Supergaussian filter transfer functions is considered, b) both modulus and phase of the Supergaussian filter transfer functions are considered.

bit more complexity, it would be enough to include more terms of the expansion, e.g., by approximating $J_0(x) \approx 1 - x^2/4$.

For the conditions studied, we can observe that the insertion of an optical filter reports a significant improvement in terms of power budget. A BER equals to 10^{-3} can be achieved with a received power equals to -20.4dBm when $|H_{gauss,2}(\Omega)|$ is used for filtering, which represents a 5.2dB improvement compared to the filter-free case. The curves obtained with $|H_{gauss,1}(\Omega)|$, $|H_{gauss,3}(\Omega)|$ and $|H_{gauss,4}(\Omega)|$ report similar power budget improvements: 4.2dB, 4.6dB and 4.8dB, respectively.

From Fig. 6.4(b) it is clear that, for some cases, the optical filter group delay has a detrimental impact on the system performance, as it was observed in [105]. Effectively, as it can be observed by comparing Fig. 6.4(a) and (b), once the phase has been considered, the power budget is reduced when the optical filters $H_{gauss,2}(\Omega)$ and $H_{gauss,3}(\Omega)$ are employed. In the case $H_{gauss,2}(\Omega)$ is used, the received power needed to assure a BER lower than 10^{-3} increases slightly to -20.2dBm, which means a small penalty of 0.2dB with respect to $|H_{gauss,2}(\Omega)|$. The most striking case occurs when $H_{gauss,3}$ is used, in which such a case we need a received power equals to -17.75dBm, which means a penalty of 2.25dB compared to the case in which the phase is not considered. The mathematical model derived in Section 6.2 can help to understand the reason of such impact.

6.3.2.1 Limiting factors

The driving factors which may be behind this degradation are (i) the decrease on the transfer function in Eq. (6.14) when the phases of $H_{fil}(\Omega_r)$ and $H^*_{fil}(-\Omega_r)$ are considered, (ii) the ICI and ISI due to the optical filter, and (iii) the nonlinear distortion products which appear as result of the imbalance caused by the optical filter (Eqs. (6.16)-(6.24)). In Fig. 6.5 we show the power spectral density of the optical signal after optical filtering, as well as several metrics with the aim of exploring the different components which affect the system performance. The results have been obtained for a received power equals to -20dBm.

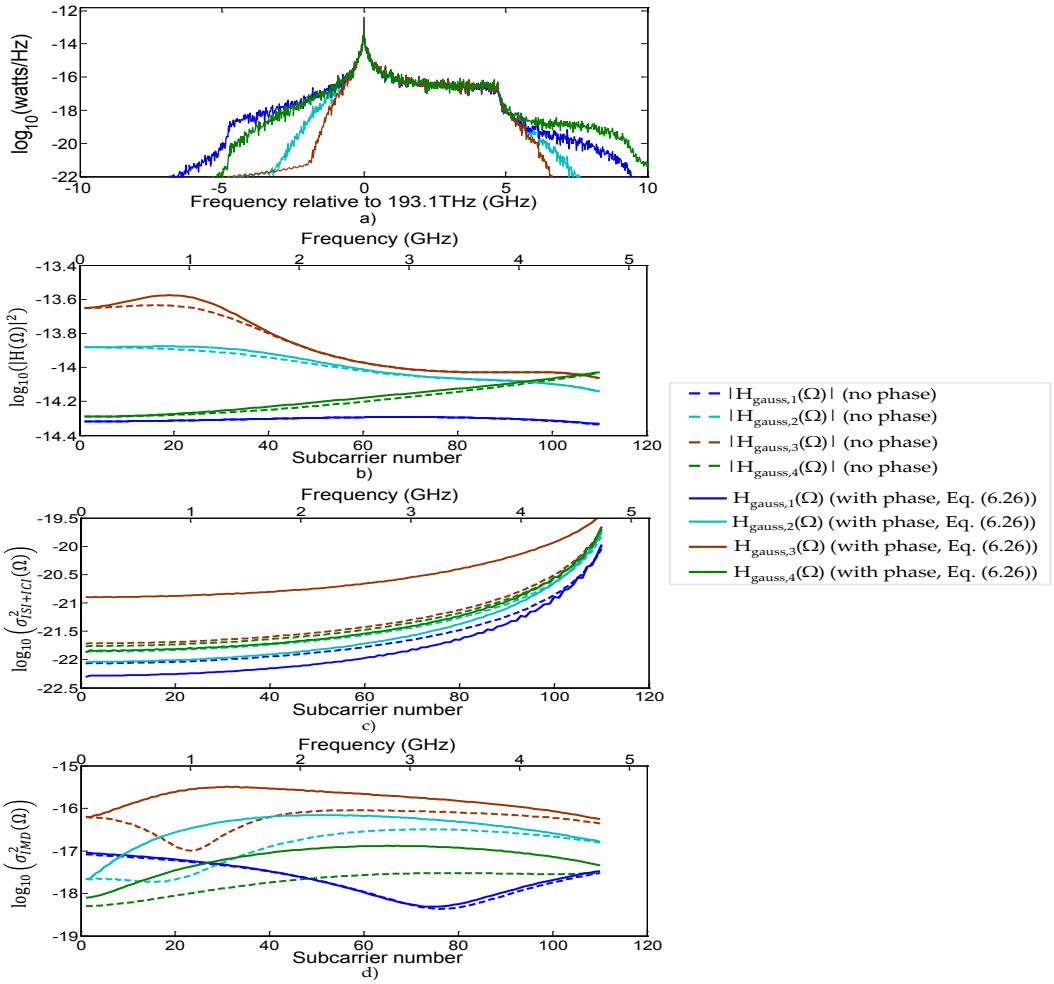

Figure 6.5: a) Power spectral density of the OOFDM signal after filtering, b) OOFDM system transfer function, c) variance of ISI and ICI, d) variance of the intermodulation distortion.

The optical spectral density of the OOFDM signal changes accordingly to the optical filter parameters used as we can observe in Fig. 6.5(a) when the filter order q or the bandwidth $\Delta\Omega_{3dB}$ are changed. The system transfer function in Fig. 6.5(b) has been obtained through the evaluation of Eq. (6.14). It is clear that, in this case, the magnitude of the transfer function does not change considerably after the phase of the filter is considered. We can

also observe that the highest transfer function magnitude is obtained with the optical filter $H_{gauss,3}$, whereas the lowest is obtained with $H_{gauss,1}$.

The variance of the distortion due to ISI & ICI, $\sigma^2_{ISI+ICI}$, has been calculated as reported through Eq. (4.23). We can observe that the ISI & ICI effects increase with the order of the filter; however, the consideration of the phase of the filter only causes an increase of ISI & ICI effects for $H_{gauss,3}$: once the phase is considered, the ISI & ICI effects increase by 2-8dB, a substantial difference which may contribute to the degradation observed in Fig. 6.4(a)-(b).

Finally, we have computed the variance of the intermodulation distortion, σ^2_{IMD}, through the evaluation of Eqs. (6.16)-(6.24). Comparing the magnitude of Fig. 6.5(c) and (d), we can conclude that when an optical filter is used the nonlinear distortion is an important issue to be considered. Generally, the intermodulation distortion increases once the phase of the filter is included, and, for the particular conditions here studied, it is the most significant reason for the degradation observed in Fig. 6.4.

We group the different impairing phenomena into the effective signal-to-noise ratio, defined as the ratio $|H(\Omega)|^2/(\sigma^2_{noise} + \sigma^2_{ISI+ICI}(\Omega) + \sigma^2_{IMD}(\Omega))$ and denoted as $SNR_{eff}(\Omega)$. In Fig. 6.6 we show the values obtained for $SNR_{eff}(\Omega_r)$, $r = 1, 2, ..N$ through the evaluation of the analytical formulation and that obtained through simulations. The results have been obtained again for a received power equals to -20dBm. We have also plotted a red line indicating the signal-to-noise ratio needed to obtain a BER equals to 10^{-3} ($log_{10}(SNR_{eff}) = 1.6543$) when 16-QAM is employed [55].

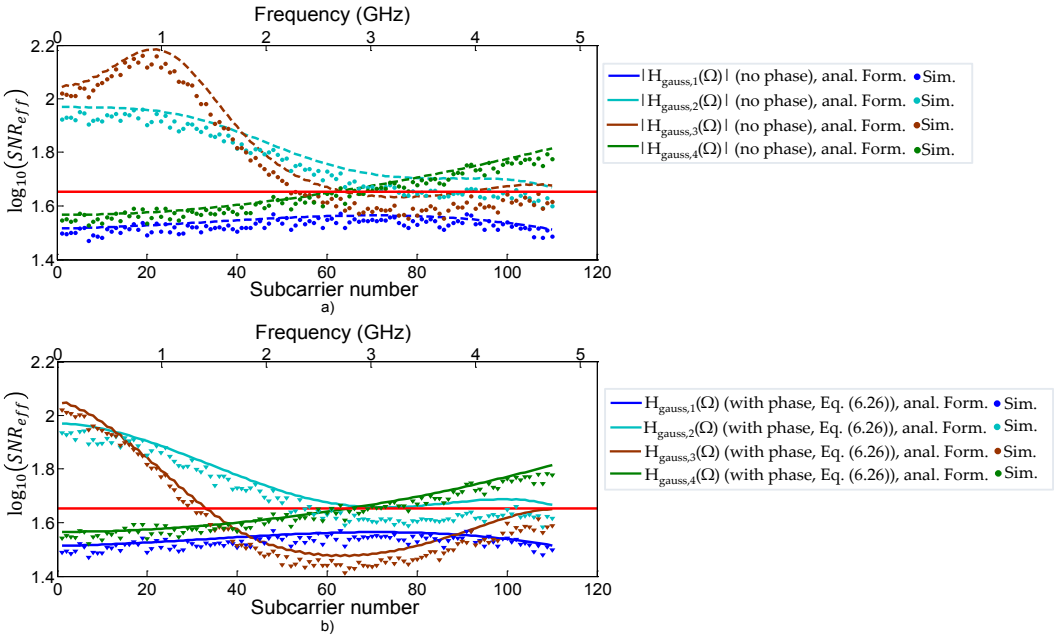

Figure 6.6: SNR_{eff} with a Supergaussian filter when a) only the modulus of the optical filter transfer function is considered, and b) both modulus and phase of the optical transfer function are considered.

First of all, we can observe from Fig. 6.6 that, apart from the expected overestimation, the results obtained through the evaluation of the analytical formulation match well with those

provided by simulations of the DM/DD OOFDM system. As expected from the results shown in Fig. 6.5, the consideration of the phase for the optical filter $H_{gauss,3}$ yields a significant SNR decrease as result of the enhancement of the nonlinear distortion, as it can be observed by comparing the results in Fig. 6.6(a) and (b).

We have identified the factors with relevant impact on the system performance of an optically filtered DM/DD OOFDM system and we have checked that the effective signal to noise ratio derived from the analytical formulation can help us to estimate it.

6.3.3 MZI and UFBG filtering approaches

In this section we explore the system performance which can be achieved using two well-known filtering structures: a MZI, and a uniform FBG. By varying a couple of their parameters (τ_{MZI} and ϕ_{upp} for the MZI, Δn and Λ for the uniform FBG), we are able to tune them and change their transfer functions. For the sake of clarity, we have plotted in Fig. 6.7 the modulus of the transfer functions with different filter parameters. In Fig. 6.7(b) we have defined as $\Lambda_0 = c/(193.1 \times 10^{12} \cdot 2 \cdot n_{eff}) = 535.35nm$.

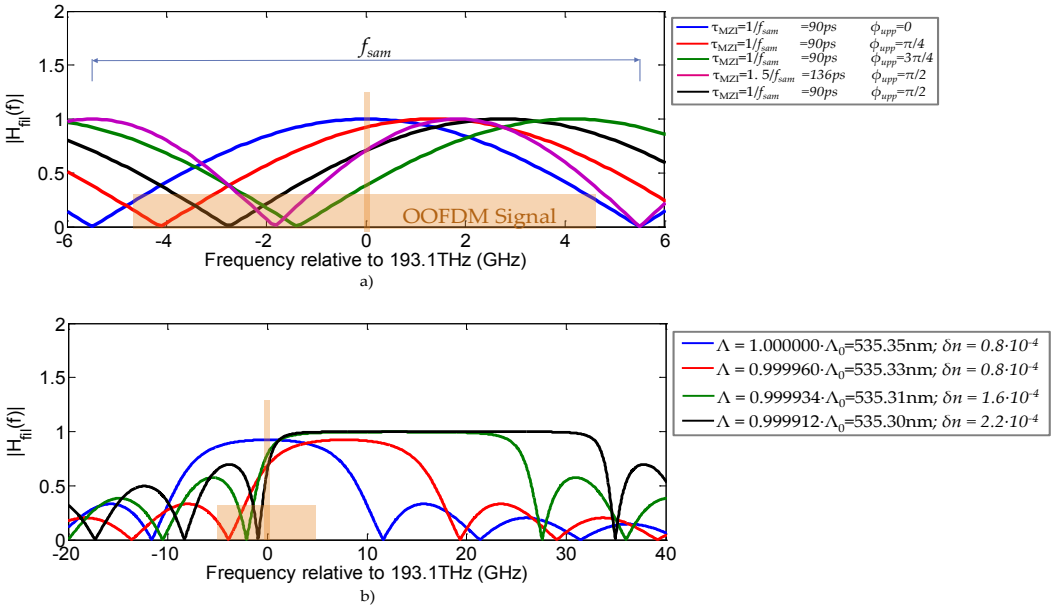

Figure 6.7: Modulus of the transfer function of a) a MZI and b) a uniform FBG.

As it can be observed in Fig. 6.7(a), the phase shift ϕ_{upp} allows us to control the location of the maximum of the transfer function, whilst the variation of τ_{MZI} allows us to control the period between the transfer function maximums. Regarding Fig. 6.7(b), both the period Λ and the refractive index variation δn are changed simultaneously to locate the optical carrier in the filter transition band; it is worth to observe that the secondary lobes which appear at the lower sideband increase with higher δn values, what necessarily affects the system performance as Eq. (6.14) indicates.

The obtained effective signal-to-noise ratio values with both filtering structures are shown in Fig. 6.8, which have been obtained once again for a received power equals to -20dBm. In Fig. 6.8(b) we have defined as $\Delta f_{FBG} = c \cdot \Delta\lambda_{FBG}/\lambda_b^2$.

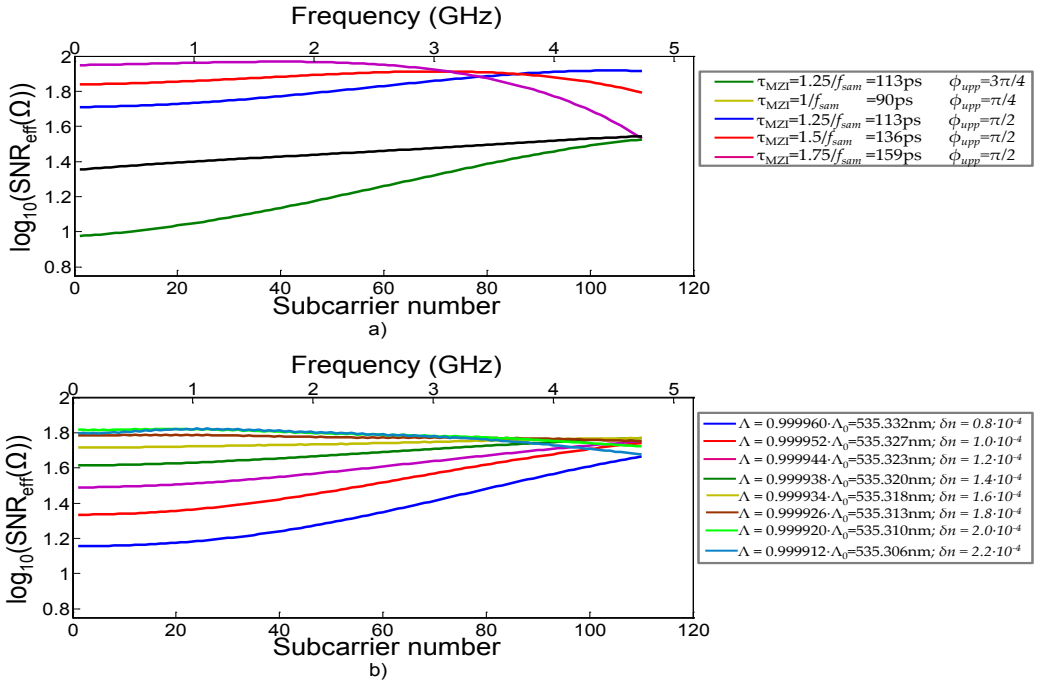

Figure 6.8: Effective SNR using a) a MZI and b) a UFBG as optical filter.

We can see in Fig. 6.8(a) that with a simple MZI we have been able to get an effective SNR around 19dB, which is obtained when $\phi_{upp} = \pi/2$. This value for the phase shift entails a trade-off point of the system, mainly determined by the optical carrier attenuation and the degree of imbalance introduced. When the value for ϕ_{upp} is changed to $\pi/4$ or $3\pi/4$ the effective SNR gets worse as a result of a decrease of the system transfer function (Eq. (6.14)). We can also observe that for $\phi_{upp} = \pi/2$, the delay τ_{MZI} can be varied over a broad range and good values of SNR_{eff} are still obtained (in Fig. 6.8, $\tau_{MZI} = [1/f_{sam} - 1.5/f_{sam}] = [90ps - 136ps]$), which is advantageous for a practical implementation. Slightly lower values of effective SNR are achieved when a uniform FBG is used: values of δn equals to 1.8×10^{-4}, 2×10^{-4} and 2.2×10^{-4} give us values of effective SNR around 18dB, provided the FBG is appropriately tuned by changing the period Λ.

6.3.4 Analysis and discussion: impact of clipping

Once we have explored the range of parameter which lead to reasonably good effective SNR values, now we determine the power budgets when a MZI, a uniform FBG and the balanced configurations explained in subsection 6.2.2.4 are used. Together with the numerical simulation results, we also show those derived from the analytical formulation when a MZI and a UFBG are employed. The derivation of the same results when the balanced configurations are employed is more challenging, since we need to finely know how the different impairments from both branches interact in amplitude, rather than in power. For this reason, its study is more appropriate within a detailed investigation on the optimization of these type of configurations.

For the MZI we set τ_{MZI} to $1.5/f_{sam} = 136$ps and ϕ_{upp} to $\pi/2$, and for the uniform FBG we set $\Delta n = 2 \times 10^{-4}$ and $\Lambda = \Lambda_0 \cdot 0.99992 = 535.310$nm. The same parameter values are

used in the balanced configurations. Given the importance of the clipping level used at the transmitter on the system performance [60], apart from the curves with the default clipping level (CL=13.8dB), some curves with smaller values of clipping level have been also plotted for each filtering structure. The results are shown in Fig. 6.9.

First of all, the results obtained from the analytical formulation match well with those obtained from simulations when a high clipping level (13.8dB) is used, what once again confirms the validity of the theory presented. The results obtained with the clipping level value are explained as follows: when the clipping level is decreased, a higher optical modulation efficiency is achieved at the expense of some clipping noise and a higher nonlinear distortion, and, thus, the improvement/penalty observed when the clipping level is decreased depends on the relative impact of the different components which affect the system performance. For example, when no optical filter is used, the system is mainly limited by the receiver noise, and the system performance can be significantly increased by reducing the clipping level. Only when the clipping level is significantly reduced and the impact of the resulting clipping noise and nonlinear distortion dominates to that due to the receiver noise, the received power needed to obtain a certain value of BER may start to increase. For the particular conditions used to obtain the results in Fig. 6.9, this inflection point happens when the clipping level is around 8dB. When no optical filter is used, a received power equals to -15.2dBm is needed to achieve a BER equals to 10^{-3} when CL=13.8dB, whilst a received power equals to -17.6dBm is needed for CL=8dB.

We have seen in previous sections that the system transfer function and the nonlinear distortion are altered when an optical filter is inserted into the dispersive link, and this variation depends on the optical filter characteristics. As result, in an optically filtered system, the system performance does not change with a reduction of the clipping level in the same way as that for a non-optically filtered system. We can observe from Fig. 6.9(a) that a received power equal -20.4dBm is needed to obtain a BER equals to 10^{-3} when $|H_{gauss,2}|$ is employed with CL=13.8dB, whilst a received power equals to -21.1dBm is needed when CL=10dB. In terms of power budget improvement, it means a difference of 3.5dB compared to the non-optically filtered system. A similar situation occurs when a MZI is used, for which a received power equals to -20.9dBm is needed to obtain a BER equals to 10^{-3} when CL=13.8dB, whilst it is reduced to -22.1dBm when CL=10dB, as it can be observed in Fig. 6.9(b). Thus, with a MZI as optical filter, we are able to get an improvement equals to 4.5dB compared to the non-optically filtered system.

On the other hand, when a UFBG is used, a reduction of the clipping level from CL=13.8dB to CL=11dB does not lead to a system improvement, and the received power needed in both cases is equal to -20.6dBm, Fig. 6.9(c), what means an improvement of 3dB. This indicates that when a uniform FBG is used the system performance is more strongly impaired by the nonlinear distortion.

The balanced detection proposed in subsection 6.2.2.4 yields to some power budget improvement, as we can see in Fig. 6.9(d). When a MZI is used, a power budget improvement equals to 5.5dB is obtained for a clipping level equals to 10dB, whereas a power budget improvement equals to 4.2dB is achieved when a UFBG is used with a clipping level equals to 12dB.

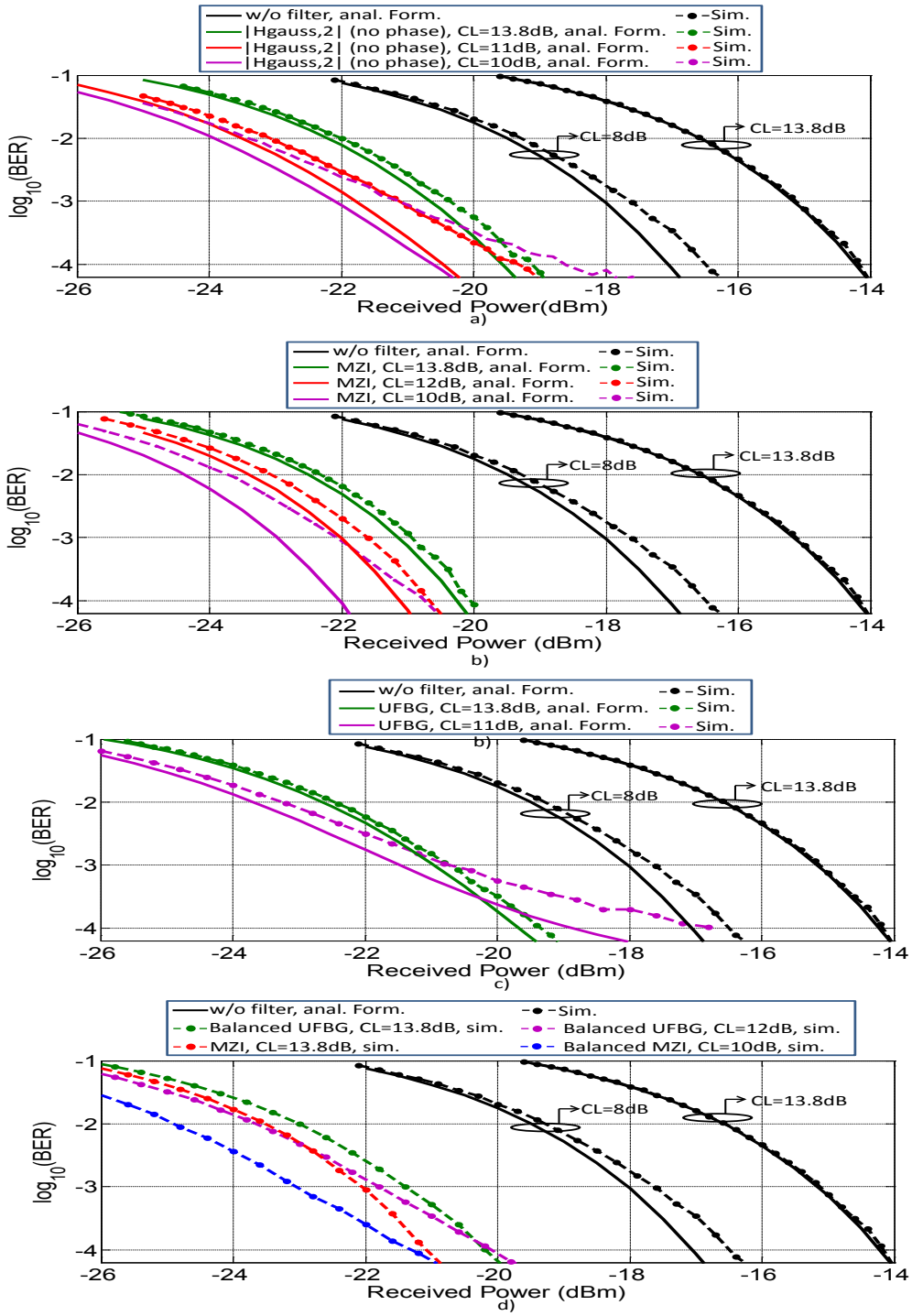

Figure 6.9: BER as a function of the received average optical power when no-optical filter is used and when a) the Supergaussian filter $|H_{gauss,2}|$, b) a MZI, c) a UFBG or d) the proposed balanced configuration is used as optical filter.

6.4 Summary

By extending the theory of Chapters 3 and 4, we have provided an analytical description of a filtered DM/DD OOFDM system which accounts both for the information part of the

detected signal and also the nonlinear distortions which impair the system performance. As the objective of this Chapter is mainly to grasp the physical mechanisms behind optical filtered DM/DD OOFDM systems, the results shown in this Chapter have obtained for particular operating conditions: a transmission information rate equal to $R = 16.8$Gbits/s and a fiber length of 25km have been set as default.

Using a simplified version of the model we have been able to verify that the linear part of the detected signal is spectrally imbalanced as a consequence of the filtering process and this translates into a higher magnitude of the overall system transfer function. As previously reported results [104], power budget improvements (around 5dB) when Supergaussian filters and flat phase transfer functions have been obtained. The isolation of the different effects has allowed us to study the influence of the optical filter group delay into the system performance, having found that the ISI & ICI effects as well as the nonlinear distortion are the responsible for the system performance reduction.

The evaluation of the system performance by means of the effective signal-to-noise ratio has proved to be an extremely useful tool to predict the system performance and the impact of the filter design parameters, in particular we have considered two commonly employed optical filters: a MZI and an uniform FBG. The MZI filter must be operated at an equilibrium point by setting the phase shift $\phi_{upp} = \pi/2$, whilst a range for the delay equal to [90ps,136ps] provides us an increase of the signal-to-noise ratio. Regarding the UFBG filtering approach, the increase of the filtering effects as result of the increase of δn leads to the increase of the effective SNR, but also of the secondary lobes appearing at the lower sideband, which may potentially limit the system performance improvement obtained.

The performance improvement obtained by inserting the optical filter in the OFDM is highly dependent on the clipping level: when no optical filter is used, a significant power budget improvement can be obtained by reducing the clipping level, whilst this reduction results in a more limited improvement in the distortion-limited power budget when an optical filter is used. For the particular conditions studied, a clipping level equal to approximately 8dB is the most convenient value for the conventional DM/DD system, whilst values higher than 10dB must be used in the optically filtered DM/DD OOFDM system. The tuning of the clipping level leads to a reduction of the power budget improvement obtained through optical filtering: the simulation results predict improvement figures of 3.3 and 3dB when a MZI or a UFBG re respectively employed.

Finally, we have proposed the use of optical balanced detection for further enhancement of optically filtered DM/DD OOFDM system performance. With this configuration, an improvement of 5.5dB is achieved by using a MZI.

Chapter 7

Conclusions and future work

7.1 Conclusions

With the purpose of filling the gap which represents the lack of a theoretical basis of optical multi-carrier directly-modulated and detected systems, this work has begun with the proposal of an analytical model for their accurate description. The proposed mathematical treatment has allowed us to include the main signal generation, transmission and detection effects, as well as providing us with a great versatility.

After proper validation by comparing the results with those obtained with simulation commercial software, the analytical model has offered us a mathematical description of the linear information signal term and the nonlinear distortion at the receiver-end side, determining jointly to a great extent the obtained system performance of DM/DD OOFDM systems. To the best of our knowledge, the proposed model represents the most accurate model up to the present day for the accounting of the main effects in DM/DD OOFDM systems. Furthermore, despite of its complexity, it can be conveniently simplified to provide a much more simple description accordingly to the needs of the particular system.

A more complete description of real DM/DD OOFDM systems has been given in Chapter 4 with the consideration of important transceiver design parameters, such as the clipping level, the number of subcarriers, the length of the cyclic extensions or the amplitude swing of the laser modulating signal. Since the number of inter-related parameters is huge, we have tried to qualitatively discuss the system performance optimization problem by describing the different trade-offs involved.

In a first approximation, the results obtained have shown that OOFDM with direct modulation is able to provide a transmission information rate around 30.7Gbits/s after propagation through 50km of single mode with a OOFDM signal occupying 4.8GHz and at a BER equal to 10^{-4}. OFDM parameters such as CL and the length of the cyclic extensions as well as the laser bias point and the amplitude swing of the laser modulating OFDM signal were

changed to obtain this result. The laser dynamics have a great influence on the system

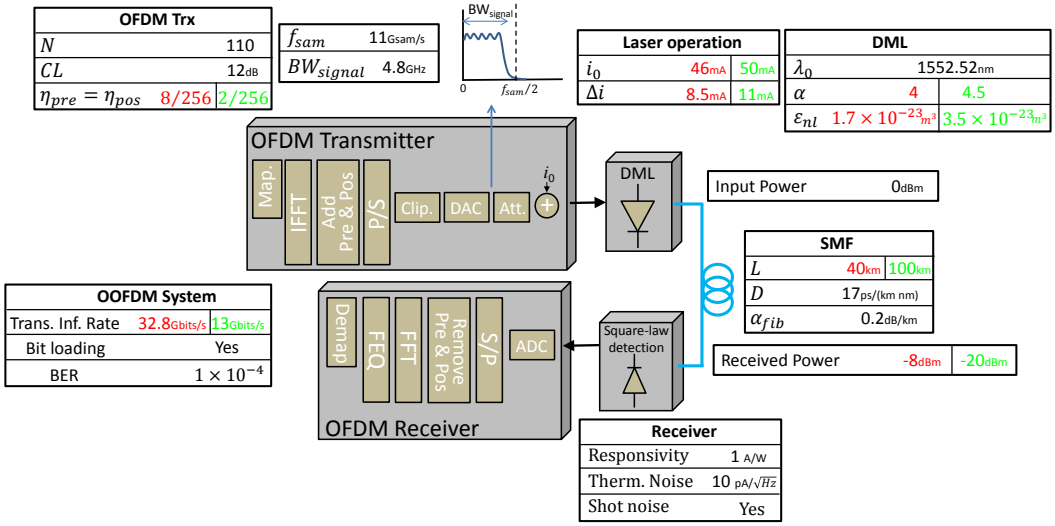

Figure 7.1: Resulting DM/DD OOFDM system obtained in Chapter 4 with variant laser parameters.

performance, and modulation parameters such as the nonlinear gain coefficient and the linewidth enhancement factor are determining: the nonlinear gain coefficient is a trade-off of the end-to-end information transmission efficiency and the nonlinear distortion, whilst a modest linewidth enhancement factor may be beneficial to overcome dispersion-induced fading, despite of the nonlinear distortion it entails. The optimization of these parameters to explore DM/DD OOFDM potentiality has result in transmission information rates equal to 32.87Gbits/s and 13.12Gbits/s for $L = 40$km and $L = 100$km, respectively. These transmission information rates have been achieved by taking advantage of the bit loading technique, using high QAM-modulation formats (64, 128 and 256-QAM), achieving thus great spectral efficiencies.

In order to deal with the underlying problem of nonlinear distortion in DM/DD OOFDM system, a novel pre-distortion technique has been proposed based on the analytical model presented in Chapter 5. In the proposed scheme, a dedicated receiver extracts and tracks some of the necessary parameters needed to reconstruct the interference terms of the system. Together with the feedback-path from the receiver to the transmitter, the proposed technique is able to achieve great nonlinear distortion reduction ratio values, arriving up to values equal to [0.02,0.13], which have been obtained after the study of the appropriate working conditions.

Transmission information rates equal to 40Gbits/s and 18.5Gbits/s have been obtained for L=40km and L=100km, respectively, with a BER in the order of 10^{-4} (see Fig. 7.2(a)). The employment of QAM modulation formats of higher order to those used in the conventional DM/DD OOFDM system (see Figs. 7.2(b) and (c)) has allowed us to obtain transmission information rate improvements equal to 9Gbits/s and 8.5Gbits/s for L=40km and L=100km, respectively.

Comparisons of the pre-distortion technique with a previously reported nonlinear mitigation technique based on nonlinear equalization at the receiver-end side have been also carried out, showing that our proposed technique achieves a higher nonlinear distortion cancellation

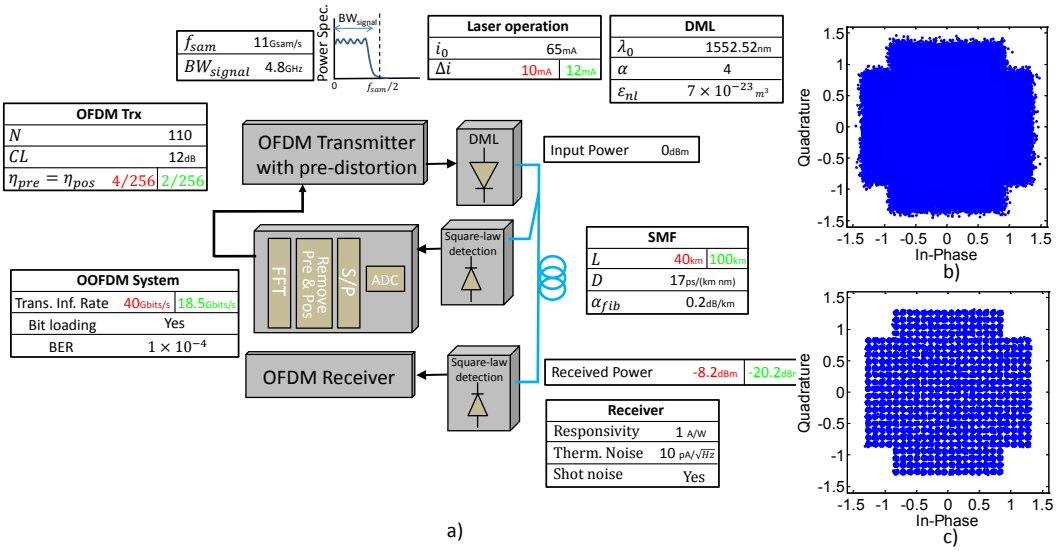

Figure 7.2: a) Resulting DM/DD OOFDM system using the pre-distortion technique proposed in Chapter 5. Constellation diagram of the received 512-QAM symbols in b) the conventional DM/DD OOFDM system. c) the DM/DD OOFDM system with pre-distortion.

efficiency. As result, our proposed technique outperforms nonlinear equalization at the receiver by several Gbits/s. Moreover, the proposed technique may be advantageous from a design perspective in a optical access network, since it may facilitate the location of complex electronic processing a the optical line terminal side.

The aim of Chapter 6 is to grasp the foundation for the improvement obtained when an optical filter is used in a DM/DD OOFDM system, as shown in Fig. 7.3. Results obtained have confirmed that optical filtering may be a suitable technique for the improvement of power budget in DM/DD OOFDM systems by a few dBs (see Fig. 7.4). The analytical formulation provided has shed some light on the influence of the filter group delay, as responsible for the decrease into the improvement observed when flat transfer functions are observed. This improvement reduction stems from mainly ISI & ICI effects and the nonlinear distortion.

The analytical formulation obtained for the description of optically filtered DM/DD OOFDM systems has demonstrated to be an useful tool to characterize the system performance through the calculation of the effective signal-to-noise ratio. Its computation has allowed us to explore optimized values for MZI and UFBG-based filters: for the MZI filter, the values of phase and delay difference between arms have been optimized, whilst the optimization of the grating period and the refractive index peak modulation of the UFBG-based filter has been carried out.

It has been found that DM/DD OOFDM systems are more strongly impaired by nonlinear distortion after the insertion of the optical filter, and, as result, their performances vary differently when the clipping level is changed. Results have shown that power budget improvements of 3.3dB and 3dB for the MZI and UFB-based filters (see Fig. 7.4(a) and (b)), respectively. In order to push further these improvement values, we have proposed the use of a balanced detection configuration, achieving a value of power budget improvement equal to 5.5dB when the MZI filter is employed (see Fig. 7.4(c)).

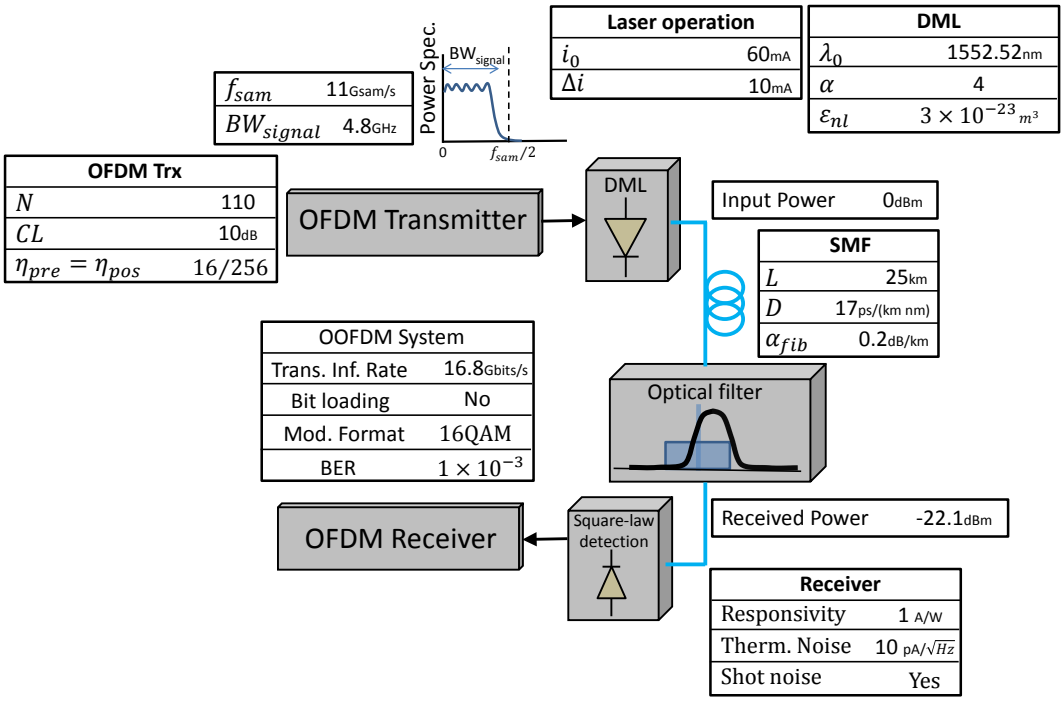

Figure 7.3: Optically filtered DM/DD OOFDM system obtained in Chapter 6.

To sum up, DM/DD OOFDM systems are suitable option to be employed in dynamical metro/access optical networks, able to provide great spectral efficiencies and versatility. The cost of such systems is also one of its main advantages, compared to other architectures such as externally modulated/directly detected systems or coherently detected systems. The laser chirp impose limitations on the link reach and the achievable transmission information rate, but, as we have seen in this work, DSP and optical signal processing techniques may make a valuable contribution to mitigate their effects. Other disadvantages arising from the nature of the information transmission (it must be conveyed in the optical intensity domain), such as the loss of the information on the phase and polarization of the optical field make DM/DD systems unflattering compared to their more complex counterparts.

7.2 Future work

From the author's point of view, research lines may be followed either in the experimental or in the theoretical areas, as described below:

7.2.1 Experimental work

It is obvious that this Ph.D. Thesis has a prominent theoretical side, and, therefore, the achievement of experimental results which may verify and extend the results presented is one of the essential steps to go on. The employment of arbitrary waveform generators and real-time oscilloscopes which allow off-line processing for the correct transmission and detection of

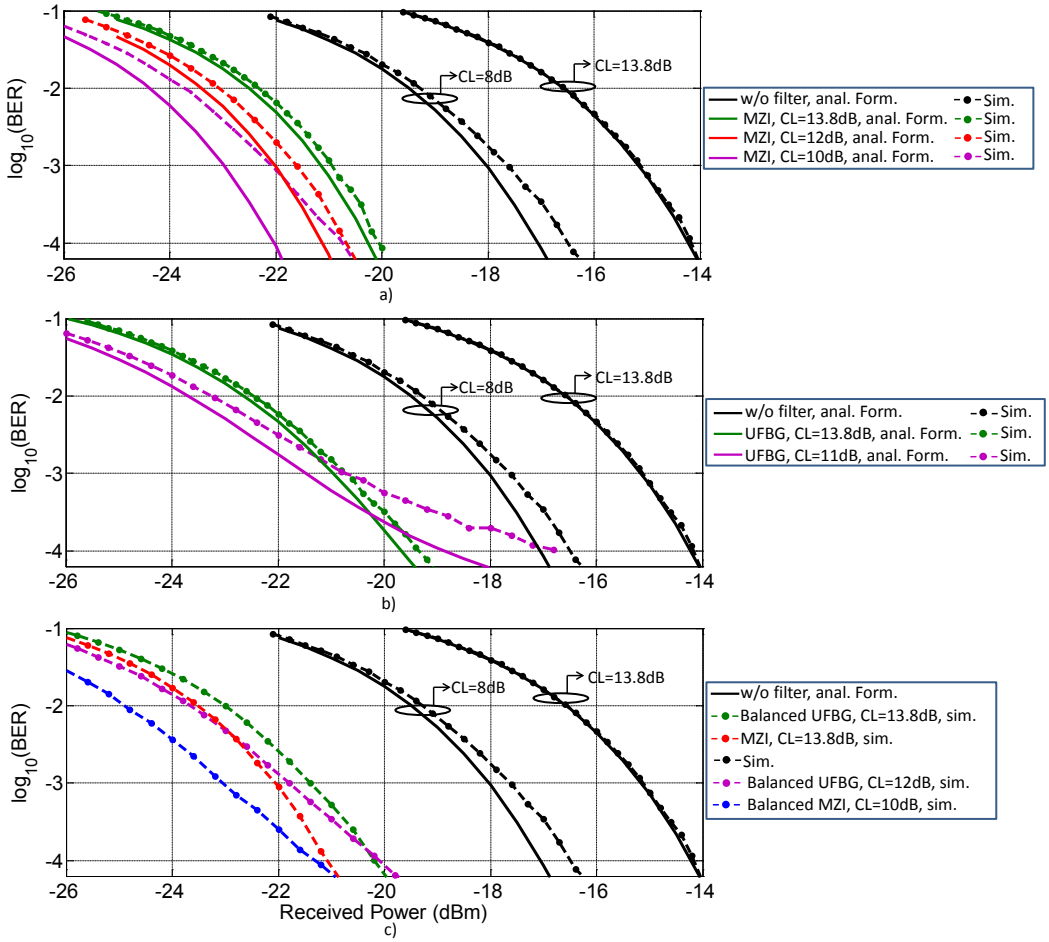

Figure 7.4: BER as a function of the received average optical power when no-optical filter is used and when a) a MZI, b) a UFBG or c) the proposed balanced configuration is used as optical filter.

OOFDM signals is an efficient way for the achievement of such experimental results. Indeed, an experimental OOFDM set-up based on this approach is currently being assembled, with satisfactory results. The real-time operation of an OOFDM system based on FPGAs would be only recommended to those interested also in the solving of real implementation issues.

Chapter 4 represents a valuable and complementary tool for the exhaustive understanding of the obtained experimental results, which are usually not very intuitive. The employment of an optical filter as suggested in Chapter 6 may be the next natural step: provided that the filter can be tuned and its transfer function adapted, its mere insertion into the basic experimental OOFDM set-up should not impose important difficulties. On the other hand, the pre-distortion technique proposed in Chapter 5 may need an important load of work in order to completely characterize the OOFDM system and identify all the magnitudes involved in the analytical model the technique is based on. Needless to say that many other architectures, techniques and approaches for the transmission and detection of OFDM signals worth to be tried in an experimental set-up.

7.2.2 Theoretical work

During all along this Ph.D. Thesis, it has been assumed that a baseband electrical signal is generated. At the aim of using more efficiently the operating bandwidth of optical modulators and, finally, of providing higher bit rates, multi-band OFDM schemes have been proposed (see e.g., [37]). The work presented may be extended to deal with frequency up-converted signals.

It has been also assumed that a laser diode with a light emission process governed by Eq. (2.24) and direct detection are used. In principle, the extension of the theory reported in this work to include other directly modulated architectures (VCSELs, spectrum sliced super luminescent sources,...), external intensity modulation (electro-absorption and Mach Zehnder modulators), and even coherently detected systems, may be carried out "straightforwardly".

The analytical model presented in Chapter 3 may be extended to account for other effects involved for the better characterization of DM/DD OOFDM systems (e.g., by including laser phase noise, the group velocity dispersion slope, optical amplification, fiber nonlinearities,...). Besides, it has been assumed an uni-directional communication system, but optical access networks can operate in a bi-directional loop-back structure, in which the Rayleigh backscattering noise is inevitable; its study, in combination with colorless optical network units with reflective modulators is of great interest.

As pointed out in Chapter 4, the quantization noise of the DAC and ADC stages is not included in the study. Expressions for the evaluation of its effects are a complement for the treatment of the PAPR/clipping of OFDM signals. Since PAPR is the main problem of OFDM signals, PAPR reduction techniques may also be very helpful for OOFDM systems.

Semiconductor optical amplifiers are nonlinear optical elements whose interaction with light are governed by similar equations to Eq. (2.24). Due to its strong nonlinear behavior, such elements are used for wavelength conversion, operation needed to perform the routing of wavelength-division multiplexed channels in the optical layer. It is thus of great interest and potential application to carry out a theoretical study in a similar way to that done in this Ph.D. Thesis on the employment of wavelength converters based on semiconductor optical amplifiers when OOFDM signals are used for information transmission.

Appendix A

Harmonic analysis of laser rate equations

The direct modulation of the laser is governed by the next equations:

$$\begin{array}{ll} \frac{dn(t)}{dt} & = I(t) - \gamma_e(n) \cdot n(t) - G(n,p) \cdot p(t) \\ \frac{dp(t)}{dt} & = \big(\Gamma \cdot G(n,p) - \gamma\big) \cdot p(t) + R_{sp}(n) \\ \frac{d\phi}{dt} & = \frac{1}{2}\alpha\Gamma v_g a_g (n(t) - n_t) \end{array} \tag{A.1}$$

where $I(t)$ is the density of injected carriers, γ_e is the carrier-recombination rate, $G(n,p)$ is the stimulated-emission rate, and γ is the net rate of stimulated emission.

Assuming that the injected density of carriers is $I(t) = I_0 + \delta I$, the magnitudes in Eq. (A.1) can be approximated by:

$$\gamma_e(n) \approx \gamma_e(n_0) + \frac{d\gamma_e}{dn}|_{n=n_0} \cdot \delta n \tag{A.2}$$

$$\begin{aligned} G(n,p) &\approx G(n_0,p_0) + \frac{\partial G(n,p)}{\partial n}|_{n=n_0,p=p_0} \cdot \delta n + \frac{\partial G(n,p)}{\partial p}|_{n=n_0,p=p_0} \cdot \delta p \\ &\approx G(n_0,p_0) + G_n(n_0,p_0) \cdot \delta n + G_p(n_0,p_0) \cdot \delta p \end{aligned} \tag{A.3}$$

$$R_{sp}(n) \approx R_{sp}(n_0) + \frac{dR_{sp}(n)}{dn}|_{n=n_0} \cdot \delta n \tag{A.4}$$

Substituting into Eq. (A.1):

$$\begin{aligned}\frac{\delta n}{dt} &= I_0+\delta I-\big(\gamma_e(n_0)+\frac{d\gamma_e}{dn}|_{n=n_0}\cdot\delta n\big)\cdot(n_0+\delta n)\\ &\quad-\Big(G(n_0,p_0)+G_n(n_0,p_0)\cdot\delta n+G_p(n_0,p_0)\cdot\delta p\Big)\cdot(p_0+\delta p) \qquad (A.5)\\ \frac{\delta p}{dt} &= \big(\Gamma\cdot G(n_0,p_0)+\Gamma\cdot G_n(n_0,p_0)\cdot\delta n+\Gamma\cdot G_p(n_0,p_0)\cdot\delta p-\gamma\big)\cdot(p_0+\delta p)\\ &\quad+\big(R_{sp}(n_0)+\frac{dR_{sp}(n)}{dn}|_{n=n_0}\big)\cdot(n_0+\delta n) \qquad (A.6)\end{aligned}$$

Assuming that $I(t)=I_0+\delta I=I_0+\delta I(\pm\Omega_1)\cdot e^{\pm j\Omega_1 t}+\delta I(\pm\Omega_2)\cdot e^{\pm j\Omega_2 t}$, the carrier and photon densities are assumed to have the following expressions:

$$\begin{aligned}n(t)\approx n_0&+\delta_1 n(\pm\Omega_1)e^{\pm j\Omega_1 t}+\delta_1 n(\pm\Omega_2)e^{\pm j\Omega_2 t}+\delta_{1,1}n(\Omega_1,\Omega_2)e^{j(\Omega_1+\Omega_2)t}\\ &+\delta_{1,1}n(-\Omega_1,-\Omega_2)e^{-j(\Omega_1+\Omega_2)t}+\delta_{1,-1}n(\Omega_1,-\Omega_2)e^{j(\Omega_1-\Omega_2)t}\\ &+\delta_{1,-1}n(-\Omega_1,\Omega_2)e^{-j(\Omega_1-\Omega_2)t} \qquad (A.7)\\ p(t)\approx p_0&+\delta_1 p(\pm\Omega_1)e^{\pm j\Omega_1 t}+\delta_1 p(\pm\Omega_2)e^{\pm j\Omega_2 t}+\delta_{1,1}p(\Omega_1,\Omega_2)e^{j(\Omega_1+\Omega_2)t}\\ &+\delta_{1,1}p(-\Omega_1,-\Omega_2)e^{-j(\Omega_1+\Omega_2)t}+\delta_{1,1}p(\Omega_1,-\Omega_2)e^{j(\Omega_1-\Omega_2)t}\\ &+\delta_{1,-1}p(-\Omega_1,\Omega_2)e^{-j(\Omega_1-\Omega_2)t} \qquad (A.8)\end{aligned}$$

From Eqs. (A.5) and (A.6), retaining only those components multiplied by $e^{\pm j\Omega_1 t}$, one can arrive at the next expressions:

$$\frac{\delta_1 n(\pm\Omega_1)}{\delta_1 p(\pm\Omega_1)}=\frac{\big(\gamma\pm j\Omega_1-\Gamma\cdot G(n_0,p_0)-\Gamma\cdot p_0\cdot G_p(n_0,p_0)\big)}{\big(\Gamma\cdot p_0\cdot G_n(n_0,p_0)+R_{sp}(n_0)+n_0\cdot\frac{dR_{sp}(n)}{dn}|_{n=n_0}\big)} \qquad (A.9)$$

$$\frac{\delta_1 p(\pm\Omega_1)}{\delta_1 I(\pm\Omega_1)}=\frac{\big(\Gamma\cdot p_0\cdot G_n(n_0,p_0)+R_{sp}(n_0)+n_0\cdot\frac{dR_{sp}(n)}{dn}|_{n=n_0}\big)}{\big(\substack{\pm j\Omega_1+\gamma_e(n_0)+n_0\cdot\frac{d\gamma_e}{dn}|_{n=n_0}+\\ p_0\cdot G_n(n_0,p_0)}\big)\cdot\big(\substack{\pm j\Omega_1-\Gamma\cdot\big(G(n_0,p_0)\big)\\ +G_p(n_0,p_0)\big)}\big)+G(n_0,p_0)+p_0\cdot G_p(n_0,p_0)} \qquad (A.10)$$

The first order optical intensity to driving current transfer function is calculated simply as:

$$H_{p_1}(\pm\Omega_1)=C_p\cdot\frac{\delta_1 p(\pm\Omega_1)}{\delta_1 I(\pm\Omega_1)} \qquad (A.11)$$

where C_p is the photon density to optical intensity conversion factor.

Proceeding in the same way, one can derive the expressions for the second order transfer functions:

$$\frac{\delta_{11}p(\Omega_1,\Omega_2)}{I(\Omega_1)\cdot I(\Omega_2)} = G_n(n_0,p_0)\cdot \frac{\begin{pmatrix}\Gamma\cdot\left(j(\Omega_1+\Omega_2)+\gamma_e(n_0)+n_0\cdot\frac{d\gamma_e}{dn}|_{n=n_0}\right)-\\ \left(R_{sp}(n_0)+n_0\cdot\frac{dR_{sp}(n)}{dn}|_{n=n_0}\right)\end{pmatrix}\cdot\left(\frac{\delta_1 n(\Omega_1)}{\delta_1 p(\Omega_1)}+\frac{\delta_1 n(\Omega_2)}{\delta_1 p(\Omega_2)}\right)\cdot\frac{\delta_1 p(\Omega_1)}{\delta_1 I(\Omega_1)}\cdot\frac{\delta_1 p(\Omega_2)}{\delta_1 I(\Omega_2)}}{\begin{pmatrix}j(\Omega_1+\Omega_2)+\gamma_e(n_0)+\\ n_0\cdot\frac{d\gamma_e}{dn}|_{n=n_0}+p_0\cdot G_n(n_0,p_0)\end{pmatrix}\cdot\left(\Gamma\cdot\begin{pmatrix}\gamma+j(\Omega_1+\Omega_2)-\\ G(n_0,p_0)+\\ p_0\cdot G_p(n_0,p_0)\end{pmatrix}\right)+\begin{pmatrix}G(n_0,p_0)+\\ p_0\cdot G_p(n_0,p_0)\end{pmatrix}\begin{pmatrix}\Gamma\cdot p_0\cdot G_n(n_0,p_0)+\\ R_{sp}(n_0)+n_0\cdot\frac{dR_{sp}(n)}{dn}|_{n=n_0}\end{pmatrix}} \tag{A.12}$$

$$\frac{\delta_{11}p(\Omega_1,-\Omega_2)}{I(\Omega_1)\cdot I(-\Omega_2)} = G_n(n_0,p_0)\cdot \frac{\begin{pmatrix}\Gamma\cdot\left(j(\Omega_1-\Omega_2)+\gamma_e(n_0)+n_0\cdot\frac{d\gamma_e}{dn}|_{n=n_0}\right)\\ -\left(R_{sp}(n_0)+n_0\cdot\frac{dR_{sp}(n)}{dn}|_{n=n_0}\right)\end{pmatrix}\cdot\left(\frac{\delta_1 n(\Omega_1)}{\delta_1 p(\Omega_1)}+\frac{\delta_1 n(-\Omega_2)}{\delta_1 p(-\Omega_2)}\right)\cdot\frac{\delta_1 p(\Omega_1)}{\delta_1 I(\Omega_1)}\cdot\frac{\delta_1 p(-\Omega_2)}{\delta_1 I(-\Omega_2)}}{\begin{pmatrix}j(\Omega_1-\Omega_2)+\gamma_e(n_0)+\\ n_0\cdot\frac{d\gamma_e}{dn}|_{n=n_0}+p_0\cdot G_n(n_0,p_0)\end{pmatrix}\cdot\left(\Gamma\cdot\begin{pmatrix}\gamma+j(\Omega_1-\Omega_2)-\\ G(n_0,p_0)+\\ p_0\cdot G_p(n_0,p_0)\end{pmatrix}\right)+\begin{pmatrix}G(n_0,p_0)+\\ p_0\cdot G_p(n_0,p_0)\end{pmatrix}\begin{pmatrix}\Gamma\cdot p_0\cdot G_n(n_0,p_0)+\\ R_{sp}(n_0)+n_0\cdot\frac{dR_{sp}(n)}{dn}|_{n=n_0}\end{pmatrix}} \tag{A.13}$$

The second order transfer function $\frac{\delta_{11}p(\Omega_1,\Omega_2)}{I(\Omega_1)\cdot I(\Omega_2)}$ can be expressed as:

$$\frac{\delta_{11}p(\Omega_1,\Omega_2)}{I(\Omega_1)\cdot I(\Omega_2)} = f(\Omega_1+\Omega_2)\cdot\frac{\delta_1 p(\Omega_1)}{\delta_1 I(\Omega_1)}\frac{\delta_1 p(\Omega_2)}{\delta_1 I(\Omega_2)} \tag{A.14}$$

where, using Eq. (A.9), we have done:

$$f(\Omega_1+\Omega_2) = G_n(n_0,p_0)\cdot \frac{\begin{pmatrix}\Gamma\cdot\left(j(\Omega_1+\Omega_2)+\gamma_e(n_0)+n_0\cdot\frac{d\gamma_e}{dn}|_{n=n_0}\right)\\ -\left(R_{sp}(n_0)+n_0\cdot\frac{dR_{sp}(n)}{dn}|_{n=n_0}\right)\end{pmatrix}\cdot\left(\frac{\left(2\gamma+j(\Omega_1+\Omega_2)-2\Gamma\cdot G(n_0,p_0)-2\Gamma\cdot p_0\cdot G_p(n_0,p_0)\right)}{\left(\Gamma\cdot p_0\cdot G_n(n_0,p_0)+R_{sp}(n_0)+n_0\cdot\frac{dR_{sp}(n)}{dn}|_{n=n_0}\right)}\right)}{\begin{pmatrix}j(\Omega_1+\Omega_2)+\gamma_e(n_0)+\\ n_0\cdot\frac{d\gamma_e}{dn}|_{n=n_0}+p_0\cdot G_n(n_0,p_0)\end{pmatrix}\cdot\left(\Gamma\cdot\begin{pmatrix}\gamma+j(\Omega_1-\Omega_2)-\\ G(n_0,p_0)+\\ p_0\cdot G_p(n_0,p_0)\end{pmatrix}\right)+\begin{pmatrix}G(n_0,p_0)+\\ p_0\cdot G_p(n_0,p_0)\end{pmatrix}\begin{pmatrix}\Gamma\cdot p_0\cdot G_n(n_0,p_0)+\\ R_{sp}(n_0)+n_0\cdot\frac{dR_{sp}(n)}{dn}|_{n=n_0}\end{pmatrix}} \tag{A.15}$$

Equivalently, the second order optical intensity to driving current can be expressed as:

$$H_{p_{11}}(\Omega_1,\Omega_2) = H'_{p_{11}}(\Omega_1+\Omega_2)\cdot H_{p_1}(\Omega_1)H_{p_1}(\Omega_2) \tag{A.16}$$

where $H'_{p_{11}}(\Omega_1+\Omega_2) = f(\Omega_1+\Omega_2)/C_p$.

Regarding the laser chirp, we can write:

$$\frac{d\delta\phi}{dt} = \omega_0+\delta\omega = \frac{1}{2}\alpha\Gamma v_g a_g(n_0+\delta n-n_t) \tag{A.17}$$

The first order transfer function is found like:

$$\begin{aligned}\delta_1\omega(\pm\Omega_1) &= \frac{1}{2}\alpha\Gamma v_g a_g\cdot\delta_1\cdot n(\pm\Omega_1)\\ &= \frac{1}{2}\alpha\Gamma v_g a_g\cdot\frac{\delta_1 n(\pm\Omega_1)}{\delta_1 p(\pm\Omega_1)}\cdot\frac{\delta_1 p(\pm\Omega_1)}{\delta I(\pm\Omega_1)}\cdot\delta I(\pm\Omega_1)\end{aligned} \tag{A.18}$$

And the second order transfer functions are given by:

$$\frac{\delta_{11}\omega(\Omega_1,\Omega_2)}{I(\Omega_1)\cdot I(\Omega_2)} = \frac{1}{2}\alpha\Gamma v_g a_g \cdot \Bigg(\frac{\Big(\gamma + j(\Omega_1+\Omega_2) - \Big(\Gamma\cdot\big(G(n_0,p_0)+p_0\cdot G_p(n_0,p_0)\big)\Big)\cdot\frac{p(\Omega_1,\Omega_2)}{I(\Omega_1)\cdot I(\Omega_2)}}{\big(\Gamma\cdot p_0\cdot G_n(n_0,p_0)+R_{sp}(n_0)+n_0\cdot\frac{dR_{sp}(n)}{dn}|_{n=n_0}\big)} - \frac{\Gamma\cdot G_n(n_0,p_0)\cdot\Big(\frac{\delta_1 n(\Omega_1)}{\delta_1 p(\Omega_1)}+\frac{\delta_1 n(\Omega_2)}{\delta_1 p(\Omega_2)}\Big)\cdot\frac{\delta_1 p(\Omega_1)}{\delta_1 I(\Omega_1)}\cdot\frac{\delta_1 p(\Omega_2)}{\delta_1 I(\Omega_2)}}{\big(\Gamma\cdot p_0\cdot G_n(n_0,p_0)+R_{sp}(n_0)+n_0\cdot\frac{dR_{sp}(n)}{dn}|_{n=n_0}\big)} \Bigg) \tag{A.19}$$

$$\frac{\delta_{11}\omega(\Omega_1,-\Omega_2)}{I(\Omega_1)\cdot I(-\Omega_2)} = \frac{1}{2}\alpha\Gamma v_g a_g \cdot \Bigg(\frac{\Big(\gamma + j(\Omega_1-\Omega_2) - \Big(\Gamma\cdot\big(G(n_0,p_0)+p_0\cdot G_p(n_0,p_0)\big)\Big)\cdot\frac{p(\Omega_1,-\Omega_2)}{I(\Omega_1)\cdot I(-\Omega_2)}}{\big(\Gamma\cdot p_0\cdot G_n(n_0,p_0)+R_{sp}(n_0)+n_0\cdot\frac{dR_{sp}(n)}{dn}|_{n=n_0}\big)} - \frac{\Gamma\cdot G_n(n_0,p_0)\cdot\Big(\frac{\delta_1 n(\Omega_1)}{\delta_1 p(\Omega_1)}+\frac{\delta_1 n(-\Omega_2)}{\delta_1 p(-\Omega_2)}\Big)\cdot\frac{\delta_1 p(\Omega_1)}{\delta_1 I(\Omega_1)}\cdot\frac{\delta_1 p(-\Omega_2)}{\delta_1 I(-\Omega_2)}}{\big(\Gamma\cdot p_0\cdot G_n(n_0,p_0)+R_{sp}(n_0)+n_0\cdot\frac{dR_{sp}(n)}{dn}|_{n=n_0}\big)} \Bigg) \tag{A.20}$$

Note that, using Eq. (A.18), the second order transfer function $\delta_{1,1}\omega(\Omega_1,\Omega_2)/\big(I(\Omega_1)\cdot I(\Omega_2)\big)$ can be expressed as:

$$\frac{\delta_{1,1}\omega(\Omega_1,\Omega_2)}{I(\Omega_1)\cdot I(\Omega_2)} = \Bigg(\frac{\delta_1\omega(\Omega_1+\Omega_2)}{\delta_1 I(\Omega_1+\Omega_2)} \Big/ \frac{\delta_1 p(\Omega_1+\Omega_2)}{I(\Omega_1+\Omega_2)} \cdot \frac{\delta_{11} p(\Omega_1,\Omega_2)}{I(\Omega_1)\cdot I(\Omega_2)} - \frac{\Gamma\cdot G_n(n_0,p_0)\cdot\Big(\frac{\delta_1 n(\Omega_1)}{\delta_1 p(\Omega_1)}+\frac{\delta_1 n(\Omega_2)}{\delta_1 p(\Omega_2)}\Big)\cdot\frac{\delta_1 p(\Omega_1)}{\delta_1 I(\Omega_1)}\cdot\frac{\delta_1 p(\Omega_2)}{\delta_1 I(\Omega_2)}}{\big(\Gamma\cdot p_0\cdot G_n(n_0,p_0)+R_{sp}(n_0)+n_0\cdot\frac{dR_{sp}(n)}{dn}|_{n=n_0}\big)} \Bigg) \tag{A.21}$$

and substituting the expression for $\delta_{11}p(\Omega_1,\Omega_2)/\Big(I(\Omega_1)\cdot I(\Omega_2)\Big)$ given by Eq. (A.14):

$$\frac{\delta_{1,1}\omega(\Omega_1,\Omega_2)}{I(\Omega_1)\cdot I(\Omega_2)} = \Bigg(\frac{\delta_1\omega(\Omega_1+\Omega_2)}{\delta_1 I(\Omega_1+\Omega_2)} \Big/ \frac{\delta_1 p(\Omega_1+\Omega_2)}{I(\Omega_1+\Omega_2)} \cdot f(\Omega_1+\Omega_2) - \frac{\Gamma\cdot G_n(n_0,p_0)\cdot\Big(\frac{\delta_1 n(\Omega_1)}{\delta_1 p(\Omega_1)}+\frac{\delta_1 n(\Omega_2)}{\delta_1 p(\Omega_2)}\Big)\cdot}{\big(\Gamma\cdot p_0\cdot G_n(n_0,p_0)+R_{sp}(n_0)+n_0\cdot\frac{dR_{sp}(n)}{dn}|_{n=n_0}\big)} \Bigg) \frac{\delta_1 p(\Omega_1)}{\delta_1 I(\Omega_1)} \cdot \frac{\delta_1 p(\Omega_2)}{\delta_1 I(\Omega_2)} \tag{A.22}$$

The derived transfer functions are useful to analytically express in an approximated way the output optical signal (both phase and and intensity) as a function of the input current.

Appendix B

Analytical study on clipping

With the assumption on the Gaussian distribution of the amplitude of the discrete OFDM signal, the probability of finding i discrete samples above or below the amplitude threshold A_{clip} within FS samples is given by the binomial distribution:

$$p_i = \binom{FS}{i} \Big(erfc\big(\sqrt{(CL/2)}\big) \Big)^i \Big(1 - erfc\big(\sqrt{(CL/2)}\big) \Big)^{FS-i} \tag{B.1}$$

which is an approximation when $2N+1 < FS$, since, then, the discrete samples are correlated and the trials are not independent. Since the OFDM symbols are windowed with a window function of size FS, the random clipping noise signal within the time interval $[-N_{symbols} \cdot FS, N_{symbols} \cdot FS - 1]$:

$$\hat{n}_{clip}[n] = \sum_{r=-N_{symbols}}^{N_{symbols}} n_{r,clip}[n - r \cdot FS] \cdot w[n - r \cdot FS] \cdot \sum_{\substack{n_p \\ n_p \in S_{\bar{p}}}} \delta[n - n_p - r \cdot FS] \tag{B.2}$$

where $n_{r,clip}$ is the rth realization of the clipping noise random process, $w[n]$ is a rectangular function (equal to 1 when $n \in [0, 1, ...FS-1]$, 0 otherwise), and the sum of kronecker delta's is the sample function which describes the ocurrence of clipping. In this case, the random time instants n_p are given by the default distribution, which has been assumed to be a binomial one, Eq. (B.1).

We calculate the power spectral density of $\hat{n}_{clip}[n]$ as:

$$\begin{aligned} \hat{n}_{\bar{p},clip}(e^{j\Omega}) &= \lim_{N_{symbols} \to +\infty} \frac{E\big[|FT\{\hat{n}_{clip}[n]\}|^2\big]}{(2N_{symbols}+1) \cdot FS} \\ &= \lim_{N_{symbols} \to +\infty} \frac{E\big[|\sum_{n=-\infty}^{\infty} \hat{n}_{clip}[n] \cdot exp(-j\Omega n)|^2\big]}{(2N_{symbols}+1) \cdot FS} \end{aligned} \tag{B.3}$$

We note that different r indices correspond to different realizations of the random process, and, therefore the samples are independent; moreover, the clipping is symmetric around the

zero value and, thus, its mean is equal to zero. Thus, we only retain the products with the same value of r index. Substituting the expression of $\hat{n}_{clip}[n]$, Eq. (B.2), into Eq. (B.3) and using the time shift property of the Fourier transform, we can arrive at the following expression:

$$\hat{n}_{\bar{p},clip}(e^{j\Omega}) = \lim_{N_{symbols}\to\infty} \frac{1}{(2N_{symbols}+1)\cdot FS} \cdot \sum_{r=-N_{symbols}}^{N_{symbols}} \sum_{n'=0}^{FS-1} \sum_{n=0}^{FS-1} E\big[n_{r,clip}[n'] \cdot n_{r,clip}[n]\big] \cdot E\Big[\sum_{\substack{n_p \\ n_p\in S_{\bar{p}}}} \delta[n'-n_p] \cdot \sum_{\substack{n_p \\ n_p\in S_{\bar{p}}}} \delta[n-n_p]\Big] \cdot exp\Big(-j\Omega(n'-n)\Big) \tag{B.4}$$

where we have also used the fact that the clipping noise random process is independent from the sampling function. Now we can divide the whole set of $2N+1$ realizations into a finite number of subsets in function of the number of clips which occur within the FS samples:

$$\begin{aligned}\hat{n}_{\bar{p},clip}(e^{j\Omega}) = & \lim_{N_{symbols}\to\infty} \frac{1}{(2N_{symbols}+1)\cdot FS} \cdot \sum_{i=0}^{i_{max}} N_{i\_clips} \sum_{n'=0}^{FS-1} \sum_{n=0}^{FS-1} E\big[n_{clip}[n'] \cdot n_{clip}[n]\big] \cdot \\ & E\Big[\sum_{\substack{n_p \\ n_p\in S_i}} \delta[n'-n_p] \cdot \sum_{\substack{n_p \\ n_p\in S_i}} \delta[n-n_p]\Big] \cdot exp\Big(-j\Omega(n'-n)\Big) \\ = & \frac{1}{FS} \cdot \sum_{i=0}^{i_{max}} p_i \sum_{n'=0}^{FS-1} \sum_{n=0}^{FS-1} E\big[n_{clip}[n'] \cdot n_{clip}[n]\big] \cdot \\ & E\Big[\sum_{\substack{n_p \\ n_p\in S_i}} \delta[n'-n_p] \cdot \sum_{\substack{n_p \\ n_p\in S_i}} \delta[n-n_p]\Big] \cdot exp\Big(-j\Omega(n-n')\Big)\end{aligned} \tag{B.5}$$

where we have used that within $2N+1$ realizations, according to Eq. (B.1), there must be $N_{i\_clips} = p_i \cdot (2N+1)$ realizations with i clips. Now S_i is the random subset of time events with cardinality equals to i, the number of clips within FS samples. Doing the variable changes $m = n$ and $u = n - n'$ and $R_{clip}[u] = E[n_{clip}[m] \cdot n_{clip}[m+u]]$, we obtain:

$$\begin{aligned}\hat{n}_{\bar{p},clip}(e^{j\Omega}) = & \frac{1}{FS} \cdot \sum_{i=0}^{i_{max}} p_i \cdot \\ & \Bigg(\sum_{u=-(FS-1)}^{0} R_{clip}[u] \sum_{m=-u}^{FS-1} E\Big[\sum_{\substack{n_p \\ n_p\in S_i}} \delta[m-n_p] \cdot \sum_{\substack{n_p \\ n_p\in S_i}} \delta[m+u-n_p]\Big] \cdot exp\Big(-j\Omega u\Big) + \\ & \sum_{u=1}^{FS-1} R_{clip}[u] \sum_{m=0}^{-u+FS-1} E\Big[\sum_{\substack{n_p \\ n_p\in S_i}} \delta[m-n_p] \cdot \sum_{\substack{n_p \\ n_p\in S_i}} \delta[m+u-n_p]\Big] \cdot exp\Big(-j\Omega u\Big)\Bigg)\end{aligned} \tag{B.6}$$

We need to study the autocorrelation of the sampling function, which can be expressed as:

$$\begin{aligned}& E\Big[\sum_{\substack{n_p \\ n_p\in S_i}} \delta[m-n_p] \cdot \sum_{\substack{n_p \\ n_p\in S_i}} \delta[m+u-n_p]\Big] = \\ & E\Big[\sum_{\substack{n_p \\ n_p\in S_i}} \big(U[m-n_p]-U[m-1-n_p]\big) \sum_{\substack{n_p \\ n_p\in S_i}} \big(U[m+u-n_p]-U[m+u-1-n_p]\big)\end{aligned} \tag{B.7}$$

where $U[m]$ is the Heaviside step function. That is, we have expressed the autocorrelation of the sampling function in terms of the counting random process $\sum_{\substack{n_p \\ n_p \in S_i}} U[m - n_p]$. An example of realization of the random sampling function and the corresponding counting process is shown in Fig. B.1.

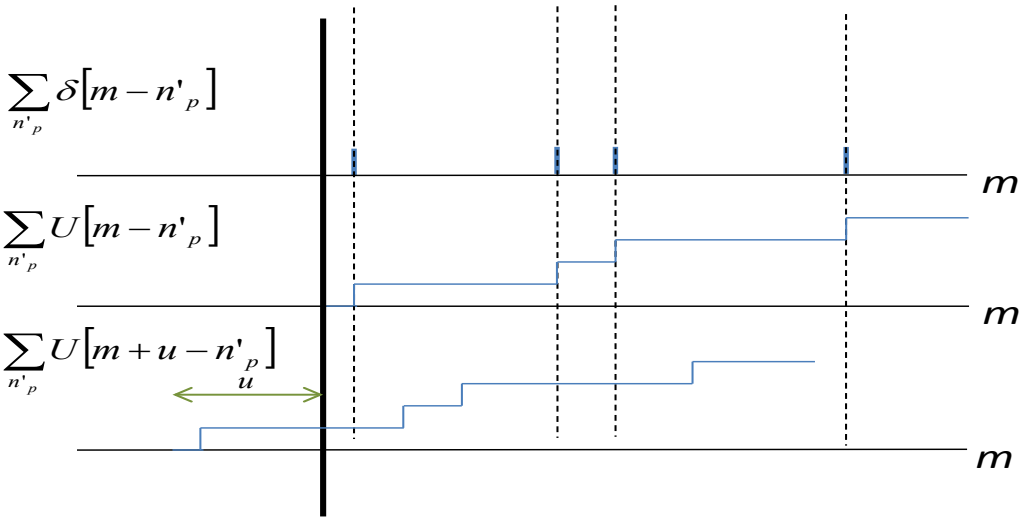

Figure B.1: Sampling function and corresponding counting process.

For sake's of nomenclature simplicity, let's define the random counting process

$$Y_m = \sum_{n=1}^{m+1} D_n, n = 0, 1, ...FS - 1 \tag{B.8}$$

being D_n a Bernoulli random variable, and Y_m a random process with hypergeometric distribution:

$$P(Y_m = q) = \frac{\binom{m+1}{q}\binom{FS-m-1}{i-q}}{\binom{FS}{i}} \tag{B.9}$$

And Eq. B.7 can be expressed as:

$$\begin{aligned} &E\Big[\sum_{\substack{n_p \\ n_p \in S_i}} \delta[m - n_p] \cdot \sum_{\substack{n_p \\ n_p \in S_i}} \delta[m + u - n_p]\Big] \\ &= E[Y_{u+m}Y_m] - E[Y_{u+m}Y_{m-1}] - E[Y_{u+m-1}Y_m] + E[Y_{u+m-1}Y_{m-1}] \end{aligned} \tag{B.10}$$

After the removal of terms which cancel out, one arrives at the simple expression:

$$\begin{aligned} &E\Big[\sum_{\substack{n_p \\ n_p \in S_i}} \delta[m - n_p] \cdot \sum_{\substack{n_p \\ n_p \in S_i}} \delta[m + u - n_p]\Big] \\ &= E[D_{m+1}D_{m+1}]\delta[u] + E[D_{m+1}D_{u+m+1}]U[u-1] \\ &= \frac{i}{FS}\delta[u] + \frac{i-1}{FS-1}\frac{i}{FS}U[u-1] \end{aligned} \tag{B.11}$$

And since the autocorrelation is an even function:

$$E\Big[\sum_{\substack{n_p\\ n_p\in S_i}}\delta[m-n_p]\cdot\sum_{\substack{n_p\\ n_p\in S_i}}\delta[m+u-n_p]\Big]$$
$$=\frac{i}{FS}\delta[u]+\frac{i-1}{FS-1}\frac{i}{FS}U[|u|-1] \tag{B.12}$$

Substituting into Eq. (B.6):

$$\hat{n}_{\bar{p},clip}(e^{j\Omega})=\frac{1}{FS}\cdot\sum_{i=0}^{i_{max}}p_i\cdot$$
$$\Big(\sum_{u=-(FS-1)}^{0}R_{clip}[u]\sum_{m=-u}^{FS-1}\Big(\frac{i}{FS}\delta[u]+\frac{i-1}{FS-1}\frac{i}{FS}U[|u|-1]\Big)\cdot exp\Big(-j\Omega u\Big)+$$
$$\sum_{u=1}^{FS-1}R_{clip}[u]\sum_{m=0}^{-u+FS-1}\Big(\frac{i}{FS}\delta[u]+\frac{i-1}{FS-1}\frac{i}{FS}U[|u|-1]\Big)\cdot exp\Big(-j\Omega u\Big)\Big)$$
$$=\sum_{i=0}^{i_{max}}p_i\cdot\Big(\frac{i}{FS}\cdot R_{clip}[0]\cdot\frac{FS}{FS}+$$
$$\frac{i-1}{FS-1}\frac{i}{FS}\sum_{u=-(FS-1)}^{FS-1}R_{clip}[u]U[|u|-1](\frac{FS}{FS}-\frac{|u|}{FS})exp\Big(-j\Omega u\Big)\Big) \tag{B.13}$$

Neglecting the effects of the finite temporal window of size FS, we can write:

$$\hat{n}_{\bar{p},clip}(e^{j\Omega})$$
$$\approx\sum_{i=0}^{i_{max}}p_i\cdot\Big(\frac{i}{FS}\cdot R_{clip}[0]+\frac{i-1}{FS-1}\frac{i}{FS}\sum_{u=-(FS-1)}^{FS-1}R_{clip}[u]U[|u|-1]exp\Big(-j\Omega u\Big)\Big)$$
$$=\sum_{i=0}^{i_{max}}p_i\cdot\Big(\frac{i}{FS}\cdot R_{clip}[0]+\frac{i-1}{FS-1}\frac{i}{FS}\sum_{u=-(FS-1)}^{FS-1}R_{clip}[u]\big(1-\delta[u]\big)exp\Big(-j\Omega u\Big)$$
$$=\sum_{i=0}^{i_{max}}p_i\cdot\Big(\frac{i}{FS}\cdot R_{clip}[0]+\frac{i-1}{FS-1}\frac{i}{FS}\big(\hat{n}_{clip}(e^{j\Omega})-R_{clip}[0]\big)\Big) \tag{B.14}$$

Doing $\sum_{i=0}^{i_{max}}p_i\frac{i}{FS}=\bar{p}$ and $\sum_{i=0}^{i_{max}}p_i\frac{i-1}{FS-1}\frac{i}{FS}=\bar{p}^2$, the previous expression can be written as:

$$\hat{n}_{\bar{p},clip}(e^{j\Omega})=\bar{p}\cdot R_{clip}[0]+\bar{p}^2\big(\hat{n}_{clip}(e^{j\Omega})-R_{clip}[0]\big) \tag{B.15}$$

That is, the spectral density can be expressed as the sum of a white component (non-correlated) multiplied by the average clipping rate $\bar{p}$, and a coloured noise component multiplied by $\bar{p}^2$ (the factor $(i-1)/(FS-1)$ instead of i/FS is due to the finite population FS). Eq. (B.15) gives us the expression of the power spectral density of the clipping noise as a function of the average sampling rate (in this case, equal to $\bar{p}$) in function of the non-sampled clipping noise.

Appendix C

Autocorrelation of discrete OFDM signals

After arranging the QAM symbols X_1, X_2,...X_N with hermitian symmetry at the IFFT input, the signal at the input of the clipping device is given by:

$$x[n] = 2\Re\Big\{ \sum_{k=1}^{N} X_k \cdot exp\Big(j \cdot 2\pi \cdot k \cdot \frac{n}{FS}\Big) \Big\} \tag{C.1}$$

where $\Re\{\cdot\}$ stands for the real part of a complex quantity.

The autocorrelation function $R_x[\varsigma]$ is calculated as:

$$R_x[\varsigma] = \langle x[n_1] \cdot x^*[n_2] \rangle;\ \varsigma = |n_1 - n_2| \tag{C.2}$$

It is interesting to make two notations: firstly, as it corresponds to linearly modulated signals, the OFDM signal is a stochastic cyclostationary process [55], that is, it presents a periodic autocorrelation function:

$$R_x[\varsigma + n \cdot FS] = R_x[\varsigma], n \in 0, 1, ...FS - 1 \tag{C.3}$$

Secondly, since some oversampling is introduced, the time samples are correlated one another. Otherwise, if all subcarriers are modulated with independent zero-mean complex QAM information symbols, the autocorrelation of the non-oversampled OFDM signal $x'[n]$ particularizes to:

$$R_{x'}[\varsigma] = \sigma_x^2 \cdot \sum_{k=-FS/2}^{FS/2-1} exp\Big(j \cdot 2\pi \cdot k \cdot \frac{\varsigma}{FS}\Big) = \sigma_x^2 \cdot FS \sum_{k=-\infty}^{\infty} \delta[\varsigma - k \cdot FS] \tag{C.4}$$

In order to determine the autocorrelation of an oversampled OFDM signal, the oversampled signal is expressed as the output of a filter with spectral nulls at those frequencies where the

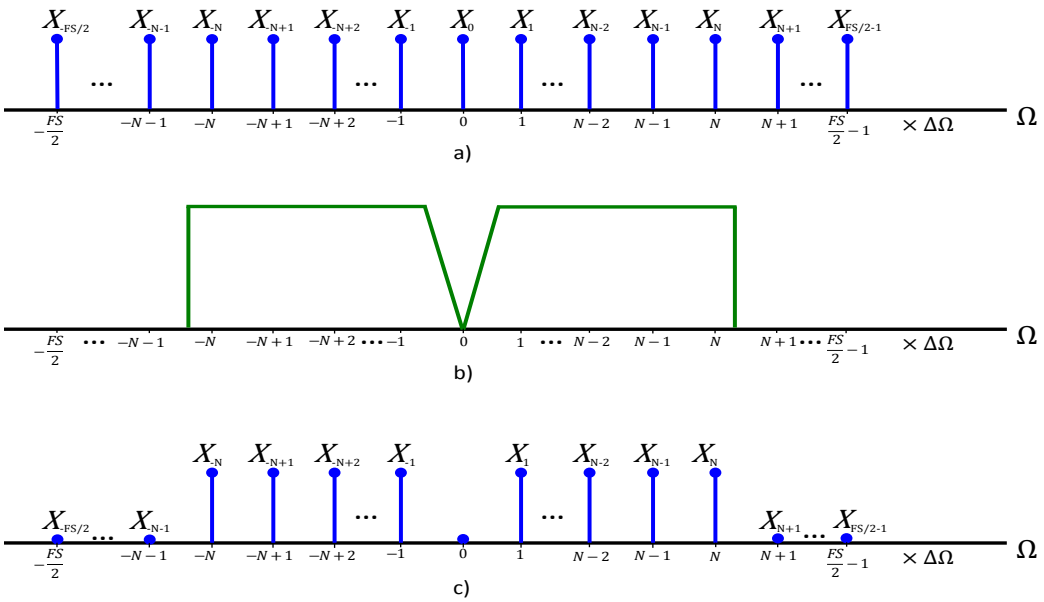

Figure C.1: a) Spectral content of a non-oversampled OFDM signal. b) Assumed filter for the introduction of oversampling. c) Spectral content of an oversampled OFDM signal.

null subcarriers of the OFDM signal are located. Fig. C.1 shows schematically the filtering process to obtain the oversampled signal.

The oversampled signal at the output of the filter can be expressed as the convolution of the non-oversampled signal with the filter's impulse response $g[n]$:

$$x[n] = \sum_{m=-\infty}^{\infty} x'[m] \cdot g[n-m] \tag{C.5}$$

Substituting Eq. (C.5) into Eq. (C.2):

$$\begin{aligned} R_x[n_1, n_2] = \langle x[n_1] \cdot x^*[n_2] \rangle &= \langle \sum_{m=-\infty}^{\infty} x'[m] \cdot g[n_1 - m] \cdot \sum_{p=-\infty}^{\infty} x'[p] \cdot g[n_2 - p] \rangle \\ &= \sum_{m=-\infty}^{\infty} \sum_{p=-\infty}^{\infty} \langle x'[m] \cdot x'[p] \rangle \cdot g[n_1 - m] \cdot g[n_2 - p] \\ &= \sum_{m=-\infty}^{\infty} \sum_{p=-\infty}^{\infty} R_{x'}[m-p] \cdot g[n_1 - m] \cdot g[n_2 - p] \end{aligned} \tag{C.6}$$

The change of variables $s = n_1 - m$ and $w = n_2 - p$ yields:

$$R_x[n_1, n_2] = \sum_{s=-\infty}^{\infty} \sum_{w=-\infty}^{\infty} R_{x'}[n_1 - s - n_2 + w] \cdot g[w] \cdot g[s] \tag{C.7}$$

We note that the inner sum can be re-written as

$$\sum_{w=-\infty}^{\infty} R_{x'}[n_1 - s - n_2 + w] \cdot g[w] = R_{x'}[n] * g[-n] \Big|_{n=n_1-s-n_2} \tag{C.8}$$

Let $f[n] = R_{x'}[n] * g[-n]$, then:

$$R_x[n_1, n_2] = \sum_{s=-\infty}^{\infty} g[s] \cdot f[n_1 - s - n_2] = f[n] * g[n]\Big|_{n=n_1-n_2} \tag{C.9}$$

Putting all these results together, we finally obtain the well-known result for the autocorrelation of the process at the output of a linear system with a stochastic random processes at the input: $R_x[\varsigma] = R_{x'}[\varsigma] * g[\varsigma] * g[-\varsigma]$. In the frequency domain we have that $X(e^{j\Omega}) = X'(e^{j\Omega}) \cdot |G(e^{j\Omega})|^2$. Using the transfer function description in Fig. C.1, the autocorrelation $R_x[\varsigma]$ can be calculated by taking the inverse Fourier transform, leading to:

$$R_x[\varsigma] = R_{x'}[\varsigma] * \frac{1}{FS}\Big(\sum_{k=-N}^{-1} exp\big(j2\pi \cdot k\frac{\varsigma}{FS}\big) + \sum_{k=1}^{N} exp\big(j2\pi \cdot k\frac{\varsigma}{FS}\big)\Big) \tag{C.10}$$

which, using Eq. (C.4), can be expressed as:

$$\begin{aligned} R_x[\varsigma] &= \sigma_x^2 \cdot \Big(\sum_{k=-N}^{-1} exp\big(j2\pi \cdot k\frac{\varsigma}{FS}\big) + \sum_{k=1}^{N} exp\big(j2\pi \cdot k\frac{\varsigma}{FS}\big)\Big) \\ &= \sigma_x^2 \left(\frac{sin\Big(2\pi\big(2N+1\big)\frac{\varsigma}{FS}\Big)}{sin\big(2\pi\frac{\varsigma}{FS}\big)} - 1 \right) \end{aligned} \tag{C.11}$$

It is easy to check that the previous expression is equal to Eq. (C.4) in the hypothetical case $2N + 1 = FS$, that is, no oversampling is introduced.

Appendix D

Penalty due to ISI & ICI effects

The penalty due to ISI is determined firstly. The discrete signal at the receiver after passing through the linear system with impulse response $h(t)$:

$$y[m] = x[m] * h[m] = \sum_{v=-L_-}^{L_+} h[v] \cdot x[m-v] \tag{D.1}$$

where $h[m] = h(m \cdot T_{sam})$ and we have assumed that the impulse response $h(t)$ has negative tail extending to $-L_- \cdot T_{sam}$ and a positive tail extending to $L_+ \cdot T_{sam}$.

Since the OFDM signal is composed of serialized OFDM symbols, $x[m] = \sum_i x_i[m - i(FS + N_g)]$, where $N_g = N_{pre} + N_{pos}$, the i-th OFDM received symbol can be expressed as:

$$y_i[m'] = \sum_i \sum_{v=-L_-}^{L_+} h[v] \cdot x_i[m - v + i(FS + N_g)], \tag{D.2}$$

Fig. D.1 depicts the convolution between $h[m]$ and $x[m]$ at time instants $m = 0$ and $m = FS - 1$.

From Fig. D.1 and assuming that only adjacent symbols introduce ISI into the current symbol, the ISI introduced by the $(i-1)$th symbol and the $(i+1)$th symbol are respectively:

$$ISI_{i-1}[m] = \sum_{v=m+i(FS+N_g)+N_{pre}+1}^{L_+} h[v] \cdot x_{i-1}[m - v + (i-1)(FS + N_g)] \tag{D.3}$$

$$ISI_{i+1}[m] = \sum_{v=-L_-}^{m+i(FS+N_g)-FS+1-N_{pos}-1} h[v] \cdot x_{i+1}[m - v + (i+1)(FS + N_g)] \tag{D.4}$$

The first term is due to the $L_+ - N_{pre} - m$ samples from the previously transmitted OOFDM symbol, and the second one is due to the $m - FS + 1 - N_{pos} - L_-$ samples from the next

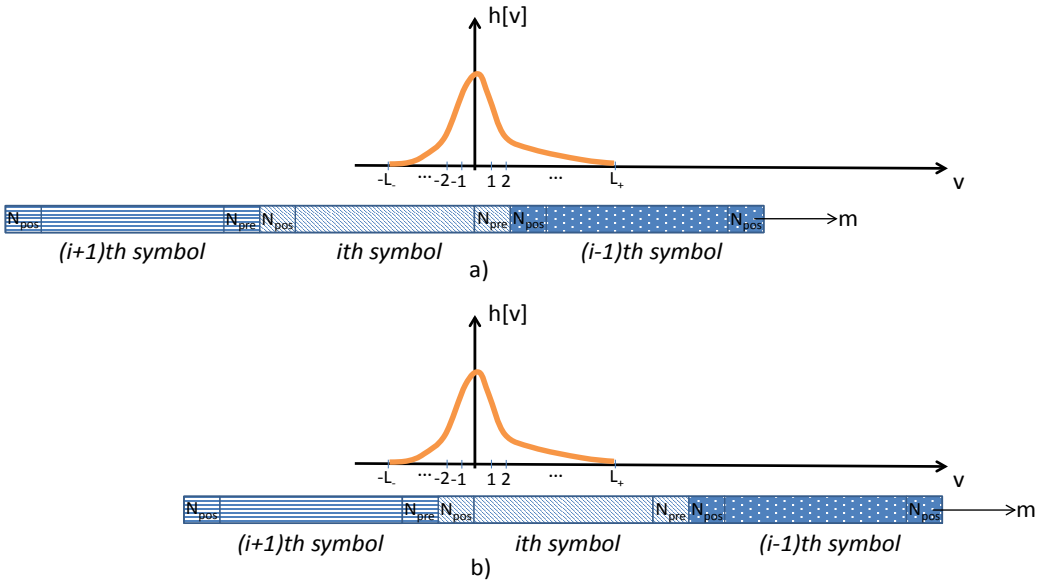

Figure D.1: Convolution between the impulse response $h[m]$ and the OFDM signal $x[m]$. a) $m = 0$ and b) $m = FS - 1$.

transmitted OOFDM symbol. At the receiver, serial to parallel conversion is performed and a DFT of size FS is calculated on each block. Doing $m' = m + i \cdot (FS + N_g)$, the resulting ISI term is given by:

$$\widehat{ISI}[k] = exp(-j2\pi\frac{N_g}{FS}) \sum_{m'=0}^{FS-1} \Bigg(\sum_{v=m'+N_{pre}+1}^{L_+} h[v] \cdot x_{i-1}[m - v - (FS + N_g)] + \sum_{v=-L_-}^{m'-FS+1-N_{pos}-1} h[v] \cdot x_{i+1}[m' - v + (FS + N_g)] \Bigg) \cdot exp\Big(- j2\pi m' \frac{k}{FS} \Big) \quad \text{(D.5)}$$

Doing the variable change $p = m' - v \Rightarrow v = m' - p$, we have:

$$\widehat{ISI}[k] = exp(-j2\pi\frac{N_g}{FS}) \sum_{m'=0}^{FS-1} \Bigg(\sum_{v=m'-L_+}^{-N_{pre}-1} h[m'-p] \cdot x_{i-1}[p-(FS + N_g)] + \sum_{v=FS-1+N_{pos}+1}^{m'+L_-} h[m' - p] \cdot x_{i+1}[p + (FS + N_g)] \Bigg) \cdot exp\Big(- j2\pi m' \frac{k}{FS} \Big) \quad \text{(D.6)}$$

Next, we interchange the order of the sums and the limits are determined as Fig. D.2.

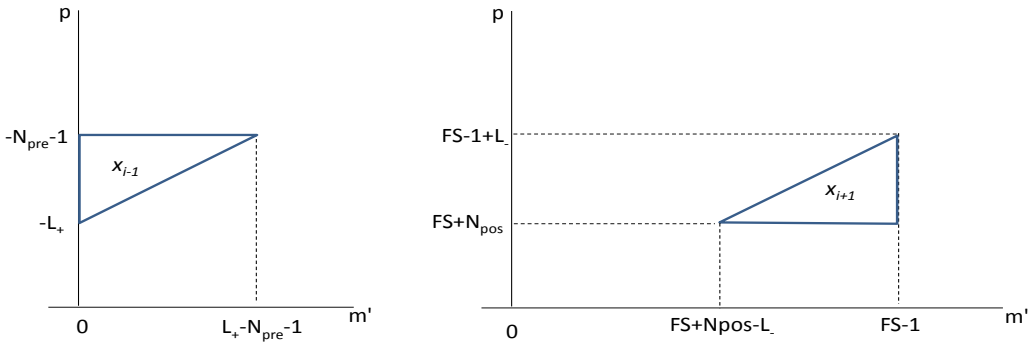

Figure D.2: Change of indexes.

$$
\begin{aligned}
\widehat{ISI}[k] &= e^{-j2\pi\frac{N_g}{FS}} \sum_{p=-L_+}^{-N_{pre}-1} \sum_{m'=0}^{p+L_+} h[m'-p]\cdot x_{i-1}[p-(FS+N_g)]\cdot e^{-j2\pi m'\frac{k}{FS}} \\
&+ e^{-j2\pi\frac{N_g}{FS}} \sum_{p=FS+N_{pos}}^{FS-1+L_-} \sum_{m'=p-L_-}^{FS-1} h[m'-p]\cdot x_{i+1}[p+(FS+N_g)]\cdot e^{-j2\pi m'\frac{k}{FS}} \\
&= e^{-j2\pi\frac{N_g}{FS}} \sum_{p=-L_+}^{-N_{pre}-1} x_{i-1}[p-(FS+N_g)]\cdot \sum_{m'=-p}^{L_+} h[m']\cdot e^{-j2\pi(m'+p)\frac{k}{FS}} \\
&+ e^{-j2\pi\frac{N_g}{FS}} \sum_{p=FS+N_{pos}}^{FS-1+L_-} x_{i+1}[p+(FS+N_g)]\cdot \sum_{m'=-L_-}^{-p+FS-1} h[m']\cdot e^{-j2\pi(m'+p)\frac{k}{FS}} \\
&= e^{-j2\pi\frac{N_g}{FS}} \sum_{p=N_{pre}+1}^{L_+} x_{i-1}[-p-(FS+N_g)]\cdot e^{j2\pi p\frac{k}{FS}} \sum_{m'=p}^{L_+} h[m']\cdot e^{-j2\pi m'\frac{k}{FS}} \\
&+ e^{-j2\pi\frac{N_g}{FS}} \sum_{p=N_{pos}}^{L_--1} x_{i+1}[p+FS+(FS+N_g)]\cdot e^{-j2\pi p\frac{k}{FS}} \sum_{m'=-L_-}^{-p-1} h[m']\cdot e^{-j2\pi m'\frac{k}{FS}} \\
&= e^{-j2\pi\frac{N_g}{FS}} \sum_{p=N_{pre}+1}^{L_+} x_{i-1}[-p-(FS+N_g)]\cdot e^{j2\pi p\frac{k}{FS}}\cdot H_{p,pos\_tail}[k] \\
&+ e^{-j2\pi\frac{N_g}{FS}} \sum_{p=N_{pos}}^{L_--1} x_{i+1}[p+FS+(FS+N_g)]\cdot e^{-j2\pi p\frac{k}{FS}}\cdot H_{p,neg\_tail}[k]
\end{aligned}
\tag{D.7}
$$

Note that $H_{p,pos\_tail}[k] = \sum_{m=p}^{L_+} h[m]\cdot exp\Big(-j2\pi m\frac{k}{FS}\Big)$ and $H_{p,neg\_tail}[k] = \sum_{m=-L_-}^{-p-1} h[m]\cdot exp\Big(-j2\pi m\frac{k}{FS}\Big)$ represent the FS-point discrete Fourier Transform of the positive and negative tails of the channel impulse response, respectively.

We finally calculate the variance of $\widehat{ISI}[k]$ as:

$$
\sigma^2_{ISI}[k] = \Big\langle \widehat{ISI}[k]\cdot(\widehat{ISI}[k])^*\Big\rangle \tag{D.8}
$$

Since the samples of different OFDM symbols are independent and with zero mean, we have:

$$\sigma^2_{ISI}[k] = \sum_{p=N_{pre}+1}^{L_+} \sum_{q=N_{pre}+1}^{L_+} \langle x_{i-1}[-p] \cdot x^*_{i-1}[-q] \rangle \cdot exp\Big(j2\pi(p-q)\frac{k}{FS}\Big) \cdot H_{p,pos\_tail}[k] \cdot H^*_{q,pos\_tail}[k] + \sum_{p=N_{pos}}^{L_--1} \sum_{q=N_{pos}}^{L_--1} \langle x_{i+1}[p+FS] \cdot x^*_{i+1}[q+FS] \rangle \cdot exp\Big(-j2\pi(p-q)\frac{k}{FS}\Big) \cdot H_{p,neg\_tail}[k] \cdot H^*_{q,neg\_tail}[k] = \quad \text{(D.9)}$$

And making use of the autcorrelation $R_x[\varsigma] = \langle x_{i+1}[p] \cdot x^*_{i+1}[p+\varsigma] \rangle$:

$$\begin{aligned}\sigma^2_{ISI}[k] = {} & R_x[0] \sum_{q=N_{pre}+1}^{L_+} |H_{q,pos\_tail}[k]|^2 \\ & + \sum_{p=N_{pre}+1}^{L_+} \sum_{\substack{q=N_{pre}+1 \\ q\neq p}}^{L_+} R_x[-q+p] \cdot exp\Big(j2\pi(p-q)\frac{k}{FS}\Big) \cdot H_{p,pos\_tail}[k] \cdot H^*_{q,pos\_tail}[k] \\ & + R_x[0] \sum_{q=N_{pos}}^{L_--1} |H_{q,neg\_tail}[k]|^2 \\ & + \sum_{p=N_{pos}}^{L_--1} \sum_{\substack{q=N_{pos} \\ q\neq p}}^{L_--1} R_x[q-p] \cdot exp\Big(-j2\pi(p-q)\frac{k}{FS}\Big) \cdot H_{p,neg\_tail}[k] \cdot H^*_{q,neg\_tail}[k] \end{aligned} \quad \text{(D.10)}$$

It remains to determine the penalty due to ICI as suggested in [87]: with a sufficiently length of the cyclic extensions, the ICI effects would be null; the effects due to ICI can be evaluated by assuming a pair of "extra" extensions Ext_{pre} and Ext_{pos} in such a way the ICI is null, and its negative would give us the ICI term (see Fig. D.3).

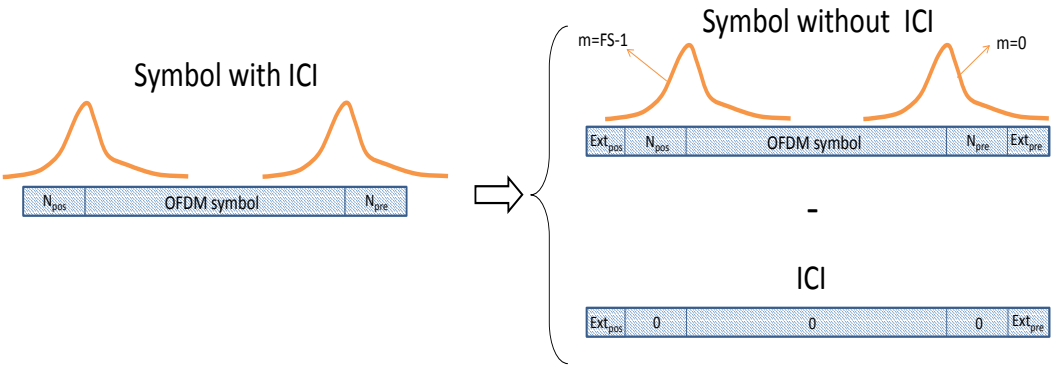

Figure D.3: ICI evaluation.

From Fig. D.3, the ICI term is given by:

$$ICI[k] = -\sum_{v=-L_-}^{m+i(FS+N_g)-FS+1-N_{pos}-1} h[v] \cdot x_i[m-v+i(FS+N_g)] - \sum_{v=m+i(FS+N_g)+N_{pre}+1}^{L_+} h[v] \cdot x_i[m-v+i(FS+N_g)] \quad \text{(D.11)}$$

Proceeding in a similar manner as with the terms in Eq. (D.3) and Eq. (D.4), the ICI term after DFT can be expressed as:

$$\widehat{ICI}[k] = \sum_{p=N_{pos}}^{L_--1} x_i[p+FS] \cdot exp\Big(j2\pi p\frac{k}{FS}\Big) \cdot H_{p,neg\_tail}[k] + \sum_{p=N_{pre+1}}^{L_+} x_i[-p] \cdot exp\Big(-j2\pi p\frac{k}{FS}\Big) \cdot H_{p,pos\_tail}[k] \quad \text{(D.12)}$$

Assuming that the samples in the two terms are uncorrelated, we have:

$$\begin{aligned}
&\sigma^2_{ICI}[k] = \\
&R_x[0] \sum_{q=N_{pre}+1}^{L_+} |H_{q,pos_tail}[k]|^2 \\
&+ \sum_{p=N_{pre}+1}^{L_+} \sum_{\substack{q=N_{pre}+1 \\ q\neq p}}^{L_+} R_x[-q+p] \cdot exp\Big(j2\pi(p-q)\frac{k}{FS}\Big) \cdot H_{p,pos_tail}[k] \cdot H^*_{q,pos_tail}[k] \\
&+ R_x[0] \sum_{q=N_{pos}}^{L_--1} |H_{q,neg_tail}[k]|^2 \\
&+ \sum_{p=N_{pos}}^{L_--1} \sum_{\substack{q=N_{pos} \\ q\neq p}}^{L_--1} R_x[q-p] \cdot exp\Big(-j2\pi(p-q)\frac{k}{FS}\Big) \cdot H_{p,neg_tail}[k] \cdot H^*_{q,neg_tail}[k]
\end{aligned} \quad \text{(D.13)}$$

Which is exactly the same expression as that for the ISI term in Eq. (D.10).

Appendix E

List of Publications

E.1 Publications derived from the realization of this Ph.D. Thesis

E.1.1 Journal Papers

1. **C. Sánchez**, B. Ortega, and J. Capmany, "System performance enhancement with pre-distorted OOFDM signal waveforms in DM/DD systems," Optics Express, vol. 22, no. 6, pp. 7269-7283, 2014.

2. **C. Sánchez**, B. Ortega, J. L. Wei, and J. Capmany, "Optical filtering in directly modulated/detected OOFDM systems," Optics Express, vol. 21, no. 25, pp. 30591-30609, 2013.

3. **C. Sánchez**, J. L. Wei, B. Ortega, and J. Capmany, "Comprehensive impairment and performance description of directly modulated/detected OOFDM systems," IEEE Journal of Lightwave Technology, vol. 31, no. 20, 2013.

4. **C. Sánchez**, B. Ortega, J. L. Wei, J. M. Tang, and J. Capmany, "Analytical formulation of directly modulated OOFDM signals transmitted over an IM/DD dispersive link," Optics Express, vol. 21, no. 6, pp. 7651-7666, 2013.

E.1.2 Conference Papers

1. **C. Sánchez**, B. Ortega, and J. Capmany, "Exploring the ultimate performance by tailoring the transmitter parameters in OOFDM systems," in Conference on Laser and Electro-Optics (CLEO), San Diego (USA), 2013, CTu2J.2.

2. **C. Sánchez**, B. Ortega, and J. Capmany, "Analytical formulation framework for directly modulated/detected OOFDM systems," in Conference on Lasers and Electro-Optics (CLEO) Europe, Munich (Germany), 2013, CI-1.5.

E.2 Related publications

E.2.1 Journal Papers

1. X. Zheng, **C. Sánchez**, B. Ortega, and J. M. Tang, "Compensation of directly modulated distributed feedback laser frequency chirps in optical orthogonal frequency division multiplexing intensity-modulation and direct-detection passive optical network systems," IET Optoelectronics, vol. 6, no. 2, pp. 75-81, 2012.

2. **C. Sánchez**, B. Ortega, and J. Capmany, "OFDM-IDMA for uplink transmission in passive optical networks," IEEE Photonics Journal, vol. 4, no. 1, pp. 1-13, 2012.

3. J. L. Wei, **C. Sánchez**, E. Hugues-Salas, P. S. Spencer, and J. M. Tang, "Wavelength-offset filtering in optical OFDM IMDD systems using directly modulated DFB lasers," IEEE Journal of Lightwave Technology, vol. 29, no. 18, pp. 2861-2870, 2011.

4. J. L. Wei, **C. Sánchez**, R. P. Giddings, E. Hugues-Salas, and J. M. Tang, "Significant improvements in optical power budgets of real-time optical OFDM PON systems," Optics Express, vol. 18, no. 20, pp. 20732-20745, 2010.

5. B. Ortega, I. Gasulla, J. Mora, G. Puerto, **C. Sánchez**, F. Grassi, M. Bolea, and J. Capmany, "IST ALPHA project: architectures for flexible photonic home and access networks," Waves, vol. 1, no. 0, pp. 6-23, 2009.

E.2.2 Conference Papers

1. J. L. Wei, E. Hugues-Salas, **C. Sánchez**, X. Q. Jin, I. Pierce, B. Ortega, and J. M. Tang,"Wavelength-offset optical filtering induced power budget improvements in end-to-end real-time optical OFDM PON systems," in Communications and Photonics conference (ACP), Guangzhou (China), pp. 1-3, 2012.

2. J. L. Wei, E. Hugues-Salas, **C. Sánchez**, X. Q. Jin, R. P. Giddings, I. Pierce, B. Ortega, C. Shu, and J. M. Tang,"Improved power budgets of end-to-end real-time optical OFDM PON systems using wavelength-offset optical filtering," in 8th International Symposium on Communication Systems, Networks & Digital Signal Processing (CSNDSP), Poznan (Poland), pp. 1-3, 2012.

3. **C. Sánchez**, B. Ortega, and J. Capmany, "Sistemas OOFDM con detección directa y sensibilidad mejorada," in XXV Simposium Nacional de la Unión Científica Internacional de Radio (URSI), Bilbao (Spain), pp. 1-3, 2010.

Bibliography

[1] W. Shieh and I. Djordjevic, *OFDM for Optical Communications*. Academic Press, 2009.

[2] *Cisco visual networking index: the zettabyte era–trends and analysis*, White Paper, Cisco, May 2013.

[3] A. Willner, R. Byer, C. Chang-Hasnain, S. Forrest, H. Kressel, H. Kogelnik, G. Tearney, C. Townes, and M. Zervas, "Optics and photonics: key enabling technologies", *Proceedings of the IEEE*, vol. 100, no. Special Centennial Issue, pp. 1604–1643, May 2012.

[4] P. Winzer and R.-J. Essiambre, "Advanced optical modulation formats", *Proceedings of the IEEE*, vol. 94, no. 5, pp. 952 –985, May 2006.

[5] D. McGhan, C. Laperle, A. Savehenko, C. Li, G. Mak, and M. O'Sullivan, "5120 km RZ-DPSK transmission over G652 fiber at 10 Gb/s with no optical dispersion compensation", in *Optical Fiber Communication Conference (OFC)*, vol. 6, Mar. 2005, PDP27.

[6] T. Foggi, E. Forestieri, G. Colavolpe, and G. Prati, "Maximum-likelihood sequence detection with closed-form metrics in OOK optical systems impaired by GVD and PMD", *Journal of Lightwave Technology*, vol. 24, no. 8, pp. 3073–3087, Aug. 2006.

[7] R. I. Killey, P. M. Watts, V. Mikhailov, M. Glick, and P. Bayvel, "Electronic dispersion compensation by signal predistortion using digital processing and a dual-drive Mach-Zehnder modulator", *Photonics Technology Letters*, vol. 17, no. 3, pp. 714–716, Mar. 2005.

[8] A. J. Lowery, "Fiber nonlinearity mitigation in optical links that use OFDM for dispersion compensation", *Photonics Technology Letters*, vol. 19, no. 19, pp. 1556–1558, Oct. 2007.

[9] Y. Benlachtar, S. J. Savory, B. C. Thomsen, G. Gavioli, P. Bayvel, and R. I. Killey, "Robust long-haul transmission utilizing electronic precompensation and MLSE equalization", in *Optical Fiber Communication Conference (OFC)*, Mar. 2007, JWA52.

[10] M. G. Taylor, "Coherent detection method using DSP for demodulation of signal and subsequent equalization of propagation impairments", *Photonics Technology Letters*, vol. 16, no. 2, pp. 674–676, Feb. 2004.

[11] E. Ip and J. M. Kahn, "Digital equalization of chromatic dispersion and polarization mode dispersion", *Journal of Lightwave Technology*, vol. 25, no. 8, pp. 2033–2043, Aug. 2007.

[12] E. Ip and J. Kahn, "Compensation of dispersion and nonlinear impairments using digital backpropagation", *Journal of Lightwave Technology*, vol. 26, no. 20, pp. 3416–3425, Oct. 2008.

[13] F. Guiomar, J. Reis, A. Teixeira, and A. Pinto, "Digital postcompensation using Volterra series transfer function", *Photonics Technology Letters*, vol. 23, no. 19, pp. 1412–1414, Oct. 2011.

[14] R. Weidenfeld, M. Nazarathy, R. Noe, and I. Shpantzer, "Volterra nonlinear compensation of 100G coherent OFDM with baud-rate ADC, tolerable complexity and low intra-channel FWM/XPM error propagation", in *Optical Fiber Communication Conference (OFC)*, Mar. 2010, OTuE3.

[15] R. Ryf, S. Randel, A. Gnauck, C. Bolle, R. Essiambre, P. Winzer, D. Peckham, A. McCurdy, and R. Lingle, "Space-division multiplexing over 10 km of three-mode fiber using coherent 6 x 6 MIMO processing", in *Optical Fiber Communication Conference (OFC)*, Mar. 2011, PDPB10.

[16] T. Omiya, M. Yoshida, and M. Nakazawa, "400 Gbit/s 256 QAM-OFDM transmission over 720 km with a 14 bit/s/hz spectral efficiency by using high-resolution FDE", *Optics Express*, vol. 21, no. 3, pp. 2632–2641, Feb. 2013.

[17] J. Armstrong, "OFDM for optical communications", *Journal of Lightwave Technology*, vol. 27, no. 3, pp. 189–204, Feb. 2009.

[18] A. J. Lowery and L. B. Du, "Optical orthogonal division multiplexing for long haul optical communications: a review of the first five years", *Optical Fiber Technology*, vol. 17, no. 5, pp. 421–438, Aug. 2011.

[19] C. F. Lam, *Passive Optical Networks: Principles and Practice*. Academic Press, 2007.

[20] T. Koonen, "Fiber to the home/fiber to the premises: what, where, and when?", *Proceedings of the IEEE*, vol. 94, no. 5, pp. 911–934, May 2006.

[21] D. Hood, *Gigabit-capable Passive Optical Networks*. Wiley, 2012.

[22] S.-M. Lee, S.-G. Mun, M.-H. Kim, and C.-H. Lee, "Demonstration of a long-reach DWDM-PON for consolidation of metro and access networks", *Journal of Lightwave Technology*, vol. 25, no. 1, pp. 271–276, Jan. 2007.

[23] R. P. Davey, D. B. Grossman, M. Rasztovits-Wiech, D. Payne, D. Nesset, A. E. Kelly, A. Rafel, S. Appathurai, and S.-H. Yang, "Long-reach passive optical networks", *Journal of Lightwave Technology*, vol. 27, no. 3, pp. 273–291, Feb. 2009.

[24] H. Song, B.-W. Kim, and B. Mukherjee, "Long-reach optical access networks: a survey of research challenges, demonstrations, and bandwidth assignment mechanisms", *Communications Surveys & Tutorials*, vol. 12, no. 1, pp. 112–123, 2010.

[25] J. Prat, *Next-Generation FTTH Passive Optical Networks: Research Towards Unlimited Bandwidth Access*. Springer, 2008.

[26] J. L. Wei, "Intensity modulation of optical OFDM signals using low-cost semiconductor laser devices for next-generation PONs", PhD thesis, Bangor University, 2010.

[27] N. Yoshimoto, J. Kani, S.-Y. Kim, N. Iiyama, and J. Terada, "DSP-based optical access approaches for enhancing NG-PON2 systems", *Communications Magazine*, vol. 51, no. 3, pp. 58–64, Mar. 2013.

[28] D. Lavery, R. Maher, D. S. Millar, B. Thomsen, P. Bayvel, and S. J. Savory, "Digital coherent receivers for long-reach optical access networks", *Journal of Lightwave Technology*, vol. 31, no. 4, pp. 609–620, Feb. 2013.

[29] R. P. Giddings, X. L. Yang, X. Q. Jin, J. M. Tang, and H. Kee, "Real-time implementation of optical OFDM transmitters and receivers for practical end-to-end optical transmission systems", *Electronics Letters*, vol. 45, no. 15, pp. 800–802, Jul. 2009.

[30] R. P. Giddings, X. Q. Jin, and J. M. Tang, "Experimental demonstration of real-time 3Gb/s optical OFDM transceivers", *Optics Express*, vol. 17, no. 19, pp. 16 654–16 665, Sep. 2009.

[31] ——, "First experimental demonstration of 6Gb/s real-time optical OFDM transceivers incorporating channel estimation and variable power loading", *Optics Express*, vol. 17, no. 22, pp. 19 727–19 738, Oct. 2009.

[32] R. P. Giddings, E. Hugues-Salas, X. Q. Jin, J. L. Wei, and J. M. Tang, "Experimental demonstration of real-time optical OFDM transmission at 7.5 Gb/s over 25-km SSMF using a 1-GHz RSOA", *Photonics Technology Letters*, vol. 22, no. 11, pp. 745–747, Jun. 2010.

[33] R. P. Giddings, E. Hugues-Salas, B. Charbonnier, and J. M. Tang, "Experimental demonstration of real-time optical OFDM transmission at 11.25 Gb/s over 500-m MMFs employing directly modulated DFB lasers", *Photonics Technology Letters*, vol. 23, no. 1, pp. 51–53, Feb. 2011.

[34] E. Hugues-Salas, R. P. Giddings, X. Q. Jin, J. L. Wei, X. Zheng, Y. Hong, C. Shu, and J. M. Tang, "Real-time experimental demonstration of low-cost VCSEL intensity-modulated 11.25Gb/s optical OFDM signal transmission over 25km PON systems", *Optics Express*, vol. 19, no. 4, pp. 2979–2988, Feb. 2011.

[35] R. P. Giddings, E. Hugues-Salas, and J. M. Tang, "Experimental demonstration of record high 19.125Gb/s real-time end-to-end dual-band optical OFDM transmission over 25km SMF in a simple EML-based IMDD system", *Optics Express*, vol. 20, no. 18, pp. 20 666–20 679, Aug. 2012.

[36] Q. W. Zhang, E. Hugues-Salas, R. P. Giddings, M. Wang, and J. M. Tang, "Experimental demonstrations of record high REAM intensity modulator-enabled 19.25Gb/s real-time end-to-end dual-band optical OFDM colorless transmissions over 25km SSMF IMDD systems", *Optics Express*, vol. 21, no. 7, pp. 9167–9179, Apr. 2013.

[37] R. P. Giddings, E. Hugues-Salas, Q. W. Zhang, J. J. Zhang, M. Wang, and J. M. Tang, "25.25-Gb/s real-time multi-band optical OFDM transmission over 300-m MMFs with IQ modulated passband", *Photonics Technology Letters*, vol. 25, no. 21, pp. 2123–2125, Nov. 2013.

[38] R. P. Giddings, "Real-time digital signal processing for optical OFDM-based future optical access networks", *Journal of Lightwave Technology*, vol. 32, no. 4, pp. 553–570, Feb. 2014.

[39] S.-H. Cho, K. W. Doo, J. H. Lee, J. Lee, S. I. Myong, and S. S. Lee, "Demonstration of a real-time 16 QAM encoded 11.52 Gb/s OFDM transceiver for IM/DD OFDMA-PON systems", in *18th OptoElectronics and Communications Conference (OECC) and International Conference on Photonics in Switching (OECC/PS)*, Jun. 2013, WP2–3.

[40] M. Chen, J. He, and L. Chen, "Real-time optical OFDM long-reach PON system over 100 km SSMF using a directly modulated DFB laser", *Journal of Optical Communications and Networking*, vol. 6, no. 1, pp. 18–25, Jan. 2014.

[41] C.-C. Wei, "Analysis and iterative equalization of transient and adiabatic chirp effects in DML-based OFDM transmission systems", *Optics Express*, vol. 20, no. 23, pp. 25 774–25 789, Nov. 2012.

[42] D.-Z. Hsu, C.-C. Wei, H.-Y. Chen, Y.-C. Lu, C.-Y. Song, C.-C. Yang, and J. Chen, "SSII cancellation in an EAM-based OFDM-IMDD transmission system employing a novel dynamic chirp model", *Optics Express*, vol. 21, no. 1, pp. 533–543, Jan. 2013.

[43] C.-C. Wei, "Small-signal analysis of OOFDM signal transmission with directly modulated laser and direct detection", *Optics Letters*, vol. 36, no. 2, pp. 151–153, Jan. 2011.

[44] D. Qian, J. Hu, J. Yu, P. N. Ji, L. Xu, T. Wang, M. Cvijetic, and T. Kusano, "Experimental demonstration of a novel OFDM-A based 10Gb/s PON architecture", *33rd European Conference and Exhibition of Optical Communication (ECOC)*, pp. 1 –2, Sep. 2007, p. Mo 5.4.1.

[45] D. Qian, N. Cvijetic, J. Hu, and T. Wang, "108 Gb/s OFDMA-PON with polarization multiplexing and direct detection", *Journal of Lightwave Technology*, vol. 28, no. 4, pp. 484–493, Feb. 2010.

[46] N. Cvijetic, M. Cvijetic, M.-F. Huang, E. Ip, Y.-K. Huang, and T. Wang, "Terabit optical access networks based on WDM-OFDMA-PON", *Journal of Lightwave Technology*, vol. 30, no. 4, pp. 493–503, Feb. 2012.

[47] C.-T. Lin, A. Ng'oma, W.-Y. Lee, C.-C. Wei, C.-Y. Wang, T.-H. Lu, J. Chen, W.-J. Jiang, and C.-H. Ho, "2 x 2 MIMO radio-over-fiber system at 60 GHz employing frequency domain equalization", *Optics Express*, vol. 20, no. 1, pp. 562–567, Jan. 2012.

[48] H.-T. Huang, C.-T. Lin, C.-H. Ho, W.-L. Liang, C.-C. Wei, Y.-H. Cheng, and S. Chi, "High spectral efficient W-band OFDM-RoF system with direct-detection by two cascaded single-drive MZMs", *Optics Express*, vol. 21, no. 14, pp. 16 615–16 620, Jul. 2013.

[49] H. Yang, S. C. J. Lee, E. Tangdiongga, C. Okonkwo, H. P. A. van den Boom, F. Breyer, S. Randel, and A. M. J. Koonen, "47.4 Gb/s transmission over 100 m graded-index plastic optical fiber based on rate-adaptive discrete multitone modulation", *Journal of Lightwave Technology*, vol. 28, no. 4, pp. 352–359, Feb. 2010.

[50] W.-R. Peng, B. Zhang, K.-M. Feng, X. Wu, A. E. Willner, and S. Chi, "Spectrally efficient direct-detected OFDM transmission incorporating a tunable frequency gap and an iterative detection techniques", *Journal of Lightwave Technology*, vol. 27, no. 24, pp. 5723–5735, Dec. 2009.

[51] X. Chen, A. Li, D. Che, Q. Hu, Y. Wang, J. He, and W. Shieh, "Block-wise phase switching for double-sideband direct detected optical OFDM signals", *Optics Express*, vol. 21, no. 11, pp. 13 436–13 441, Jun. 2013.

[52] T. M. F. Alves, M. Morant, A. V. T. Cartaxo, and R. Llorente, "Transmission of OFDM wired-wireless quintuple-play services along WDM LR-PONs using centralized broadband impairment compensation", *Optics Express*, vol. 20, no. 13, pp. 13 748–13 761, Jun. 2012.

[53] J.-H. Yan, Y.-W. Chen, K.-H. Shen, and K.-M. Feng, "An experimental demonstration for carrier reused bidirectional PON system with adaptive modulation DDO-OFDM downstream and QPSK upstream signals", *Optics Express*, vol. 21, no. 23, pp. 28 154–28 166, Nov. 2013.

[54] C. Zhang, Q. Zhang, C. Chen, N. Jiang, D. Liu, K. Qiu, S. Liu, and B. Wu, "Metro-access integrated network based on optical OFDMA with dynamic sub-carrier allocation and power distribution", *Optics Express*, vol. 21, no. 2, pp. 2474–2479, Jan. 2013.

[55] J. G. Proakis, *Digital Communications*, 4th ed. McGrawHill, 2000.

[56] M. Cvijetic and I. B. Djordjevic, *Advanced optical communication systems and networks*. Artech House, 2013.

[57] A. Peled and A. Ruiz, "Frequency domain data transmission using reduced computational complexity algorithms", in *IEEE International Conference on Acoustics, Speech, and Signal Processing (ICASSP)*, vol. 5, 1980, pp. 964–967.

[58] R. v. Nee and R. Prasad, *OFDM for Wireless Multimedia Communications*. Artech House, 2000.

[59] D. J. F. Barros and J. M. Kahn, "Optical modulator optimization for orthogonal frequency-division multiplexing", *Journal of Lightwave Technology*, vol. 27, no. 13, pp. 2370–2378, Jul. 2009.

[60] E. Vanin, "Performance evaluation of intensity modulated optical OFDM system with digital baseband distortion", *Optics Express*, vol. 19, no. 5, pp. 4280–4293, Feb. 2011.

[61] C. R. Berger, Y. Benlachtar, R. I. Killey, and P. A. Milder, "Theoretical and experimental evaluation of clipping and quantization noise for optical OFDM", *Optics Express*, vol. 19, no. 18, pp. 17 713–17 728, Aug. 2011.

[62] D. Hillerkuss, R. Schmogrow, T. Schellinger, M. Jordan, M. Winter, G. Huber, T. Vallaitis, R. Bonk, P. Kleinow, F. Frey, M. Roeger, S. Koenig, A. Ludwig, A. Marculescu, J. Li, M. Hoh, M. Dreschmann, J. Meyer, S. B. Ezra, N. Narkiss, B. Nebendahl, F. Parmigiani, P. Petropoulos, B. Resan, A. Oehler, K. Weingarten, T. Ellermeyer, J. Lutz, M. Moeller, M. Huebner, J. Becker, C. Koos, W. Freude, and J. Leuthold, "26 tbit $s-1$ line-rate super-channel transmission utilizing all-optical fast Fourier transform processing", *Nature Photonics*, vol. 5, no. 6, pp. 364–371, May 2011.

[63] J.-K. K. Rhee, N. Cvijetic, N. Wada, and T. Wang, "Optical orthogonal frequency division multiplexed transmission using all-optical discrete Fourier transform", *Laser & Photonics Reviews*, vol. 7, no. 4, pp. 539–553, Jul. 2013.

[64] A. J. Lowery, "Design of arrayed-waveguide grating routers for use as optical OFDM demultiplexers", *Optics Express*, vol. 18, no. 13, pp. 14 129–14 143, Jun. 2010.

[65] G. Agrawal and N. Dutta, *Semiconductor Lasers*. Van Nostrand Reinhold, 1993.

[66] K. Petermann, *Laser Diode Modulation and Noise*. Springer, 1988.

[67] B. J. C. Schmidt, A. J. Lowery, and J. Armstrong, "Experimental demonstrations of electronic dispersion compensation for long-haul transmission using direct-detection optical OFDM", *Journal of Lightwave Technology*, vol. 26, no. 1, pp. 196–203, Jan. 2008.

[68] W. Shieh, H. Bao, and Y. Tang, "Coherent optical OFDM: theory and design", *Optics Express*, vol. 16, no. 2, pp. 841–859, Jan. 2008.

[69] H. Bao and W. Shieh, "Transmission simulation of coherent optical OFDM signals in WDM systems", *Optics Express*, vol. 15, no. 8, pp. 4410–4418, Apr. 2007.

[70] E. Ip, A. P. T. Lau, D. J. F. Barros, and J. M. Kahn, "Coherent detection in optical fiber systems", *Optics Express*, vol. 16, no. 2, pp. 753–791, Jan. 2008.

[71] G. Li, "Recent advances in coherent optical communication", *Advances in Optics and Photonics*, vol. 1, no. 2, pp. 279–307, Apr. 2009.

[72] D. J. F. Barros and J. M. Kahn, "Comparison of orthogonal frequency-division multiplexing and On-Off keying in direct-detection multimode fiber links", *Journal of Lightwave Technology*, vol. 29, no. 15, pp. 2299–2309, Aug. 2011.

[73] X. Zheng, X. Q. Jin, R. P. Giddings, J. L. Wei, E. Hugues-Salas, Y. H. Hong, and J. M. Tang, "Negative power penalties of optical OFDM signal transmissions in directly modulated DFB laser-based IMDD systems incorporating negative dispersion fibers", *Photonics Journal*, vol. 2, no. 4, pp. 532 –542, Aug. 2010.

[74] J. M. Tang and K. A. Shore, "30-Gb/s signal transmission over 40-km directly modulated DFB-laser-based single-mode-fiber links without optical amplification and dispersion compensation", *Journal of Lightwave Technology*, vol. 24, no. 6, pp. 2318 –2327, Jun. 2006.

[75] R. Bracewell, *The Fourier Transform and Its Applications*, 3rd ed. McGraw-Hill Higher Education, 2000.

[76] M. Abramowitz and I. A. Stegun, *Handbook of mathematical functions*. Dover publications, 1965.

[77] E. Peral and A. Yariv, "Large-signal theory of the effect of dispersive propagation on the intensity modulation response of semiconductor lasers", *Journal of Lightwave Technology*, vol. 18, no. 1, pp. 84–89, Jan. 2000.

[78] J. A. P Morgado and A. V. T Cartaxo, "Laser optimization guidelines for dispersion supported transmission systems operating at arbitrary bit rates", *Journal of Lightwave Technology*, vol. 26, no. 13, pp. 1807–1816, Jul. 2008.

[79] A. Chorti and M. Brookes, "On the effects of memoryless nonlinearities on M-QAM and DQPSK OFDM signals", *Transactions on Microwave Theory and Techniques*, vol. 54, no. 8, pp. 3301–3315, Aug. 2006.

[80] T. Wang, J. G. Proakis, and J. R. Zeidler, "Techniques for suppression of intercarrier interference in OFDM systems", in *IEEE Wireless Communications and Networking Conference (WCNC)*, vol. 1, 2005, pp. 39–44.

[81] H. Ochiai and H. Imai, "Performance analysis of deliberately clipped OFDM signals", *Transactions on Communications*, vol. 50, no. 1, pp. 89–101, Jan. 2002.

[82] D. Dardari, "Joint clip and quantization effects characterization in OFDM receivers", *Transactions on Circuits and Systems*, vol. 53, no. 8, pp. 1741–1748, Aug. 2006.

[83] D. Dardari, V. Tralli, and A. Vaccari, "A theoretical characterization of nonlinear distortion effects in OFDM systems", *Transactions on Communications*, vol. 48, no. 10, pp. 1755–1764, Oct. 2000.

[84] H. E. Rowe, "Memoryless nonlinearities with gaussian inputs: elementary results", *Bell System Technical Journal*, vol. 61, no. 7, 1519â–1526, Sep. 1982.

[85] R. Gross and D. Veeneman, "SNR and spectral properties for a clipped DMT ADSL signal", in *IEEE International Conference on Communications (ICC)*, vol. 2, Jul. 1994, pp. 843–847.

[86] A. R. S. Bahai, M. Singh, A. J. Goldsmith, and B. Saltzberg, "A new approach for evaluating clipping distortion in multicarrier systems", *Journal on Selected Areas in Communications*, vol. 20, no. 5, pp. 1037–1046, Jun. 2002.

[87] W. Henkel, G. Taubock, P. Odling, P. Borjesson, and N. Petersson, "The cyclic prefix of OFDM/DMT - an analysis", in *International Zurich Seminar on Broadband Communications*, 2002, pp. 22–1–22–3.

[88] D. J. F. Barros and J. M. Kahn, "Optimized dispersion compensation using orthogonal frequency-division multiplexing", *Journal of Lightwave Technology*, vol. 26, no. 16, pp. 2889–2898, Aug. 2008.

[89] G. P. Agrawal, *Fiber-Optic Communication Systems*, 3rd ed. John Wiley & Sons, 2002.

[90] P. K. Vitthaladevuni, M. S. Alouini, and J. C. Kieffer, "Exact BER computation for cross QAM constellations", *Transactions on Wireless Communications*, vol. 4, no. 6, pp. 3039–3050, Nov. 2005.

[91] J. A. P Morgado and A. V. T. Cartaxo, "Directly modulated laser parameters optimization for metropolitan area networks utilizing negative dispersion fibers", *Journal of Selected Topics in Quantum Electronics*, vol. 9, no. 5, pp. 1315–1324, Sep. 2003.

[92] E. Giacoumidis, J. L. Wei, X. Q. Jin, and J. M. Tang, "Improved transmission performance of adaptively modulated optical OFDM signals over directly modulated DFB laser-based IMDD links using adaptive cyclic prefix", *Optics Express*, vol. 16, no. 13, pp. 9480–9494, Jun. 2008.

[93] Z. Liu, M. A. Violas, and N. B. Carvalho, "Digital predistortion for RSOAs as external modulators in radio over fiber systems", *Optics Express*, vol. 19, no. 18, pp. 17641–17646, Aug. 2011.

[94] T. F. Alves, J. Morgado, and A. Cartaxo, "Linearity improvement of directly modulated PONs by digital pre-distortion of coexisting OFDM-based signals", in *Advanced Photonics Congress*, Optical Society of America, 2012, AW4A.2.

[95] Y. Bao, Z. Li, J. Li, X. Feng, B. ou Guan, and G. Li, "Nonlinearity mitigation for high-speed optical OFDM transmitters using digital pre-distortion", *Optics Express*, vol. 21, no. 6, pp. 7354–7361, Mar. 2013.

[96] D. Lam, A. M. Fard, B. Buckley, and B. Jalali, "Digital broadband linearization of optical links", *Optics Letters*, vol. 38, no. 4, pp. 446–448, Feb. 2013.

[97] N. S. André, K. Habel, H. Louchet, and A. Richter, "Adaptive nonlinear Volterra equalizer for mitigation of chirp-induced distortions in cost effective IMDD OFDM systems", *Optics Express*, vol. 21, no. 22, pp. 26527–26532, Nov. 2013.

[98] W. Yan, T. Tanaka, B. Liu, M. Nishihara, L. Li, T. Takahara, Z. Tao, J. C. Rasmussen, and T. Drenski, "100 Gb/s optical IM-DD transmission with 10G-class devices enabled by 65 GSamples/s CMOS DACcore", in *Optical Fiber Communication Conference (OFC)*, Optical Society of America, 2013, OM3H.1.

[99] M. H. M Costa, "Writing on dirty paper", *Transactions on Information Theory*, vol. 29, no. 3, pp. 439–441, May 1983.

[100] G. Shulkind and M. Nazarathy, "Estimating the Volterra series transfer function over coherent optical OFDM for efficient monitoring of the fiber channel nonlinearity", *Optics Express*, vol. 20, no. 27, pp. 29035–29062, Dec. 2012.

[101] W. Yan, B. Liu, L. Li, Z. Tao, T. Takahara, and J. C. Rasmussen, "Nonlinear distortion and DSP-based compensation in metro and access networks using discrete multitone", in *European Conference and Exhibition on Optical Communication (ECOC)*, 2012, Mo.1.B.2.

[102] A. V. Oppenheim, R. W. Schafer, and J. R. Buck, *Discrete-time Signal Processing*, 2nd ed. Prentice-Hall, 1999.

[103] L. S. Yan, Y. Wang, B. Zhang, C. Yu, J. McGeehan, L. Paraschis, and A. E. Willner, "Reach extension in 10-Gb/s directly modulated transmission systems using asymmetric and narrowband optical filtering", *Optics Express*, vol. 13, no. 13, pp. 5106–5115, Jun. 2005.

[104] J. L. Wei, C. Sánchez, R. P. Giddings, E. Hugues-Salas, and J. M. Tang, "Significant improvements in optical power budgets of real-time optical OFDM PON systems", *Optics Express*, vol. 18, no. 20, pp. 20 732–20 745, Sep. 2010.

[105] J. L. Wei, C. Sánchez, E. Hugues-Salas, P. S. Spencer, and J. M. Tang, "Wavelength-offset filtering in optical OFDM IMDD systems using directly modulated DFB lasers", *Journal of Lightwave Technology*, vol. 29, no. 18, pp. 2861–2870, Sep. 2011.

[106] J. Capmany, "On the cascade of incoherent discrete-time microwave photonic filters", *Journal of Lightwave Technology*, vol. 24, no. 7, pp. 2564–2578, Jul. 2006.

[107] C. K. Madsen and J. H. Zhao, *Optical Filter Design and Analysis: A Signal Processing Approach*. Wiley-Interscience, Jun. 1999.

[108] J. Yu, Z. Jia, M.-F. Huang, M. Haris, P. N. Ji, T. Wang, and G.-K. Chang, "Applications of 40-Gb/s chirp-managed laser in access and metro networks", *Journal of Lightwave Technology*, vol. 27, no. 3, pp. 253–265, Feb. 2009.

[109] M. A. Muriel and A. Carballar, "Phase reconstruction from reflectivity in uniform fiber Bragg gratings", *Optics Letters*, vol. 22, no. 2, pp. 93–95, Jan. 1997.

[110] T. Erdogan, "Fiber grating spectra", *Journal of Lightwave Technology*, vol. 15, no. 8, pp. 1277–1294, Aug. 1997.

[111] Z. Al-Qazwini and H. Kim, "Symmetric 10-Gb/s WDM-PON using directly modulated lasers for downlink and RSOAs for uplink", *Journal of Lightwave Technology*, vol. 30, no. 12, pp. 1891–1899, Jun. 2012.

[112] D. J. Barros and J. M. Kahn, "OFDM vs. OOK with MLSD for IM/DD systems", in *Optical Fiber Communication Conference (OFC)*, 2010, OThE1.

[113] C. Browning, K. Shi, S. Latkowski, P. M. Anandarajah, F. Smyth, B. Cardiff, R. Phelan, and L. P. Barry, "Performance improvement of 10Gb/s direct modulation OFDM by optical injection using monolithically integrated discrete mode lasers", *Optics Express*, vol. 19, no. 26, B289–B294, Dec. 2011.

[114] H.-Y. Chen, C. C. Wei, D.-Z. Hsu, M. Yuang, J. Chen, Y.-M. Lin, P.-L. Tien, S. Lee, S.-H. Lin, W.-Y. Li, C.-H. Hsu, and J.-L. Shih, "A 40-Gb/s OFDM PON system based on 10-GHz EAM and 10-GHz direct-detection PIN", *Photonics Technology Letters*, vol. 24, no. 1, pp. 85–87, Jan. 2012.

[115] N. Cvijetic, "OFDM for next-generation optical access networks", *Journal of Lightwave Technology*, vol. 30, no. 4, pp. 384–398, Feb. 2012.

[116] D. Qian, N. Cvijetic, J. Hu, and T. Wang, "108 Gb/s OFDMA-PON with polarization multiplexing and direct detection", *Journal of Lightwave Technology*, vol. 28, no. 4, pp. 484–493, Feb. 2010.

[117] I. B. Djordjevic and B. Vasic, "Orthogonal frequency division multiplexing for high-speed optical transmission", *Optics Express*, vol. 14, no. 9, pp. 3767–3775, May 2006.

[118] B. J. Dixon, R. D. Pollard, and S. Iezekiel, "Orthogonal frequency division multiplexing in wireless communication systems with multimode fibre feeds", in *Radio and Wireless Conference (RAWCON)*, 2000, pp. 79–82.

[119] R. P. Giddings, X. Q. Jin, E. Hugues-Salas, E. Giacoumidis, J. L. Wei, and J. M. Tang, "Experimental demonstration of a record high 11.25Gb/s real-time optical OFDM transceiver supporting 25km SMF end-to-end transmission in simple IMDD systems", *Optics Express*, vol. 18, no. 6, pp. 5541–5555, Mar. 2010.

[120] E. Hugues-Salas, X. Q. Jin, R. P. Giddings, Y. Hong, S. Mansoor, A. Villafranca, and J. M. Tang, "Directly modulated VCSEL-based real-time 11.25-Gb/s optical OFDM transmission over 2000-m legacy MMFs", *Photonics Journal*, vol. 4, no. 1, pp. 143–154, Feb. 2012.

[121] *10-gigabit-capable passive optical networks (XG-PON): general requirements*, IEEE, 802.11, Piscataway, NJ, 1997.

[122] N. Jolley, H. Kee, R. Rickard, and J. M. Tang, "Generation and propagation of a 1550 nm 10 Gbit/s optical orthogonal frequency division multiplexed signal over 1000m of multimode fibre using a directly modulated DFB", in *Optical Fiber Communication Conference (OFC)*, 2005, OFP3.

[123] A. J. Lowery, L. Du, and J. Armstrong, "Orthogonal frequency division multiplexing for adaptive dispersion compensation in long haul WDM systems", in *Optical Fiber Communication Conference (OFC)*, Mar. 2006, PDP39.

[124] M. S. Moreolo, R. Muñoz, and G. Junyent, "Novel power efficient optical OFDM based on Hartley transform for intensity-modulated direct-detection systems", *Journal of Lightwave Technology*, vol. 28, no. 5, pp. 798 –805, Mar. 2010.

[125] W.-R. Peng, X. Wu, V. R. Arbab, B. Shamee, L. C. Christen, J.-Y. Yang, K.-M. Feng, A. E. Willner, and S. Chi, "Experimental demonstration of a coherently modulated and directly detected optical OFDM system using an RF-tone insertion", in *Optical Fiber communication Conference (OFC)*, Feb. 2008, OMU2.

[126] W.-R. Peng, I. Morita, and H. Tanaka, "Enabling high capacity direct-detection optical OFDM transmissions using beat interference cancellation receiver", in *36th European Conference and Exhibition on Optical Communication (ECOC)*, Sep. 2010, Tu.4.A.2.

[127] B. Schmidt, Z. Zan, L. Du, and A. Lowery, "100 Gbit/s transmission using single-band direct-detection optical OFDM", in *Optical Fiber Communication Conference (OFC)*, Mar. 2009, PDPC3.

[128] B. Schmidt, Z. Zan, L. Du, and A. Lowery, "120 Gbit/s over 500-km using single-band polarization-multiplexed self-coherent optical OFDM", *Journal of Lightwave Technology*, vol. 28, no. 4, pp. 328 –335, Feb. 2010.

[129] B. Schrenk, G. de Valicourt, M. Omella, J. Lazaro, R. Brenot, and J. Prat, "Direct 10-Gb/s modulation of a single-section RSOA in PONs with high optical budget", *Photonics Technology Letters*, vol. 22, no. 6, pp. 392–394, Mar. 2010.

[130] W. Shieh and C. Athaudage, "Coherent optical orthogonal frequency division multiplexing", *Electronics Letters*, vol. 42, no. 10, pp. 587 –589, May 2006.

[131] W.-R. Peng, B. Zhang, K.-M. Feng, X. Wu, A. Willner, and S. Chi, "Spectrally efficient direct-detected OFDM transmission incorporating a tunable frequency gap and an iterative detection techniques", *Journal of Lightwave Technology*, vol. 27, no. 24, pp. 5723–5735, Dec. 2009.

[132] Y.-M. Lin, "Demonstration and design of high spectral efficiency 4Gb/s OFDM system in passive optical networks", in *Optical Fiber Communication Conference (OFC)*, Mar. 2007, OThD7.

[133] Y.-M. Lin and P.-L. Tien, "Next-generation OFDMA-based passive optical network architecture supporting radio-over-fiber", *Journal on Selected Areas in Communications*, vol. 28, no. 6, pp. 791–799, Aug. 2010.

[134] X. Zheng, J. L. Wei, and J. M. Tang, "Transmission performance of adaptively modulated optical OFDM modems using subcarrier modulation over SMF IMDD links for access and metropolitan area networks", *Optics Express*, vol. 16, no. 25, pp. 20 427–20 440, Dec. 2008.